J.-H. Richard

Mercury contaminated groundwater: Speciation analysis, modeling, and remediation

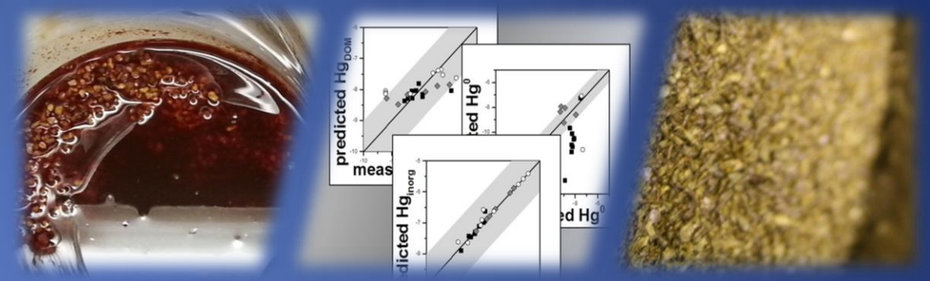

Mercury contaminated groundwater: Speciation analysis, modeling, and remediation

doctoral thesis

of

Jan-Helge Richard

TU Braunschweig, Institut für Geoökologie, Umweltgeochemie

Mercury contaminated groundwater: Speciation analysis, modeling, and remediation

Von der

Fakultät Architektur, Bauingenieurwesen und Umweltwissenschaften

der Technischen Universität Carolo-Wilhelmina

zu Braunschweig

zur Erlangung des Grades eines

Doktors der Naturwissenschaften (Dr. rer. nat.)

genehmigte

Dissertation

von

Jan-Helge Richard

geboren am 03. Februar 1982

aus Fulda

Eingereicht am: 03. Februar 2016
Disputation am: 23. Mai 2016

Berichterstatter: Prof. Dr. Harald Biester

Prof. Dr. Stephan Weber

2016

Abstract

Mercury (Hg) is a toxic element and has gained much attention in recent decades mainly because of its tendency to be enriched in the aquatic food web. It has been used for centuries in numerous applications and can still be found in soils and groundwater at many former industrial production sites. In the present thesis three such sites were examined, where soil and groundwater had been contaminated due to the use of highly soluble Hg^{2+}-salts as wood preservatives or the application of elemental Hg (Hg^0) in the production of caustic soda and chlorine. Distribution of Hg species and species transformation processes were studied in the aquifer of one of the sites. The importance of redox change derived hydrous ferric oxides (HFOs) for Hg^{2+} reduction and Hg mobility in the aquifer could be shown for the first time here. Measured Hg concentrations in HFO of up to 4 wt.-% were not predicted by geochemical modeling.

Species distribution of dissolved Hg is often determined on the basis of such models, but prediction accuracy for Hg speciation has never been evaluated by comparison with analyses on natural samples. Therefore, in a second study, Hg species measurements (Hg^0, inorganic Hg^{2+}, Hg^{2+} bound to dissolved organic matter (DOM)) were performed on groundwater samples from the three sites and were compared with predicted species distribution from three geochemical modeling programs (PHREEQC, Visual MINTEQ, WHAM). Here, DOM quality in terms of functional group composition (thiols and weaker binding sites) and binding site abundance could be identified as a crucial parameter for prediction accuracy in contaminated groundwater.

Hg speciation is a key factor to be determined for choosing the right remediation strategy. In fast flowing and highly Hg contaminated groundwater permeable reactive barriers would be advantageous but cannot be applied for remediation, due to the lack of an appropriate filter medium. Hence, long-term effectiveness of brass shavings as Hg filter material has been investigated in a third study. At one of the test sites a pilot plant has been installed and was operated over a period of 2.5 years. It could be demonstrated that reaction kinetics and cleaning performance of brass are clearly superior to those of other filter materials.

However, possible applications of brass shavings are restricted through high Zn concentrations in the effluent of the test filters at natural pH of the site (pH 6.6).

The present work provides new insights into species transformation processes strongly influencing mobility and bioavailability of Hg in the environment. The crucial role of DOM composition for predicting dissolved inorganic and DOM bound Hg by geochemical models could be identified. Performance and limitations of brass shavings as filter material were determined in a pilot project for the remediation of Hg contaminated groundwater.

Zusammenfassung

Quecksilber (Hg) ist ein toxisches Schwermetall welches unter anderem aufgrund seiner Tendenz im Nahrungsnetz angereichert zu werden in den letzten Jahrzehnten große Aufmerksamkeit erlangt hat. Es wurde über Jahrhunderte in zahllosen Anwendungen eingesetzt und ist daher heute in Böden und Grundwasser vieler (ehemaliger) Industriestandorte angereichert. In der vorliegenden Arbeit wurden drei solcher Standorte untersucht, an denen es aufgrund der Verwendung von leicht löslichen Hg^{2+}-Salzen in der Holzkonservierung beziehungsweise dem Einsatz von elementarem Hg (Hg^0) bei der Herstellung von Natronlauge und Chlor zur Kontamination von Boden und Grundwasser gekommen war. An einem der Standorte wurde die Verteilung von Hg-Spezies im Grundwasserleiter sowie auftretende Spezies Umwandlungsprozesse näher untersucht. Hierbei ließ sich erstmals unter Feldbedingungen die große Bedeutung von durch Redox-Schwankungen gebildeten Eisenhydroxiden (HFOs) für die Hg^{2+} Reduktion und Quecksilber-Mobilität in zeitweise anoxischen Aquiferen nachweisen.

An frisch gefällten HFOs wurden dabei Hg-Konzentrationen von bis zu 4 Gew.-% ermittelt. Die Entstehung solch hoher Hg-Gehalte ließ sich jedoch nicht mittels geochemischer Modelle nachvollziehen. Die Speziesverteilung von Hg wird aber oft allein auf Grundlage solcher Modelle berechnet, ohne dass diese bisher über den Vergleich mit chemischen Analysen an natürlichen Proben evaluiert worden wären. Daher wurden in einer zweiten Studie Hg-Spezies Messungen (Hg^0, anorganisches Hg^{2+} und an gelöste organische Substanz (DOM) gebundenes Hg^{2+}) an Grundwasserproben von allen drei Standorten durchgeführt und mit der von geochemischer Modellier-Software (PHREEQC, Visual MINTEQ, WHAM) prognostizierten Speziesverteilung verglichen. Als entscheidender Parameter für die Qualität der Modellvorhersagen in Hg kontaminierten Grundwässern konnte dabei die DOM-Qualität im Sinne von Implementierung beziehungsweise angenommener Häufigkeit wichtiger funktioneller Gruppen (reduzierte Schwefel- bzw. Sauerstoffgruppen) identifiziert werden.

Die Kenntnis der Speziesverteilung auf einem Hg-belasteten Standort ist ein Schlüsselfaktor zur Wahl der richtigen Sanierungsstrategie. In schnell fließenden, stark mit anorganischem Hg^{2+} kontaminierten Grundwässern wäre dabei der Einsatz von reaktiven Wänden eine sinnvolle Sanierungstechnik. Deren Anwendung ist aber in Ermangelung eines geeigneten Hg-Filtermediums stark eingeschränkt. Daher wurde in einer dritten Studie die Langzeit-Effektivität von Messinggranulat als mögliches Hg Filtermaterial untersucht. An einem der untersuchten Standorte wurde dazu eine Pilotanlage installiert und über einen Zeitraum von 2½ Jahren betrieben. Hier erwiesen sich Reaktionskinetik und Reinigungsleistung von Messing gegenüber denen konventioneller Filtermaterialien als deutlich überlegen. Bei pH-Werten unter 8,5 beschränken jedoch erhöhte Zn-Konzentrationen im Ablauf der Versuchsfilter das mögliche Einsatzgebiet von Messinggranulat.

In der vorliegenden Arbeit konnten neue Erkenntnisse zu Spezies Umwandlungsprozessen gewonnen werden, welche starken Einfluss auf Mobilität und Bioverfügbarkeit von Hg in der Umwelt haben. Die Zusammensetzung gelöster organischer Substanz (DOM) konnte als kritischer Parameter für die Vorhersagequalität von anorganischem und DOM gebundenen Hg in geochemischen Modellen identifiziert werden. Außerdem konnte das Potenzial von Messinggranulat als Filtermaterial zur Reinigung von Hg kontaminiertem Grundwasser ermittelt und die hydrochemischen Grenzparameter für dessen Einsatz bestimmt werden.

Table of contents

Chapter 1: Introduction

1 Structure of the thesis

The present thesis comprises of five chapters. It begins with an introduction (chapter 1) where a review of the relevant literature is presented, deducing the research need for the conducted studies and aiming to give the reader the necessary background for the following section. The main part of the thesis (chapters 2-4) consists of three manuscripts that have already been published (chapter 2) or have been submitted for publication in international peer-reviewed journals. A synthesis of the combined studies of this thesis is given in chapter 5 together with an outlook on further research work.

2 Mercury in the environment

2.1 Characteristics of mercury.

Mercury (Hg) is the only metal liquid at room temperature, has a very high vapor pressure ($1.71 \cdot 10^{-7}$ MPa at 20°C, NIST, 2006), and forms alloys (amalgams) at ambient conditions with most other metals (with iron being an important exception from the rule). Hg is known to the ancients and due to its very special characteristics (liquid, amalgam forming, toxic), it has been used for numerous purposes e.g. in gold processing, base chemicals production, in batteries and electrical switches, as a pesticide, an antiseptic, and for measuring temperature and pressure (Hylander and Meili, 2005). Industrial usage has led to a dramatic increase of anthropogenic Hg release during the last century, surpassing natural, mainly volcanic, primary emissions by a factor of three to four (UNEP, 2013). Today, Hg use in artisanal small-scale gold mining (ASGM) followed by high temperature processes such as coal combustion, waste incineration, cement, and metal production are the largest anthropogenic emission sources, summing up to a total of ~2000 t a^{-1} (Mason et al., 2012). The long atmospheric residence time and resulting long-distance transport of elemental Hg (Hg^0) ensued in an increase of Hg even in remote ecosystems (Fitzgerald et al., 1998). Hg^0 is a neurotoxin and long-term exposure to Hg^0 containing vapors can lead to serious health issues like tremor or renal insufficiency (WHO, 2016). While all forms of Hg are considered to be noxious, the organomercury

compounds di- and monomethylmercury ($(CH_3)_2Hg$ and CH_3Hg^+, respectively) are by far the most toxic forms of Hg. CH_3Hg^+ is produced by microorganisms in reducing environments (e.g. lake sediments) through methylation of Hg^{2+}. It is fat-soluble and forms complexes with cysteine. Therefore CH_3Hg^+ is bioaccumulated in the food web, making it the Hg compound most involved in Hg exposure to humans, mainly via consumption of fish (WHO, 2016).

2.2 Mercury species in the environment.

As mentioned above, Hg can occur in different chemical forms, so called species, greatly differing in terms of physico-chemical properties (water solubility, volatility, surface interaction, bonding or complex formation behavior,…) and resulting environmental dynamics. Hg has three stable oxidation states, Hg^0, Hg^{1+}, and Hg^{2+}. Elemental Hg forms alloys with other metals at ambient temperatures (amalgams). Silver and gold amalgams are prominent examples, one still occasionally used as dental filling material, the other an important intermediate product of gold extraction in ASGM. As already mentioned, Hg^0 is volatile and its solubility is consequently defined by a Henry`s law constant (1.3 mol m^{-3} Pa^{-1}; Sander, 2015). Therefore Hg^0 in solution is also called dissolved gaseous mercury (DGM). In its monovalent state (Hg^{1+}), Hg is usually present as the binuclear mercurous ion (Hg_2^{2+}). Several stable mercurous compounds (mainly halides) are known in the laboratory, but as soon as ligands are added that reduce the activity of Hg^{2+} to a significantly greater extent than that of Hg_2^{2+} (e.g. OH^-, Cl^-, S^{2-}, CN^- and many others), Hg_2^{2+} readily disproportionates to Hg^0 and Hg^{2+} (Cotton, 1972). Therefore Hg^{1+} is of no relevance in natural systems and calomel (Hg_2Cl_2) is probably the only mercurous compound that can sometimes be found in nature as a weathering product at Hg mineral deposits (Anthony et al., 2003). In the environment, Hg is most often found in its divalent state in form of the mercuric ion (Hg^{2+}). Hg^{2+} compounds show solubilities ranging from below 10 ng L^{-1} (cinnabar, α-HgS; Merian et al., 2004) to 250 g L^{-1} (mercury(II)chlorate, $Hg(ClO_3)_2$, Perry, 2011). In aqueous solution Hg^{2+} may be found as free, uncoordinated ion, but in natural waters it readily forms complexes with different ligands. As a type B or “soft” metal ion (Ahrland et al., 1958; Pearson, 1963) it prefers complexes with sulfur

(S), selenium (Se), the halides (chloride, bromine, iodine), phosphorus (P), and certain nitrogen (N) ligands (Cotton et al., 1999).

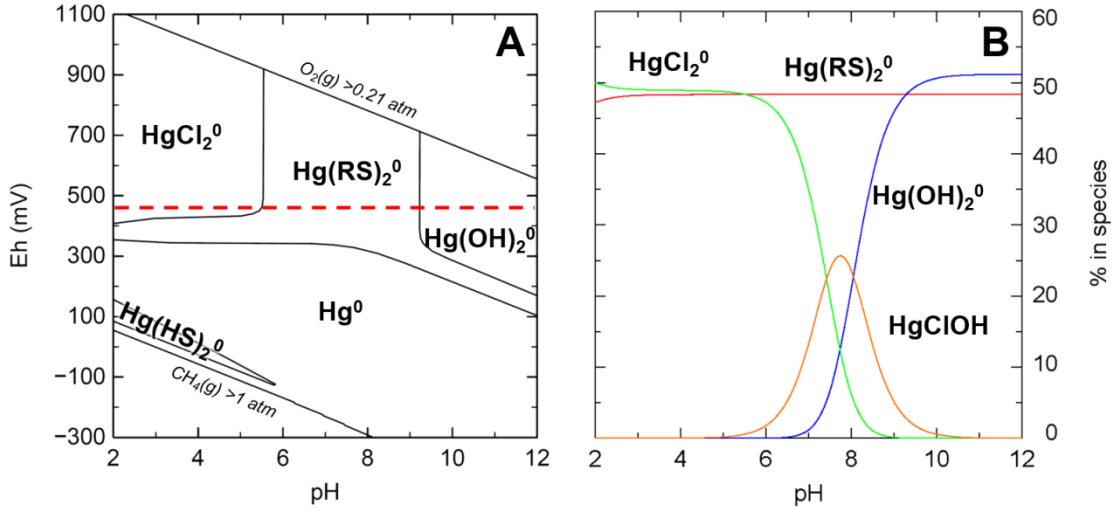

Figure 1. (A) Eh-pH and (B) pH-species distribution diagrams of a contaminated groundwater. The dashed red line in (A) represents the redox potential (Eh) for which (B) was calculated. $Hg(RS)_2^0$ is a two-coordinated complex of Hg with DOM thiol groups. Minor species (below 5%) were excluded from (B).

The preferred coordination number is 2, the complex character is covalent (Cotton, 1972), and Hg^{2+}-complexes are usually comparatively stable (VanLoon and Duffy, 2011). In natural waters, Hg^{2+} shows a strong tendency to bind to reduced S or thiol (RSH) groups in organic matter (Qian et al., 2002). Thus, Hg speciation in the environment is often dominated by Hg complexation to dissolved organic matter (DOM) on the aqueous phase (Meili et al., 1991), and Hg binding to soil organic matter (SOM) on the solid phase (Manceau et al., 2015). However, when Hg-DOM binding site ratios are higher (e.g. where DOM concentrations are low or Hg concentrations high), other ligands gradually come into play. Such a situation is depicted in Figure 1, where dominant Hg species in a contaminated groundwater (Hg: 40 µg L^{-1}, DOC: 4 mg L^{-1}) at different pH and redox conditions (Eh) are shown (Figure 1 A). Stabilities of Hg chloro-hydroxy complexes strongly depend on pH (Figure 1 B). In contrast, pH hardly influences Hg binding to DOM thiols ($Hg(RS)_2^0$) at the Eh for which Figure 1 B has been calculated. Depending on the prevailing Eh, Hg^{2+} may also be reduced to Hg^0 (Figure 1 A). In dark environments (e.g. soils, sediments, or groundwater), where Hg photoreduction (Amyot et al., 1997) can be excluded as a reaction mechanism, Hg^0 formation can be due to electron-transfer from

organic matter (Allard and Arsenie, 1991), bacteria (Barkay et al., 2003), or reduced iron species (Fe^{2+}; Charlet et al., 2002). Inorganic Hg^{2+} reduction by reduced organic matter and biotic reduction through iron or sulfate reducing bacteria (IRB, SRB) were studied in controlled lab experiments, aiming to mimic the situation in dark anoxic environments (Gu et al., 2011; Hellal et al., 2015), Nevertheless, relative importance of these reaction pathways in natural systems is still largely unknown. Indications exist, that inorganic reduction by Fe^{2+} might play an important role in anoxic groundwater (Lamborg et al., 2013). It could also be shown that kinetics of surface catalyzed Hg^{2+} reduction by Fe^{2+} is fast enough (Amirbahman et al., 2013) to account for a substantial part of Hg^0 formation in anoxic environments. When dissolved Fe^{2+} is oxidized and precipitates e.g. at redox interfaces of anoxic groundwater, hydrous ferric oxides (HFOs) are formed. However, the role of such abundant and highly reactive Fe-hydroxides for Hg^0 formation and Hg mobility in aquifers has not yet been explored.

3 Determination of mercury species

3.1 Mercury species measurement in solids

Three different general concepts exist to determine Hg species in solid materials: (i) Chemical extraction methods (ii) XAS (X-ray absorption spectroscopy) methods (iii) Thermodesorption. Apart from the compound specific extraction of CH_3Hg^+ (Rogers, 1975), chemical methods usually yield operationally defined Hg species groups separated on the basis of different chemical behavior i.e. leachability with different extracting agents. The first multistep chemical extraction methods for Hg speciation were presented in the 1980s (Giulio and Ryan, 1987). Bloom et al. (2003) developed a five step selective sequential extraction (SSE) method where a pre-weighed sample aliquot is treated with a series of continuously stronger reagents to determine bioavailable, semi- and non-mobile fractions (Figure 2). The US environmental protection agency published a different leaching method where inorganic and organic extractable, semi-mobile, and non-mobile Hg fractions are determined in a four step analytical protocol (US EPA, 2005). In a benchmark test with standard materials, results of both methods were similar and mostly reasonable,

except for Hg^0 and HgS standards. Here the EPA method gave inconsistent results while the SSE method was more reliable (Carter and Briscoe, 2012).

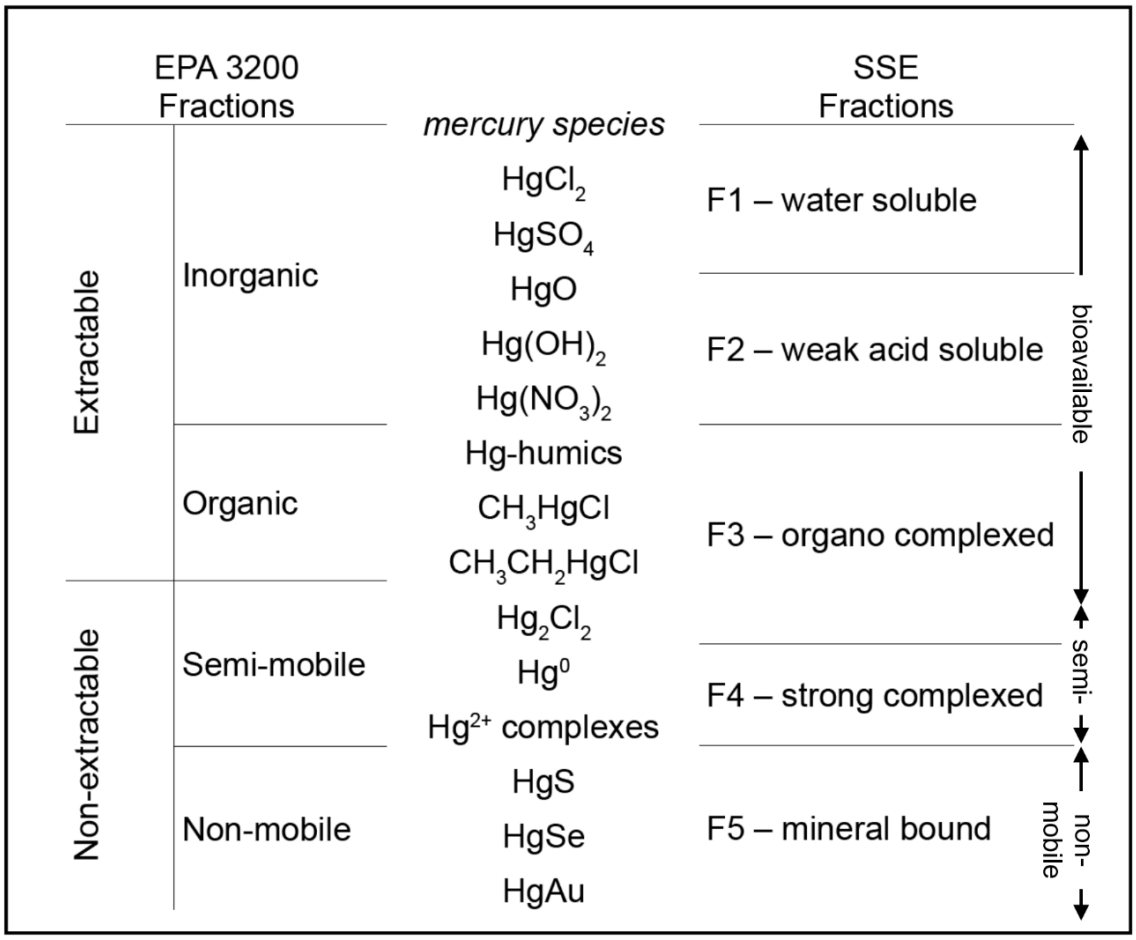

Figure 2. Comparison of chemical extraction method EPA 3200 (US EPA, 2005) and selective sequential extraction (SSE; Bloom et al., 2003) for determination of Hg species in solids. (altered after Carter and Briscoe, 2012).

Even though chemical extraction methods can be very helpful to asses transport behavior and possible ecological impact of the Hg found at a certain location, they give no clear information about the actual Hg compounds present in the sample. Here XAS methods are more explicit. XANES (X-ray absorption near edge structure spectroscopy) and EXAFS (extended X-ray absorption fine structure spectroscopy) are both synchrotron based techniques where the sample is exposed to an intense monochromatic X-ray beam. The exact wavelength of the beam is modulated around the energy level needed to excite a core level electron and evoke X-ray absorption. When this energy level is reached (at the so called absorption edge) absorption increases dramatically. XANES evaluates this part of the absorption spectra, while EXAFS examines

the undulating decrease of absorption in the latter part of the spectra at higher energies/wavelengths. By combining both techniques, oxidation state, type of nearest neighbors, coordination number, bond distance, and orbital symmetry of a certain element, in our case Hg, can be determined (Ginder-Vogel and Sparks, 2010). Hence, XAS is a powerful tool to determine Hg oxidation number and bonding (i.e. speciation) in many solids (e.g. ores, contaminated soils and sediment; Esbrí et al., 2010) or solution extracts (e.g. DOM; Skyllberg et al., 2005). However, synchrotron radiation (SR) facilities are rare (only ~70 exist worldwide; lightsources.org, 2015) so access to them is limited. A second drawback is, that the Hg concentration in the sample needs to be above 50 mg kg^{-1} even when using brightest third-generation SR sources to get a reasonable signal noise ratio (Skyllberg, 2010). Here, thermodesorption comes into play. Biester (1994) developed a Hg-speciation method based on the fact that different Hg species, when heated, decompose at different temperatures. An atomic absorption spectrometer (AAS) is coupled to a pyrolysis unit where a sample is heated continuously (heating rate: ~0.5°C s^{-1}) (Figure 3). Hg^0 is

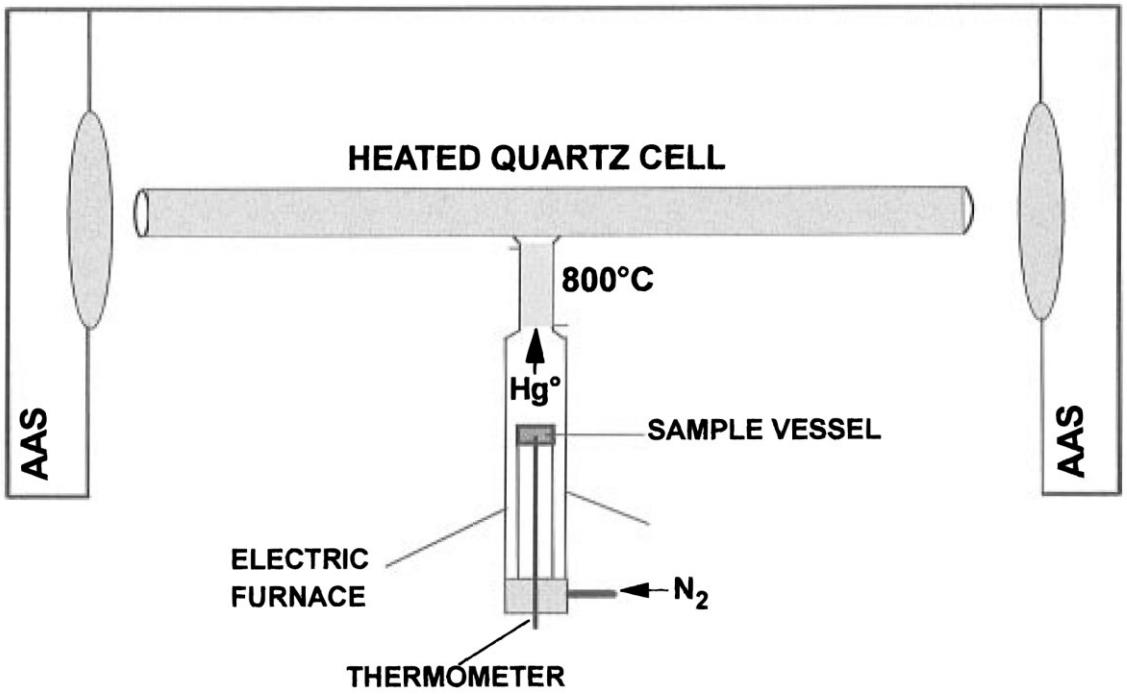

Figure 3. Schematic diagram of the Hg thermodesorption apparatus used in this thesis for Hg species measurements in solids, consisting of a pyrolysis unit coupled to an atomic absorption spectrometer (Figure taken from Biester and Scholz, 1996).

liberated from the sample first and with increasing temperature also oxidized Hg gets thermally reduced to Hg^0 and is released. Strength of Hg binding defines here, when Hg^0 is formed and gets liberated. Hg^0 is subsequently transported to a heated quartz cell (carrier gas: N_2 at 300 mL min^{-1} flow), where it gets detected by AAS. Resulting thermo-desorption spectra can be used to determine Hg speciation in solids by comparing obtained spectra from a sample with those of Hg standard materials (Figure 4).

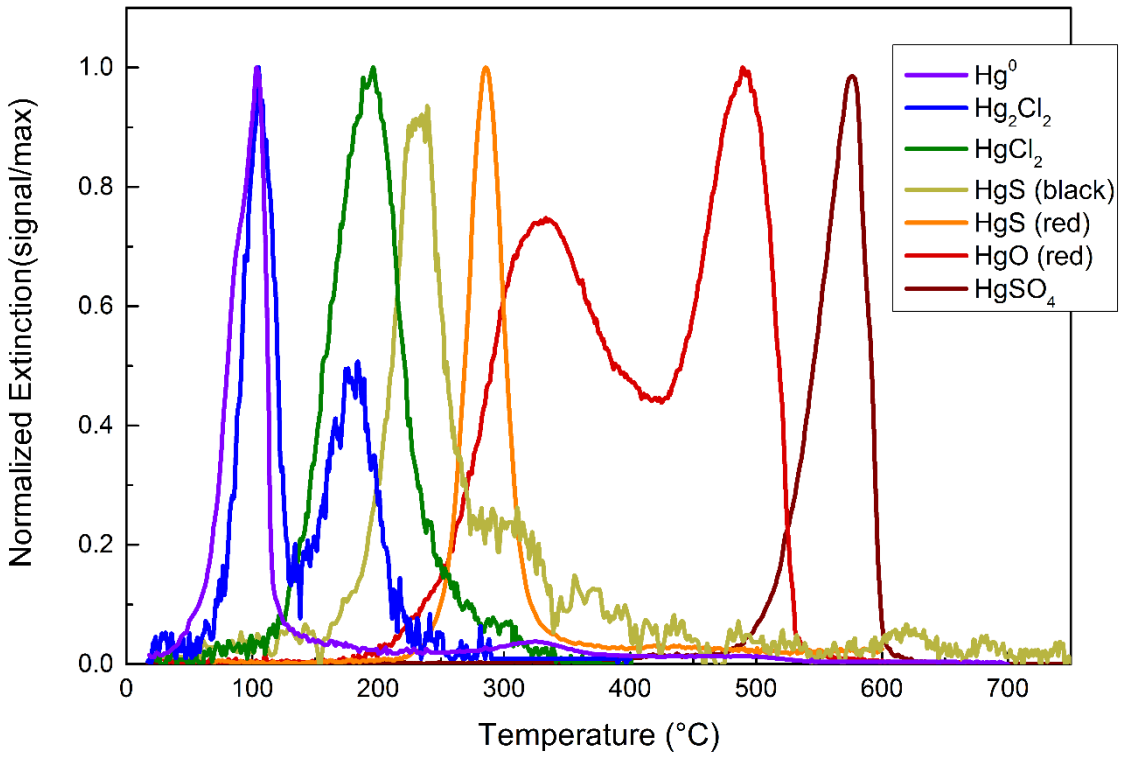

Figure 4. Thermodesorption curves of Hg standard materials.

Advantages of the method are the simple setup, comparatively short measuring times, and a low detection limit of less than 0.5 mg kg^{-1}. Since the 1990s Hg-thermodesorption was adopted by other research groups (e.g. do Valle et al., 2005; Coufalík et al., 2014; Reis et al., 2015; Rumayor et al., 2015) and became a widely accepted and often applied Hg speciation technique in the mercury community (Horvat, 2013). Application of thermo-desorption to determine Hg species in ores, (Biester et al., 1999), soils (Higueras et al., 2003), stream and lake sediments (Biester et al., 1999; Bouffard and Amyot, 2009), attic dust (Gosar et al., 2006), coal, and fly ashes (Rumayor et al., 2015), and peat

(Coufalík et al., 2014) demonstrate the versatility and widespread scope of application of this technique. Thus, thermodesorption was used in the present work for determination of Hg species in solids.

3.2 Mercury species measurement in solutions

Some Hg species in aqueous solution can be measured directly. For example, dissolved Hg^0 can be purged from solution (Brosset, 1987) and measured by cold vapor atomic absorption/fluorescence spectrometry (CV-AAS or CV-AFS, respectively), either directly or after preconcentration on a gold trap. CH_3Hg^+ can be determined using either gas chromatography (GC; Hippler et al., 2009) or high pressure liquid chromatography (HPLC; Brombach et al., 2014) for trace-matrix separation. CH_3Hg^+ is then determined by subsequent detection using inductively coupled plasma mass spectrometry (ICP-MS; Chen et al., 2005) or CV-AFS (Brombach et al., 2014). Free Hg^{2+} ions can also be measured directly in solution using an ion selective electrode (ISE) (Jumal et al., 2012), at least in lab experiments with Hg enriched solutions (detection limit: 120 µg L^{-1}; Juarez-Gomez et al., 2013). Aqueous Hg complexes, however, can only be determined indirectly (Powell et al., 2005) in high purity binary systems of Hg with the respective ligand by e.g. potentiometric (Oram et al., 1996) or spectrophotometric (Bahram et al., 2011) titration and cannot be measured in natural samples. Yet, methods exist to determine operationally defined Hg species groups, differing in chemical or physical properties (Leopold et al., 2010). Iverfeldt and Lindqvist (1982, 1986) developed a method to distinguish between inorganic and organic Hg^{2+} on the basis of reducibility by stannous chloride ($SnCl_2$). Inorganic species that can be reduced by $SnCl_2$ (all inorganic Hg^{2+} complexes except Hg (poly)sulfides), were named “reactive” Hg. Hg binding in “non-reactive” Hg species (DOM complexes, CH_3Hg^+, dissolved Hg (poly)sulfides) is too strong for Hg^{2+} to get reduced by $SnCl_2$. Hence, these Hg species can only be determined after cracking the bonds between Hg and the respective ligand by digestion with a strong oxidizing agent (e.g. BrCl; USEPA, 2002). The method was further developed and combined with Hg^0-stripping by Brosset (1987) and Meili et al. (1991), renaming “reactive” and “non-reactive” species groups to Hg^{II}_a and Hg^{II}_b. Based on their work, speciation analysis of

aqueous Hg in the present thesis was done following an analytical protocol published in Bollen et al. (2008).

4 Hydrogeochemical modeling

4.1 Reasons for modeling and theoretic background

Hg speciation measurements in aqueous solutions are challenging and often impossible at environmental concentration levels (Skyllberg, 2010). Therefore, hydrogeochemical modeling can be a valuable tool to calculate species distributions (Nordstrom et al., 1979). Building up on speciation, processes like species transformation, dissolution and precipitation (Delany, 1986), sorption (Gaines and Thomas, 1953), surface complexation (Dzombak and Morel, 1990), and kinetically controlled reactions (Plummer et al., 1978) can be predicted and even reactive transport (Yeh and Tripathi, 1989) can subsequently be modeled. First, formation constants of aqueous complexes have to be determined in lab experiments in high purity binary systems of in our case Hg and the respective ligand. Based on the mass action law, these constants can then be applied to calculate the concentration (more precisely: thermodynamic activity) of a single complex in solution from the concentrations (activities) of Hg and the ligand at thermodynamic equilibrium. A simple example is given by equations 1 and 2.

$$Hg^{2+} + 2\,Cl^{-} \rightarrow HgCl^{0}_{2\,(aq)} \tag{1}$$

$$K = \frac{\{HgCl^{0}_{2\,(aq)}\}}{\{Hg^{2+}\}\{Cl^{-}\}^{2}} \tag{2}$$

with:

K = complex formation constant

{x} = activity of component x

Similar equations can be set up for dissolution/precipitation, sorption, and redox reactions. Equilibrium constants have been determined for reactions of numerous complexes/minerals of all relevant ions usually dominating solution

chemistry (major elements, e.g. Na, Ca, Mg,…) and also of many trace elements, including Hg (Powell et al., 2005). When elemental concentrations and other key parameters (pH, Eh, temperature) were measured, the hydrochemical composition of a water sample in terms of elemental speciation can then be calculated at thermodynamic equilibrium by solving a system of linear equations. At the outset of geochemical modeling, all calculations had to be performed by hand (Garrels and Mackenzie, 1967) but nowadays several computer programs exist, that can solve such linear or non-linear equation systems with hundreds of parameters within seconds. Among the software programs most frequently used for geochemical modeling are PHREEQC (Parkhurst and Apello, 2013), Geochemist´s Workbench® (Bethke and Yeakel, 2016), WHAM (Tipping et al., 2011), and Visual MINTEQ (Gustafsson, 2013).

4.2 Modeling mercury hydrogeochemistry

Geochemical modeling has been used for prediction of Hg speciation in many different environmental compartments such as stream water (Barringer et al., 2010; Muresan et al., 2011), lakes (Wollenberg and Peters, 2009; Chiasson-Gould et al., 2014), wetlands (Reddy and Aiken, 2001), and soil solutions (Tipping et al., 2010). Based on speciation also more refined models were set up. Gemici et al. (2009) applied PHREEQC to calculate saturation indices of Hg minerals in mine water. Lin et al. (2011) used Hg complexation to DOM as predicted by geochemical modeling (Visual MINTEQ with DOM submodel “Stockholm Humic Model”) to explain the correlation of dissolved Hg and DOC in contaminated stream water. The adsorption behavior of Hg and other trace elements was studied in situ in forming lake sediments and compared to results of geochemical modeling, both indicating Hg being bound mainly to organic matter (Feyte et al., 2010). Besides processes at equilibrium, also time dependent, kinetic reactions of Hg were modeled. Rate constants of kinetic Hg release by pH change triggered desorption and mineral dissolution in aquifers (e.g. through CO_2 intrusion) were published by Bearup et al. (2012). These constants provide constraints on relevant processes for setting up reactive transport models. Such a model with equilibrium and kinetic biogeochemical reactions implemented was presented by Bessinger et al. (2012), where they simulated 1-D reactive Hg and arsenic (As) transport from contaminated

sediments through a subaqueous sediment cap. Also by combining geo- and biochemical reactive transport modeling, Johannesson and Neumann (2013) were able to explain changes in Hg concentration along a flowpath in a deep confined aquifer. Their model suggested release of sorbed Hg by microbially mediated iron (Fe) reduction and subsequent Fe mineral dissolution as cause for increasing Hg. Following decrease of Hg was ascribed to biotic sulfate reduction causing coprecipitation of Hg on FeS and precipitation of Hg as ß-HgS (metacinnabar). Finally, Leterme et al. (2014) published a three phase kinetic reactive transport model simulating Hg fate in soil by coupling an unsaturated flow model (Hydrus-1D; Šimůnek et al., 2008) with Hg speciation,

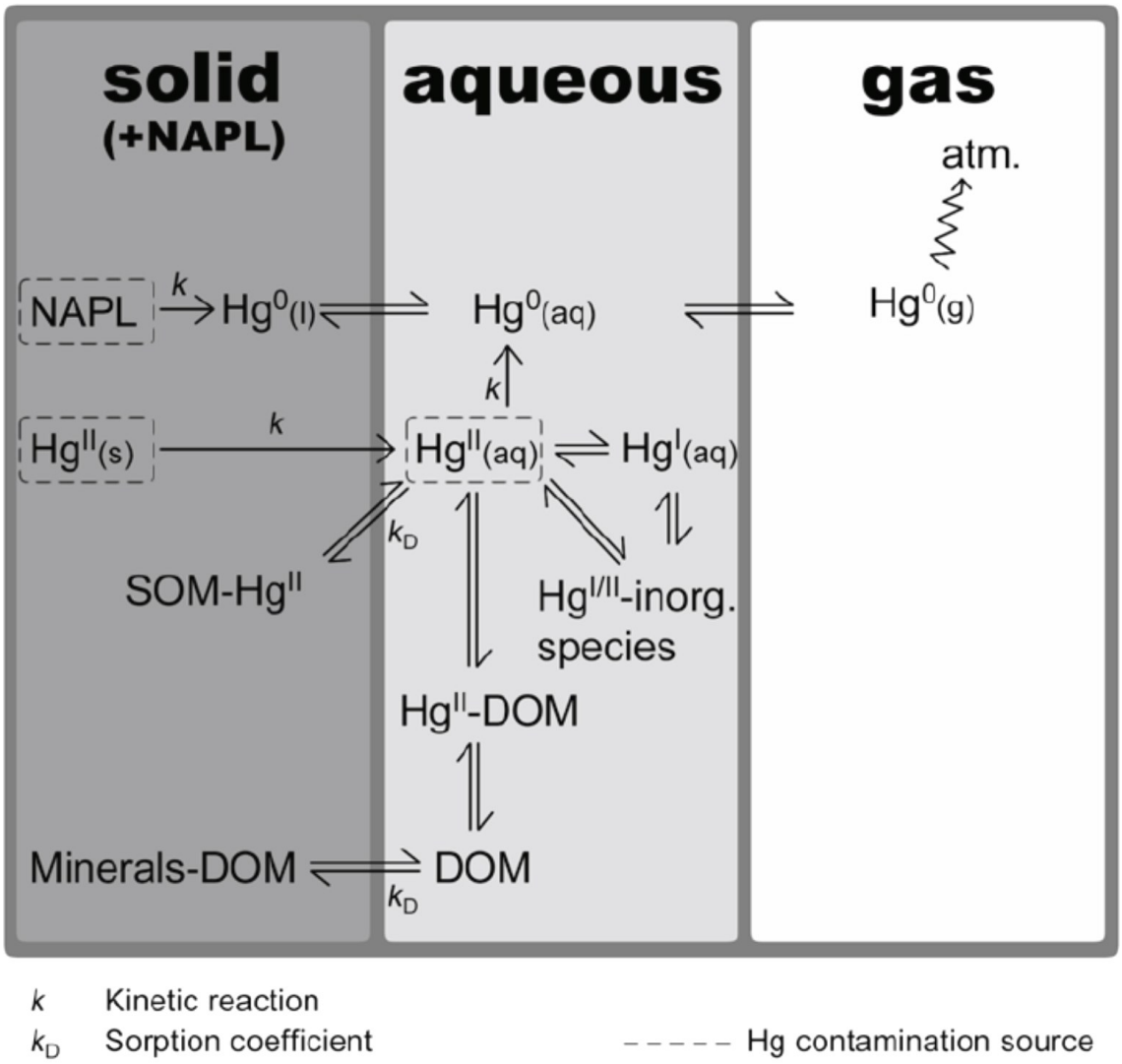

Figure 5. Conceptual model of Hg speciation and reactions in the solid, aqueous, and gas phase of a soil, as implemented in the reactive transport model by Leterme et al. (2014).

sorption, precipitation (PHREEQC), and volatilization in an integrating software (HP1; Jacques and Šimůnek, 2010). The concept of their model is depicted in Figure 5. Sensitivity analysis (Leterme and Jacques, 2015) indicated that the constants describing Hg binding to soil organic matter, the assumed DOM concentration, and the DOM thiol binding constant were the critical parameters of their model. This illustrates the general importance of organic matter for Hg geochemical modeling (constants describing Hg-DOM binding are the highest constants in Hg hydrogeochemistry) and explains the need for accurate Hg-DOM binding constants. In fact, formation constants for Hg-DOM complexes were highly controversial in the past until Skyllberg (2008) presented a now widely accepted log K of 22 ± 2 (M^{-1}) for the formation of Hg complexes with thiols, the most Hg affine binding group in DOM (equation 3 with RSH being a DOM thiol group and $Hg(RS)_2^0$ a two-coordinated Hg complex with DOM-thiols).

$$2\,RSH + Hg^{2+} = Hg(RS)_2^0 + 2\,H^+ \quad (3)$$

This log K value is now frequently applied for prediction of Hg DOM complexation in geochemical modeling (Johannesson and Neumann, 2013; Leterme et al., 2014) assuming that thiols are totally dominating Hg binding to DOM as shown for soil organic matter (Xia et al., 1999) and that thiols correspond to a defined proportion of DOC (0.15 wt.% according to Skyllberg, 2008). However, since speciation calculations build the basis of even the most sophisticated geochemical modeling approaches, there is an urgent need to evaluate[1] modeled speciation results. For doing so no better way exists than comparing them with analytical results (Nordstrom and Campbell, 2014) but for Hg speciation this has never been done with natural samples.

5 Mercury contaminated sites

Because Hg was used for many different purposes throughout the centuries, it still can be found at many former industrial production sites. Hg was set to rank

[1] the verb “evaluate“ is used intentionally here, because it was argued against the frequently used term “validate” (c.f. Nordstrom, 2012). “Validation” implies the absoluteness of right and wrong and should therefore better be avoided in natural science.

3 on the US-EPA and ATSDR 2015 priority list of hazardous substances (ATSDR, 2015), because of its high toxicity and its frequent occurrence on the 799 most contaminated sites in the USA (Superfund sites). Hg was reported to be a contaminant of concern at 290 of these sites, with 144 showing Hg groundwater contamination (US EPA, 2007). From the Hg contaminated sites 102 were landfills and 15 chemical production sites. On 14 sites a distinct groundwater plume was encountered. Other reported sites include wood impregnation (Schöndorf et al., 1999), mirror and thermometer production (City of Fuerth, 2005; Rajgopal et al., 2006), metal processing, military, transportation, mining (US EPA, 2007), and hat industry sites (Lerman-Sinkoff, 2014).

5.1 Mercury in groundwater

Natural background Hg concentrations in groundwater are usually at the low ng L^{-1} level (Cizdziel, 2004). Even on contaminated sites low solubility of elemental Hg (~60 µg L^{-1}, Merck, 2014) and Hg^{2+} adsorption to Fe-(hydr)oxides (Anderson, 1979), clay, manganese oxides (Farrell et al., 1998), and in particular soil organic matter (Skyllberg et al., 2006) often prevent or retard Hg intrusion into the aquifer (Barringer et al., 2013a). When groundwater is affected, reported maximum concentrations range from 0.16 µg L^{-1} down-gradient a site of former wastewater infiltration beds (Lamborg et al., 2013) to 23 mg L^{-1} at the location of a former chlor alkali plant (Orica, 2016). Hg transport in groundwater is controlled less by the physical properties of an aquifer (porous or fissured, hydraulic conductivity, flow velocity) than by its organic matter content, its mineral inventory, and the prevailing geochemical conditions (Figure 6). Bollen et al. (2008) described strong retardation of Hg in a highly permeable aquifer with effective groundwater velocities of up to 10 m d^{-1} due to sorption processes and Hg^0 formation/precipitation in the aquifer (one of the sites investigated in the present work). On the other hand, Johannesson and Neumann (2013) proposed on the basis of geochemical modeling, that mobilization of sorbed natural Hg through reductive dissolution of Fe^{3+}-(hydr)oxides was the driving factor behind rising Hg concentrations along a flow

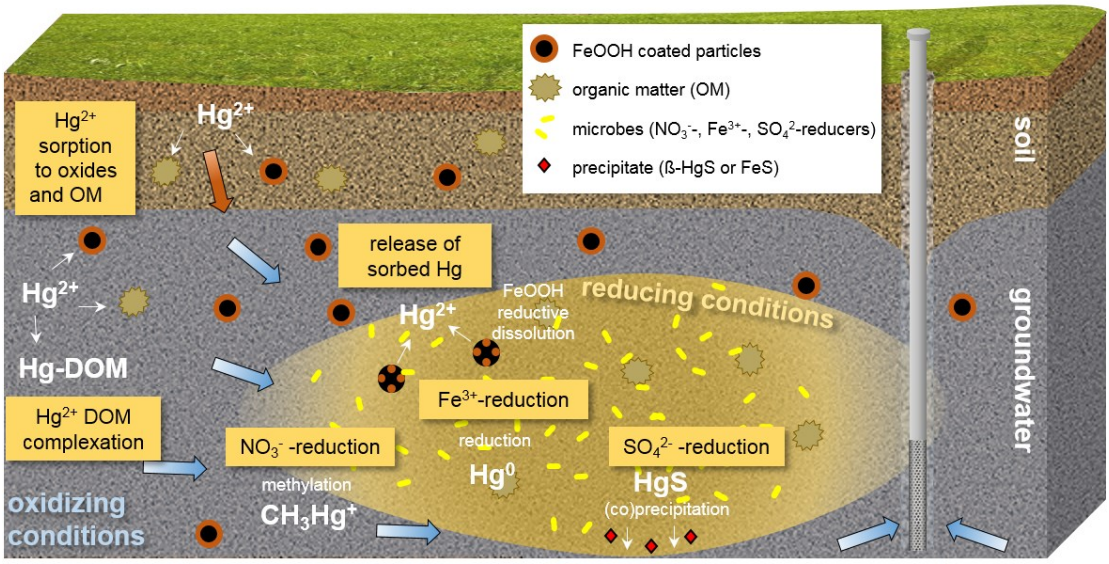

Figure 6. Relevant processes for mercury mobility in groundwater (based on Barringer et al., 2013a and Lamborg et al., 2013).

path within a deep, confined aquifer. Barringer and Szabo (2006) also found elevated Hg in groundwater being associated with reducing conditions in the aquifer. Lamborg et al. (2013) concluded that such reductive Hg mobilization resulted in increased CH_3Hg^+ production in the nitrate reducing zone of an oxygen depleted aquifer and the formation of Hg^0 when iron reduction was evident. At strongly reducing conditions, however, Hg concentrations tend to decrease when reduced sulfur (H_2S) is produced from sulfate reduction as Hg is sorbed to or coprecipitated with pyrite (FeS; Behra et al., 2001) or highly insoluble metacinnabar (β-HgS) gets precipitated (Bessinger et al., 2012). However, some Hg can still remain in solution when polysulfide complexes (Jay et al., 2000) or nanocolloidal ß-HgS (Gerbig et al., 2011) are formed. Also transport of Hg sorbed to particles/colloids of clay (Ryan and Gschwend, 1994), Fe-(hydr)oxide (Ryan and Gschwend, 1990), organic matter (Zhu et al., 2014), or organo-oxide agglomerates (Chadwick et al., 2006) may occur in some aquifers (Barringer et al., 2006). Particulate Hg transport can be of special importance when water levels of reducing groundwater are fluctuating (Ryan and Gschwend, 1994) or when groundwater is pumped with varying pumping rates (Szabo et al., 2010).

Hg contamination of aquifers is of greatest concern when groundwater is used for drinking water supply. For example, in the coastal plain of New Jersey, USA, more than 600 domestic (Sites and Oberholtzer, 1992; Barringer and Szabo, 2006) and also some public-supply wells (Fischer et al., 2010) showed Hg concentrations above the legal limit (2µg L^{-1}). No possible Hg point sources could be identified and origin of Hg could not be determined. Past agricultural use of mercurial pesticides was assumed to be the main Hg source besides atmospheric deposition, since background Hg concentrations of groundwater in neighboring forested areas was below 10 ng L^{-1}(Barringer et al., 2013a). Koterba et al. (2006) reported similar findings for a surficial aquifer in Delaware (USA), where elevated Hg concentrations were detected in some of the production wells of the local water company.

Besides the threat Hg constitutes in aquifers, exfiltration of Hg contaminated groundwater to surface water can also occur, endangering aquatic life and posing risk also to humans via bioaccumulation and possible uptake through fish consumption. Hissler and Probst (2006) described the interactions between groundwater and river Thur (France) in an area heavily polluted with Hg by emissions from a chlor-alkali plant. Bradley et al. (2012) demonstrated that the primary source of Hg in a coastal plain stream reach was groundwater discharge. Barringer et al. (2013b) found indications that Hg flux from groundwater substantially contributed to the total Hg inventory of a major river, containing fish with highest Hg tissue concentrations in the state of New Jersey (USA).

5.2 Remediation of mercury contaminated sites

When Hg contaminated sites have to be remediated the appropriate technique depends on the Hg species present on the site and their respective concentrations, their spatial and vertical distribution, and general characteristics of the site. When only building structures or soil are affected, the task of remediation is mainly the removal of contaminated material without further pollution of the surroundings (Meschede and Vogelsberger, 1999; Terra, 2010). After the contaminated material has been removed, it has to be disposed in a suitable landfill (often after immobilization treatment with e.g. elemental sulfur;

Phipps et al., 2014) or Hg has to be separated from soil/construction debris. Hg containing soils from two former CAPs in the Netherlands (Pensaert and Gerbrands, 2012) and Australia (Golder, 2012) were excavated and treated by soil washing to remove soluble Hg compounds and/or wet classification to withdraw higher contaminated fine grained soil fractions. However, at both sites Hg concentrations of treated soil did not meet the remediation target values (CMJA, 2012; Phipps et al., 2014). Thermal treatment of soils (NIMD, 2014), as applied at a former pulp and tissue mill with included CAP in Washington (State) (USA), appears to be more effective and Hg concentrations in treated soils were below target values (Phipps et al., 2014). A combined method of soil washing with subsequent vacuum distillation was successfully applied at a former chemical manufacturing site in Marktredwitz (Hempel and Thoeming, 1999). In situ techniques for soil remediation like vitrification and in situ thermodesorption were employed on some sites with varying degrees of success (US EPA, 2007). In situ immobilization by polysulfides (Biester and Zimmer, 1998) or in situ extraction by L-Cysteine (Bollen and Biester, 2011) were also proposed as possible remediation approaches. However, for choosing the right remediation strategy one has always to consider that Hg, besides being poisonous, is also redox sensitive and species transformations may occur before or during remediation. Hence, the initial species of contamination may (have) turn(ed) into other potentially more soluble or volatile Hg forms.

Once Hg contaminated the aquifer and groundwater has to be treated, different remediation techniques may be applied. The right remediation strategy depends on the Hg concentration range, the volume of water to be treated, estimated remediation times, and hydrogeological setup (groundwater flow velocity, hydraulic conductivity, groundwater hydrochemistry,…). Most often groundwater is cleaned in an onsite treatment plant (Merly and Hube, 2014), a so called pump & treat (P&T) unit. Here Hg is removed from solution either by complexation on sulfonated flocculants with subsequent flocculation and filtration (Pensaert and Gerbrands, 2012), by reduction of inorganic Hg through addition of $SnCl_2$ and subsequent air stripping (US EPA, 2007), or by filtration through bed filters (Merly and Hube, 2014). Frequently used filter materials for Hg removal from aqueous solution are sulfurized granular activated carbons

(Asasian and Kaghazchi, 2015), Hg specific adsorption resins with thiol-functional groups (Monier et al., 2015), and zeolites (Murthy et al., 2013). While activated carbon and zeolites are comparatively cheap, they suffer from low loading capacities. In contrast, Hg specific adsorption resins show higher loading capacities but are about ten times more expensive (Schöndorf, 2011). (Bio)fouling of activated carbon (Newcombe et al., 1997) or adsorption resins (Beril Gönder et al., 2006) can also be an issue, so selecting the right filter material can be a difficult task.

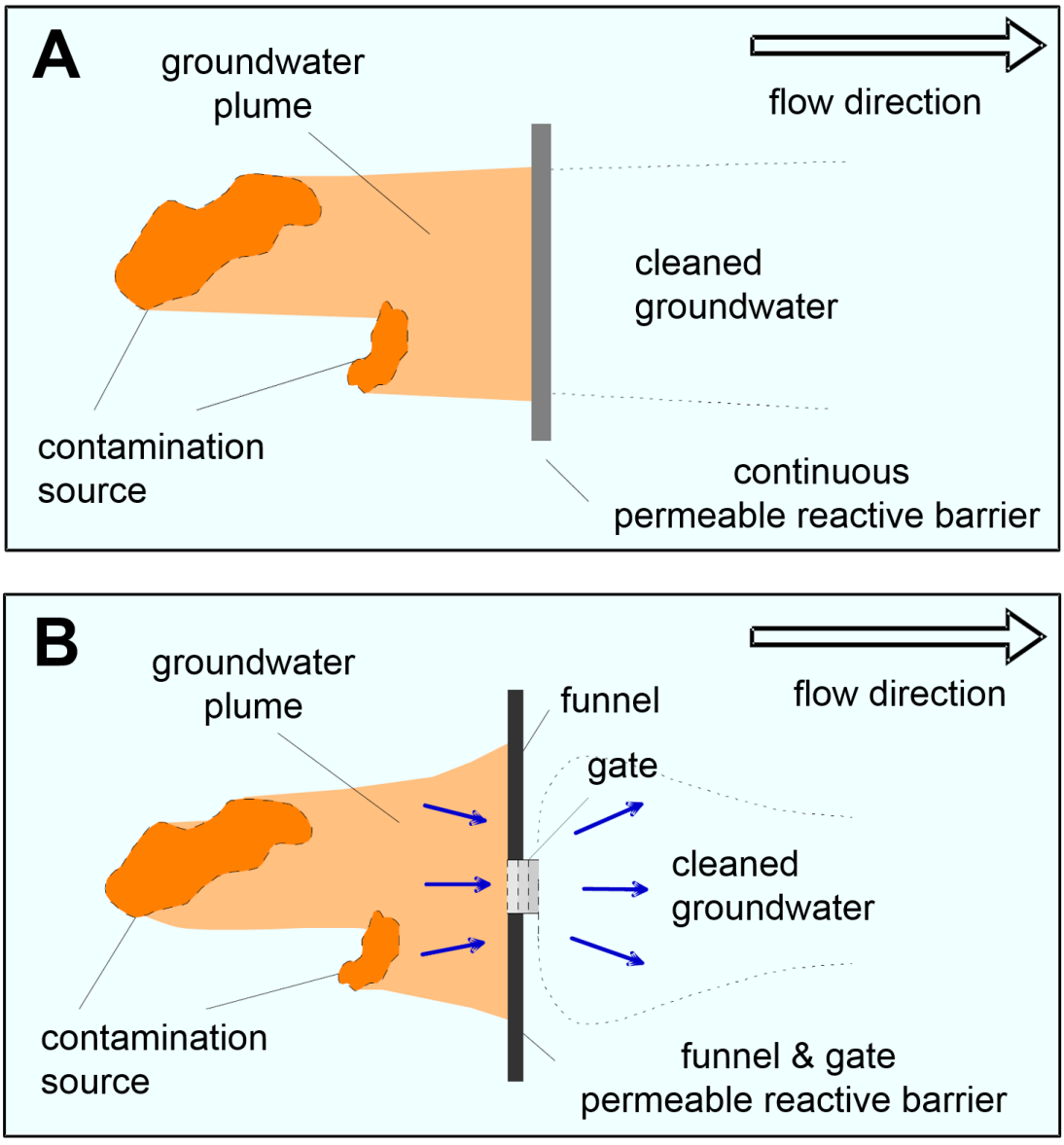

Figure 7. Fundamental functionality of permeable reactive barriers (PRBs), altered after Birke et al., 2006. (A) Continuous PRB. (B) Funnel & gate PRB.

When predicted remediation times are long, application of in situ technologies namely permeable reactive barriers (PRBs, Figure 7) may be reasonable (Birke,

2004) due to lower operating costs compared to P&T units. Here the contaminant plume is treated in situ without the need for pumping just by flowing through a proper reactive (filter) material. Two main configurations of PRBs exist, continuous PRBs and funnel & gate PRBs. In continuous PRBs the reactive material is evenly distributed over the whole width of the barrier. In contrast, funnel & gate systems consist of two or more impermeable structures, forming the so called “funnel”, that guide the groundwater flow through a permeable “gate” filled with the reactive material. The choice between the two PRB types depends on the hydrogeological characteristics of the site, the costs of the reactive material, and how often it needs to be replaced (Birke et al., 2006; Thiruvenkatachari et al., 2008). Hydraulic conductivity (*K*) of a PRB always has to exceed that of the treated aquifer to avoid lateral or vertical bypass. This is of special importance in funnel & gate systems. Here water from a wide flow cross section is merged and channeled through a gate with much smaller flow area, resulting in an increased flow velocity. Hence, fast reaction kinetics and high hydraulic conductivities are key factors for choosing the right reactive material for (funnel & gate) PRBs.

For Hg treatment two full scale PRBs are reported in the literature, both situated at the site of former CAPs. Both were designed as funnel & gate systems and were reported to work without major problems since they were put into operation (Merly and Hube, 2014). One was completed in 2001 in Hallein (Austria), has a total length of 245 m, a barrier depth of up to 24 m and *K* of the aquifer is ~2 x 10^{-3} m s^{-1} (Merly and Hube, 2014; Phipps et al., 2014). The treated water volume is about 25 m^3 h^{-1} but maximum Hg concentrations (~10 µg L^{-1}) are relatively low. Nevertheless, the filter material already had to be exchanged and disposed when the sorption capacity was reached (Merly and Hube, 2014). The other PRB was built in 2005 at a petrochemical complex in Camaçari (Brazil) and treats water with relatively high Hg concentrations (up to 360 µg L^{-1}; Nobre et al., 2012). No information about treated water volume per time unit is given but reported hydraulic conductivity (*K*) of the aquifer (<5 x 10^{-6} m s^{-1}) suggests that the treated amount of water must be low. In both PRBs granular activated carbon/gravel mixtures were used as gate fillings.

Hence, activated carbon (AC) appears to be a proper filter material for PRBs when either Hg concentration or flow of treated water is low. AC is, however, no reasonable choice when both, Hg and flow, are high due to its low loading capacity (Schöndorf, 2011). Hg specific exchange resins might be suitable for PRBs under such conditions and the use of resins in PRBs was frequently proposed for other contaminants (e.g. Watson et al., 2002; Barton et al., 2004). However, use of exchange resins has not been reported to be brought into practice (Obiri-Nyarko et al., 2014), most likely because of high costs (Schöndorf, 2011), the risk of (bio)fouling (Beril Gönder et al., 2006), or possible floating due to low densities of the resins (<0.8 g cm^{-3}). Thus, there is a lack of an appropriate Hg filter material for the long-term use in PRBs that is cost-effective, shows high reaction kinetics and a high hydraulic conductivity, and does not have the tendency for (bio)fouling. Amalgamating materials were proposed as proper filter materials here (Biester et al., 2000; Huttenloch et al., 2003) and brass shavings were shown to meet all specified prerequisites under lab conditions (Wenke et al., 2016). However, they have never been tested with real groundwater in long-term tests under realistic conditions.

6 Research motivation and objectives

6.1 Research needs

With regard to the state of knowledge presented above, several key issues arose in the field of Hg contaminated groundwater that demanded further research. They form the focus of the present thesis and are as follows:

It is well known that Hg^{2+} can be reduced to Hg^0 in the environment, posing the risk of volatilization and Hg long range transport. Indications exist, that kinetically fast inorganic reduction by Fe^{2+} might play an important role for Hg^0 formation in anoxic groundwater. When dissolved Fe^{2+} is oxidized and precipitates, hydrous ferric oxides (HFOs) are formed but the role of such abundant and highly reactive Fe-hydroxides for Hg^{2+} reduction and Hg mobility in groundwater has not yet been studied.

Hg speciation is important for risk assessment and prediction of Hg mobility. Measuring Hg species in aqueous solutions is problematic and often impossible

at environmental concentration levels. Hence, hydrogeochemical modeling can be a valuable tool to calculate speciation and, building up on that, construct more complex models up to the simulation of Hg reactive transport. Nevertheless, even the most sophisticated model is based on speciation calculations which, in case of Hg, have never been evaluated by comparison with analytical results from natural samples.

When predicted remediation times for Hg contaminated aquifers are long the installation of permeable reactive barriers (PRBs) is advantageous. On some Hg contaminated sites PRBs have been installed and work without major problems. However, for sites with high Hg concentrations and fast flowing groundwater no appropriate reactive material for the use as PRB filling exists. Here brass shavings were proposed as an alternative to conventional materials but their performance has not yet been tested in long-term operation under realistic conditions with real groundwater.

6.2 Objectives of the thesis

Based on the specified key issues, the three main objectives of the present thesis were to

1) **study the role of freshly precipitated Fe-hydroxides for Hg species transformation and Hg mobility**

   Hydrous ferric oxides (HFOs) were obtained from inside a remediation plant that treats Hg contaminated groundwater. Behind a mixing chamber where oxic and anoxic well waters mix, filters were installed, were removed after 200 days, and retained HFOs were collected. Additionally, water from 1 temporarily anoxic and 4 oxic wells was sampled and freshly precipitated HFOs were extracted. Hg concentrations and speciation were measured in obtained HFOs and groundwater and compared with results from a geochemical model in which well water mixing, HFO precipitation, and Hg speciation was simulated.

2) **evaluate Hg speciation models**

   This objective was addressed by measuring hydrochemistry and Hg species (Hg^0, inorganic, and dissolved organic matter (DOM) bound

Hg^{2+}) in groundwater from three different Hg contaminated sites. Determined Hg speciation was compared with Hg species predictions from geochemical modeling based on measured hydrochemistry and total Hg concentrations. As DOM is an important complexing ligand for Hg, its role for modeling accuracy was investigated in different modeling scenarios. Here, assumed DOM quality and form of implementation in the models was varied.

3) **examine the long-term performance of brass shavings as Hg filter material for permeable reactive barriers (PRBs)**

After a pretest, evaluating two different brass shaving types in bypass to an existing pump & treat remediation plant, a pilot plant was built at a Hg contaminated site where the installation of a PRB is under consideration. Large scale test columns (~30 cm diameter) were filled with brass shavings and brass/gravel mixtures and fed with Hg contaminated groundwater for 2.5 years. Water from filter effluences and from inside the filter beds was periodically analyzed for Hg and other hydrochemical parameters. Hydraulic conductivity was monitored during the whole testing period. Influence of pH on Zn release and Hg removal was studied by raising pH, using three different techniques (calcite, NaOH, Magno-Dol). After decommissioning of the filter, brass shavings were analyzed for Hg content, chemical change, and surface alteration.

References

Ahrland, S., Chatt, J., Davies, N.R., 1958. The relative affinities of ligand atoms for acceptor molecules and ions. Q. Rev. Chem. Soc. 12, 265–276. doi:10.1039/QR9581200265

Allard, B., Arsenie, I., 1991. Abiotic reduction of mercury by humic substances in aquatic system — an important process for the mercury cycle. Water. Air. Soil Pollut. 56, 457–464. doi:10.1007/BF00342291

Amirbahman, A., Kent, D.B., Curtis, G.P., Marvin-DiPasquale, M.C., 2013. Kinetics of Homogeneous and Surface-Catalyzed Mercury(II) Reduction by Iron(II). Environ. Sci. Technol. 47, 7204–7213. doi:10.1021/es401459p

Amyot, M., Gill, G.A., Morel, F.M.M., 1997. Production and Loss of Dissolved Gaseous Mercury in Coastal Seawater. Environ. Sci. Technol. 31, 3606–3611. doi:10.1021/es9703685

Anderson, A., 1979. Mercury in soils, in: Nriagu, J.O. (Ed.), The Biogeochemistry of Mercury in the Environment. Elsevier/North-Holland Biomedical Press, pp. 79–122.

Anthony, J.W., Bideaux, R.A., Bladh, K.W., Nichols, M.C. (Eds.), 2003. Handbook of Mineralogy, Mineralogical Society of America.

Asasian, N., Kaghazchi, T., 2015. Sulfurized activated carbons and their mercury adsorption/desorption behavior in aqueous phase. Int. J. Environ. Sci. Technol. 12, 2511–2522. doi:10.1007/s13762-015-0818-x

ATSDR, 2015. Agency for Toxic Substances & Disease Registry - Priority List of Hazardous Substances.

Bahram, M., Pesyan, N.N., Naseri, A., Tasbihforosh, M., 2011. Determination of stability constants of 5-(2-hydroxybenzylidene)-2-thioxodihydropyrimidine-4, 6 (1H, 5H)-dione with copper (II) and mercury (II) ions. Turk J Chem 35, 255–264.

Barkay, T., Miller, S.M., Summers, A.O., 2003. Bacterial mercury resistance from atoms to ecosystems. FEMS Microbiol. Rev. 27, 355–384. doi:10.1016/S0168-6445(03)00046-9

Barringer, J.L., Riskin, M.L., Szabo, Z., Reilly, P.A., Rosman, R., Bonin, J.L., Fischer, J.M., Heckathorn, H.A., 2010. Mercury and Methylmercury Dynamics in a Coastal Plain Watershed, New Jersey, USA. Water. Air. Soil Pollut. 212, 251–273. doi:10.1007/s11270-010-0340-1

Barringer, J.L., Szabo, Z., 2006. Overview of investigations into mercury in ground water, soils, and septage, new jersey coastal plain. Water. Air. Soil Pollut. 175, 193–221. doi:10.1007/s11270-006-9130-1

Barringer, J.L., Szabo, Z., Reilly, P.A., 2013a. Occurrence and Mobility of Mercury in Groundwater, in: Bradley, P. (Ed.), Current Perspectives in Contaminant Hydrology and Water Resources Sustainability. InTech.

Barringer, J.L., Szabo, Z., Reilly, P.A., Riskin, M.L., 2013b. Variable Contributions of Mercury from Groundwater to a First-Order Urban Coastal Plain Stream in New Jersey, USA. Water. Air. Soil Pollut. 224, 1–25. doi:10.1007/s11270-013-1475-7

Barringer, J.L., Szabo, Z., Schneider, D., Atkinson, W.D., Gallagher, R.A., 2006. Mercury in ground water, septage, leach-field effluent, and soils in residential areas, New Jersey coastal plain. Sci. Total Environ. 361, 144–162. doi:10.1016/j.scitotenv.2005.05.037

Barton, C.S., Stewart, D.I., Morris, K., Bryant, D.E., 2004. Performance of three resin-based materials for treating uranium-contaminated groundwater within a PRB. J. Hazard. Mater. 116, 191–204. doi:10.1016/j.jhazmat.2004.08.028

Bearup, L.A., Navarre-Sitchler, A.K., Maxwell, R.M., McCray, J.E., 2012. Kinetic Metal Release from Competing Processes in Aquifers. Environ. Sci. Technol. 46, 6539–6547. doi:10.1021/es203586y

Behra, P., Bonnissel-Gissinger, P., Alnot, M., Revel, R., Ehrhardt, J.J., 2001. XPS and XAS Study of the Sorption of Hg(II) onto Pyrite. Langmuir 17, 3970–3979. doi:10.1021/la0014510

Beril Gönder, Z., Kaya, Y., Vergili, I., Barlas, H., 2006. Capacity loss in an organically fouled anion exchanger. Desalination, Selected paper from the 10th Aachen Membrane Colloquium 10th Aachen Membrane Colloquium 189, 303–307. doi:10.1016/j.desal.2005.07.012

Bessinger, B.A., Vlassopoulos, D., Serrano, S., O'Day, P.A., 2012. Reactive Transport Modeling of Subaqueous Sediment Caps and Implications for the Long-Term Fate of Arsenic, Mercury, and Methylmercury. Aquat. Geochem. 18, 297–326. doi:10.1007/s10498-012-9165-4

Bethke, C.M., Yeakel, S., 2016. The Geochemist´s Workbench GWB Essentials Guide. Aqueous Solutions, LLC.

Biester, H., 1994. Möglichkeiten der Anwendung eines temperaturgesteuerten Pyrolyseverfahrens zur Bestimmung der Bindungsform des Quecksilbers in Böden und Sedimenten, Heidelberger geowissenschaftliche Abhandlungen / Geologisch-Paläontologisches Institut; Institut für Sedimentforschung; Laboratorium für Geochronologie; Mineralogisch-Petrographisches Institut der Universität Heidelberg, ISSN 1430-8665 ; ZDB-ID: 1549881. Inst. für Sedimentforschung, Heidelberg.

Biester, H., Gosar, M., Müller, G., 1999. Mercury speciation in tailings of the Idrija mercury mine. J. Geochem. Explor. 65, 195–204. doi:10.1016/S0375-6742(99)00027-8

Biester, H., Scholz, C., 1996. Determination of mercury binding forms in contaminated soils: Mercury pyrolysis versus sequential extractions. Environ. Sci. Technol. 31, 233–239.

Biester, H., Schuhmacher, P., Müller, G., 2000. Effectiveness of mossy tin filters to remove mercury from aqueous solution by Hg(II) reduction and Hg(0) amalgamation. Water Res. 34, 2031–2036. doi:10.1016/S0043-1354(99)00379-6

Biester, H., Zimmer, H., 1998. Solubility and changes of mercury binding forms in contaminated soils after immobilization treatment. Environ. Sci. Technol. 32, 2755–2762.

Birke, V. (Ed.), 2004. Permeable reactive barriers (prbs) in europe: Potentials and expectations. Battelle Press, Columbus, OH.

Birke, V., Ebert, M., Finkel, M., Rosenau, D., 2006. Anwendung von durchströmten Reinigungswänden zur Sanierung von Altlasten.

Bloom, N.S., Preus, E., Katon, J., Hiltner, M., 2003. Selective extractions to assess the biogeochemically relevant fractionation of inorganic mercury in sediments and soils. Anal. Chim. Acta 479, 233–248. doi:10.1016/S0003-2670(02)01550-7

Bollen, A., Biester, H., 2011. Mercury extraction from contaminated soils by l-cysteine: Species dependency and transformation processes. Water. Air. Soil Pollut. 219, 175–189. doi:10.1007/s11270-010-0696-2

Bollen, A., Wenke, A., Biester, H., 2008. Mercury speciation analyses in HgCl2-contaminated soils and groundwater—Implications for risk assessment and remediation strategies. Water Res. 42, 91–100. doi:10.1016/j.watres.2007.07.011

Bouffard, A., Amyot, M., 2009. Importance of elemental mercury in lake sediments. Chemosphere 74, 1098–1103. doi:10.1016/j.chemosphere.2008.10.045

Bradley, P.M., Journey, C.A., Lowery, M.A., Brigham, M.E., Burns, D.A., Button, D.T., Chapelle, F.H., Lutz, M.A., Marvin-DiPasquale, M.C., Riva-Murray, K., 2012. Shallow Groundwater Mercury Supply in a Coastal Plain Stream. Environ. Sci. Technol. 46, 7503–7511. doi:10.1021/es301540g

Brombach, C.-C., Gajdosechova, Z., Chen, B., Brownlow, A., Corns, W.T., Feldmann, J., Krupp, E.M., 2014. Direct online HPLC-CV-AFS method for traces of methylmercury without derivatisation: a matrix-independent method for urine, sediment and biological tissue samples. Anal. Bioanal. Chem. 407, 973–981. doi:10.1007/s00216-014-8254-1

Brosset, C., 1987. The behavior of mercury in the physical environment. Water. Air. Soil Pollut. 34, 145–166. doi:10.1007/BF00184757

Carter, A., Briscoe, M.L., 2012. an overview of techniques for mercury speciation of contaminated sediments. Brooks Rand Laboratories.

Chadwick, S.P., Babiarz, C.L., Hurley, J.P., Armstrong, D.E., 2006. Influences of iron, manganese, and dissolved organic carbon on the hypolimnetic cycling of amended mercury. Sci. Total Environ. 368, 177–188. doi:10.1016/j.scitotenv.2005.09.039

Charlet, L., Bosbach, D., Peretyashko, T., 2002. Natural attenuation of TCE, As, Hg linked to the heterogeneous oxidation of Fe (II): an AFM study. Chem. Geol. 190, 303–319.

Chen, D., Jing, M., Wang, X., Agilent Technologies, 2005. Determination of Methyl Mercury in Water and Soil by HPLC-ICP-MS.

Chiasson-Gould, S.A., Blais, J.M., Poulain, A.J., 2014. Dissolved Organic Matter Kinetically Controls Mercury Bioavailability to Bacteria. Environ. Sci. Technol. 48, 3153–3161. doi:10.1021/es4038484

City of Fuerth, 2005. Funding program for mercury contamination-Förderprogramm zur Quecksilbersanierung [WWW Document]. URL http://www.fuerth.de/home/stadtentwicklung/newsarchiv/archiv-2005/foerderprogramm-zur-quecksilbersanierung.aspx (accessed 1.24.16).

Cizdziel, J., 2004. Mercury concentrations in groundwater collected from wells on and near the Nevada Test Site, USA. Bull. Environ. Contam. Toxicol. 72, 202–210.

CMJA, 2012. Site Audit: Excavation of Shallow Impacted Soils, Block G, Former ChlorAlkali Plant, Botany Industrial Park.

Cotton, F.A., And Geoffrey Wilkinson, 1972. Advanced Inorganic Chemistry: a Comprehensive Text, 3rd Edition,. 1972.

Cotton, F.A., Wilkinson, G., Murillo, C.A., Bochmann, M., 1999. Advanced Inorganic Chemistry, Auflage: 6. Auflage. ed. John Wiley & Sons, New York.

Coufalík, P., Zvěřina, O., Komárek, J., 2014. Determination of mercury species using thermal desorption analysis in AAS. Chem. Pap. 68, 427–434. doi:10.2478/s11696-013-0471-0

Delany, J.M., 1986. Precipitation kinetics option for the EQ6 geochemical reaction path code. Lawrence Livermore National Laboratory, University of California.

do Valle, C.M., Santana, G.P., Augusti, R., Egreja Filho, F.B., Windmöller, C.C., 2005. Speciation and quantification of mercury in Oxisol, Ultisol, and Spodosol from Amazon (Manaus, Brazil). Chemosphere 58, 779–792. doi:10.1016/j.chemosphere.2004.09.005

Dzombak, D.A., Morel, F.M.M., 1990. Surface Complexation Modeling: Hydrous Ferric Oxide. John Wiley & Sons.

Esbrí, J.M., Bernaus, A., Ávila, M., Kocman, D., García-Noguero, E.M., Guerrero, B., Gaona, X., Álvarez, R., Perez-Gonzalez, G., Valiente, M., Higueras, P., Horvat, M., Loredo, J., 2010. XANES speciation of mercury in three mining districts – Almadén, Asturias (Spain), Idria (Slovenia). J. Synchrotron Radiat. 17, 179–186. doi:10.1107/S0909049510001925

Farrell, R.E., Huang, P.M., Germida, J.J., 1998. Biomethylation of mercury (II) adsorbed on mineral colloids common in freshwater sediments. Appl. Organomet. Chem. 12, 613–620.

Feyte, S., Tessier, A., Gobeil, C., Cossa, D., 2010. In situ adsorption of mercury, methylmercury and other elements by iron oxyhydroxides and organic matter in lake sediments. Appl. Geochem. 25, 984–995. doi:10.1016/j.apgeochem.2010.04.005

Fischer, J.M., Szabo, Z., Barringer, J.L., Jacobsen, E., 2010. Mercury in a north Atlantic Coastal Plain aquifer system; a flowpath study, in: Geological Society of America Abstracts. Presented at the Northeastern Section (45th Annual) and Southeastern Section (59th Annual) Joint Meeting, Baltimore, p. 178.

Fitzgerald, W.F., Engstrom, D.R., Mason, R.P., Nater, E.A., 1998. The Case for Atmospheric Mercury Contamination in Remote Areas. Environ. Sci. Technol. 32, 1–7. doi:10.1021/es970284w

Gaines, G.L.J., Thomas, H.C., 1953. Adsorption Studies on Clay Minerals. II. A Formulation of the Thermodynamics of Exchange Adsorption. J. Chem. Phys. 21, 714–718. doi:10.1063/1.1698996

Garrels, R.M., Mackenzie, F.T., 1967. Origin of the chemical compositions of some springs and lakes. Equilib. Concepts Nat. Water Syst. 67, 222–242.

Gemici, Ü., Tarcan, G., Melis Somay, A., Akar, T., 2009. Factors controlling the element distribution in farming soils and water around the abandoned Halıköy mercury mine (Beydağ, Turkey). Appl. Geochem. 24, 1908–1917. doi:10.1016/j.apgeochem.2009.07.004

Gerbig, C.A., Kim, C.S., Stegemeier, J.P., Ryan, J.N., Aiken, G.R., 2011. Formation of Nanocolloidal Metacinnabar in Mercury-DOM-Sulfide Systems. Environ. Sci. Technol. 45, 9180–9187. doi:10.1021/es201837h

Ginder-Vogel, M., Sparks, D.L., 2010. The Impacts of X-Ray Absorption Spectroscopy on Understanding Soil Processes and Reaction Mechanisms, in: Synchrotron-Based Techniques in Soils and Sediments, Developments in Soil Science. pp. 1–26.

Giulio, R.T.D., Ryan, E.A., 1987. Mercury in soils, sediments, and clams from a North Carolina peatland. Water. Air. Soil Pollut. 33, 205–219. doi:10.1007/BF00191389

Golder, 2012. Remediation Options Appraisal Report Former Chlor Alkali Plant, Orica Botany, NSW (No. Risk-based management of mercury-impacted sites).

Gosar, M., Šajn, R., Biester, H., 2006. Binding of mercury in soils and attic dust in the Idrija mercury mine area (Slovenia). Sci. Total Environ. 369, 150–162. doi:10.1016/j.scitotenv.2006.05.006

Gu, B., Bian, Y., Miller, C.L., Dong, W., Jiang, X., Liang, L., 2011. Mercury reduction and complexation by natural organic matter in anoxic environments. Proc. Natl. Acad. Sci. 108, 1479–1483. doi:10.1073/pnas.1008747108

Gustafsson, J.P., 2013. Tutorial to Visual MINTEQ version 3.0.

Hellal, J., Guédron, S., Huguet, L., Schäfer, J., Laperche, V., Joulian, C., Lanceleur, L., Burnol, A., Ghestem, J.-P., Garrido, F., Battaglia-Brunet, F., 2015. Mercury mobilization and speciation linked to bacterial iron oxide and sulfate reduction: A column study to mimic reactive transfer in an anoxic aquifer. J. Contam. Hydrol. 180, 56–68. doi:10.1016/j.jconhyd.2015.08.001

Hempel, M., Thoeming, J., 1999. Remediation Techniques for Hg-Contaminated Sites, in: Ebinghaus, D.R., Turner, D.R.R., Lacerda, P.D.L.D. de, Vasiliev, P.D.O., Salomons, P.D.W. (Eds.), Mercury Contaminated Sites, Environmental Science. Springer Berlin Heidelberg, pp. 113–130.

Higueras, P., Oyarzun, R., Biester, H., Lillo, J., Lorenzo, S., 2003. A first insight into mercury distribution and speciation in soils from the Almadén mining district, Spain. J. Geochem. Explor. 80, 95–104. doi:10.1016/S0375-6742(03)00185-7

Hippler, J., Hoppe, H.W., Mosel, F., Rettenmeier, A.W., Hirner, A.V., 2009. Comparative determination of methyl mercury in whole blood samples using GC–ICP-MS and GC–MS techniques. J. Chromatogr. B, SPECIAL SECTION ON 11th INTERNATIONAL SYMPOSIUM ON BIOCHROMATOGRAPHY AND NANOSEPARATIONSMontpellier, France, 14-16 October 2008 877, 2465–2470. doi:10.1016/j.jchromb.2009.06.004

Hissler, C., Probst, J.-L., 2006. Chlor-alkali industrial contamination and riverine transport of mercury: Distribution and partitioning of mercury between water, suspended matter, and bottom sediment of the Thur River, France. Appl. Geochem., Mercury: Distribution, Transport, and Geochemical and Microbial Transformations from Natural and Anthropogenic Sources 21, 1837–1854. doi:10.1016/j.apgeochem.2006.08.002

Horvat, M., 2013. Advances in analytical technology - what is available and what is needed? Presented at the ICMGP 2013 Edinburgh.

Huttenloch, P., Roehl, K.E., Czurda, K., 2003. Use of Copper Shavings To Remove Mercury from Contaminated Groundwater or Wastewater by Amalgamation. Environ. Sci. Technol. 37, 4269–4273. doi:10.1021/es020237q

Hylander, L.D., Meili, M., 2005. The Rise and Fall of Mercury: Converting a Resource to Refuse After 500 Years of Mining and Pollution. Crit. Rev. Environ. Sci. Technol. 35, 1–36. doi:10.1080/10643380490492485

Iverfeldt, Å., Lindqvist, O., 1986. Atmospheric oxidation of elemental mercury by ozone in the aqueous phase. Atmospheric Environ. 1967 20, 1567–1573. doi:10.1016/0004-6981(86)90245-3

Iverfeldt, Å., Lindqvist, O., 1982. Distribution equilibrium of methyl mercury chloride between water and air. Atmospheric Environ. 1967 16, 2917–2925. doi:10.1016/0004-6981(82)90042-7

Jacques, D., Šimůnek, J., 2010. Notes on HP1–a software package for simulating variablysaturated water flow, heat transport, solute transport and biogeochemistry in porous media. HP1 Version 2.

Jay, J.A., Morel, F.M.M., Hemond, H.F., 2000. Mercury Speciation in the Presence of Polysulfides. Environ. Sci. Technol. 34, 2196–2200. doi:10.1021/es9911115

Johannesson, K.H., Neumann, K., 2013. Geochemical cycling of mercury in a deep, confined aquifer: Insights from biogeochemical reactive transport modeling. Geochim. Cosmochim. Acta 106, 25–43. doi:10.1016/j.gca.2012.12.010

Juarez-Gomez, J., Perez-Garcia, F., Ramirez-Silva, M.T., Rojas-Hernandez, A., Galan-Vidal, C.A., Paez-Hernandez, M.E., 2013. Solid-contact Hg(II)-selective electrode based on a carbon-epoxy composite containing a new dithiophosphate-based ionophore. Talanta 114, 235–242. doi:10.1016/j.talanta.2013.05.013

Jumal, J., Yamin, B.M., Ahmad, M., Heng, L.Y., 2012. Mercury Ion-Selective Electrode With Self-plasticizing Poly(n–buthylacrylate) Membrane Based On 1,2-Bis-(N'–benzoylthioureido)cyclohexane As Ionophore. APCBEE Procedia, 2nd International Conference on Chemistry and Chemical Process (ICCCP 2012) May 5-6, 2012 3, 116–123. doi:10.1016/j.apcbee.2012.06.056

Koterba, M.T., Andres, A.S., Vrabel, J., Crilley, D.M., Szabo, Z., DeWild, J.F., Aiken, G.R., Reyes-Padro, B., 2006. Occurrence and Distribution of Mercury in the SurficialAquifer, Long Neck Peninsula, Sussex County, Delaware, 2003-04 (USGS Numbered Series No. 2006-5011), Scientific Investigations Report.

Lamborg, C.H., Kent, D., Swarr, G., Munson, K., Kading, T., O'Connor, A., Fairchild, G., LeBlanc, D., Wiatrowski, H., 2013. Mercury Speciation and Mobilization in a Wastewater-contaminated Groundwater Plume. Environ. Sci. Technol. 13239–13249. doi:10.1021/es402441d

Leopold, K., Foulkes, M., Worsfold, P., 2010. Methods for the determination and speciation of mercury in natural waters—A review. Anal. Chim. Acta 663, 127–138. doi:10.1016/j.aca.2010.01.048

Lerman-Sinkoff, S.T., 2014. Transport and Fate of Historic Mercury Pollution from Danbury, CT through the Still and Housatonic Rivers (Bachelor Thesis). Honors College.

Leterme, B., Blanc, P., Jacques, D., 2014. A reactive transport model for mercury fate in soil—application to different anthropogenic pollution sources. Environ. Sci. Pollut. Res. 21, 12279–12293. doi:10.1007/s11356-014-3135-x

Leterme, B., Jacques, D., 2015. A reactive transport model for mercury fate in contaminated soil—sensitivity analysis. Environ. Sci. Pollut. Res. 22, 16830–16842. doi:10.1007/s11356-015-4876-x

lightsources.org, 2015. Light Source Facility Information [WWW Document]. URL http://www.lightsources.org/light-source-facility-information (accessed 1.21.16).

Lin, Y., Larssen, T., Vogt, R.D., Feng, X., Zhang, H., 2011. Transport and fate of mercury under different hydrologie regimes in polluted stream in mining area. J. Environ. Sci. 23, 757–764. doi:10.1016/S1001-0742(10)60473-1

Manceau, A., Lemouchi, C., Enescu, M., Gaillot, A.-C., Lanson, M., Magnin, V., Glatzel, P., Poulin, B.A., Ryan, J.N., Aiken, G.R., Gautier-Luneau, I., Nagy, K.L., 2015. Formation of Mercury Sulfide from Hg(II)–Thiolate Complexes in Natural Organic Matter. Environ. Sci. Technol. 49, 9787–9796. doi:10.1021/acs.est.5b02522

Mason, R.P., Choi, A.L., Fitzgerald, W.F., Hammerschmidt, C.R., Lamborg, C.H., Soerensen, A.L., Sunderland, E.M., 2012. Mercury biogeochemical cycling in the ocean and policy implications. Environ. Res., Mercury in Marine Ecosystems: Sources to Seafood Consumers 119, 101–117. doi:10.1016/j.envres.2012.03.013

Meili, M., Iverfeldt, A., Håkanson, L., 1991. Mercury in the surface water of Swedish forest lakes —concentrations, speciation and controlling factors. Water. Air. Soil Pollut. 56, 439–453. doi:10.1007/BF00342290

Merck, 2014. Safety Data Sheet Mercury:

Merian, E., Anke, M., Ihnat, M., Stoeppler, M. (Eds.), 2004. Elements and their compounds in the environment: occurence, analysis and biological relevance, 2nd completely rev. and enl. ed. ed. Wiley-VCH, Weinheim.

Merly, C., Hube, D., 2014. IMaHg Project: Enhanced knowledge in mercury fate and transport for Improved Management of Hg soil contamination: Remediation of Mercury Contaminated Sites (No. Project No. SN-03/08). SNOWMAN network.

Meschede, T., Vogelsberger, R., 1999. Mercury Decontamination of a Chloralkali Plant in Alexandria, Egypt, in: Ebinghaus, D.R., Turner, D.R.R., Lacerda, P.D.L.D. de, Vasiliev, P.D.O., Salomons, P.D.W. (Eds.), Mercury Contaminated Sites, Environmental Science. Springer Berlin Heidelberg, pp. 457–463.

Monier, M., Elsayed, N.H., Abdel-Latif, D., 2015. Synthesis and application of ion-imprinted resin based on modified melamine–thiourea for selective removal of Hg(II). Polym. Int. 64, 1465–1474. doi:10.1002/pi.4942

Muresan, B., Pernet-Coudrier, B., Cossa, D., Varrault, G., 2011. Measurement and modeling of mercury complexation by dissolved organic matter isolates from freshwater and effluents of a major wastewater treatment plant. Appl. Geochem. 26, 2057–2063. doi:10.1016/j.apgeochem.2011.07.003

Murthy, Z.V.P., Parikh, P.A., Patel, N.B., 2013. Application of β-Zeolite, Zeolite Y, and Mordenite as Adsorbents to Remove Mercury from Aqueous Solutions. J. Dispers. Sci. Technol. 34, 747–755. doi:10.1080/01932691.2012.685839

Newcombe, G., Drikas, M., Hayes, R., 1997. Influence of characterised natural organic material on activated carbon adsorption: II. Effect on pore

volume distribution and adsorption of 2-methylisoborneol. Water Res. 31, 1065–1073. doi:10.1016/S0043-1354(96)00325-9

NIMD National Institute for Minamata Diseas, Japanese Ministry of the Environment, 2014. Recovery of mercury from mercury-polluted soil by thermaltreatment [WWW Document]. URL http://www.nimd.go.jp/archives/english/tenji/c_corner/c09.html (accessed 1.24.16).

NIST, National Institute for Standards and Technology, Huber, M.L., Laesecke, A., Friend, D.G., 2006. NISTIR 6643: The vapor pressure of mercury.

Nobre, R.C.M., Nobre, M.M.M., Pereira, P.A., 2012. Field Performance of a 7-Year PRB to Remediate a Mercury Contaminated Plume. Presented at the Eighth International Conference on Remediation of Chlorinated and Recalcitrant Compounds Battelle Memorial Institute, Columbus, OH, Monterey, CA.

Nordstrom, D.K., 2012. Models, validation, and applied geochemistry: Issues in science, communication, and philosophy. Appl. Geochem. 27, 1899–1919. doi:10.1016/j.apgeochem.2012.07.007

Nordstrom, D.K., Campbell, K.M., 2014. Modeling Low-Temperature Geochemical Processes, in: Treatise on Geochemistry. Elsevier, pp. 27–68.

Nordstrom, D.K., Plummer, L.N., Wigley, T.M.L., WOLERY, T.J., BALL, J.W., JENNE, E.A., BASSETT, R.L., CRERAR, D.A., FLORENCE, T.M., FRITZ, B., HOFFMAN, M., HOLDREN, G.R., LAFON, G.M., MATTIGOD, S.V., McDUFF, R.E., MOREL, F., REDDY, M.M., SPOSITO, G., THRAILKILL, J., 1979. A Comparison of Computerized Chemical Models for Equilibrium Calculations in Aqueous Systems, in: Chemical Modeling in Aqueous Systems, ACS Symposium Series. AMERICAN CHEMICAL SOCIETY, pp. 857–892.

Obiri-Nyarko, F., Grajales-Mesa, S.J., Malina, G., 2014. An overview of permeable reactive barriers for in situ sustainable groundwater remediation. Chemosphere 111, 243–259. doi:10.1016/j.chemosphere.2014.03.112

Oram, P.D., Fang, X., Fernando, Q., Letkeman, P., Letkeman, D., 1996. The Formation Constants of Mercury(II)−Glutathione Complexes. Chem. Res. Toxicol. 9, 709–712. doi:10.1021/tx9501896

Orica, 2016. Mercury Remediation [WWW Document]. URL http://www.orica.com/Locations/Asia-Pacific/Australia/Botany/Botany-Transformation-Projects/Mercury-Remediation#.VpvMI1Lpx3Q (accessed 1.17.16).

Parkhurst, D.L., Apello, C.A.J., 2013. Description of Input and Examples for PHREEQC Version 3—A Computer Program for Speciation, Batch-Reaction, One-Dimensional Transport, and Inverse Geochemical Calculations (No. book 6, chap. A43), U.S. Geological Survey Techniques and Methods.

Pearson, R.G., 1963. Hard and Soft Acids and Bases. J. Am. Chem. Soc. 85, 3533–3539. doi:10.1021/ja00905a001

Pensaert, S., Gerbrands, B., 2012. Remediation of a former chlor-alkali plant in the netherlands. Presented at the Mercury contaminated sites-technical Meeting NICOLE, Brussels.

Perry, D.L., 2011. Handbook of Inorganic Compounds, Second Edition. CRC Press.

Phipps, O., Barrett, J., Hesketh, P., Brown, R., 2014. Risk-based management of mercury-impacted sites. NICOLE Network for Industrially Contaminated Land in Europe.

Plummer, L.N., Wigley, T.M.L., Parkhurst, D.L., 1978. The kinetics of calcite dissolution in CO 2 -water systems at 5 degrees to 60 degrees C and 0.0 to 1.0 atm CO 2. Am. J. Sci. 278, 179–216. doi:10.2475/ajs.278.2.179

Powell, K.J., Brown, P.L., Byrne, R.H., Gajda, T., Hefter, G., Sjöberg, S., Wanner, H., 2005. Chemical speciation of environmentally significant heavy metals with inorganic ligands. Part 1: The Hg2+– Cl–, OH–, CO32–, SO42–, and PO43– aqueous systems (IUPAC Technical Report). Pure Appl. Chem. 77. doi:10.1351/pac200577040739

Qian, J., Skyllberg, U., Frech, W., Bleam, W.F., Bloom, P.R., Petit, P.E., 2002. Bonding of methyl mercury to reduced sulfur groups in soil and stream organic matter as determined by x-ray absorption spectroscopy and binding affinity studies. Geochim. Cosmochim. Acta 66, 3873–3885. doi:10.1016/S0016-7037(02)00974-2

Rajgopal, T., Ravimohan, H., Mascarenhas, P., 2006. Epidemiological surveillance of employees in a mercury thermometer plant: An occupational health study. Indian J. Occup. Environ. Med. 10, 11. doi:10.4103/0019-5278.22889

Reddy, M.M., Aiken, G.R., 2001. Fulvic Acid-Sulfide Ion Competition for Mercury Ion Binding in the Florida Everglades. Water. Air. Soil Pollut. 132, 89–104. doi:10.1023/A:1012073503678

Reis, A.T., Coelho, J.P., Rucandio, I., Davidson, C.M., Duarte, A.C., Pereira, E., 2015. Thermo-desorption: A valid tool for mercury speciation in soils and sediments? Geoderma 237–238, 98–104. doi:10.1016/j.geoderma.2014.08.019

Rogers, R.D., 1975. Methylation of Mercury in a Terrestrial Environment. U.S. Environmental Protection Agency, Office of Research and Development, Environmental Monitoring and Support Laboratory, Monitoring Systems Research and Development Division.

Rumayor, M., Diaz-Somoano, M., Lopez-Anton, M.A., Martinez-Tarazona, M.R., 2015. Application of thermal desorption for the identification of mercury species in solids derived from coal utilization. Chemosphere 119, 459–465. doi:10.1016/j.chemosphere.2014.07.010

Ryan, J.N., Gschwend, P.M., 1994. Effect of Solution Chemistry on Clay Colloid Release from an Iron Oxide-Coated Aquifer Sand. Environ. Sci. Technol. 28, 1717–1726. doi:10.1021/es00058a025

Ryan, J.N., Gschwend, P.M., 1990. Colloid mobilization in two Atlantic coastal plain aquifers: Field studies. Water Resour. Res. 26, 307–322. doi:10.1029/WR026i002p00307

Sander, R., 2015. Compilation of Henry's law constants (version 4.0) for water as solvent. Atmospheric Chem. Phys. 15, 4399–4981. doi:10.5194/acp-15-4399-2015

Schöndorf, T., 2011. literature review about Hg contaminated sites in terms of the market potential for the Hg-reactor process - (Recherche und Auswertung von Quecksilberschadensfällen im Hinblick auf das Marktpotenzial für das Hg-Reaktor-Verfahren). UFZ TASK.

Schöndorf, T., Egli, M., Biester, H., Mailahn, W., Rotard, W., 1999. Distribution, Bioavailability and Speciation of Mercury in Contaminated Soil and Groundwater of a Former Wood Impregnation Plant, in: Ebinghaus, D.R., Turner, D.R.R., Lacerda, P.D.L.D. de, Vasiliev, P.D.O., Salomons, P.D.W. (Eds.), Mercury Contaminated Sites, Environmental Science. Springer Berlin Heidelberg, pp. 181–206.

Šimůnek, J., van Genuchten, M.T., Šejna, M., 2008. Development and Applications of the HYDRUS and STANMOD Software Packages and Related Codes. Vadose Zone J. 7, 587. doi:10.2136/vzj2007.0077

Sites, A., Oberholtzer, L., 1992. Mercury Point-of-entry Treatment Study. New Jersey Department of Environmental Protection and Energy.

Skyllberg, U., 2010. Mercury biogeochemistry in soils and sediments, in: Synchrotron-Based Techniques in Soils and Sediments, Developments in Soil Science. pp. 379–410.

Skyllberg, U., 2008. Competition among thiols and inorganic sulfides and polysulfides for Hg and MeHg in wetland soils and sediments under suboxic conditions: Illumination of controversies and implications for MeHg net production. J. Geophys. Res. 113. doi:10.1029/2008JG000745

Skyllberg, U., Bloom, P.R., Qian, J., Lin, C.-M., Bleam, W.F., 2006. Complexation of Mercury(II) in Soil Organic Matter: EXAFS Evidence for Linear Two-Coordination with Reduced Sulfur Groups. Environ. Sci. Technol. 40, 4174–4180. doi:10.1021/es0600577

Skyllberg, U., Qian, J., Frech, W., 2005. Combined XANES and EXAFS study on the bonding of methyl mercury to thiol groups in soil and aquatic organic matter. Phys. Scr. 2005, 894. doi:10.1238/Physica.Topical.115a00894

Szabo, Z., Barringer, J.L., Jacobsen, E., Smith, N.P., Gallagher, R.A., Sites, A., 2010. Variability of mercury concentrations in domestic well water, New Jersey Coastal Plain, in: Geological Society of America Abstracts. Presented at the Northeastern Section (45th Annual) and Southeastern Section (59th Annual) Joint Meeting, Baltimore, p. 178.

Terra, 2010. Mercury remediation in Meckenbeuren- Dismantling of a former kyanization hall (Quecksilber-Sanierung in Meckenbeuren Ehemaliges Gelände der Holzindustrie Meckenbeuren (HIM) Dekontamination/Rückbau der ehemaligen Kyanisierungshalle) [WWW Document]. URL http://www.terra-firmengruppe.de/download_cms/pdf/referenzen/umweltservice/pdb_meckenbeuren_fraenkel_ag.pdf (accessed 1.24.16).

Thiruvenkatachari, R., Vigneswaran, S., Naidu, R., 2008. Permeable reactive barrier for groundwater remediation. J. Ind. Eng. Chem. 14, 145–156. doi:10.1016/j.jiec.2007.10.001

Tipping, E., Lofts, S., Hooper, H., Frey, B., Spurgeon, D., Svendsen, C., 2010. Critical Limits for Hg(II) in soils, derived from chronic toxicity data. Environ. Pollut. 158, 2465–2471. doi:10.1016/j.envpol.2010.03.027

Tipping, E., Lofts, S., Sonke, J.E., 2011. Humic Ion-Binding Model VII: a revised parameterisation of cation-binding by humic substances. Environ. Chem. 8, 225. doi:10.1071/EN11016

UNEP, 2013. Global Mercury Assessment 2013: Sources, Emissions, Releases and Environmental Transport. UNEP Chemicals Branch, Geneva, Switzerland.

US EPA, 2007. Treatment Technologies for Mercury in Soil, Waste and Water (No. EPA-542-R-07-003). US EPA.

US EPA, 2005. Method 3200, Mercury species fractionation and quantification by microwave assisted extraction, selective solvent extraction and/or solid phase extraction.

USEPA, 2002. Method 1631, Revision E: Mercury in Water by Oxidation, Purge and Trap, and Cold Vapor Atomic Fluorescence Spectrometry.

VanLoon, G.W., Duffy, S.J., 2011. Environmental chemistry: a global perspective. Oxford University Press, Oxford; New York.

Watson, D.B., Phillips, D.H., Gu, B., 2002. Performance evaluation of in-situ iron reactive barriers at the Oak Ridge Y-12 site (No. DE-AC05-00OR22725).

Wenke, A., Bollen, A., Richard, J.-H., Biester, H., 2016. Potential of Brass to Remove Inorganic Hg(II) from Aqueous Solution through Amalgamation (in press). Water Environment Research.

WHO, 2016. WHO | Mercury and health [WWW Document]. WHO. URL http://www.who.int/mediacentre/factsheets/fs361/en/ (accessed 1.15.16).

Wollenberg, J.L., Peters, S.C., 2009. Mercury emission from a temperate lake during autumn turnover. Sci. Total Environ. 407, 2909–2918. doi:10.1016/j.scitotenv.2008.12.017

Xia, K., Skyllberg, U.L., Bleam, W.F., Bloom, P.R., Nater, E.A., Helmke, P.A., 1999. X-ray Absorption Spectroscopic Evidence for the Complexation of Hg(II) by Reduced Sulfur in Soil Humic Substances. Environ. Sci. Technol. 33, 257–261. doi:10.1021/es980433q

Yeh, G.T., Tripathi, V.S., 1989. A critical evaluation of recent developments in hydrogeochemical transport models of reactive multichemical components. Water Resour. Res. 25, 93–108. doi:10.1029/WR025i001p00093

Zhu, Y., Ma, L.Q., Dong, X., Harris, W.G., Bonzongo, J.C., Han, F., 2014. Ionic strength reduction and flow interruption enhanced colloid-facilitated Hg transport in contaminated soils. J. Hazard. Mater. 264, 286–292. doi:10.1016/j.jhazmat.2013.11.009

Chapter 2: Mercury (II) reduction and co-precipitation of metallic mercury on hydrous ferric oxide in contaminated groundwater[1]

Abstract

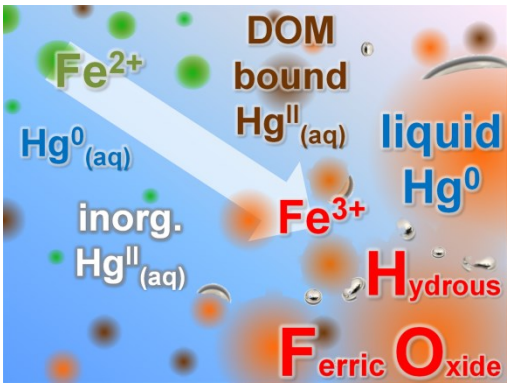

Mercury (Hg) speciation and sorption analyses in contaminated aquifers are useful for understanding transformation, retention, and mobility of Hg in groundwater. In most aquifers hydrous ferric oxides (HFOs) are among the most important sorbents for trace metals; however, their role in sorption or mobilization of Hg in aquifers has been rarely analyzed. In this study, we investigated Hg chemistry and Hg sorption to HFO under changing redox conditions in a highly $HgCl_2$-contaminated aquifer (up to 870 $\mu g \cdot L^{-1}$ Hg). Results from aqueous and solid phase Hg measurements were compared to modeled (PHREEQC) data. Speciation analyses of dissolved mercury indicates that Hg^{II} forms were reduced to Hg^0 under anoxic conditions, and adsorbed to or co-precipitated with HFO. Solid phase Hg thermo-desorption measurements revealed that between 55 and 93% of Hg bound to HFO was elemental Hg (Hg^0). Hg concentrations in precipitates reached more than 4 weight %, up to 7000 times higher than predicted by geochemical models that do not consider unspecific sorption to and co-precipitation of elemental Hg with HFO. The observed process of Hg^{II} reduction and Hg^0 formation, and its retention and co-precipitation by HFO is thought to be crucial in $HgCl_2$-contaminated aquifers

[1] this chapter has been published in Science of the Total Environment
DOI: 10.1016/j.scitotenv.2015.08.116

with variable redox-conditions regarding the related decrease in Hg solubility (factor of ~10^6), and retention of Hg in the aquifer.

1 Introduction

Mercury (Hg) is among the most toxic contaminants, but the actual toxicity and harmful potential are strongly dependent on its chemistry (UNEP, 2002). Inorganic ionic, mainly divalent mercury, Hg^{II}, and metallic mercury, $Hg^0_{(l)}$, have been used in numerous industrial processes resulting in soil and groundwater contamination. In the environment, mercury is subject of several species transformation processes resulting in changes of mobility and toxicity of which the formation of methyl-Hg is most relevant for Hg uptake in aquatic food chains. As a type B metal, Hg shows strong affinity for sulfur and its transport in aquatic systems is mainly determined by sulfur bearing dissolved organic matter (DOM) (Ravichandran, 2004; Nagy et al., 2011). However, DOM concentrations in groundwater are usually low (< 1 $mg \cdot L^{-1}$) (Malcolm, 1991). As a noble metal, Hg is easily reduced to its elemental form, either by humic matter enhanced photoreduction (Si and Ariya, 2011) or in oxygen depleted (subsurface) environments (Lamborg et al., 2013).

There are only few studies of mercury in groundwater, that mainly focus on total or methyl-Hg. A summary of the existing work is given elsewhere (Barringer et al., 2013). Even fewer studies address the fate of $HgCl_2$ and Hg^0 in groundwater. Bollen et al. (2008) observed the formation of Hg^0 in aquifer sediments at a mercury(II)chloride ($HgCl_2$) contaminated site and dissolved gaseous mercury (DGM) has been shown to occur in an anoxic groundwater contaminated by a wastewater plume (Lamborg et al., 2013). Under anoxic conditions, iron (Fe) containing minerals are important electron acceptors (Ehrlich and Newman, 2008) for the microbial degradation of organic matter, and are dissolved as Fe^{II} ions (Liang et al., 1993). Upon contact with oxygen, Fe^{II} gets oxidized and starts to precipitate as ferrihydrite ($Fe(OH)_3$) and other amorphous or poorly crystalline hydrous ferric oxides (HFOs). HFO formation and dissolution is an important process in many aquifers (Herbert Jr, 1996) and groundwater/freshwater interfaces (Dekov et al., 2014). Moreover, HFOs are known to be important temporary sinks, but also carriers of pollutants due to

their large reactive surface areas including inner and outer sorption sites (Dzombak and Morel, 1990; Sparks, 2005). Hg sorbed to Fe-minerals can get exchanged (Jiskra et al., 2014), and dissolution of HFO can lead to the release of trapped Hg (Johannesson and Neumann, 2013). Large efforts were made in the past to determine sorption constants for many pollutants, including mercury (Dzombak and Morel, 1990), in order to predict their sorption behavior on HFO precipitates by geochemical modeling. Such constants are based on lab experiments with HFO derived from Fe(III) salts and equilibrated with Hg^{II} solutions (Dzombak and Morel, 1990). Other important Hg species such as DOM-bound Hg or Hg^0 were disregarded and possible effects on the oxidation state of Hg resulting from redox changes have been widely neglected. Less is known about the role of HFOs for Hg^{II} reduction, but recent laboratory studies (Charlet et al., 2002; Peretyazhko et al., 2006; Wiatrowski et al., 2009; Amirbahman et al., 2013; Pasakarnis et al., 2013) have shown the importance of Fe^{II} as a reducing agent for Hg^0 formation. Recently, Lamborg et al. (2013) found indications for the relevance of this process in the iron reducing zone of an anoxic aquifer. It is not known, however, how important HFOs are for precipitation and retention of Hg^0 in contaminated aquifers. In this study, we investigated the role of HFO as Hg sorbent in a $HgCl_2$-contaminated aquifer showing variable redox conditions. We analyzed Hg speciation in aqueous phase and on HFO, quantified Hg retained, and compared the results to those obtained by geochemical modeling to evaluate to what extent geochemical models are able to reproduce measured Hg compounds and their quantities.

2 Materials and methods

2.1 Sampling site.

The sampling site (Figure 1) is a former wood impregnation facility located in the Black Forest (Southern Germany). $HgCl_2$ had been used as a wood preservative for decades, resulting in extensive contamination of soil and groundwater. Hydrogeology of the site is characterized by late Quarternary fluvial sediments overlaying Paleozoic granite basement (LUBW, 2014). Part of the affected aquifer is rich in organic material (peat), which causes depletion of oxygen and temporary anoxic conditions. Multiple groundwater wells have been

installed on the site for monitoring purposes, and a pump & treat remediation facility is operated. Water is pumped through high-density polyethylene (HDPE) pipes from several oxic wells (W2, W35-W38) and one mostly anoxic well W7a, that becomes oxic when groundwater levels are low. W7a water can also mix with oxygen rich groundwater or river water, depending on groundwater levels and flow. This leads to periodic oxidation events and formation of HFO colloids and particles.

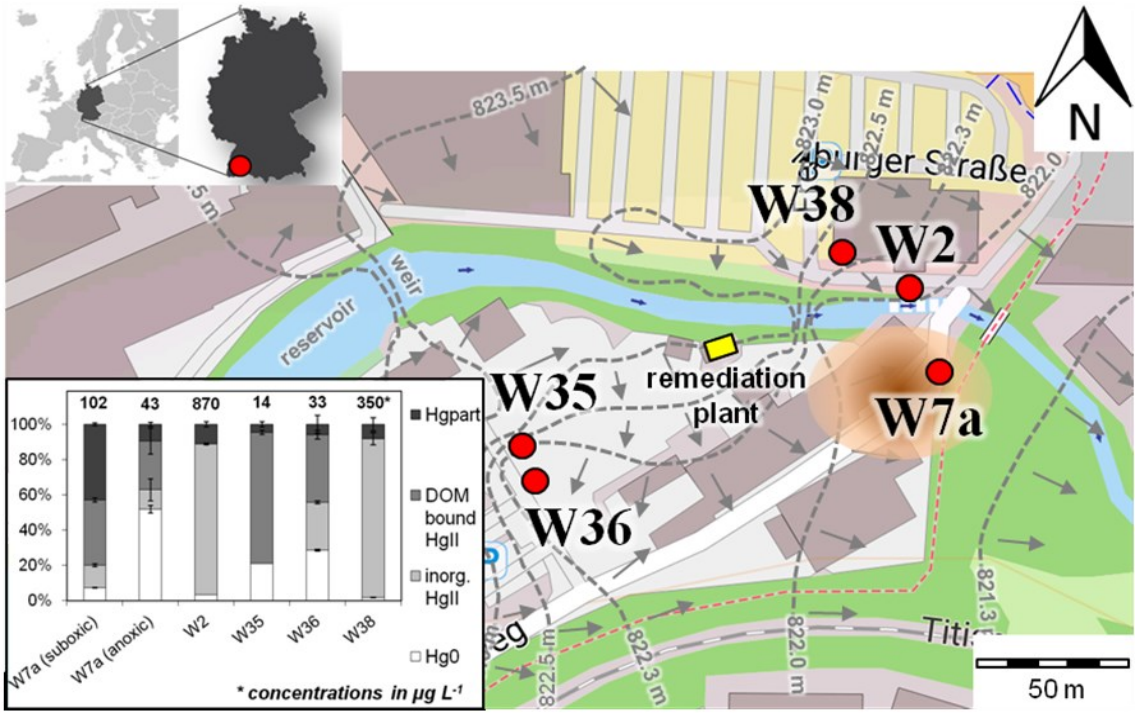

Figure 1. Site map with groundwater contours of upper aquifer, well locations and area of temporary anoxia and HFO formation/dissolution in the aquifer (basemap: OpenStreetMap, groundwater isohypses: HPC AG). Hg speciation and total concentrations of groundwater are shown in inset graph.

2.2 Sampling and sample treatment.

Precipitate samples were collected from filters inside the pump & treat facility and from the temporarily anoxic well W7a. Filters inside the pump & treat facility consisted of six synthetic fiber filter pads with undefined pore size, that had been installed for 200 days in parallel between a mixing chamber for oxic- and anoxic groundwater and the treatment units (see also Figure S4). How many redox cycles well W7a went through during this time period was not monitored, but redox conditions inside the mixing chamber were always oxic. Filter pads

were installed behind cartridge filters (5µm) monitored for oversaturation by the plant operator, thus solely freshly precipitated, not yet coagulated material was obtained. Precipitates were washed off the filter pads using Milli-Q water (18.2 MΩ·cm) and suspensions were centrifuged at 5000 rpm. The supernatant was discarded and the retained precipitate was stored in sealed polypropylene (PP) containers below 8°C until further analysis. To obtain precipitate samples from the temporarily anoxic groundwater well 50 L of unfiltered water were collected in a PP container during a suboxic event (0.9 $mg \cdot L^{-1}$ O_2, 9.7°C). Sampling was done after stationary conditions of field parameters (pH, electric conductivity) were reached, using a 1.4 inch polybutylene terephthalate (PBT) groundwater testing pump (WP 4012, Whale Pumps, U.K.). Sample for extraction of precipitates was transported to the lab under oxic conditions at ambient temperature (~15°C) to allow complete oxidation and HFO precipitation and filtered through 0.45 µm polyamide (PA) membrane filters within 48h. Precipitates were rinsed from the filters with Milli-Q water, centrifuged, collected after the supernatant was discarded, split into 6 replicates, and stored in sealed PP containers below 8°C until further analysis.

All water samples were taken in a 500 mL fluorinated polyethylene (FLPE) bottle, thoroughly washed with demineralized water and double distilled nitric acid (HNO_3), and preconditioned with sample water. Samples for determination of dissolved concentrations were filtered through 0.45 µm polyamide (PA) membrane syringe filters in the field directly after sampling. Total concentrations were determined from unfiltered samples and particulate concentrations were calculated by subtracting dissolved from total concentrations. To avoid precipitation subsamples for cation analysis were acidified immediately after extraction by adding one percent (v/v) of double distilled HNO_3 and stored in sealed PP containers below 8°C until analysis. Subsamples for anion analysis were kept in air free, sealed PP containers below 8°C until analysis. Because sampling was done in an oxic environment oxidation of reduced nitrogen forms to nitrate cannot be ruled out except for well 7a, where a field photometer was used to determine ammonium and nitrite in the field. However, Eh, pH, electric conductivity, temperature, and oxygen content were determined using an air free flow chamber to avoid contact with the atmosphere. Subsamples for total

mercury and total filtered mercury determination were stabilized with 1/60 M $K_2Cr_2O_7$-HNO_3 in the field and oxidized in the lab with BrCl solution according to EN standard method 1483 (EN and European Committee for Standardization, 2007) and USEPA method 1631 (USEPA, 2002) (more detailed information on Hg speciation analyses in chapter 2.4.2.).

2.3 Precipitate analyses.

2.3.1 Determination of Fe, sulfur, organic carbon, and Hg.

Specimens (~1g) of all precipitate samples were dried at 105°C (>24h) to determine water content according to standard method ISO 11465 (ISO, 1996), grinded, and digested in aqua regia according to ISO standard method 11466 (ISO, 1997). Fe, Mn, and Al concentrations were determined using an inductively coupled plasma optical emission spectrometer (ICP-OES Varian 715 ES, Agilent Technologies Inc., USA). Hg content in digests was determined by means of cold-vapor (CV) ICP-OES (vapor generator VGA 77P, coupled to ICP-OES. Calibration range: 0-150 µg·L-1, Limit of quantification (LOQ): 18 µg·L-1, sample dilution to approx. 60 µg·L-1). For total mercury analyses, fresh specimens of precipitates were digested in aqua regia, and subsequently corrected for water content. Concentrations of sulfur (S), total carbon (TC), and organic carbon (Corg) on the dried samples were determined using a CNS elemental analyzer (Euro EA 3000, Hekatech GmbH, Germany). Corg concentrations were determined in carbonate free samples after pretreatment with hydrochloric acid (HCl, 25%).

2.3.2 Determination of solid phase Hg binding forms.

Hg binding form analyses were performed using thermo-desorption cold-vapor atomic absorption spectrometry (TD-CV-AAS) according to the method of Biester and Scholz (1996) (also e.g. Rumayor et al., 2013, 2015; Reis et al., 2015). Precipitate specimens from the filter pads and from well W7a were heated continuously at a heating rate of 0.5°C·s^{-1} in a N_2 gas flow (300 mL·min^{-1}) and the released mercury was continuously detected by means of atomic absorption spectroscopy. Hg thermo-desorption (Hg-TD) curves of replicate (>3) measurements were combined to averaged curves and compared to those of the standard materials Hg^0, meta-HgS, HgS, and $HgCl_2$ on quartz sand, divalent

mercury (Hg^{II}) sorbed to HFO, and Hg bound to humic acid. Hg^0, meta-HgS, HgS, and $HgCl_2$ standards were obtained by adding aliquots of metallic mercury (99.999%, Alfa Aesar GmbH, Germany), metacinnabar (HgS black, Sigma Aldrich Corp. USA), cinnabar (HgS red, 99%, Sigma Aldrich Corp. USA), and mercury(II)chloride ($HgCl_2$, p.a., Carl Roth GmbH, Germany) to quartz sand/powder, respectively, until a concentration of app. 5 $mg \cdot kg^{-1}$ was reached. Hg^{II}/HFO standard was produced by adding 1mL of a $7 \cdot 10^{-4}$ molar $Hg^{(II)}Cl_2$ solution to 40mL of a 0.4 molar Fe(III) salt solution ($Fe(NO_3)_3 \cdot 9H_2O$, p.a., Bernd Kraft GmbH, Germany). HFO was then precipitated adjusting pH to >7 by adding sodium hydroxide (NaOH). Two standards of Hg bound to humic acids were analyzed. One was PGS 10 “Humic Acid” (LOT#BCBK5107V, total Hg: 286 ± 10 $\mu g \cdot kg^{-1}$, Sigma Aldrich Corp. USA). The other one was obtained by extraction from a peat sample (Harz Mountains, Germany) with 0.5 molar NaOH solution and subsequent precipitation of humic acid by adjusting pH to 1 with HCl (total Hg: 1.63 ± 0.02 $mg \cdot kg^{-1}$). Fitting of Gauss shaped peaks, calculation of peak areas, normalizing, and averaging of TD curves were performed using Origin 9.0 software (OriginLab Corp., USA).

2.4 Water analyses.

2.4.1 Determination of cations, anions, and field parameters.

Water samples were analyzed for major cations by means of ICP-OES. Major anions were determined using an ion exchange chromatograph (761 Compact IC, Metrohm AG, Switzerland). Redox sensitive ions (Fe^{2+}, ammonium (NH_4^+), nitrite (NO_2^-)) in water from W7a were analyzed in the field immediately after sampling using a field photometer (Data Line LED-Photometer, Windaus GmbH, Germany). Fe^{2+} was determined, using a test kit (Winlab® iron Fe^{2+}/Fe^{3+}) based on the phenantroline method (Eaton and Franson, 2005). NH_4^+ and NO_2^- were quantified with the indophenole blue method (Aquanal®-plus ammonium 37440) and the red-violet azo dye method (Aquanal®-plus nitrite 37450), respectively. Nitrate (NO_3^-) in W7a water could not be measured in the field and was calculated by subtraction of NH_4^+ and NO_2^- from NO_3^- concentration as determined by IC after arrival in the lab in the anion subsample transported under oxic conditions.

Alkalinity was determined in the field by titration according to ISO standard method 9963-1 (ISO, 1996). Mercury was analyzed using a cold vapor atomic absorption spectrometer (CV-AAS, mercury analyzer Hg-254 NE, Seefelder Messtechnik GmbH, Germany, calibration range: 0-35 ng Hg absolute, LOQ: 3 ng absolute), according to EN standard method 1483 (EN, 2007).

2.4.2 Aqueous Hg speciation.

Speciation of aqueous phase Hg was determined according to the protocol given in Bollen et al. (2008), modified after Brosset (1987) and Meili et al. (1991) (see also Figure S1). The following operationally defined Hg species were determined: "*Purgeable, dissolved gaseous elemental mercury*" (Hg^0), "*dissolved, inorganic divalent mercury, reducible with $SnCl_2$*" (Hg^{II}_a), "*Dissolved Hg, bound to BrCl-oxidizable humic compounds or dissolved Hg-sulfide species*" (DOM-bound, Hg^{II}_b), and "*particulate Hg*" (Hg_{part}). Purgeable Hg^0 and Hg^{II}_a were determined onsite within a few minutes after sampling. The maximum sample volume analyzed per single measurement was 20 mL, resulting in a LOQ of 0.15 $\mu g \cdot L^{-1}$ (3ng/20mL).

2.4.3 Determination of dissolved organic carbon.

Filtered samples (0.45µm) were analyzed by means of thermocatalytic oxidation at 950°C with subsequent NDIR detection of CO_2, using a TOC analyzer (multi N/C 2100, Analytik Jena AG, Germany).

2.5 Analytical quality assurance.

Standard reference materials (SRMs) were analyzed to assure quality of digests and analyzes. The following SRMs were utilized: "Lake Sediment" IAEA-SL-1: (ICP-OES), "Chinese Soil" NCS-DC 73322: (CNS, CV-ICP-OES (digested)), "Trace Metals" RTC 1-WP: (CV-AAS, CV-ICP-OES, ICP-OES), "natural water from Lake Superior" EC ION-915: (IC, Alkalinity, pH, TOC), "River Water" NRC SLRS-5: (ICP-OES, photometer). See Supplementary Material for recovery rates and limits of quantification (Table S1).

2.6 Modeling of Hg sorption to HFO.

Sorption of mercury to HFO was modeled using PHREEQC (Parkhurst and Apello, 2013), version 3.1.2 (database: minteq.v4.dat, expanded with additional

sulfide (Dyrssen and Wedborg, 1991; Drott et al., 2013) and DOC (Skyllberg, 2008) complexes; see Table S3 in Supplementary Material for Hg equilibrium constants). The smaller one of the two published complex formation constants for $HOHgSH^0$ (cf. Skyllberg, 2008) was applied, because Drott et al.(2013) have shown that it is the more reasonable one. DOC was assumed to contain 0.15% thiol (RSH) functional groups (Qian et al., 2002; Skyllberg, 2008; Skyllberg et al., 2005, 2003) on a mass basis. All modeling was based on the cation-anion-balances of the groundwater samples, including data on Hg (and if possible Fe) speciation, pH, temperature and Eh. For the implementation of HFO as a surface sorption site, two different models were used: The sorption models of Dzombak and Morel (1990) (D&M) and Tiffreau et al. (1995), both implemented with a Borkovec diffuse double layer (DDL, with the DDL thickness considered to be equal the Debye length), and coupled to the precipitation of ferrihydrite ($Fe(OH)_3$ as HFO source. Hg complexation constants of both models were originally developed by the authors on the basis of the same experimental data set published by Avotins (1975). The D&M model is based on the modification of an existing HFO sorption theory for other cations, and assumes a weak and a strong binding site. The Tiffreau model, however, was developed solely for mercury and employs only one binding site, but includes also ternary surface complexes between the HFO surface, Hg^{II}, Hydroxide (OH-), and Chloride (Cl-). The sorption of Hg^0 is not considered in any of the models. To model the amount of Hg sorbed to HFO, we used four different scenarios: Two for the situation in groundwater well W7a and two for the situation after mixing anoxic and oxic well waters in the mixing chamber. For W7a, water analyses of suboxic and anoxic events were used, respectively. Hg sorption to HFO in the mixing chamber was modeled using a water analysis of real mixed water as well as a modeled water composition calculated by mixing the waters from Table 1 in PHREEQC, using the approximate mixing ratios from long term pumping rates of the remediation plant, respectively (see Table 1).

3 Results and discussion

3.1 Characterization of groundwater samples.

Main cations in solution were uniformly dominated by alkali earth metals in all samples. Anions showed considerable variation (see Figure S3), mainly caused by chloride (Cl^-) and fluoride (F^-) salts attributed to the use of such salts for wood impregnation at different locations at the site. Wells W2 and W35-W38 were oxic during the whole study period, whereas well W7a was found to be suboxic at one sampling date and anoxic at the other (Table 1Table). Total unfiltered iron contents of W2 and W35-W38 were below limit of quantification (LOQ) calculated from calibration of the ICP-OES system, the anoxic sample from W7a exhibited a total iron concentration of 2.5 $mg \cdot L^{-1}$. Dissolved (<0.45µm) iron was found to be mainly Fe^{2+}, but the presence of particulate Fe (Fe_{part}), and the Eh (263 mV) indicated that iron oxidation had already begun to take place (Equation 1).

$$Fe^{2+} = Fe^{3+} + e^- \quad (1)$$

In the sample from the suboxic event (Eh: 397 mV) dissolved Fe was below LOQ whereas Fe_{part} was found to be higher than 32 $mg \cdot L^{-1}$. DOC concentrations were 0.8 to 5.3 $mg \cdot L^{-1}$ (Table 1), and therefore relatively high when compared to typical DOC concentrations in groundwater (0.5 $mg \cdot L^{-1}$) (Malcolm, 1991). High DOC concentrations were not restricted to W7a (~4.5 $mg \cdot L^{-1}$), but other wells with comparatively low Hg concentrations (W35, W36) were also enriched in dissolved organic matter (5.3 and 3.4 $mg \cdot L^{-1}$ DOC, respectively. See also chapter 3.2.).

All samples were slightly acidic to neutral (pH: 6.3-6.8). Lowest Eh values were found in the anoxic W7a sample and highest in well W36 (524 mV, Table 1). Water analysis of a sample of water collected behind the mixing chamber is also shown (Table 1). Overall water chemistry does not differ much from “theoretical” mixed water calculated with PHREEQC using the given mixing ratios, except for Na^+, Cl^-, NO_3^-, and Fe concentrations. In contrast to the wells that were sampled in summer, the mixed water sample was taken in winter. Therefore, elevated Na^+ and Cl^- concentrations were most likely due to the use

of road salt on the car park in the northern part of the site. The elevated NO_3^- concentration in the measured mixed water compared to the calculated one, likely reflected lower denitrification rates in soils and aquifer caused by lower temperatures. Fe concentrations were found to be much lower than theoretical ones. This is not surprising, since the sample was taken behind the cartridge filters. However, Fe_{part} and $Fe_{filtered}$ were above calculated Fe solubility (<1µg·L^{-1}). This indicates a transport of freshly precipitated, not yet coagulated Fe particles that could pass the cartridge filters and Fe^{3+} colloids, and/or dissolved Fe^{2+}. The occurrence of Fe_{part} and $Fe_{filtered}$ therefore show that the Fe oxidation and precipitation process was not yet fully completed when the water reached the filter pads.

3.2 Speciation of aqueous phase mercury in groundwater.

. Hg-bound to DOM (Hg^{II}_b) was the most abundant Hg form in DOC-rich samples (W35 and W36), but total Hg (Hg_{tot}) concentrations were found to be comparatively low (Figure 1; Table 1). Highest Hg_{tot} concentrations were encountered in the wells with lowest DOC content, (W2 and W38, Table 1) with inorganic divalent mercury (Hg^{II}_a, mainly $(HgCl_2)^0$, according to geochemical modeling; cf. Figure S3b+g) being the dominant species group. This inverse relationship between Hg content and DOC concentration might be explained by an enhanced solid phase sorption of Hg in peat rich, DOC releasing parts of the aquifer. Dissolved gaseous mercury was found to be dominant in W7a during the anoxic event (22.5 µg·L^{-1}), consistent with thermodynamic equilibrium calculations (Figure S3c). During the suboxic event most Hg in W7a was particulate, due to binding to suspended HFO, corresponding with the high content of Fe particles (Table 1).

3.3 Composition of HFO precipitates.

Concentrations of Fe, S, C_{org}, Al, Mn, and Hg in HFO precipitates are summarized in Table 2. Element concentrations in the samples indicate that the sampled precipitates were agglomerates of HFO with aluminosilicates and other mineral precipitates rather than pure iron oxides. However, HFO was the dominant compound in all samples. Total mercury contents of the precipitates were extremely high, varying between 0.93 ± 0.04% (m/m) in those sampled

directly from W7a and 4.4 ± 0.3% in samples from the filter pads installed after the mixing chamber. Organic carbon contents were found to be 1.6 ± 0.4 and 4.7 ± 0.7% in W7a and filter pad samples, respectively, indicating co-precipitation of DOM on iron hydroxides as described elsewhere (Henneberry et al., 2012; Riedel et al., 2013). Binding of Hg to reduced sulfur (-S) or thiol (-SH) functional groups bearing co-precipitated organic matter (e.g. Henneberry et al., 2011; Gu et al., 2014) could therefore be important. Iron oxides in high-DOC water also can get covered with a coating of organic matter (Fu and Quan, 2006; Gu et al., 1994, 1995). However, molar Hg concentrations in precipitate samples exceeded the sulfur (S) content by a factor between two and eight (Table 2).

Table 1. Concentrations of major solutes, field parameters, mixing ratios, well depths, Fe, and Hg species in groundwater and water behind the mixing chamber. Errors represent one standard deviation of threefold measurements (Fe, DOC, Hg_{total}, Hg^0) or combined standard deviation of threefold measurements of initial values (Fe_{part}, Hg_{part}, Hg^{II}_a and Hg^{II}_b). Fe^{II} and Fe^{III} are "dissolved" concentrations (<0.45 µm). Shown analyses are from different sampling events. Concentrations of calculated mixed water as calculated by PHREEQC, using the given mixing ratios.

	W7a (suboxic)	W7a (anoxic)	W2	W35	W36	W38	measured mixed Water	calculated mixed Water
mixing ratios	29.4%		29.4%	5.9%	5.9%	29.4%	-	-
well depth (m)	9.0		11.9	5.3	5.3	18.0	-	-
pH	6.40	6.42	6.34	6.77	6.42	6.22	6.39	6.38
Eh (mV)	397	263	n.d.	474	524	n.d.	n.d.	-
Temp (°C)	9.7	10.1	11.9	15.2	15.2	11.8	8.9	11.6
Conductivity ($\mu S \cdot cm^{-1}$)	319	393	520	760	490	347	562	-
Alkalinity ($mmol \cdot L^{-1}$)	1.89	1.67	0.76	7.09	3.98	1.43	n.d.	-
$mg \cdot L^{-1}$								
Ca	27.7	35.0	33.6	87.8	55.8	30.8	37.1	37.6
Na	21.7	25.1	9.7	31.0	22.3	25.4	41.4	20.7
Mg	5.2	5.3	8.8	11.0	6.5	8.9	9.7	7.8
K	3.5	3.3 ± 0.1	5.0	44.7	14.1	2.0	5.1	6.0
NH_4^+	n.d.	0.32 ± 0.02	n.d.	n.d.	n.d.	n.d.	n.d.	-
F	0.2	0.2	0.1	7.5	2.8	0.09	0.3	0.6
Cl	48.5	64.6	117	22.1	30.2	62.7	122	76
NO_2^-	n.d.	0.02	n.d.	n.d.	n.d.	n.d.	n.d.	-
Br	< LOQ	0.03	< LOQ	< LOQ	< LOQ		< LOQ	-
NO_3^-	0.9	0.1*	7.0	1.3	6.8	4.6	20.4	4.7
SO_4^{2-}	2.7	3.3	12.7	18.5	18.7	12.0	16.9	10.3
DOC	4.6 ± 0.2	4.1 ± 1.2	1.1 ± 0.0	5.3 ± 0.0	3.4 ± 0.1	0.8 ± 0.0	1.9 ± 0.6	2.4
O_2	0.9	0.0	4.1	3.6	3.6	4.2	1.7	3.1
$\mu g \cdot L^{-1}$								
Fe_{total}	< LOQ	2537 ± 46	< LOQ	< LOQ	< LOQ	< LOQ	99 ± 1	523
$Fe_{filtered}$	< LOQ	760 ± 15	< LOQ	< LOQ	< LOQ	< LOQ	43 ± 3	
Fe^{II}	n.d.	736 ± 9	n.d.	n.d.	n.d.	n.d.	n.d.	-
Fe^{III}	n.d.	24 ± 22	n.d.	n.d.	n.d.	n.d.	n.d.	-
Fe_{part}	>32,000[#]	1776 ± 61	n.d.	n.d.	n.d.	n.d.	56 ± 4	-
Mn		2873	272	43.7	53.2	22.3	195	937
Hg_{total}	101.5 ± 0.2	43.3 ± 0.1	871 ± 10	14.3 ± 0.1	32.7 ± 1.0	349 ± 4	403 ± 11	375
Hg^0	7.4 ± 0.3	22.5 ± 0.9	29.8 ± 0.2	3.2 ± 0.0	9.3 ± 0.2	6.4 ± 0.5	n.d.	-
inorganic Hg (Hg^{II}_a)	13.0 ± 0.7	4.8 ± 2.7	752 ± 5	<0.2*	8.9 ± 0.3	346 ± 13	n.d.	-
DOM bound Hg (Hg^{II}_b)	37.5 ± 1.1	12.0 ± 3.2	<0.2*	11.0 ± 0.2	12.6 ± 0.8	<0.2*	n.d.	-
Hg_{part}	43.6 ± 0.9	4.0 ± 0.5	97 ± 14	0.7 ± 0.2	1.9 ± 1.7	31 ± 14	n.d.	-

*< LOQ below limit of quantification n.d. not determined *calculated by subtracting NH_4^+ and NO_2^- from lab measured NO_3^-*

[#] estimated from amount of obtained Fe precipitates

Table 2. Elemental composition (wt%) of suspended material and precipitates from temporarily anoxic groundwater well W7a and retained precipitates from filter pads behind the mixing chamber, where oxic and anoxic groundwaters mix. Hg (fresh) is total Hg, and Hg (dried) is the Hg concentration after drying and vaporization of Hg^0.

		precipitates from well W7a	precipitates behind mixing chamber
Fe	(%)	15.1 ± 3.2	13.4 ± 2.4
Hg (fresh)	(%)	0.93 ± 0.04	4.4 ± 0.3
Hg (dried)	(%)	0.16 ± 0.02	0.32 ± 0.1
C_{org}	(%)	1.6 ± 0.4	4.7 ± 0.7
S	(%)	0.09 ± 0.02	0.09 ± 0.01
Al	(%)	6.8 ± 0.9	1.1 ± 0.5
Mn	(%)	0.14 ± 0.03	0.15 ± 0.09

3.4 Mercury speciation analyses of precipitates.

Results of solid phase Hg thermo-desorption measurements are shown in Figure 2. Fresh samples from filter pads after the groundwater mixing chamber (Figure 2a) showed one dominant peak in the range of ~30 to 120°C with a maximum extinction temperature (E_{max}) of 69 ± 4°C. Samples from the temporarily anoxic well W7a (Figure 2b) exhibited two distinct peaks in the range of ~ 30-120°C and 120 to 250°C with E_{max} temperatures of 71 ± 18 and 185 ± 9°C, respectively. Comparison with standard materials (Figure 2e to h) indicate the first peak is Hg^0 (Figure 2e, E_{max}: 95 ± 13°C). The slight shift of the peak maxima is assumed to be due to: A) The high water content of the samples (107 ± 5%), leading to a temperature gradient inside the sample vessel and to a slower warming of the thermocouple during Hg-TD-AAS measurement, and B) A finer dispersion of Hg^0 in the samples than in the standard material (Hg droplets in a sand matrix), leading to higher surface areas and faster diffusion during heating. The second peak is assumed to reflect Hg^{II}-species. Figure 2c and d show thermo-desorption profiles of the precipitates after drying at 105°C for > 24 h. We concluded that these curves reflect the release of Hg^{II} bound to the precipitates, after all Hg^0 has been evaporated during drying.

Figure 2f-h show thermo-desorption curves of $HgCl_2$, Hg bound to humic acid, and $HgCl_2$ spiked HFO.

Thermo-desorption profiles of the dried precipitate samples (E_{max}: 199 ± 10°C) matched the $HgCl_2$ standard (Figure 2f, E_{max}: 193 ± 11°C), but Hg^{II} adsorbed to ferrihydrite (Figure 2h, E_{max}: 215 ± 7°C) is also similar so no definite allocation could be made. The analyzed standards of sulfur bound Hg like meta-cinnabar (meta-HgS, Figure 2e), cinnabar (HgS, Figure 2e), and Hg bound to thiol groups in organic matter (Figure 2g) showed somewhat higher E_{max} temperatures: 227 ± 8°C (meta-HgS), 230 ± 2°C (HA from peat), 229 ± 10°C (commercial HA: PGS 10), and 324 ± 4°C (HgS). Fitting of Gaussian shaped curves to the spectra of W7a samples and calculation of peak areas yielded in a relative proportion of 55 ± 11% of Hg^0 (5.1 ± 1.2 $g \cdot kg^{-1}$) and 45 ± 11 % of adsorbed Hg^{II}. Calculated from the difference between Hg contents found in fresh and dried samples of W7a (Table 2), the proportion of Hg^0 was even higher (83 ± 4%). Samples from the filter pads also exhibited residual Hg^{II} after drying (7.5 ± 3.9% of total Hg, Table 2) but the Hg^{II} peak was almost entirely overlapped by Hg^0 and emerged only after drying (Figure 2a+c).

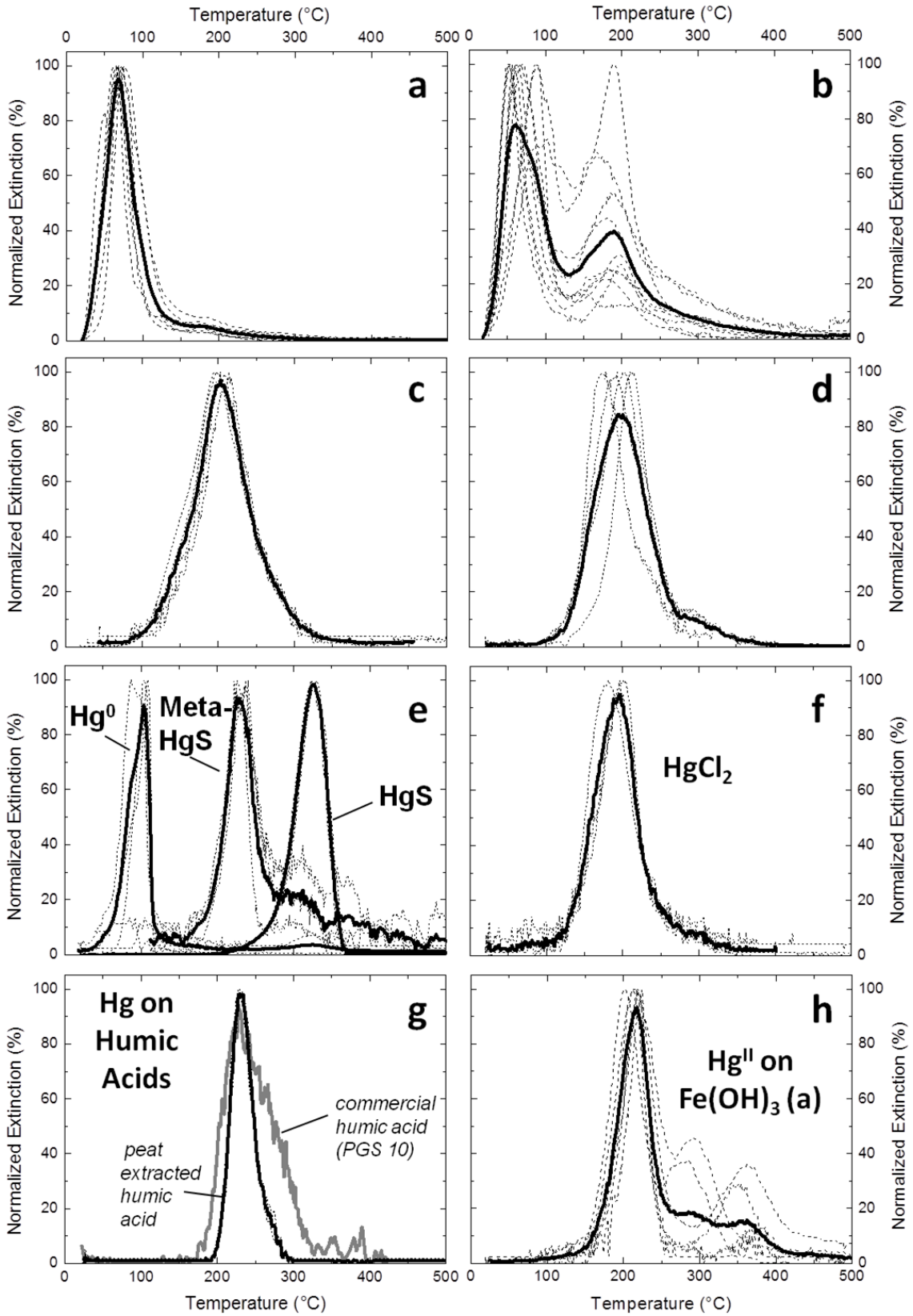

Figure 2. Hg-TD-CVAAS spectra for precipitate samples and standard materials (dashed curves are single measurements, solid lines averaged curves). Hg-TD curves of fresh and furnace dried precipitates, obtained from filters behind mixing chamber are depicted in (a) and (c), respectively. Spectra from fresh and furnace dried precipitates extracted from temporarily anoxic groundwater well W7a are shown in (b) and (d), whereas Hg release curves of standard materials are drawn in (e)-(h).

Regardless of the method of calculation, most Hg in all precipitate samples was Hg^0. But because uncharged, metallic mercury cannot be chemisorbed, a reasonable explanation for the high Hg^0 concentrations found on the precipitates could be its physical sorption and co-precipitation. Before precipitation, however, Hg^0 somehow has to be formed through reduction of Hg^{II}. Three possible processes could account for this: Abiotic reduction of Hg^{II} by organic matter (Gu et al., 2011), microbial reduction (Barkay et al., 2003; Wiatrowski et al., 2006), or reduction during oxidation of Fe^{II} as recently shown in lab experiments (Charlet et al., 2002; Peretyazhko et al., 2006; Wiatrowski et al., 2009; Amirbahman et al., 2013; Pasakarnis et al., 2013). Direct reduction through organic matter at least does not seem to be dominant here. In contrast to aqueous phase Hg speciation, where humic bound Hg (Hg^{II}_b) was found to be a major species in samples from W7 (Table 1), Hg-TD measurements indicated that Hg^{II} in the precipitates was not primarily bound to humic substances (Figure 2). Nevertheless, the presence of organic matter is certainly a precondition for Hg^0 formation, if not as a direct reducing agent for Hg^{II} at least indirectly as substrate for microorganisms. Bacterial activity is also indispensible for the formation of Hg^0, at the least for providing dissolved Fe^{II} through reduction of iron during anaerobic organic matter mineralization. Many eubacteria are also able to directly reduce Hg^{II} (e.g. Geobacter sp.) (e.g. Barkay et al., 2003), although very high Hg concentrations are lethal even to so called “mercury-resistant” bacteria (von Canstein et al., 2002). Because molar concentration of Fe^{II} exceeded that of Hg^{II} by more than 60 times in the anoxic groundwater well (Table 1) Hg^0 formation through (surface catalyzed) reduction of Hg^{II} by HFO bound Fe^{II}, either directly to Hg^0 (Pasakarnis et al., 2013) or via prior formation of Hg^I and subsequent further reduction (Amirbahman et al., 2013) is also likely to occur.. In natural systems most likely all of these processes simultaneously contribute to Hg^{II} reduction, although abiotic, DOM or Fe^{II} induced reduction is most likely predominant due to high DOC and Fe concentrations and fast reaction kinetics (Amirbahman et al., 2013; Matthiessen, 1998). Mishra et al. (2011) have shown that the effectiveness of mixed Fe^{II}/Fe^{III} phases in reducing biomass bound Hg^{II} strongly depends on Hg binding site distribution (carboxylic

or sulfhydryl groups). Gu et al. (2011) demonstrated that Hg^{II} reduction by humic acid (HA) peaked at HA concentrations of 0.2 $mg \cdot L^{-1}$, decreased rapidly with increasing HA concentrations and was undetectable above HA contents of 5 $mg \cdot L^{-1}$, due to effective prevention of reduction by Hg^{II} binding to reduced S or thiol functional groups. Therefore, DOM quality (humic/fulvic acid and thiol binding sites) and variability of aqueous Hg concentrations would be the key factors to be determined in order to elucidate relative contributions of possible reduction pathways for Hg^0 production.

As discussed in chapter 3.3., co-precipitation of Hg-DOM complexes on HFO could also have occured. Gu et al. (2011) investigated interactions of Hg^0 with DOM and found increasing Hg^0 sorption with increased organic matter. However, they also showed that physically sorbed Hg^0 was oxidized to Hg^{II} by ligand-induced oxidative complexation and subsequent formation of Hg^{II}-thiol complexes took place. They stated: “Reduced DOM (…) sequesters Hg(0), but as Hg(II), not as Hg(0) itself”. This in turn means, that if Hg^0 would have been predominantly sorbed not directly onto HFO itself but on HFO-DOC co-precipitates, a distinct signal of HA-bound Hg in thermo desorption curves of the precipitates (Figure 2) should be visible, which is not the case. Therefore we concluded, that DOM-HFO co-precipitates did not play a dominant role in Hg^0 precipitation here.

3.5 Modeling Hg speciation and sorption to HFO.

Hg^0 was calculated to be the dominant dissolved Hg species in the anoxic sample from well W7a whereas Hg-sulfide complexes were restricted to strongly reducing conditions not observed on the site (see predominance diagrams in Figure S3, Supplementary Material). Thermo desorption diagrams also indicated irrelevance of Hg sulfide species, since no HgS was found on the HFO precipitates (Figure 2). DOM-complexes were calculated to predominate in lesser contaminated wells (W35, W36) but were predicted to be negligible in wells with highest Hg concentrations (W2, W38). Here inorganic Hg forms were dominating, most likely due to an oversaturation of humic binding sites. Thus, modeling results were in excellent agreement with measured aqueous Hg speciation (Figure 1, Table 1).

Results of the modeled sorption of Hg on HFO are shown in Table 3, wherein the modeled concentrations of the different sorption species of Hg were summed up, related to the amount of HFO calculated to precipitate, and converted into mass fractions (wt %).

Table 3. Results of Hg sorption modeling to HFO with the models from Dzombak & Morel (1990) (D&M) and Tiffreau et al. (1995). Portions of mercury (wt %) on hydrous ferric oxide were obtained by summing up calculated Hg species sorbed to HFO and relating them to the amount of precipitated ferrihydrite ($Fe(OH)_3$) as predicted in the models. Values in brackets are percentages of modeled to measured Hg^{II} and total Hg concentrations, respectively.

	modeled Hg content (wt %)		**measured Hg content (wt %)**	
	D&M	Tiffreau	Hg^{II}	total Hg
W7a oxic	0.001 *(0.9 and 0.2%)*	0.03 *(18.7 and 3.1%)*	0.16 ± 0.02	0.93 ± 0.04
W7a anoxic	0.001 *(0.4 and 0.01%)*	0.01 *(8.5 and 0.4%)*		
modeled mixed water	0.02 *(5.6 and 0.4%)*	0.19 *(60.2 and 4.4%)*	0.32 ± 0.10	4.43 ± 0.35
real mixed water	0.003 *(1.0 and 0.1%)*	0.11 *(33.9 and 2.5%)*		

Proportions of Hg sorption to HFO calculated by means of the Tiffreau model are closer to the measured values in all four scenarios, but the predicted Hg concentrations were always lower than the observed ones. The model predicted a maximum of 60% (Table 3) of the measured Hg in dried precipitates (Hg^{II}). Certainly, the underestimation of Hg^{II} sorption can be attributed to differences between artificial and natural HFO. Surface area and reactivity of lab produced HFO used for development and calibration of the two models, were most likely lower than those of natural ferrihydrite due to the aging of HFO prior to sorption experiments (Dzombak and Morel, 1990). However, when compared to the total Hg concentrations, the predictive power of the models decreases to a maximum prediction rate of only 4.4%. This poor model performance was clearly caused by the non-implementation of Hg^0 as possible sorption species. This limitation of

the models may be of less importance when HFO is produced from Fe^{III} salts as for example commonly used in water treatment (Faust and Aly, 1998). But it can be crucial in natural systems where HFO originates from oxidation of Fe^{II} rich, anoxic waters, in which Hg^{II} can get reduced to Hg^0.

4 Conclusions

In summary, Hg^{II} reduction and co-precipitation on HFO as Hg^0 can be a key process in groundwater when redox conditions change from iron reduction to iron oxidation and formation of HFO takes place. Although site specific relative contributions of possible Hg^{II} reduction pathways (organic matter induced/microbial reduction or Fe^{II} as electron donor) were not quantified, general significance of the overall process has to be emphasized. Through Hg^{II} reduction to Hg^0 the behavior of Hg changes dramatically. Hg mobility in the gas phase is enhanced since Hg^0 is much more volatile than Hg^{II} (Henry`s law constants of Hg^0 and $HgCl_2$ are $1.1 \cdot 10^{-1}$ and $1.4 \cdot 10^{-6}$ $M \cdot atm^{-1}$, respectively (Ryaboshapko et al., 2001)). On the other hand, HFOs can serve as a temporal sink of Hg due to their strong Hg enrichment capacity as shown in this study. In this case, even re-reduction and subsequent dissolution of HFO would not lead to an immediate release of large amounts of Hg in solution, as Hg liberation would be limited by the relatively low solubility of Hg^0 (60 $\mu g \cdot L^{-1}$; Merck, 2014) compared to Hg^{II} (e.g. $HgCl_2$: 74 $g \cdot L^{-1}$; Merck, 2010). Bollen et al.(2008) showed that the formation of Hg^0 in a contaminated aquifer significantly contributed to the stationary nature of a $HgCl_2$ plume. However, Lamborg et al.(2013) observed a net Hg mobilization of sorbed naturally occuring Hg^{II} through wastewater induced anoxia and production of less strongly sorbing Hg^0. Hence, profound site-specific knowledge is needed to determine the risk potential of Hg in contaminated groundwater. Hg-thermo-desorption measurements were a useful tool enlightening understanding of sorption processes in Hg contaminated aquifers. Sorption of Hg^0 could not be predicted by geochemical modeling using PHREEQC and the available models for Hg binding to HFO, which do not yet consider formation, sorption or co-precipitation of Hg^0 on HFO, as shown in this study.

Acknowledgments

We thank the regional council of Freiburg i. Brsg. (Germany) for the permission to work on the investigated site and the Harres Pickel Consulting Group (HPC AG, Germany) for the excellent cooperation. Six anonymous reviewers provided valuable critiques and helped to enhance this manuscript.

Supplementary material

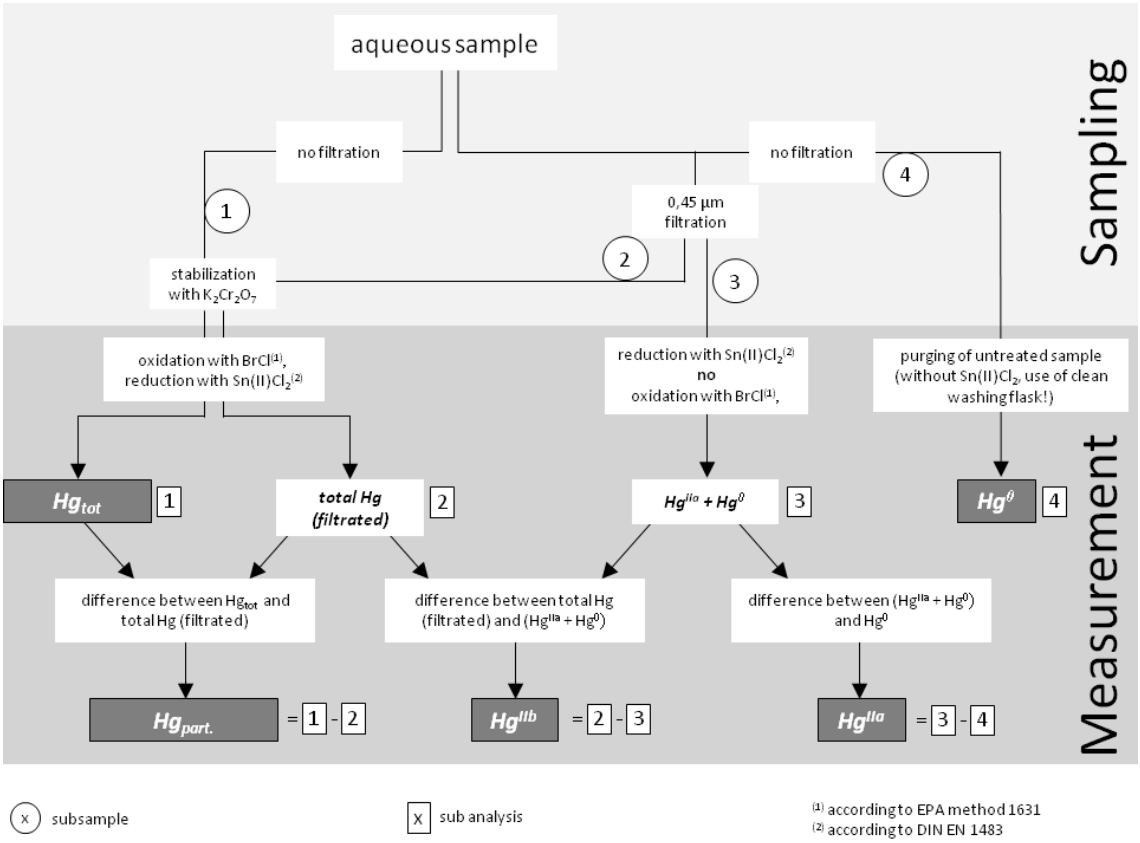

Figure S1. Scheme of sampling and analytical procedure used for aqueous phase Hg speciation measurements.

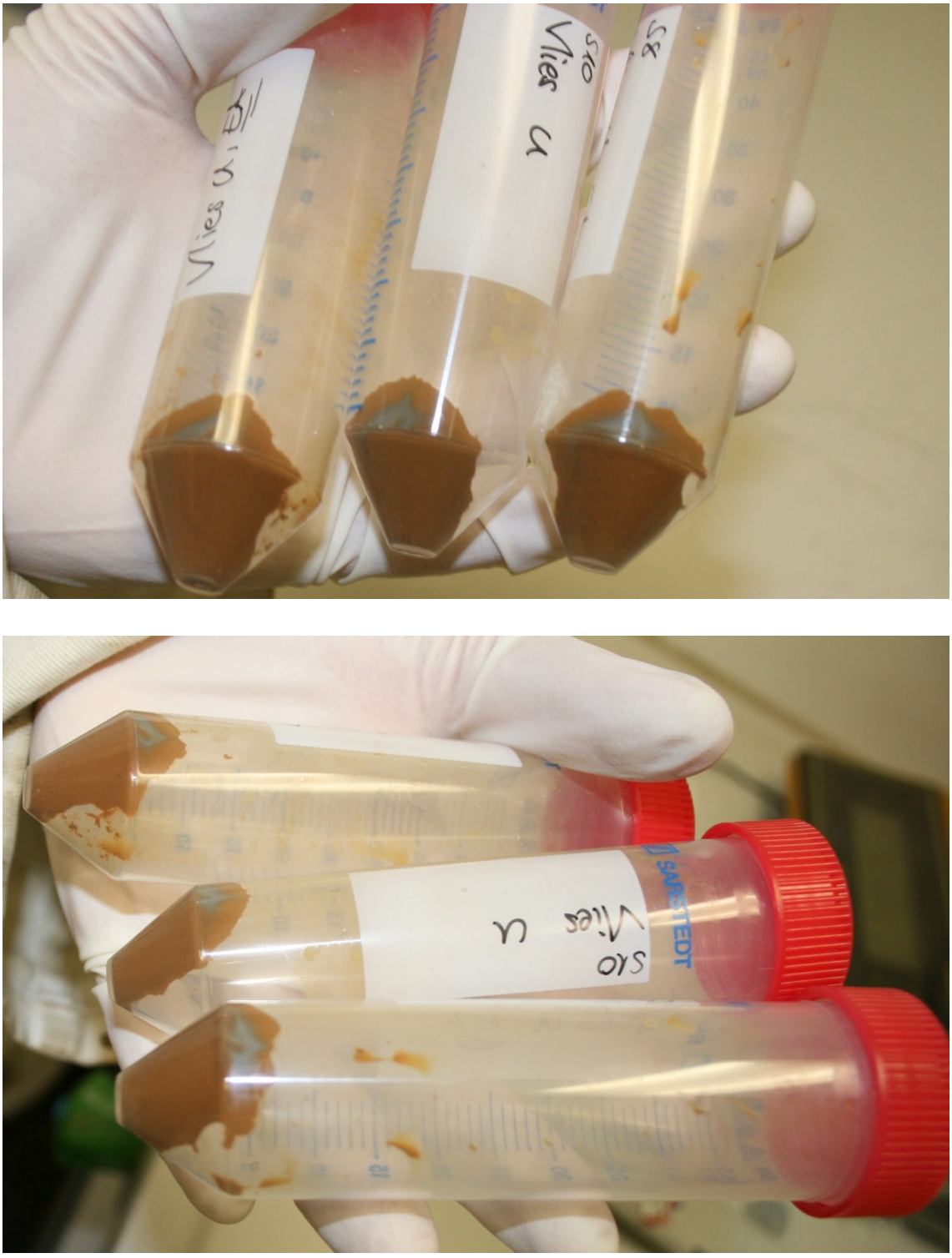

Figure S2. Centrifuged precipitate samples from filter pads with grayish streaks of metallic mercury (Hg^0).

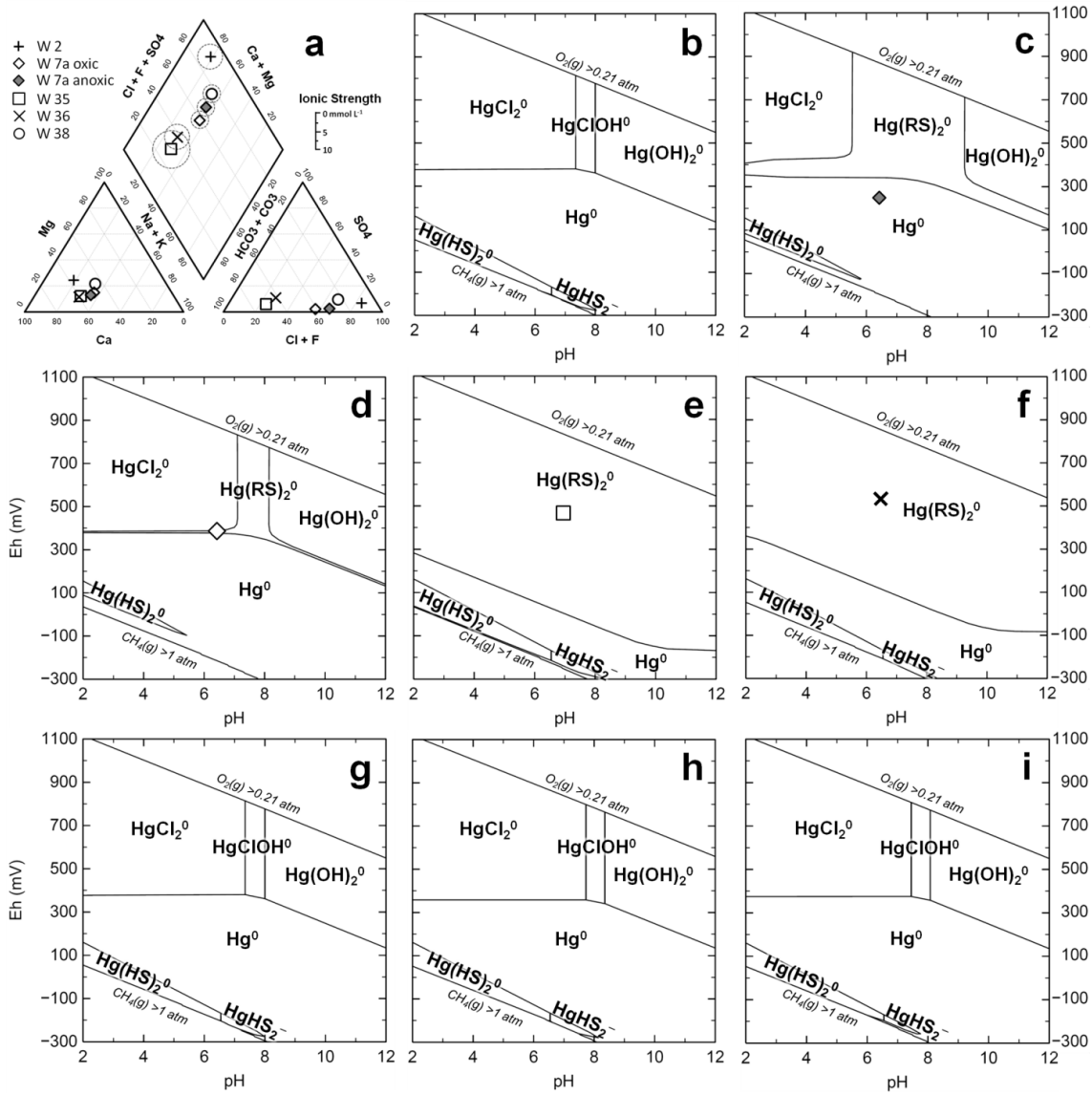

Figure S3. Characterization of groundwater: (a) Piper plot, constructed using template from USGS. (b -h) Predominance diagrams of Hg species in solution, calculated using PhreePlot (Kinniburgh and Cooper, 2014) from groundwater analyses presented in Table S2. Hg(RS)20 is a two coordinated Hg complex with thiol groups from dissolved organic matter. Concentration of thiol groups was assumed to be 0.15% of DOC on a mass basis (Qian et al., 2002; Skyllberg et al., 2003, 2005; Skyllberg, 2008) (b) W2: 871 µg·L-1 Hg, 1.1 mg·L-1 DOC (c) W7a (anoxic): 43 µg·L-1 Hg, 4.1 mg·L-1 DOC (d) W7a (suboxic): 102 µg·L-1 Hg, 4.6 mg·L-1 DOC (e) W35: 14.3 µg·L-1 Hg, 5.3 mg·L-1 DOC (f) W36: 32.7 µg·L-1 Hg, 3.4 mg·L-1 DOC (g) W38: 349 µg·L-1 Hg, 0.8 mg·L-1 DOC (h) mixed water (measured): 403 µg·L-1 Hg, 1.9 mg·L-1 DOC (i) mixed water (calculated): 375 µg·L-1 Hg, 2.3 mg·L-1 DOC.

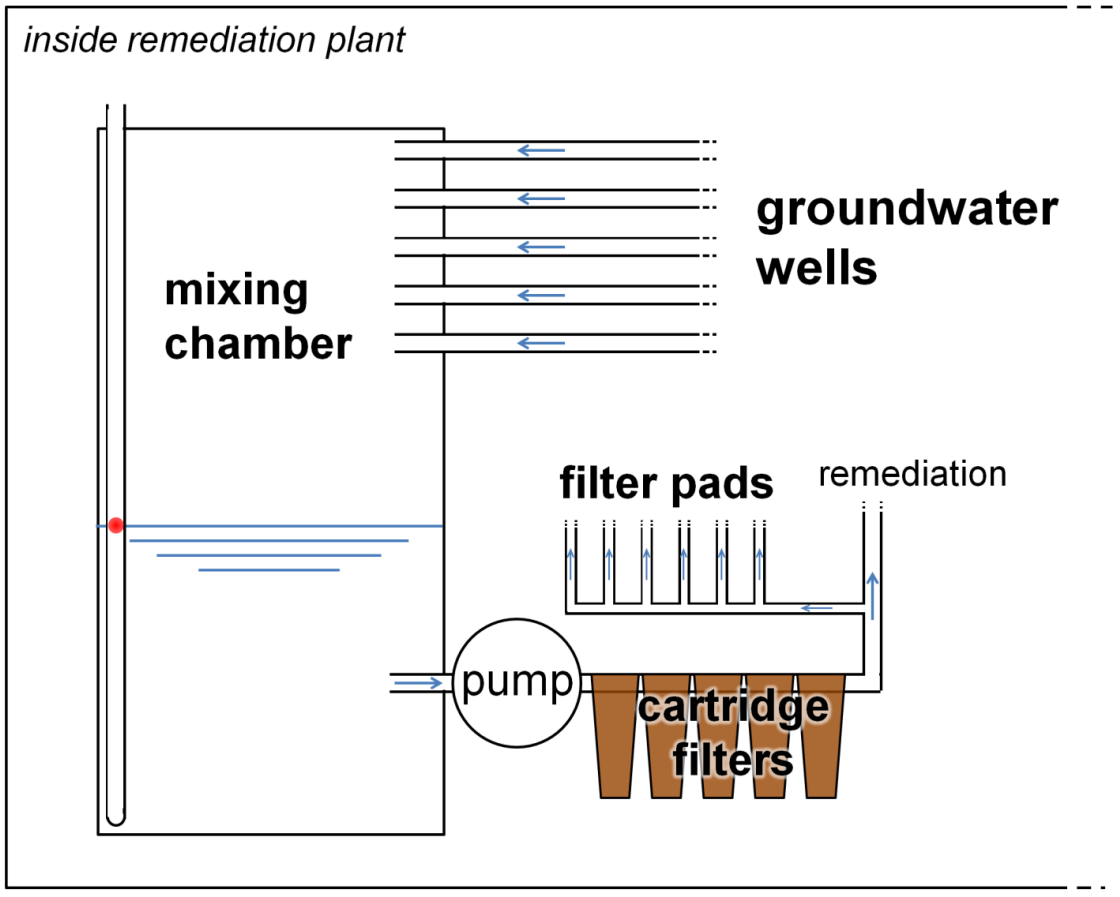

Figure S4. Scheme of the HFO sampling setup inside the remediation plant. Minimum residence time of mixed water is 15 minutes. Pipe material from the wells to the remediation plant and inside the plant is HDPE. PVC hoses were used for the last meter to the filter pads.

Table S1. Limits of quantification, applied standard reference materials, and recovery rates for different analytes.

Analyte	Unit	Analytical Instrument	Limit of Quantification (LOQ)*	Standard Reference Material (SRM)	Certified Concentration	Obtained Concentration	Recovery Rate
Hg	$\mu g \cdot L^{-1}$	CV-AAS	0.15	"Trace Metals" RTC 1-WP	78.0 ± 4.0	78.8 ± 1.5	101.0%
Hg	$\mu g \cdot L^{-1}$	CV-ICP-OES	17.9	"	63.6 ± 1.6	66.3 ± 4.3	104.3%
Hg in digest	$\mu g \cdot kg^{-1}$	CV-AAS	97.4#	"Chinese Soil" NCS-DC 73322	590 ± 50	480 ± 22.5	81.3%
C_{org}	%	CNS Analyzer	0.0003	"Chinese Soil" NCS-DC 73322	0.62 ± 0.08	0.60 ± 0.01	97.3%
S	%	CNS Analyzer	0.0005	Sulfanilamid	18.62	18.64 ± 0.02	100.1%
NO_2^-	$mg \cdot L^{-1}$	Photometer	0.01				
NH_4^+	$mg \cdot L^{-1}$	Photometer	0.25				
DOC	$mg \cdot L^{-1}$	TIC/TOC Analyzer	0.51	"natural water from Lake Superior" EC ION-915	1.37 ± 0.41	1.62 ± 0.05	118.0%
Cl^-	$mg \cdot L^{-1}$	IC	0.49	"	1.42 ± 0.21	1.48 ± 0.30	104.2%
NO_3^-	$mg \cdot L^{-1}$	IC	0.02	"	25.7 ± 3.5	24.2 ± 4.1	94.2%
SO_4^{2-}	$mg \cdot L^{-1}$	IC	0.75	"	26.0 ± 2.0	24.4 ± 0.9	93.7%
F^-	$mg \cdot L^{-1}$	IC	0.01	"	0.03	0.04	133.3%
Br^-	$mg \cdot L^{-1}$	IC	0.02	"			
Ca	$mg \cdot L^{-1}$	ICP-OES	3.4	"	10.5 ± 0.4	10.8 ± 0.1	102.6%
Na	$mg \cdot L^{-1}$	ICP-OES	3.2	"	5.38 ± 0.10	5.46 ± 0.01	101.4%
K	$mg \cdot L^{-1}$	ICP-OES	0.87	"	0.84 ± 0.04	0.75 ± 0.04	89.1%
Mn	$\mu g \cdot L^{-1}$	ICP-OES	14	"	4.3 ± 0.2	4.4 ± 0.2	101.1%
Fe	$\mu g \cdot L^{-1}$	ICP-OES	36	"	91.2 ± 5.8	96.7 ± 1.7	106.0%
Fe	$\mu g \cdot L^{-1}$	Photometer	33	"	91.2 ± 5.8	96.5 ± 0.7	105.8%
Fe in digest	$g \cdot kg^{-1}$	ICP-OES	2.3#	"Lake Sediment" IAEA-SL-1	67.4 ± 2.4	65.5 ± 0.5	97.1%

* Calculated from respective calibration according to DIN 32645 or Neitzel (2002).

For comparison with SRM, concentration converted from mass per volume to mass concentration by dividing through weight-in mass of SRM.

Table S2. Results of HFO sorption modeling.

Dzombak&Morel			**Tiffreau**		
7a.2 oxic	*mol/l*	*mg/l*	***7a.2 oxic***	*mol/l*	*mg/l*
Amount Ferrihydrit	5.73E-04	51	Amount Ferrihydrit	5.73E-04	51
			SurfaOHgCl	6.93E-08	
Hfo_sOHg+	1.13E-09		SurfaOHg+	2.78E-09	
Hfo_wOHg+	2.49E-09		SurfaOHgOH	1.56E-09	
Hg in DDL	8.27E-11		Hg in DDL	6.89E-11	
Hg sorbed	3.70E-09	7.4E-04	Hg sorbed	7.37E-08	1.5E-2
Hg Portion HFO (%)	6.46E-04	**0.00146**	Hg Portion HFO (%)	1.29E-02	**0.029**
7a.3 anoxic	*mol/l*	*mg/l*	***7a.3 anoxic***	*mol/l*	*mg/l*
Amount Ferrihydrit	3.17E-05	2.82	Amount Ferrihydrit	3.17E-05	2.82
			SurfaOHgCl	3.14E-09	
Hfo_sOHg+	2.66E-11		SurfaOHg+	1.34E-10	
Hfo_wOHg+	5.67E-11		SurfaOHgOH	8.59E-11	
Hg in DDL	1.81E-12		Hg in DDL	1.74E-12	
Hg sorbed	8.50E-11	1.70E-05	Hg sorbed	1.87E-09	3.7E-04
Hg Portion HFO (%)	2.68E-04	**0.0006**	Hg Portion HFO (%)	5.89E-03	**0.013**
Mixed Water (measured)	*mol/l*	*mg/l*	***Mixed Water (measured)***	*mol/l*	*mg/l*
Amount Ferrihydrit	1.68E-06	0.15	Amount Ferrihydrit	1.68E-06	0.15
Hfo_sOHg+	6.36E-12		SurfaOHgCl	7.76E-10	
Hfo_wOHg+	1.78E-11		SurfaOHg+	2.19E-11	
Hg in DDL	8.70E-13		SurfaOHgOH	1.19E-11	
Hg sorbed	2.50E-11	5.0E-06	Hg in DDL	8.34E-13	
			Hg sorbed	7.58E-07	1.6E-04
Hg Portion HFO (%)	1.50E-03	**0.003**	Hg Portion HFO (%)	4.84E-02	**0.11**
Mixed Water (calculated)	*mol/l*	*mg/l*	***Mixed Water (calculated)***	*mol/l*	*mg/l*
Amount Ferrihydrit	9.3E-06	0.83	Amount Ferrihydrit	9.3E-06	0.83
			SurfaOHgCl	7.49E-09	
Hfo_sOHg+	9.68E-11		SurfaOHg+	3.05E-10	
Hfo_wOHg+	6.45E-10		SurfaOHgOH	1.79E-10	
Hg in DDL	3.92E-12		Hg in DDL	4.29E-12	
Hg sorbed	7.46E-10	1.5E-06	Hg sorbed	7.98E-09	1.6E-03
Hg Portion HFO (%)	8.02E-03	**0.018**	Hg Portion HFO (%)	8.59E-02	**0.19**

Table S3. Applied equilibrium constants (log K values) of aqueous Hg species and complexes.

AQUEOUS COMPLEXES

Name	Reaction	log K
$Hg(CO_3)_2^{2-}$	Hg(OH)2 + 2H+ + 2CO3-2 = Hg(CO3)2-2 + 2H2O	21.772
$Hg(Cyanide)_2$	2Cyanide- + 2H+ + Hg(OH)2 = Hg(Cyanide)2 + 2H2O	38.944
$Hg(Cyanide)_3$-	3Cyanide- + 2H+ + Hg(OH)2 = Hg(Cyanide)3- + 2H2O	42.504
$Hg(Cyanide)_4^{2-}$	4Cyanide- + 2H+ + Hg(OH)2 = Hg(Cyanide)4-2 + 2H2O	45.164
$Hg(HS)_2$	2H+ + 2HS- + Hg(OH)2 = Hg(HS)2 + 2H2O	45.242*
$Hg(NH_3)_2^{2+}$	Hg(OH)2 + 2NH4+ = Hg(NH3)2+2 + 2H2O	5.506
$Hg(NH_3)_3^{2+}$	Hg(OH)2 + 3NH4+ = Hg(NH3)3+2 + H+ + 2H2O	-3.138
$Hg(NH_3)_4^{2+}$	Hg(OH)2 + 4NH4+ = Hg(NH3)4+2 + 2H+ + 2H2O	-11.482
$Hg(NO_3)_2$	2H+ + Hg(OH)2 + 2NO3- = Hg(NO3)2 + 2H2O	5.38
$Hg(OH)_3^-$	H2O + Hg(OH)2 = Hg(OH)3- + H+	-14.897
$Hg(SR)_2$	2RS- + Hg(OH)2 + 2H+ = Hg(SR)2 + 2H2O	48.142#
Hg^{2+}	2H+ + Hg(OH)2 = Hg+2 + 2H2O	6.194
$Hg^0_{(aq)}$	0.5Hg2+2 + e- = Hg	6.5667
Hg_2^{2+}	4H+ + 2Hg(OH)2 + 2e- = Hg2+2 + 4H2O	43.185
$HgBr^+$	Br- + 2H+ + Hg(OH)2 = HgBr+ + 2H2O	15.803
$HgBr_2$	2Br- + 2H+ + Hg(OH)2 = HgBr2 + 2H2O	24.2725
$HgBr_2I_2^{2-}$	2Br- + 2H+ + Hg(OH)2 + 2I- = HgBr2I2-2 + 2H2O	32.3994
$HgBr_3^-$	3Br- + 2H+ + Hg(OH)2 = HgBr3- + 2H2O	26.7025
$HgBr_3I^{2-}$	3Br- + 2H+ + Hg(OH)2 + I- = HgBr3I-2 + 2H2O	30.1528
$HgBr_4^{2-}$	4Br- + 2H+ + Hg(OH)2 = HgBr4-2 + 2H2O	27.933
HgBrCl	Br- + Cl- + 2H+ + Hg(OH)2 = HgBrCl + 2H2O	22.1811
HgBrI	Br- + 2H+ + Hg(OH)2 + I- = HgBrI + 2H2O	27.3133
$HgBrI_3^{2-}$	Br- + 2H+ + Hg(OH)2 + 3I- = HgBrI3-2 + 2H2O	34.2135

Continued on next page

Table S3. Equilibrium constants (log K values) of aqueous Hg species and complexes from applied database – Continued.

AQUEOUS COMPLEXES

Name	Reaction	log K
HgBrOH	Br- + H+ + Hg(OH)2 = HgBrOH + H2O	12.433
$HgCl^+$	Cl- + 2H+ + Hg(OH)2 = HgCl+ + 2H2O	13.494
$HgCl_2$	2Cl- + 2H+ + Hg(OH)2 = HgCl2 + 2H2O	20.194
$HgCl_3^-$	3Cl- + 2H+ + Hg(OH)2 = HgCl3- + 2H2O	21.194
$HgCl_4^{2-}$	4Cl- + 2H+ + Hg(OH)2 = HgCl4-2 + 2H2O	21.794
HgClI	Cl- + 2H+ + Hg(OH)2 + I- = HgClI + 2H2O	25.532
HgClOH	Cl- + H+ + Hg(OH)2 = HgClOH + H2O	10.444
$HgCyanide^+$	Cyanide- + 2H+ + Hg(OH)2 = HgCyanide+ + 2H2O	23.194
$HgCO_3$	Hg(OH)2 + 2H+ + CO3-2 = HgCO3 + 2H2O	18.272
HgF^+	F- + 2H+ + Hg(OH)2 = HgF+ + 2H2O	7.763
$HgHCO_3^+$	Hg(OH)2 + 3H+ + CO3-2 = HgHCO3+ + 2H2O	22.542
$HgHS_2^-$	Hg(OH)2 + H+ + 2HS- = HgHS2- + 2H2O	38.642*
HgI^+	2H+ + Hg(OH)2 + I- = HgI+ + 2H2O	19.603
HgI_2	2H+ + Hg(OH)2 + 2I- = HgI2 + 2H2O	30.8225
HgI_3^-	2H+ + Hg(OH)2 + 3I- = HgI3- + 2H2O	34.6025
HgI_4^{2-}	2H+ + Hg(OH)2 + 4I- = HgI4-2 + 2H2O	36.533
$HgNH_3^{2+}$	H+ + Hg(OH)2 + NH4+ = HgNH3+2 + 2H2O	5.75
$HgNO_3^+$	2H+ + Hg(OH)2 + NO3- = HgNO3+ + 2H2O	5.7613
$HgOH^+$	H+ + Hg(OH)2 = HgOH+ + H2O	2.797
$HgRS^+$	RS- + Hg(OH)2 + 2H+ = HgRS+ + 2H2O	26.145[#]
HgS_2^{2-}	2HS- + Hg(OH)2 = HgS2-2 + 2H2O	29.342*
HOHgSH	Hg(OH)2 + HS- + H+ = HOHgSH + H2O	22.447°

* log K from Drott et al. (2013) [#] log K from Skyllberg (2008)

° log K from Dyrssen & Wedborg (1991) as published in Skyllberg (2008). The lower of the two published constants has been used, according to Drott et al. (2013). All inserted log K values have been converted using thermodynamic data from Wagman et al. (1982) to fit format of applied minteq.v4.dat database.

References

Amirbahman, A., Kent, D.B., Curtis, G.P., Marvin-DiPasquale, M.C., 2013. Kinetics of Homogeneous and Surface-Catalyzed Mercury(II) Reduction by Iron(II). Environ. Sci. Technol. 47, 7204–7213. doi:10.1021/es401459p

Avotins, P., 1975. Adsorption and coprecipitation studies of mercury on hydrous iron oxide. (Thesis (Ph. D.)). Stanford University, Dept. of Applied Earth Sciences, Stanford.

Barkay, T., Miller, S.M., Summers, A.O., 2003. Bacterial mercury resistance from atoms to ecosystems. FEMS Microbiol. Rev. 27, 355–384. doi:10.1016/S0168-6445(03)00046-9

Barringer, J.L., Szabo, Z., Reilly, P.A., 2013. Occurrence and Mobility of Mercury in Groundwater, in: Bradley, P. (Ed.), Current Perspectives in Contaminant Hydrology and Water Resources Sustainability. InTech.

Biester, H., Scholz, C., 1996. Determination of mercury binding forms in contaminated soils: Mercury pyrolysis versus sequential extractions. Environ. Sci. Technol. 31, 233–239.

Bollen, A., Wenke, A., Biester, H., 2008. Mercury speciation analyses in HgCl2-contaminated soils and groundwater—Implications for risk assessment and remediation strategies. Water Res. 42, 91–100. doi:10.1016/j.watres.2007.07.011

Brosset, C., 1987. The behavior of mercury in the physical environment. Water. Air. Soil Pollut. 34, 145–166. doi:10.1007/BF00184757

Charlet, L., Bosbach, D., Peretyashko, T., 2002. Natural attenuation of TCE, As, Hg linked to the heterogeneous oxidation of Fe (II): an AFM study. Chem. Geol. 190, 303–319.

Dekov, V.M., Vanlierde, E., Billström, K., Garbe-Schönberg, C.-D., Weiss, D.J., Gatto Rotondo, G., Van Meel, K., Kuzmann, E., Fortin, D., Darchuk, L., Van Grieken, R., 2014. Ferrihydrite precipitation in groundwater-fed river systems (Nete and Demer river basins, Belgium): Insights from a combined Fe-Zn-Sr-Nd-Pb-isotope study. Chem. Geol. 386, 1–15. doi:10.1016/j.chemgeo.2014.07.023

DIN Deutsches Institut für Normung e. V., DIN German Institute for Standardization (Ed.), 2008. DIN 32645 (2008-11-00) Chemical analysis - Decision limit, detection limit and determination limit under repeatability conditions - Terms, methods, evaluation (Nachweis-, Erfassungs- und Bestimmungsgrenze unter Wiederholbedingungen - Begriffe, Verfahren, Auswertung).

Drott, A., Björn, E., Bouchet, S., Skyllberg, U., 2013. Refining Thermodynamic Constants for Mercury(II)-Sulfides in Equilibrium with Metacinnabar at Sub-Micromolar Aqueous Sulfide Concentrations. Environ. Sci. Technol. 47, 4197–4203. doi:10.1021/es304824n

Dyrssen, D., Wedborg, M., 1991. The sulphur-mercury(II) system in natural waters. Water. Air. Soil Pollut. 56, 507–519. doi:10.1007/BF00342295

Dzombak, D.A., Morel, F.M.M., 1990. Surface Complexation Modeling: Hydrous Ferric Oxide. John Wiley & Sons.

Eaton, A.D., Franson, M.A.H., 2005. Standard Methods for the Examination of Water & Wastewater. American Public Health Association.

Ehrlich, H.L., Newman, D.K., 2008. Geomicrobiology, Fifth Edition. CRC Press.

EN, European Committee for Standardization, 2007. Method 1483, Water quality- Determination of mercury- Method using atomic absorption spectrometry; German version.

Faust, S.D., Aly, O.M., 1998. Chemistry of Water Treatment, Second Edition. CRC Press.

Fu, H., Quan, X., 2006. Complexes of fulvic acid on the surface of hematite, goethite, and akaganeite: FTIR observation. Chemosphere 63, 403–410. doi:10.1016/j.chemosphere.2005.08.054

Gu, B., Bian, Y., Miller, C.L., Dong, W., Jiang, X., Liang, L., 2011. Mercury reduction and complexation by natural organic matter in anoxic environments. Proc. Natl. Acad. Sci. 108, 1479–1483. doi:10.1073/pnas.1008747108

Gu, B., Mishra, B., Miller, C., Wang, W., Lai, B., Brooks, S.C., Kemner, K.M., Liang, L., 2014. X-ray fluorescence mapping of mercury on suspended mineral particles and diatoms in a contaminated freshwater system. Biogeosciences 11, 5259–5267. doi:10.5194/bg-11-5259-2014

Gu, B., Schmitt, J., Chen, Z., Liang, L., McCarthy, J.F., 1995. Adsorption and desorption of different organic matter fractions on iron oxide. Geochim. Cosmochim. Acta 59, 219–229. doi:10.1016/0016-7037(94)00282-Q

Gu, B., Schmitt, J., Chen, Z., Liang, L., McCarthy, J.F., 1994. Adsorption and desorption of natural organic matter on iron oxide: mechanisms and models. Environ. Sci. Technol. 28, 38–46. doi:10.1021/es00050a007

Henneberry, Y.K., Kraus, T.E.C., Fleck, J.A., Krabbenhoft, D.P., Bachand, P.M., Horwath, W.R., 2011. Removal of inorganic mercury and methylmercury from surface waters following coagulation of dissolved organic matter with metal-based salts. Sci. Total Environ. 409, 631–637. doi:10.1016/j.scitotenv.2010.10.030

Henneberry, Y.K., Kraus, T.E.C., Nico, P.S., Horwath, W.R., 2012. Structural stability of coprecipitated natural organic matter and ferric iron under reducing conditions. Org. Geochem. 48, 81–89. doi:10.1016/j.orggeochem.2012.04.005

Herbert Jr, R.B., 1996. Metal retention by iron oxide precipitation from acidic ground water in Dalarna, Sweden. Appl. Geochem. 11, 229–235.

ISO, International Organization for Standardization, 1997. Method 11466, Soil quality- Extraction of trace elements soluble in aqua regia, German version.

ISO, International Organization for Standardization, 1996a. Method 11465, Soil quality - Determination of dry matter and water content on a mass basis - Gravimetric method, German version.

ISO, International Organization for Standardization, 1996b. Method 9963-1, Water quality- Determination of alkalinity -Part 1: Determination of total and composite alkalinity, German version.

Jiskra, M., Saile, D., Wiederhold, J.G., Bourdon, B., Björn, E., Kretzschmar, R., 2014. Kinetics of Hg(II) exchange between organic ligands, goethite, and natural organic matter studied with an enriched stable isotope approach. Environ. Sci. Technol. doi:10.1021/es503483m

Johannesson, K.H., Neumann, K., 2013. Geochemical cycling of mercury in a deep, confined aquifer: Insights from biogeochemical reactive transport modeling. Geochim. Cosmochim. Acta 106, 25–43. doi:10.1016/j.gca.2012.12.010

Kinniburgh, D.G., Cooper, D., 2014. PhreePlot: Creating graphical output with PHREEQC.

Lamborg, C.H., Kent, D., Swarr, G., Munson, K., Kading, T., O'Connor, A., Fairchild, G., LeBlanc, D., Wiatrowski, H., 2013. Mercury Speciation and Mobilization in a Wastewater-contaminated Groundwater Plume. Environ. Sci. Technol. 13239–13249. doi:10.1021/es402441d

Liang, L., McCarthy, J.F., Jolley, L.W., McNabb, J.A., Mehlhorn, T.L., 1993. Iron dynamics: Transformation of Fe(II)/Fe(III) during injection of natural organic matter in a sandy aquifer. Geochim. Cosmochim. Acta 57, 1987–1999. doi:10.1016/0016-7037(93)90088-E

LUBW, 2014. Hydrogeological Map of Baden Württemberg [WWW Document]. URL http://udo.lubw.baden-wuerttemberg.de/public/pages/map/default/index.xhtml (accessed 9.24.14).

Malcolm, R.L., 1991. Factors to be considered in the isolation and characterization of aquatic humic substances, in: Humic Substances in the Aquatic and Terrestrial Environment. Springer, pp. 7–36.

Matthiessen, A., 1998. Reduction of divalent mercury by humic substances — kinetic and quantitative aspects. Sci. Total Environ. 213, 177–183. doi:10.1016/S0048-9697(98)00090-4

Meili, M., Iverfeldt, A., Håkanson, L., 1991. Mercury in the surface water of Swedish forest lakes —concentrations, speciation and controlling factors. Water. Air. Soil Pollut. 56, 439–453. doi:10.1007/BF00342290

Merck, 2014. Safety Data Sheet Mercury:

Merck, 2010. Safety Data Sheet: Mercury(II)Chloride (HgCl2):

Mishra, B., O'Loughlin, E.J., Boyanov, M.I., Kemner, K.M., 2011. Binding of Hg II to High-Affinity Sites on Bacteria Inhibits Reduction to Hg 0 by Mixed Fe II/III Phases. Environ. Sci. Technol. 45, 9597–9603. doi:10.1021/es201820c

Nagy, K.L., Manceau, A., Gasper, J.D., Ryan, J.N., Aiken, G.R., 2011. Metallothionein-Like Multinuclear Clusters of Mercury(II) and Sulfur in Peat. Environ. Sci. Technol. 45, 7298–7306. doi:10.1021/es201025v

Neitzel, V., 2002. Calibration of Analytical Methods (part 2) non linear calibration functions (Die Kalibration von Analysenverfahren (Teil 2) Nicht lineare Kalibrationsfunktionen). Chem. Labor Biotech. 53.

Parkhurst, D.L., Apello, C.A.J., 2013. Description of Input and Examples for PHREEQC Version 3—A Computer Program for Speciation, Batch-Reaction, One-Dimensional Transport, and Inverse Geochemical Calculations (No. book 6, chap. A43), U.S. Geological Survey Techniques and Methods.

Pasakarnis, T.S., Boyanov, M.I., Kemner, K.M., Mishra, B., O'Loughlin, E.J., Parkin, G., Scherer, M.M., 2013. Influence of Chloride and Fe(II) Content on the Reduction of Hg(II) by Magnetite. Environ. Sci. Technol. 47, 6987–6994. doi:10.1021/es304761u

Peretyazhko, T., Charlet, L., Grimaldi, M., 2006. Production of gaseous mercury in tropical hydromorphic soils in the presence of ferrous iron: a laboratory study. Eur. J. Soil Sci. 57, 190–199. doi:10.1111/j.1365-2389.2005.00729.x

Qian, J., Skyllberg, U., Frech, W., Bleam, W.F., Bloom, P.R., Petit, P.E., 2002. Bonding of methyl mercury to reduced sulfur groups in soil and stream

organic matter as determined by x-ray absorption spectroscopy and binding affinity studies. Geochim. Cosmochim. Acta 66, 3873–3885. doi:10.1016/S0016-7037(02)00974-2

Ravichandran, M., 2004. Interactions between mercury and dissolved organic matter—a review. Chemosphere 55, 319–331. doi:10.1016/j.chemosphere.2003.11.011

Reis, A.T., Coelho, J.P., Rucandio, I., Davidson, C.M., Duarte, A.C., Pereira, E., 2015. Thermo-desorption: A valid tool for mercury speciation in soils and sediments? Geoderma 237–238, 98–104. doi:10.1016/j.geoderma.2014.08.019

Riedel, T., Zak, D., Biester, H., Dittmar, T., 2013. Iron traps terrestrially derived dissolved organic matter at redox interfaces. Proc. Natl. Acad. Sci. 110, 10101–10105. doi:10.1073/pnas.1221487110

Rumayor, M., Diaz-Somoano, M., Lopez-Anton, M.A., Martinez-Tarazona, M.R., 2015. Application of thermal desorption for the identification of mercury species in solids derived from coal utilization. Chemosphere 119, 459–465. doi:10.1016/j.chemosphere.2014.07.010

Rumayor, M., Diaz-Somoano, M., Lopez-Anton, M.A., Martinez-Tarazona, M.R., 2013. Mercury compounds characterization by thermal desorption. Talanta 114, 318–322. doi:10.1016/j.talanta.2013.05.059

Ryaboshapko, A., Ilyin, I., Bullock, R., Ebinghaus, R., 2001. INTERCOMPARISON STUDY OF NUMERICAL MODELS FOR LONG-RANGE ATMOSPHERIC TRANSPORT OF MERCURY: Stage I. Comparison of chemical modules for mercury transformations in a cloud/fog environment, MSC-E Technical Report 2/2001. METEOROLOGICAL SYNTHESIZING CENTRE - EAST, Moscow, Russia.

Si, L., Ariya, P.A., 2011. Aqueous photoreduction of oxidized mercury species in presence of selected alkanethiols. Chemosphere 84, 1079–1084. doi:10.1016/j.chemosphere.2011.04.061

Skyllberg, U., 2008. Competition among thiols and inorganic sulfides and polysulfides for Hg and MeHg in wetland soils and sediments under suboxic conditions: Illumination of controversies and implications for MeHg net production. J. Geophys. Res. 113. doi:10.1029/2008JG000745

Skyllberg, U., Qian, J., Frech, W., 2005. Combined XANES and EXAFS study on the bonding of methyl mercury to thiol groups in soil and aquatic organic matter. Phys. Scr. 2005, 894. doi:10.1238/Physica.Topical.115a00894

Skyllberg, U., Qian, J., Frech, W., Xia, K., Bleam, W.F., 2003. Distribution of mercury, methyl mercury and organic sulphur species in soil, soil solution and stream of a boreal forest catchment. Biogeochemistry 64, 53–76. doi:10.1023/A:1024904502633

Sparks, D.L., 2005. Sorption | Metals, in: Hillel, D., Hatfield, J.L., Powlson, D.S., Rosenweig, C., Scow, K.M., Singer, M.J., Sparks, D.L. (Eds.), Encyclopedia of Soils in the Environment. Elsevier Ltd., Oxford UK, pp. 532–537.

Tiffreau, C., Lützenkirchen, J., Behra, P., 1995. Modeling the Adsorption of Mercury(II) on (Hydr)oxides: I. Amorphous Iron Oxide and α-Quartz. J. Colloid Interface Sci. 172, 82–93. doi:10.1006/jcis.1995.1228

UNEP, 2002. Global Mercury Assessment 2002. UNEP Chemicals Branch, Geneva, Switzerland.

USEPA, Office of Science and Technology, 2002. Method 1631, Revision E: Mercury in Water by Oxidation, Purge and Trap, and Cold Vapor Atomic Fluorescence Spectrometry.

USGS, n.d. Piper Plot MS-Excel Spreadsheet Template: [WWW Document]. Excel Hydrol. URL http://nevada.usgs.gov/tech/excelforhydrology/WaterQualityTools/PiperPlot-QW.XLS (accessed 9.25.14).

Von Canstein, H., Kelly, S., Li, Y., Wagner-Dobler, I., 2002. Species Diversity Improves the Efficiency of Mercury-Reducing Biofilms under Changing Environmental Conditions. Appl. Environ. Microbiol. 68, 2829–2837. doi:10.1128/AEM.68.6.2829-2837.2002

Wagman, D.D., Evans, W.H., Parker, V.B., Schumm, R.H., Halow, I., 1982. The NBS Tables of Chemical Thermodynamic Properties. Selected Values for Inorganic and C1 and C2 Organic Substances in SI Units.

Wiatrowski, H.A., Das, S., Kukkadapu, R., Ilton, E.S., Barkay, T., Yee, N., 2009. Reduction of Hg(II) to Hg(0) by Magnetite. Environ. Sci. Technol. 43, 5307–5313. doi:10.1021/es9003608

Wiatrowski, H.A., Ward, P.M., Barkay, T., 2006. Novel Reduction of Mercury(II) by Mercury-Sensitive Dissimilatory Metal Reducing Bacteria. Environ. Sci. Technol. 40, 6690–6696. doi:10.1021/es061046g

Chapter 3: Comparing modeled and measured mercury speciation in contaminated groundwater: The importance of DOM composition[1]

Abstract

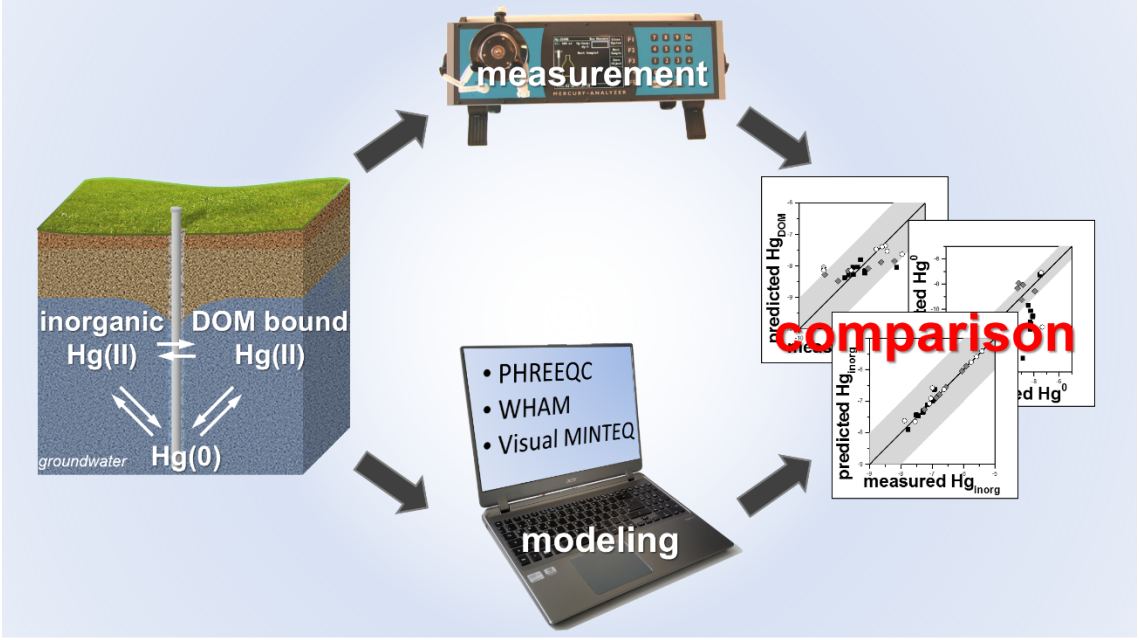

The risk of mercury (Hg) in contaminated groundwater strongly depends on its chemical species. Thus, besides analytical speciation, reliable modeling of Hg species in groundwater is crucial to predict the mobility and toxicity of Hg in subsurface environments. Available geochemical speciation codes have not been tested for their accuracy in predicting Hg speciation in groundwater. Our study compares analyses of Hg species in groundwater of three different highly Hg contaminated sites with predictions of Hg species by three geochemical codes (WHAM, Visual MINTEQ, and PHREEQC) with and without implementation of Hg complexation by dissolved organic matter (DOM). Chemical composition, dissolved elemental, oxidized, and DOM bound Hg were analyzed in all groundwater samples (total Hg: 0.02 to 4 µmol L^{-1}). Hg complexation by DOM was modeled using three main approaches: Binding to humic (HAs) and fulvic acids (FAs) using DOM binding sub-models of WHAM and Visual MINTEQ, binding to thiol-groups, or a combination of both. Hg(0)

[1] this chapter has been published in revised form in Environmental Science & Technology DOI: 10.1021/acs.est.6b00500

modeling results were poor in all codes and scenarios. DOM composition was found to be crucial for modeling total inorganic and DOM bound Hg. Combining weaker binding sites by adjusting equilibrium constants in WHAMs DOM submodel with strongly binding thiol groups gave best results.

1 Introduction

While mercury (Hg) in general is considered to be one of the most toxic contaminants, the actual degree of toxicity depends on the Hg compounds present (UNEP, 2002). Mobility of Hg is strongly related to its speciation, as different Hg compounds show different physical properties. Water solubility of Hg compounds for instance ranges from practically insoluble Hg sulfide (cinnabar), (solubility: <0.05 nmol L^{-1}; Merian et al., 2004) to highly soluble Hg salts such as mercury(II)chloride ($HgCl_2$) or mercury(II)chlorate ($Hg(ClO_3)_2$ (solubilities: 0.27 and 0.68 mol L^{-1}, respectively; Merck, 2010; Perry, 2011). Some Hg species can be subject to transport in gaseous form, too. Henry constants for these Hg compounds range from 9.3 10^{-2} to 1.4$10^{-6}$ M atm^{-1} for Hg(0) and $HgCl_2$, respectively (Sander, 1999; Ryaboshapko et al., 2001). Transformation processes between Hg species are of crucial importance for risk assessment e.g. microbial methylation of inorganic Hg to extremely toxic and biomagnifying monomethylmercury (CH_3Hg^+) surpasses direct anthropogenic CH_3Hg^+ release by far (UNEP, 2013). In natural aquatic environments Hg mobility is mostly controlled by complexation to reduced sulfur groups of organic matter (Qian et al., 2002; Skyllberg et al., 2000, 2003). Analytical procedures for the measuring inorganic soluble Hg species in environmental samples do usually not determine defined Hg complexes, but operational defined Hg fractions based on volatilization (Hg(0)) or chemical reducibility (reactive species such as Hg chloro- or hydroxo-complexes (Brosset, 1987; Meili et al., 1991)). Here, organic matter bound Hg is defined as the non-stannous-chloride ($SnCl_2$)-reducible, non-reactive, complex bound Hg fraction (Brosset, 1987; Meili et al., 1991). In contrast to the comparatively well established, thermodynamic modeling of defined inorganic aqueous Hg complexes (e.g. $Hg(OH)_2^0$, $HgCl_2^0$,...), modeling of dissolved organic matter (DOM) bound Hg is restricted to complexation constants of DOM functional groups like thiols,

carboxylic, and phenolic acids and of operationally defined DOM fractions such as humic or fulvic acids.

In nature, humic substances can either act as sinks or, in dissolved, colloidal or suspended form, as transport vectors for Hg. The dissolved organic carbon (DOC) content is a parameter to quantify the amount of organic substances in aqueous solutions. However, DOC concentrations alone do not yield any information concerning the quality of the encountered organic matter and its ability to bind Hg. Since DOM comprises of numerous organic compounds (Swift, 1999) showing different chemical properties and complexing behavior, a more comprehensive characterization of DOM was needed. Therefore, separation techniques based on adsorption onto resins and pH dependent precipitation were developed (Thurman and Malcolm, 1981) for isolation and separation of DOM-fractions. Fulvic (FAs) and humic acids (HAs) were found to be the most important sub-fractions regarding cation complexation. The differentiation between FAs and HAs is operationally defined by precipitation from alkaline extracts of organic matter, defining HAs as being soluble in solutions above pH 1 only whereas FAs are soluble under both, acid and alkaline conditions(Aiken, 1985). FAs show more carboxylic than phenolic acid groups and HAs exhibit rather equal amounts of both types of binding sites (Gustafsson, 2001). For the implementation in geochemical modeling codes equilibrium constants for cation complexation with FA or HA were determined from experimental data (Lövgren and Sjöberg, 1989; Milne et al., 2003; Khwaja et al., 2006; Tipping, 2007; Tipping et al., 2011). Reduced sulfur groups have been shown to be the most important ligand for Hg binding to DOM (Qian et al., 2002; Khwaja et al., 2006; Nagy et al., 2011; Xia et al., 1999) exhibiting highest equilibrium constants (Haitzer et al., 2002; Khwaja et al., 2006; Skyllberg, 2008). Geochemical modeling has been used to predict Hg speciation in seawater (Grassi and Netti, 2000; Bessinger et al., 2012; Stockdale et al., 2015), lakes (Wollenberg and Peters, 2009; Feyte et al., 2010; Chiasson-Gould et al., 2014), rivers (Barringer et al., 2010; Muresan et al., 2011; Bessinger et al., 2012; Miller et al., 2012; Carling et al., 2013) and groundwater (Grassi and Netti, 2000; Maprani et al., 2005; Gemici et al., 2009; Bearup et al., 2012; Johannesson and Neumann, 2013). However speciation codes have not yet

been validated by comparison to chemical Hg species analyses on natural samples.

In this study we compare data of Hg speciation measurements in groundwater of three different contaminated sites to Hg speciation as predicted by the geochemical modeling codes WHAM VII, Visual MINTEQ 3.1 and PHREEQC 3.1 In their original form WHAM and Visual MINTEQ (VM) already support Hg complexation to DOM. Here DOM is described by complexation constants for Hg to FAs and HAs only, without further differentiation of FA or HA functional groups. Therefore, in a second step, databases of all tested codes were extended with equilibrium constants for Hg binding to thiol groups. However, it was shown in previous studies that when thiol groups are saturated with Hg, other functional groups become relevant (Xia et al., 1999; Haitzer et al., 2002; Tipping, 2007). Thus, in a third step, we additionally evaluated Hg species modeling including both, thiol binding and Hg complexation to FAs and HAs as provided by WHAM and VM.

2 Materials and methods

2.1 Sampling sites.

Groundwater was sampled at three Hg contaminated sites which differ in contamination history and hydrochemical conditions of the aquifer. Sampling wells on each site were selected to represent the encountered variability best:

Site A is a chemical production site in South-Eastern France where the Castner-Kellner (or mercury-cell) process has been applied for decades to produce sodium hydroxide (NaOH) and chlorine (Cl) from sodium chloride (NaCl). Metallic Hg and Hg contaminated brine has been spilled causing contamination of soil and groundwater. The aquifer here is characterized by alluvial sediments (fine sands to coarse gravels) with interstratified silt layers poor in organic matter. Hg was not the only contaminant in groundwater at this site but a variety of inorganic and organic pollutants are known to be present in the aquifer (e.g. (per)chlorate, polychlorinated biphenyls (PCBs), chloromethanes, -ethanes, and -ethenes, BTEX, halogenated aromatics, DDT and its derivates) resulting in complex and diverse hydrochemical conditions.

Sampled wells were distributed over the whole site to capture maximum variability of different Hg and DOC concentrations and hydrochemical conditions.

Site B is a former wood impregnation facility located south-west of the city of Freiburg (Southern Germany). Mercury chloride (HgC_{l2}) solution had been used for wood preservation through dipping and pressuring of wooden parts (kyanizing). During time of operation several tons of Hg were released to soils and groundwater (Schöndorf et al., 1999). The aquifer material consists of fluvial loose gravel and sands superposed by loess soil. A more detailed site description can be found elsewhere (Bollen et al., 2008). Sampled wells follow a transect along the groundwater contamination plume.

Site C is located in the Black Forest (Southern Germany). Kyanization was applied for wood preservation in a similar manner as at Site B. However, hydrogeology and resulting groundwater chemistry differ from those of site B. Here the aquifer is characterized by late quarternary fluvial carbonate free sediments containing interstratified peat layers overlaying the paleozoic granite basement (LUBW, 2014). More details can be found in Richard et al. (2016). Wells from the whole site were sampled reflecting the versatility of Hg and DOC concentrations at the site.

2.2 Sampling and sample treatment.

Water was pumped from the wells using submersible groundwater testing pumps (site A: MP 1, Grundfos, Denkmark, site B: Comet-Combi 12-2T, Comet-Pumpen, Germany, site C: WP4012, Whale Pumps, U.K.) After stationary condition of field parameters (pH, DO, temperature, conductivity) were reached, samples were taken either in 500 mL bottles (fluorinated polyethylene (FLPE)), thoroughly washed with demineralized water and double distilled nitric acid (HNO3) or in new 2000 mL borosilicate glass bottles (site A), both preconditioned with sample water, respectively. Samples were filtered through 0.45 µm polyamide (PA) membrane syringe filters in the field directly after sampling. Subsamples for cation analysis were acidified by adding one percent (v/v) of double distilled HNO3 and stored in sealed containers (Polypropylene (PP)) below 8°C until analysis. Subsamples for anion analysis were kept in air

free, sealed PP containers below 8°C until analysis. Redox-potential (Eh), pH, conductivity (EC), and dissolved oxygen (DO) were determined using a sealed flow cell to prevent oxygen contact of the water at site B and C. Pumping capacity of the applied pump was too high to use a flow cell at site A, so field parameters were determined in a 10 L container directly at the outflow of the submerged pumping hose. Subsamples for total dissolved Hg (Hgtot) determination were stabilized with 1/60 M $K_2Cr_2O_7$-HNO_3 and BrCl solution according to EN standard method 1483 (EN, 2007) and USEPA method 1631 (USEPA, 2002).

2.3 Water analyses.

2.3.1 Determination of cations, anions, and alkalinity:

Water samples were analyzed for major cations and trace elements by means of inductively coupled plasma optical emission spectrometry (ICP-OES, Varian 715 ES, Agilent Technologies Inc., USA) and ICP-mass spectrometry (ICP-MS, Agilent 7700, Agilent Technologies Inc., USA), respectively. Anions were determined using an ion exchange chromatograph (761 Compact IC, Metrohm AG, Switzerland). Alkalinity was determined in the field by titration according to ISO standard method 9963-1 (ISO, 1996).

2.3.2 Hg determination and speciation:

Dissolved Hg was analyzed using a cold vapor atomic absorption spectrometer (CV-AAS, mercury analyzer Hg-254 NE, Seefelder Messtechnik GmbH, Germany), according to EN standard method 1483 (EN, 2007). Speciation of aqueous phase Hg was determined according to the protocol given in Bollen et al., (2008) and Richard et al. (2016), modified after Brosset (1987) and Meili et al. (1991) (Figure S1). The following operational defined Hg species were determined from duplicate or triplicate measurements: “Total dissolved Hg” (Hg_{tot}), “purgeable, dissolved gaseous elemental Hg" (Hg(0)), “dissolved, reactive inorganic divalent Hg” ($Hg(II)_a$), “total inorganic Hg” (Hg_{inorg} = Hg(0) + $Hg(II)_a$) and “dissolved divalent Hg, bound to BrCl-oxidable organic compounds” (DOM-bound, $Hg(II)_b$ or Hg_{DOM}). Hg(0) and $Hg(II)_a$ were determined on site within a few minutes after sampling (site A and C), or immediately after arrival in the lab (site B). However, since $Hg(II)_b$ was calculated by subtraction of $Hg(II)_a$

and Hg(0) from Hg_{tot}, inaccuracies for this species can arise when proportions of the measured initial values are significantly different (Leopold et al., 2010). Therefore we selected only samples in which calculated $Hg(II)_a$ and $Hg(II)_b$ concentrations surpassed the combined standard deviations from replicate measurements of the initial values.

2.3.3 Determination of dissolved organic carbon:

Filtered samples (0.45 µm) were acidified to pH 2 using hydrochloric acid (HCl, 2M) to remove carbonates. Analysis of DOC was performed subsequently by means of thermocatalytic oxidation at 950°C with subsequent NDIR detection of CO_2, using a TOC analyzer (multi N/C 2100, Analytik Jena AG, Germany).

2.3.4 Analytical quality assurance:

Standard reference materials (SRMs) “Trace Metals” RTC 1-WP: (CV-AAS), “natural water from Lake Superior” EC ION-915 (IC, Alkalinity, pH, TOC), “River Water” NRC SLRS-5: (ICP-OES) were analyzed to assure quality of analyses. See Table S1 for recovery rates and limits of quantification.

2.4 Statistics and graphic presentation.

All statistical analyses and graphic production was done using Origin 9.0 software (OriginLab Corporation, USA).

2.5 Modeling.

2.5.1 Basic information and applied databases:

For modeling Hg speciation, total Hg concentrations, cation and anion analysis were entered in the geochemical codes together with temperature, dissolved oxygen and pH. When redox reactions or complexation by humic matter were implemented in the model code, Eh/pE-values and/or DOC concentrations were added. Three different codes were applied: WHAM VII, developed by Lofts and Tipping (Tipping et al., 2011), Visual MINTEQ 3.1, based on MINTEQA2 (Allison et al., 1991) (U.S. Environmental Protection Agency), extended and further developed by Gustafsson (2013), and PHREEQC 3.1 developed by Parkhurst and Apello (2013). First, unaltered databases as provided with the modeling codes were applied. Minteq.dat and minteq.v4.dat databases were

used in PHREEQC, containing equilibrium constants for 42 and 43 aqueous inorganic Hg species, respectively, including dissolved elemental Hg(0). In VM and WHAM the standard aqueous complexes databases (thermo.vdb and default.db7) were used, containing equilibrium constants for 56 and 8 different inorganic Hg species and complexes, respectively. In additional modeling scenarios, complemented versions of the original databases were applied, where equilibrium constants of dissolved HgS-complexes were updated and constants for Hg to DOM bound thiols were added (cf. equilibrium constants in Table S2).

WHAM and VM already provide submodels for the interaction of trace elements with DOM. In WHAM, "Humic Ion Binding Model VII" was used for modeling Hg complexation to DOM. This model follows a mechanistic approach with a series of discrete-site pKa values for metal binding to strong and weak binding sites. These sites may stand for carboxylic and phenolic acids (Tipping, 1998, 1994; Tipping et al., 2011) but can also refer to other functional groups like, in the case of Hg, reduced sulfur or thiols (Tipping, 2007). In VM the "Stockholm Humic Model (SHM)" and the "NICA-Donnan (ND)" model were applied for humic complexation modeling. SHM is similar to Model VII in WHAM. Its main difference is in the electrostatic submodel, based on the Basic Stern concept (Gustafsson, 2001). The ND-model, however, assumes a continuous distribution of pKa values and implies a non ideal competitive adsorption (NICA) binding isotherm coupled with an electrostatic submodel based on the Donnan concept (Kinniburgh et al., 1999; Milne et al., 2001, 2003). In VM and also in PHREEQC (using the extended database), modeling of Hg(0), inorganic, and DOM bound Hg(II) could be performed at the same time. Hence, direct comparison of modeling results with measurements was possible. However, WHAM and PHREEQC (using the default database) are only capable of modeling two Hg species groups (Hg_{inorg} + Hg_{DOM} or Hg(II) + Hg(0), respectively). Therefore, either measured inorganic Hg species (Hg(0) and $Hg(II)_a$) or divalent Hg ($Hg(II)_a$ and $Hg(II)_b$) had to be combined to one species in order to compare the measurements with modeling results.

2.5.2 Quantification of prediction accuracy:

To quantify model accuracy and to describe systematic prediction errors root-mean-square errors (RMSEs) and mean signed differences (MSDs) were calculated (equation 1 and 2), with xpredicted and xmeasured referring to a species` concentration in log (mol L^{-1}), as predicted by the model or as measured, respectively. The number of samples analyzed is denoted as n.

$$RMSE = \sqrt{\frac{\sum(x_{predicted} - x_{measured})^2}{n}} \quad (1)$$

$$MSD = \frac{\sum(x_{predicted} - x_{measured})}{n} \quad (2)$$

2.5.3 Modeling Scenarios:

Eight modeling scenarios were applied in this study, differing in assumed DOM content, composition, binding site implementation, and equilibrium constants (Table S3). They can be classified in four groups: (i) No implementation of DOM (scenario 1). (ii) DOM implemented as FAs and HAs (scenarios 2-4). (iii) DOM implemented as thiol groups (scenarios 5, 6) using log Ks from Skyllberg (2008). (iv) DOM implemented as a combination of thiol groups and FAs and HAs (scenarios 7, 8).

Scenario 1 (no DOM) was applied in PHREEQC and VM.

In **Scenario 2** (VM, WHAM) DOM was set to 100% FA (e.g. Christensen et al. (1999); Christensen and Christensen (1999); Unsworth et al. (2006) Ndungu, (2012)). Measured DOC was converted to FA concentrations assuming a carbon content of 52.3% C for FA in groundwater as found by Artinger et al. (2000). In **Scenario 3** (VM), the default DOM-composition parameters of VM were used (100% FA, containing 50% C with 82.5% being active in terms of cation binding (Sjöstedt et al., 2010).In **Scenario 4** (VM, WHAM), denoted as “Malcolm”, DOC was assumed to be comprised of 13% FA and 1.5% HA, typical for DOM composition in groundwater (Malcolm, 1991). Other DOC fractions (low molecular weight acids, hydrophilic neutrals, hydrophobic neutrals, bases) (Malcolm, 1991) were neglected as possible complexing agents because only FA and HA are implemented in WHAM and VM. Carbon

content of FA and HA were assumed to be 52.3% and 57% C, respectively (Artinger et al., 2000).

In **Scenario 5** (PHREEQC, VM, WHAM) a proportion of 0.15 wt.% of thiols on DOC was assumed, as determined from soil extracts and surface waters (Skyllberg, 2008). In **Scenario 6** (PHREEQC, VM, WHAM), RMSEs of HgDOM and Hginorg were optimized by systematic variation of the thiol to DOC ratio. It is known that DOM composition in groundwater differs from that in surface waters (Malcolm, 1991; Maurice and Leff, 2002; Wong and Williams, 2009) so that thiol to DOC ratios in groundwater are also likely to deviate from those determined in surface waters.

In **Scenario 7** (VM, WHAM), Hg thiol binding was applied using the thiol to DOC ratio from Scenario 6. Additionally, Hg binding to other functional groups (e.g. carboxylic and phenolic acids) from FAs and HAs was assumed to take place after thiol groups have been saturated according to Haitzer et al. (2002). This was achieved by assuming a DOM composition as described in Scenario 4 and systematically lowering the intrinsic binding constants of Hg-DOM complexes in the SHM (log K_A) and Model VII (log K_{MA}) DOM binding submodels in VM and WHAM to optimize RMSEs. **Scenario 8** (WHAM) is a “best fit” scenario, where the proportion of Hg binding, „reactive” thiols on DOC was set to 0.03% according to Haitzer et al. (2002) and log KMA values for FA and HA as well as the factor ΔLK_2 used for generation of stronger binding sites were varied systematically to achieve minimum RMSEs.

3 Results and discussion

3.1 Hg concentrations and characterization of groundwater samples.

Total Hg concentrations determined in groundwater are depicted in Figure 1. Chemical water composition of all modeled samples from all sites is given in Tables S4 to S6.

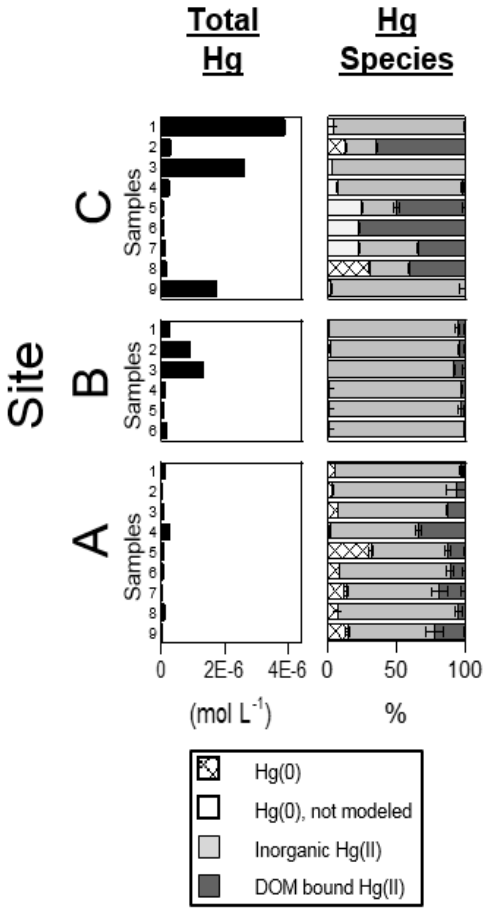

Figure 1. Total Hg concentrations and measured Hg species as proportions of total Hg.

Site A: Here, total dissolved Hg concentrations ranged from 20 to 245 nmol L^{-1} (median: 60 nmol L^{-1}). Since most contaminants known to be present in groundwater on the site could not (adequately) be implemented in the geochemical codes applied due to missing IUPAC recommended stability constants, analyses for this study were limited to major and trace elements and standard anions. Sodium (Na^+) and chloride (Cl^-) from the leakage of brine and/or the storage of NaCl salt on the site were found to be elevated in all

samples resulting in highest ionic strengths of all sites (32 to 192 mmol L^{-1}). Due to acid and brine spillages, pH in groundwater was highly variable (1.9 to 11.5). Redox potentials (Eh: 289 to 727 mV) and DOC (range: 73 to 1307 µmol L^{-1}, median: 117 µmol L^{-1}) also varied strongly. The two samples with lowest pH and highest DOC content were excluded from modeling because either Hg speciation could not be measured or DOC was likely comprised mainly by organochlorine pollutants, based on previous measurements.

Site B: Here, total dissolved Hg concentrations ranged from 60 nmol L^{-1} to 1.3 µmol L^{-1} (median: 229 nmol L^{-1}). Groundwater chemistry was uniform in all samples with pH and Eh ranging from 6.5 to 6.7 and 383 to 480 mV, and ionic strength from 5.8 to 6.9 mmol L^{-1}, respectively (Bollen et al., 2008). Average DOC concentrations of 58 ± 8 µmol L^{-1} were the lowest of all three sites.

Site C: Hydrochemical conditions at site C showed larger diversity than at site B, related to the more complex hydrogeology at this site. Ionic strength ranged from 3.7 to 10.3 mmol L^{-1} and pH between 6.1 and 7.4. Concentrations of total dissolved Hg were between 57 nmol L^{-1} and 3.9 µmol L^{-1}, making this site the most contaminated one investigated (median: 244 nmol L^{-1}). Here, DOC concentrations ranged between 66.7 and 442 µmol L^{-1} (median: 282 µmol L^{-1}) due to the comparatively higher organic matter content of the partially peat rich aquifer material at this site. A weak negative correlation between DOC content and total Hg was observed (R^2: 0.46, p-value: 0.04) that might be attributed to an enhanced solid phase sorption of Hg in peat layers. Redox potential could only be measured in two samples (sample 2 and 8) and was 393 and 524 mV.

3.2 Measured mercury species

Inorganic divalent Hg as dissolved $HgCl_2$ was the initial Hg species released to soil and groundwater at site B and C. At site A it is assumed that metallic Hg from the electrolysis cells had been oxidized to Hg(II)-chloro-complexes in the NaCl-brine, based on Hg speciation measurements in brine coming from the cells (total Hg: 18.4 µmol L^{-1}, >99.98% $Hg(II)_a$). The brine was subsequently released to soil and groundwater through leakages in tubing and brine reservoirs. Results of Hg speciation measurements in groundwater from all sites are shown in Figure 1. **Inorganic Hg(II)** ($Hg(II)_a$) was found to be dominant in

samples from site A and B. On site C, where mean DOC concentrations exceeded those of site A and B (see above), a negative correlation of $Hg(II)_a$ and DOC concentrations was observed (R^2:0.80, p-value: 0.001). Consequently, **DOM bound Hg(II)** ($Hg(II)_b$) dominated Hg speciation in lesser polluted samples from site C, resulting in a positive correlation between $Hg(II)_b$ and DOC (R^2:0.76, p-value: 0.002). However, $Hg(II)_b$ was below ten percent of total Hg in samples from all sites having Hg concentrations higher than 500 nmol L^{-1}, most likely due to an oversaturation of strong DOM binding sites so that $Hg(II)_a$ was found to be the dominant species in these samples.

Dissolved **elemental Hg** (Hg(0)) was above limit of quantification (~0.4 nmol L^{-1}) in all but one sample, but its relative abundance varied significantly. While Hg(0) proportions of total Hg were found to be comparatively low in samples from site B (0.7 ± 0.4%), site-A-samples showed 9.9 ± 9.0% Hg(0) on the average and site-C- samples had an average Hg(0) proportion of 14.4 ± 10.8%. Hg(0) concentrations were found to be relatively low compared to Hg(0) solubility (300 nmol L^{-1}) (Merck, 2014) in samples from site A and B with average concentrations of 3.5 and 8 nmol L^{-1} (maximum: 15 and 35 nmol L^{-1}), respectively. In samples from site C concentrations of up to 150 nmol L^{-1} were reached (average: 46 nmol L^{-1}). While Hg(0) in groundwater at site A could at least partly be residual metallic Hg that did not get oxidized in the brine, the importance of Hg(0) for Hg speciation at Site C, however, is most probably a consequence of the relatively high aquifer organic matter contents at this site. High organic matter concentrations support Hg(0) formation through Hg(II) reduction by bacteria (Barkay et al., 2003; Wiatrowski et al., 2006) or humic acids (Gu et al., 2011). The importance of hydrous ferric oxides (HFOs) on Hg(0) formation on this site could also be shown recently (Richard et al., 2016).

3.3 Modeled mercury species

The geochemical codes predicted inorganic Hg(II) to be comprised by different Hg complexes, but these differences could not be evaluated since the operationally defined species analyses provide only total inorganic Hg(II). However, more than 99 percent of Hginorg in all samples was predicted to be

comprised of ten different hydroxo-, chloro-, and bromo-species or Hg(0) (Figures S2 and S3) in all modeling codes and scenarios. WHAM modeled inorganic speciation was necessarily dominated by Hg-chloro complexes except for two samples with high Hg hydroxides, since only these two types of complexes are included in the WHAM database (Table S2). Using VM and PHREEQC (minteq.v4.dat database), inorganic Hg speciation was very similar due to mostly identical equilibrium constants (Table S2) and showed also bromo, bromo-hydroxyl and bromo-chloro-complexes (mainly in samples from site A) besides chloro and hydroxyl complexes and Hg(0). In contrast, applying PHREEQC with the minteq.dat database predicted Hg(0) and $Hg(OH)_2^0$ to be dominant and Hg chloro-complexes being of less importance. As mentioned above, the applied analytical protocol for Hg speciation measurements yields only total inorganic Hg(II), so the proportions of all predicted inorganic Hg(II) species had to be combined in order to compare modeling results with measurements.

When the NICA-Donnan DOM binding submodel was applied in VM the model frequently failed to converge (arithmetic overflow mainly for samples from site B and C). Because prediction accuracy for the remaining samples was also lower compared to the SHM submodel (Table 1), the ND submodel was only applied in modeling scenarios 2-4.

3.4 Comparing modeling results and measurements

Even though the three applied codes did not always perform equal in the different modeling scenarios in terms of RMSEs, no significant difference in overall prediction accuracy could be found ($p>0.05$) except when the ND DOM submodel was used in VM. Here, Hg_{DOM} and Hg(0) was predicted significantly worse than with the SHM DOM submodel or with other codes. Prediction accuracy decreased significantly with decreasing concentrations ($p<0.05$ in 8 and 11 of 17 modeling runs for Hg_{inorg} and Hg_{DOM}, respectively) except when modeling Hg(0). This is of particular importance, because speciation modeling is often applied when Hg concentrations are too low for species measurements (Skyllberg, 2010). Between the three investigated sites no significant difference

was found when modeling total Hg_{inorg} ($p>0.05$). Hg(0) was predicted best at site B (significant at the 99% level) and Hg_{DOM} was significantly better predicted for samples from site A than for samples from the other sites ($p<0.001$).

3.4.1 Modeling of Hg(0):

Predicted Hg(0) concentrations showed large deviation from the measured results in all modeling scenarios independent of code or database used (Table 1, Figure S4). Negative MSD values in Table 1 show that Hg(0) was in most cases underestimated, except when modeled in PHREEQC using the minteq.dat database. Measured Eh used for calculation of Hg(0) concentrations represent a mixed potential that is often not in agreement with calculated Eh from single redox couples (Linberg and Runnels, 1984). Moreover, Hg(0) formation in aquifers is frequently not controlled by the redox potential in the water phase alone, but also by surface catalyzed Hg(II) reduction e.g. by Fe minerals (Amirbahman et al., 2013; Richard et al., 2016), reduced organic matter (Gu et al., 2011), or microbial activity (Barkay et al., 2003; Wiatrowski et al., 2006). Therefore, geochemical models that do not consider interaction with solid phases and biota necessarily fall short when used for prediction of dissolved Hg(0) concentrations, resulting in large underestimation. Because of this, Hg(0) is further discussed only in combination with inorganic Hg(II) as total inorganic Hg (Hg_{inorg}).

Table 1. Combined Root Mean Squared Errors (RMSEs) and Mean Signed Differences (MSDs) of modeled compared to measured concentrations of Hg species (log mol L^{-1}) in all samples from all sites.

		Root Mean Squared Error (RMSE)					Mean Signed Difference (MSD)				
Modeling Scenario	**Applied Code**	**DOM bound Hg**	**tot inorg. Hg**	**inorg. Hg(II)**	**tot Hg(II)**	**Hg(0)**	**DOM bound Hg**	**tot inorg. Hg**	**inorg. Hg(II)**	**tot Hg(II)**	**Hg(0)**
no DOM											
1 "no DOM"	**V-MINTEQ**				0.18	2.22				-0.03	-1.22
	PHREEQC (minteq.dat)				1.04	1.55				-0.58	0.23
	PHREEQC (minteq.v4.dat)				0.26	2.26				-0.05	-1.28
DOM as FA+HA											
2 "100% FA"	**V-MINTEQ SHM**	1.38	2.59	2.41	0.06	3.90	1.09	-1.94	-1.92	0.04	-3.24
	V-MINTEQ ND	1.58	5.20	5.82	0.04	7.26	1.34	-4.26	-5.23	0.03	-6.47
	WHAM	1.34	2.65				1.11	-1.96			
3 "default DOM"	**V-MINTEQ SHM**	1.35	2.25	2.11	0.05	3.60	1.06	-1.66	-1.63	0.04	-2.95
	V-MINTEQ ND	1.56	4.95	5.55	0.04	7.00	1.33	-4.01	-4.94	0.03	-6.17
4 "Malcolm"	**V-MINTEQ SHM**	0.93	0.27	0.36	0.11	2.33	0.50	-0.09	-0.13	-0.01	-1.44
	V-MINTEQ ND	1.32	3.11	3.76	0.05	5.47	1.17	-1.99	-2.90	0.05	-5.18
	WHAM	0.89	0.49				0.59	-0.17			
DOM as thiols											
5 "0.15% thiols"	**PHREEQC (minteq.v4.dat)**	0.83	4.17	4.17	0.06	3.83	0.52	-1.57	-1.58	0.01	-2.18
	V-MINTEQ	0.82	4.87	4.86	0.61	5.00	0.51	-1.49	-1.48	-0.27	-2.86
	WHAM	0.83	4.39				0.52	-1.64			
6 "optimized thiols"	**PHREEQC (minteq.v4.dat)**	0.64	0.15	0.26	0.13	2.31	0.03	0.04	0.02	-0.01	-1.34
	V-MINTEQ	0.64	0.15	0.19	0.61	2.36	0.02	0.04	0.05	-0.28	-1.45
	WHAM	0.64	0.15				0.02	0.04			
DOM as thiols and FA+HA											
7 "Malcolm + optimized thiols"	**V-MINTEQ SHM**	0.65	0.15	0.22	0.62	2.27	0.07	0.03	0.03	-0.29	-1.29
	WHAM	0.64	0.14				0.07	0.03			
8 "best fit"	**WHAM**	0.59	0.13				0.03	0.04			

3.4.2 Inorganic and DOM bound Hg:

DOM as FA+HA: While modeling **scenarios 2 and 3** ("100% FA" and "default DOM") resulted in underestimations of Hg_{inorg} of up to ten orders of magnitude (Figure 2), deviations in **scenario 4** ("Malcolm") were mostly within one order of magnitude. RMSEs in Table 1 show that Hg_{inorg} in scenarios 2-4 was slightly better predicted by VM using the SHM submodel than by WHAM (minimum RMSEs: 0.27 and 0.49 in scenario 4, respectively). RMSEs of Hg_{DOM} were smaller than those of Hg_{inorg} in scenario 2 (1.34-1.58) and 3 (1.35 and 1.56). However, even though RMSEs of Hg_{DOM} decreased in scenario 4 (minimum: 0.89), they were not as good as the ones of Hg_{inorg}. In scenarios 2-4 Hg_{DOM} was overestimated by all codes (positive MSDs in Table 1) but WHAM performed slightly better in predicting Hg_{DOM} than VM with SHM. Measured and predicted concentrations of Hg_{inorg} from all "no-thiols-scenarios" showed linear correlation (R^2: 0.56-0.89; slope: 1.10-4.75, best result: VM-SHM in scenario 4, Table S7). However, for Hg_{DOM} correlation could only be found for one code and only in scenario 4 (WHAM, R^2: 0.21, slope 0.19, p:0.03, Table S8).

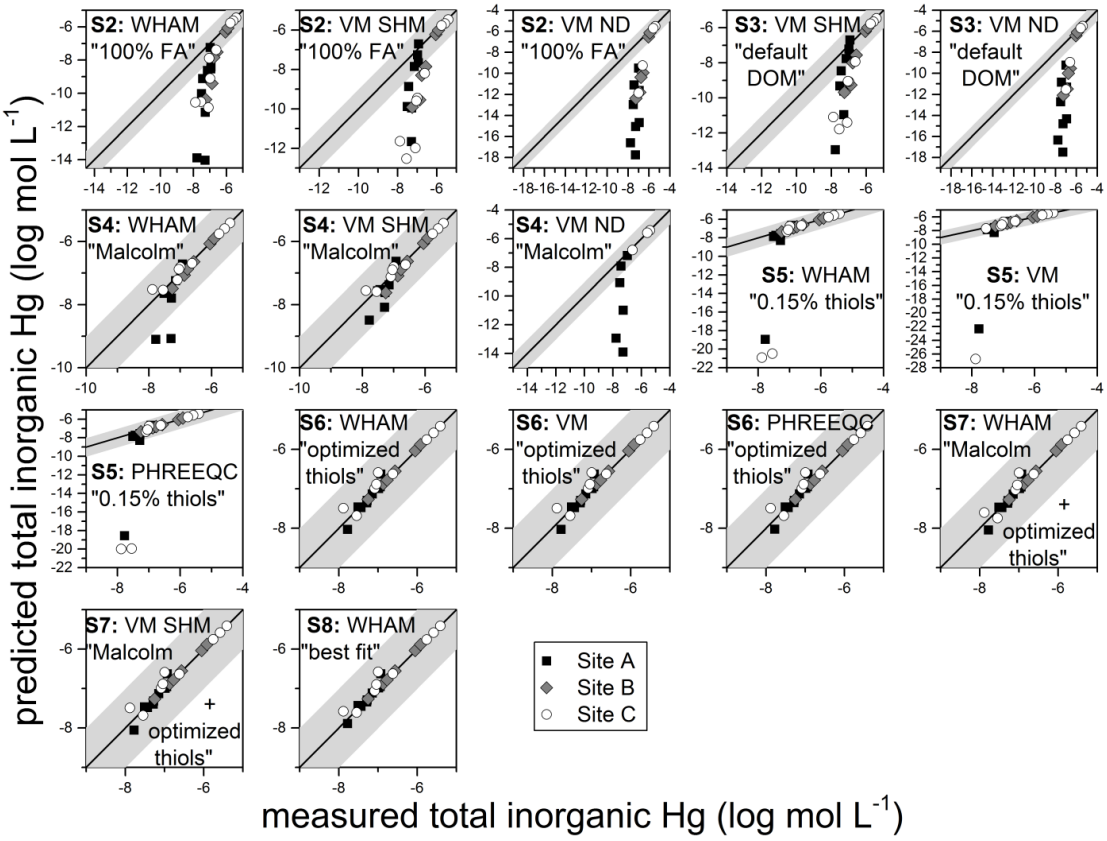

Figure 2: Comparison of measured and predicted concentrations of total inorganic Hg (Hg_{inorg} = $Hg(0) + Hg(II)_a$). "S" is scenario, VM is Visual MINTEQ. Note the different scales for each

scenario. Solid line and shaded area represent 1:1 line and one order of magnitude alongside 1:1 line, respectively.

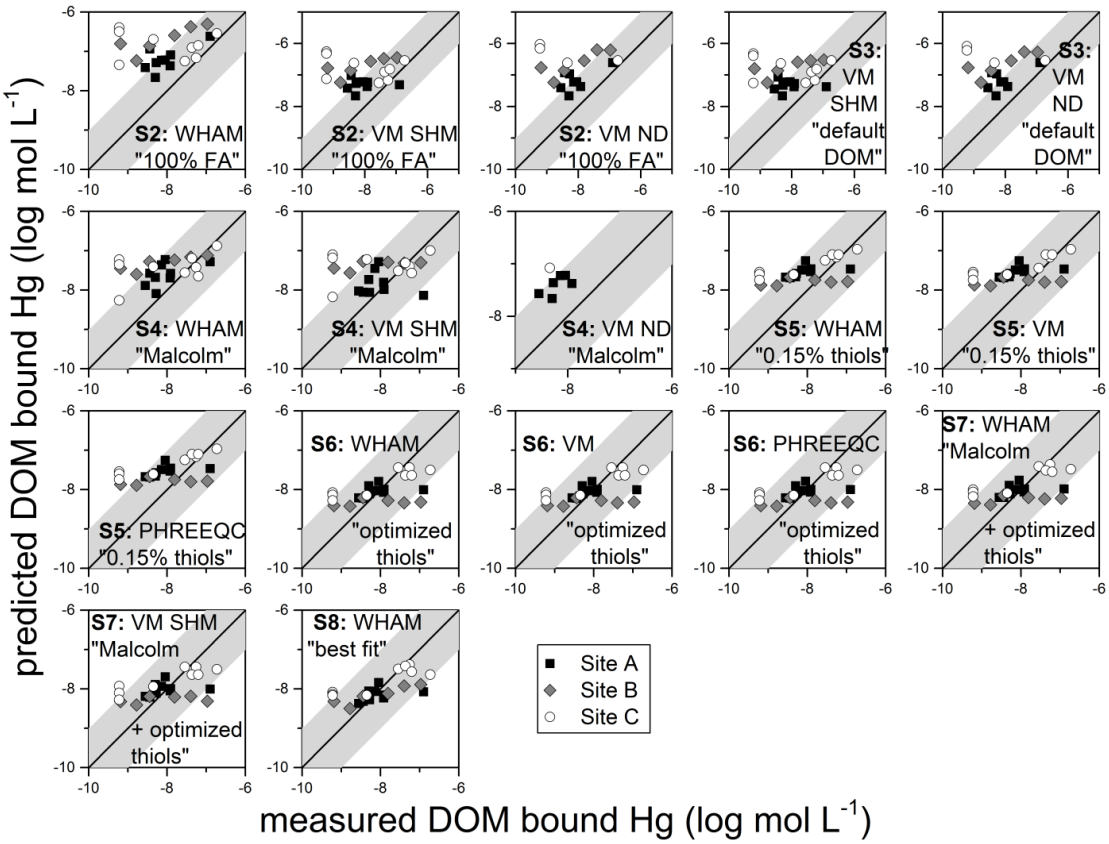

Figure 3. Comparison of measured and predicted concentrations of DOM bound Hg. ”S” is scenario, VM is Visual MINTEQ. Note different scales for each scenario. Solid line and shaded area represent 1:1 line and one order of magnitude alongside 1:1 line, respectively.

DOM as thiols (scenarios 5, 6): When Hg complexation with DOM was based on binding to thiol groups only, prediction accuracy for Hg_{DOM} and Hg_{inorg} of all applied codes (WHAM, VM, PHREEQC) was similar (Table 1). This is attributed to the fact, that the binding constants of Hg to thiol-groups which had been added to the databases were the same in all codes and higher than all other equilibrium constants, making other differences between the databases insignificant. In **scenario 5** (“0.15% thiols”) Hg_{inorg} was extremely underestimated in samples with the lowest concentrations (Figure 2) leading to the highest RMSE values for this species group in all scenarios (4.17-4.87). Prediction of Hg_{DOM} was better in scenario 5 than in the “FA+HA-DOM” scenarios 2-4 (RMSE: 0.82 to 0.83) but positive MSDs (0.51-0.52) indicated that Hg_{DOM} was still overestimated. For **scenario 6** (“optimized thiols”) the estimated

proportion of thiols on DOC was systematically varied between 0.15 and 0.01% to reach lowest RMSEs, leading to a thiol proportion of 0.04375%. Hg_{inorg} concentrations of samples with lowest Hg contents were predicted much better now (Figure 2) resulting in RMSEs of 0.15 and even better linear correlations between predicted and measured concentrations (R^2: 0.95, slope: 0.99 for all codes, Table S7) than in scenario 4. RMSEs of Hg_{DOM} decreased to 0.64 and MSDs were close to zero now, meaning that Hg_{DOM} was neither systematically under- nor overestimated. All codes in scenario 5 and 6 gave results for Hg_{DOM} which showed significant ($p<0.01$) linear correlation to measurements, but correlations (R^2 0.31-0.32) were poor if compared to Hg_{inorg} (Table S8).

DOM as thiols and FA+HA: In scenarios 7 and 8, Hg binding was not restricted to thiol groups but also included weaker binding sites (e.g. carboxylic and phenolic acids). Results of **scenario 7** were practically equal to scenario 6 but WHAM gave slightly better results than VM. Fitted intrinsic DOM binding constants were 1.125 (WHAMs log K_{MA}) and 0.1 (VMs log K_A). However, differences between the codes are more likely due to problems with the multi-problem generator of VM than to a general preeminence of WHAM over VM. Because all samples had to be modeled individually in VM, fitting of the intrinsic Hg binding constant log K_A in the SHM submodel could not be performed as thoroughly as this was possible with the log K_{MA} in WHAM, using WHAM´s batch processing mode. Therefore, only WHAM was used for **scenario 8**, where three parameters of the DOM binding submodel (log K_{MA}s for HA and FA and ΔLK_2) had to be optimized. In modeling scenario 8 fitted values for log KMA and ΔLK_2 were 3.1 and 3.3 for FA and HA, respectively. Here, the proportion of “reactive” thiols in DOC was set to 0.03 wt.%, corresponding to the amount of strong Hg binding sites found in DOM isolated from wetland water (5 x 10-9 mol mg^{-1} DOM) (Haitzer et al., 2002). Assuming this lowest thiol to DOC ratio of all thiol-containing scenarios, the modeling setup resulted in the best RMSEs for Hg_{inorg} and Hg_{DOM} of all scenarios (0.13 and 0.59, respectively) and modeled concentrations of Hg_{inorg} were in line with those measured (R^2: 0.97, slope 0.98). Linear correlation of modeled and measured Hg_{DOM} values was weaker (R^2: 0.45, slope 0.27) but results were better than in all other scenarios (Figure 3). However, since the slope of Hg_{DOM} was still far from 1 (gradient of ideal 1 to

1 relationship), prediction error for samples with lowest and highest Hg_{DOM} content was larger than one order of magnitude (Figure 3). Two main reasons could account for this: (i) the applied Hg-thiol equilibrium constants from the literature (Skyllberg, 2008, 2011), which were derived from organic matter extracted from soil and peat, are too high for thiols in DOM from groundwater, or (ii) the actual proportion of reactiver(free) thiols in groundwater DOM is even lower than assumed in scenario 8. The first option is not very likely, as there is no chemical explanation why the binding strength of thiol groups should be different for DOM from soil, peat, surface, or groundwater. The second option appears to be more probable, though. It is known that DOM composition in groundwater differs from that in surface waters (Malcolm, 1991; Maurice and Leff, 2002; Wong and Williams, 2009). Functional group bearing humic substances were found to comprise a much smaller proportion of total DOM in groundwater than in surface water (Malcolm, 1991). Therefore it is also likely that reactive thiol groups are less abundant in groundwater than in surface or soil water.

In summary, no significant difference in prediction accuracy was found between the tested speciation codes except for the NICA-Donnan DOM binding submodel in Visual-MINTEQ which performed significantly worse than the SHM DOM submodel and the other codes. Good compliance of modeled and measured data could be achieved for DOM bound and total inorganic Hg when modeling combined strong (thiol) and weaker binding sites. However, while model predictions of Hg_{inorg} were accurate and predicted Hg_{DOM} concentrations were satisfactory, Hg(0) was in most cases underestimated and modeling results were generally poor in all codes and scenarios. This was likely due to (i) a general redox disequilibrium in most groundwaters (Linberg and Runnels, 1984) and (ii) the non-implementation of Hg interactions with minerals and biota in the applied models. Nevertheless, the results of this study clearly show that DOM composition is a key parameter in modeling Hg species in groundwater. Instead of assuming DOM to be comprised of 100% fulvic acids (e.g. Christensen et al., 1999; Christensen and Christensen, 1999; Unsworth et al., 2006; Ndungu, 2012) and readily altering default binding constants of DOM complexation to fit model results to the experimental findings, as often applied,

we suggest to adapt DOM composition. The application of DOM composition from the literature, where typical fulvic and humic acid proportions for different types of surface- and groundwaters are provided (Malcolm, 1991; Artinger et al., 2000) can be a good starting point. For Hg speciation, however, our study shows that thiol functional groups are of greatest importance also in groundwater, even if their concentration is probably lower than in surface water. Consequently, speciation modeling scenarios of Hg in groundwater with direct implementation of thiol groups gave better results than the application of the DOM binding submodels provided by WHAM and VM, where thiol groups are only implicitly represented as strong binding sites (Tipping, 2007). Best prediction accuracy for the highly contaminated groundwater investigated in our study was achieved when both concepts were combined, using the DOM binding submodels to introduce weaker binding sites which are relevant for Hg binding when thiols are saturated (Haitzer et al., 2002). However, for verifying our results and improve accuracy of Hg speciation models, experimental quantification of thiol groups in groundwater DOM is needed.

Notes

The authors declare no competing financial interest.

Acknowledgment

We thank the regional council of Freiburg i. Brsg., Germany, the French Geological Survey (BRGM) and the Harres Pickel Consulting Group (HPC AG, Germany) for the permissions to work on the investigated sites and the excellent cooperation.

Supporting Information

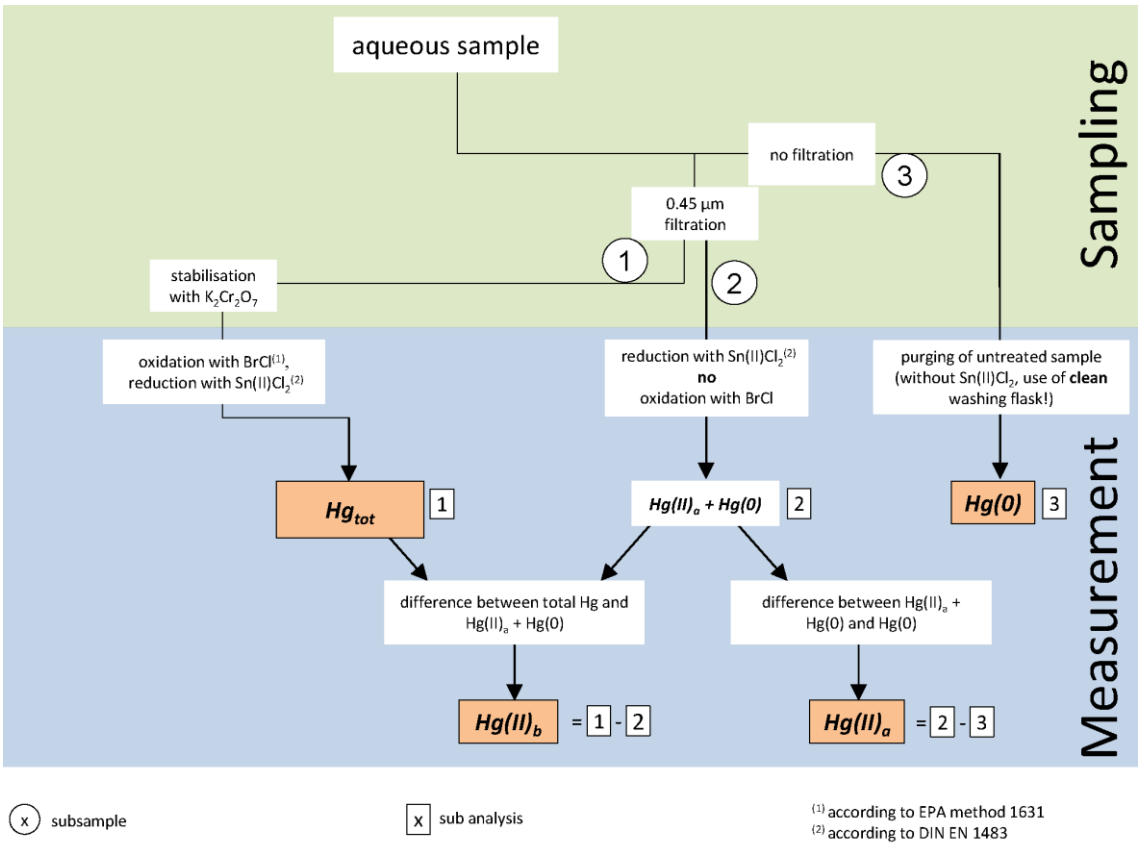

Figure S1. Scheme of analytical protocol followed during Hg speciation measurements.

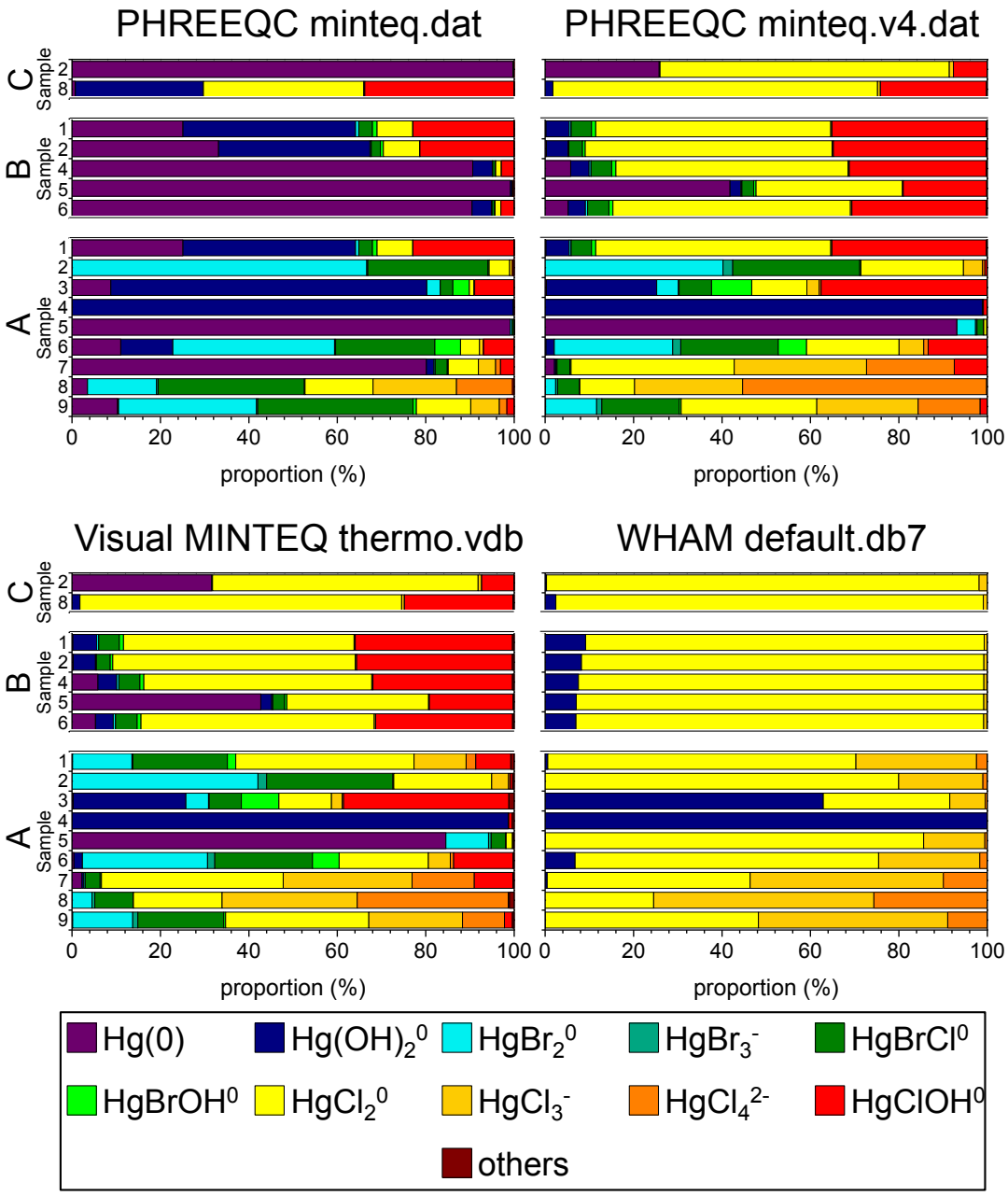

Figure S2. Inorganic speciation of samples from sites A, B, and C as calculated with PHREEQC using minteq.dat and minteq.v4.dat database, Visual MINTEQ, and WHAM 7, broken down to the applied database. Only samples that were modeled in scenario 1 are shown.

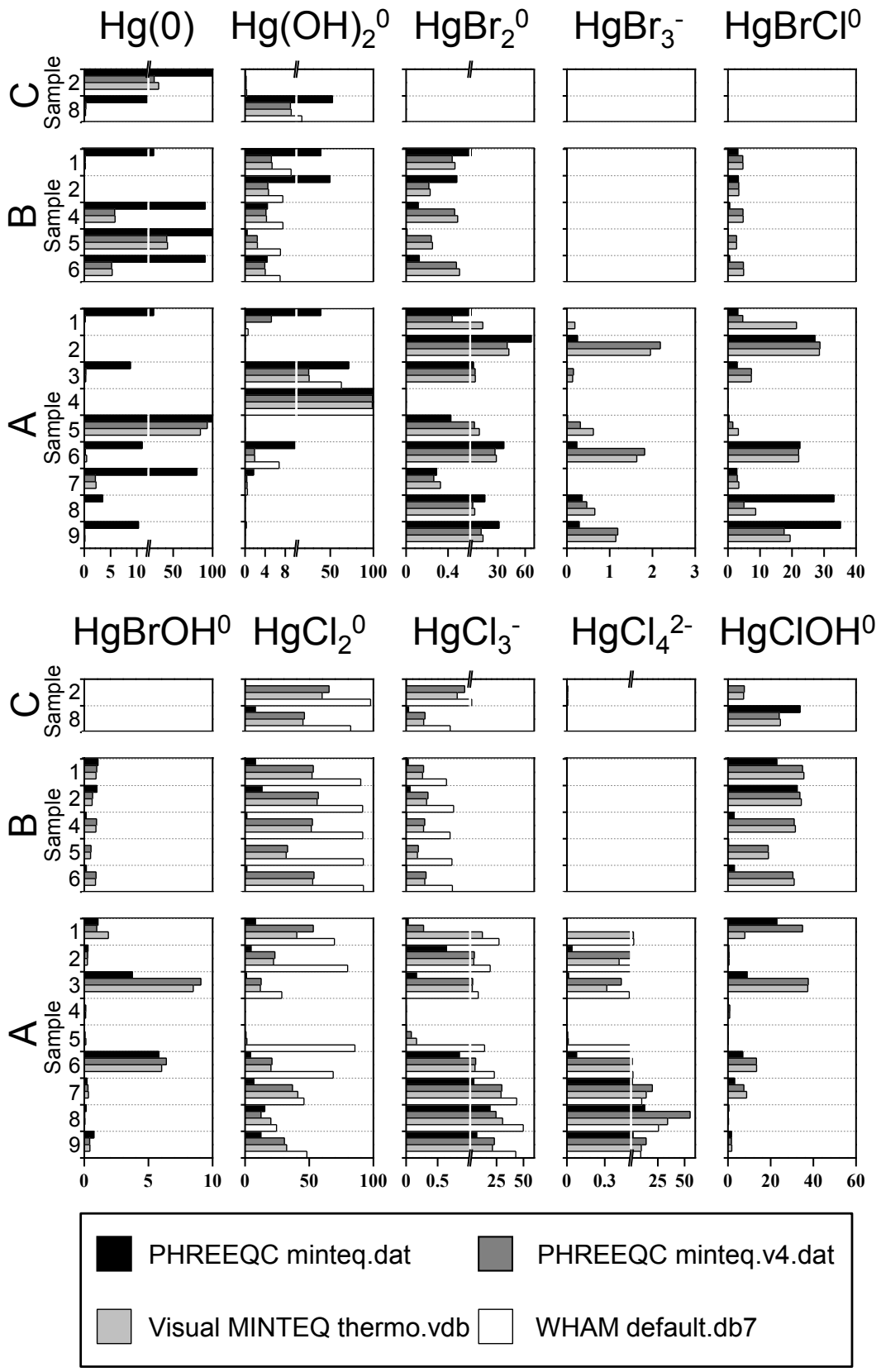

Figure S3. Inorganic speciation of samples from sites A, B, and C as calculated with PHREEQC using minteq.dat and minteq.v4.dat database, Visual MINTEQ, and WHAM 7, broken down to most frequent species. Only samples that were modeled in scenario 1 are shown.

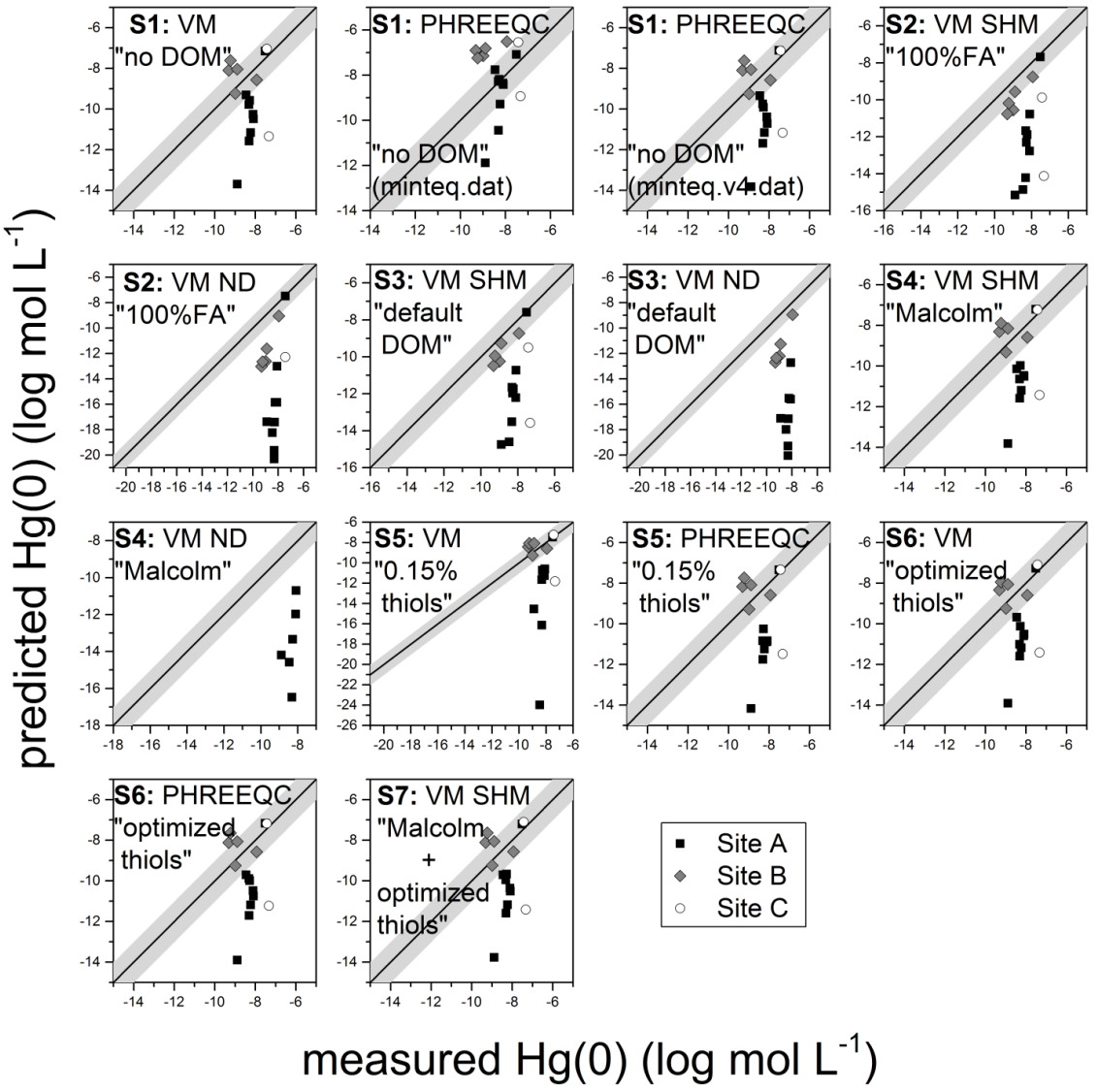

Figure S4. Comparison of measured and predicted concentrations of dissolved elemental mercury (Hg(0)). ”S” is scenario, VM is Visual MINTEQ Note different scales for each scenario.. Solid line and shaded area represent 1:1 line and one order of magnitude alongside 1:1 line, respectively.

Table S1. Limits of quantification, applied standard reference materials, and recovery rates for different analytes.

Analyte	Unit	Analytical Instrument	Limit of Quantification (LOQ)*	Standard Reference Material (SRM)	Certified Concentration	Obtained Concentration	Recovery Rate
Hg	$nmol \cdot L^{-1}$	CV-AAS	0.75	"Trace Metals" RTC 1-WP	389 ± 20	393 ± 7.5	101.0%
DOC	$\mu mol \cdot L^{-1}$	TIC/TOC Analyzer	42	"natural water from Lake Superior" EC ION-915	114 ± 34	110 ± 12	96.8%
Cl^-	$\mu mol \cdot L^{-1}$	IC	13.9	"	40.1 ± 6.0	40.2 ± 2.5	100.3%
F^-	$\mu mol \cdot L^{-1}$	IC	0.7	"	2.5	2.1	83.9%
NO_3^-	$\mu mol \cdot L^{-1}$	IC	0.3	"	1.6 ± 0.2	1.4 ± 0.1	90.1%
SO_4^{2-}	$\mu mol \cdot L^{-1}$	IC	7.8		3.4 ± 0.4	3.4 ± 0.3	100.7%
Br^-	$\mu mol \cdot L^{-1}$	IC	0.3	"		0.01 ± 0.00	
Ca	$mmol \cdot L^{-1}$	ICP-OES	0.08	"River Water" NRC SLRS-5	0.26 ± 0.01	0.27 ± 0.00	102.6%
Na	$\mu mol \cdot L^{-1}$	ICP-OES	140	"	234.0 ± 4.3	237.3 ± 0.6	101.4%
K	$\mu mol \cdot L^{-1}$	ICP-OES	22.2	"	21.5 ± 1.0	19.1 ± 1.0	89.1%
Mg	$\mu mol \cdot L^{-1}$	ICP-OES	36.6	"	118.5 ± 8.9	123.3 ± 0.4	104.1%
Mn	$nmol \cdot L^{-1}$	ICP-OES	255	"	78.8 ± 3.3	79.7 ± 3.1	101.1%
Si	$\mu mol \cdot L^{-1}$	ICP-OES	5	"	42.0 ± 4.8	44.6 ± 0.2	106.1%

* Calculated from respective calibration according to DIN 32645 or Neitzel (2002).

Table S2. Used equilibrium constants (log K values) of aqueous Hg species and complexes.

AQUEOUS COMPLEXES		EQUILIBRIUM CONSTANTS					
Name	Reaction	PHREEQC minteq.dat	PHREEQC minteq.v4.dat	Visual Minteq thermo.vdb and shmgeneric 14.vdb		WHAM default.db7	
		log K	log K	log K	ΔLK_2	log K	ΔLK_2
$Hg(CO_3)_2^{2-}$	Hg(OH)2 + 2H+ + 2CO3-2 = Hg(CO3)2-2 + 2H2O		21.772	21.74			
$Hg(Cyanide)_2$	2Cyanide- + 2H+ + Hg(OH)2 = Hg(Cyanide)2 + 2H2O	40.6513	38.944	38.91			
$Hg(Cyanide)_2Cl^-$	Cl- + 2Cyanide- + 2H+ + Hg(OH)2 = Hg(Cyanide)2Cl- + 2H2O	40.3735					
$Hg(Cyanide)_3^-$	3Cyanide- + 2H+ + Hg(OH)2 = Hg(Cyanide)3- + 2H2O	44.4042	42.504	42.47			
$Hg(Cyanide)_3Br^{2-}$	Br- + 3Cyanide- + 2H+ + Hg(OH)2 = Hg(Cyanide)3Br-2 + 2H2O	44.9415					
$Hg(Cyanide)_3Cl^{2-}$	Cl- + 3Cyanide- + 2H+ + Hg(OH)2 = Hg(Cyanide)3Cl-2 + 2H2O	43.8332					
$Hg(Cyanide)_4^{2-}$	4Cyanide- + 2H+ + Hg(OH)2 = Hg(Cyanide)4-2 + 2H2O	47.4094	45.164	45.13			
$Hg(HS)_2$	2H+ + 2HS- + Hg(OH)2 = Hg(HS)2 + 2H2O	43.8178	44.516 / *45.242**	44.58 / *45.242**			
$Hg(N_3)_2$	Hg(OH)2 + 2 N3-1 + 2 H+ = Hg(N3)2 + 2 H+			21.52			
$Hg(NH_3)_2^{2+}$	Hg(OH)2 + 2NH4+ = Hg(NH3)2+2 + 2H2O	5.0341	5.506	5.47			
$Hg(NH_3)_3^{2+}$	Hg(OH)2 + 3NH4+ = Hg(NH3)3+2 + H+ + 2H2O	-3.2493	-3.138				
$Hg(NH_3)_4^{2+}$	Hg(OH)2 + 4NH4+ = Hg(NH3)4+2 + 2H+ + 2H2O	-11.7307	-11.482	-11.52			
$Hg(NO_2)_2$	Hg(OH)2 + 2 NO2-1 + 2 H+ = Hg(NO2)2 + 2 H2O			16.07			

Continued on next page

Table S2. Used equilibrium constants (log K values) of aqueous Hg species and complexes - Continued.

AQUEOUS COMPLEXES		EQUILIBRIUM CONSTANTS					
Name	Reaction	PHREEQC minteq.dat	PHREEQC minteq.v4.dat	Visual Minteq thermo.vdb and shmgeneric 14.vdb		WHAM default.db7	
		log K	log K	log K	ΔLK_2	log K	ΔLK_2
$Hg(NO_2)_3^-$	Hg(OH)2 + 3 NO2-1 + 2 H+ = Hg(NO2)3- + 2 H2O			17.61			
$Hg(NO_2)_4^{2-}$	Hg(OH)2 + 4 NO2-1 + 2 H+ = Hg(NO2)4-2 + 2 H2O			18.02			
$Hg(NO_3)_2$	2H+ + Hg(OH)2 + 2NO3- = Hg(NO3)2 + 2H2O	4.7791	5.38	5.38			
$Hg(OH)_3^-$	H2O + Hg(OH)2 = Hg(OH)3- + H+	-15.0042	-14.897				
$Hg(SCN)_2$	Hg(OH)2 +2 SCN-1 +2 H+ = Hg(SCN)2 + 2 H2O			23.66			
$Hg(RO)_2$	2ROH + Hg(OH)2 = Hg(RO)2 + 2H+			(6.7)	3.1		
$Hg(SCN)_3^-$	Hg(OH)2 +3 SCN-1 +2 H+ = Hg(SCN)3- + 2 H2O			26.47			
$Hg(SCN)_4^{2-}$	Hg(OH)2 + 4 SCN-1 + 2 H+ = Hg(SCN)4-2 + 2 H2O			28.27			
$Hg(SO_3)_2^{2-}$	Hg(OH)2 + 2 SO3-2 + 2 H+ = Hg(SO3)2-2 + H2O			29.62			
$Hg(SO_3)_2^{4-}$	Hg(OH)2 + 3 SO3-2 + 2 H+ = Hg(SO3)2-4 + H2O			30.66			
$Hg(SO_4)_2^{2-}$	Hg(OH)2 + 3 SO4-2 + 2 H+ = Hg(SO4)2-2 + 2 H2O			9.64			
$Hg(SR)_2$	2RS- + Hg(OH)2 +2H+ = Hg(SR)2 + 2H2O		*48.142°*	*48.142°*			
$Hg(SR)_2$	Hg2+ + 2RS- = Hg(SR)2					*42°*	
Hg^{2+}	2H+ + Hg(OH)2 = Hg+2 + 2H2O	6.097	6.194	6.164			
$Hg^0_{(aq)}$	0.5Hg2+2 + e- = Hg	6.9316	6.5667	6.5667			

Continued on next page

Table S2. Used equilibrium constants (log K values) of aqueous Hg species and complexes - Continued.

AQUEOUS COMPLEXES		EQUILIBRIUM CONSTANTS					
Name	Reaction	PHREEQC minteq.dat	PHREEQC minteq.v4.dat	Visual Minteq thermo.vdb and shmgeneric 14.vdb		WHAM default.db7	
		log K	log K	log K	ΔLK_2	log K	ΔLK_2
Hg_2^{2+}	4H+ + 2Hg(OH)2 + 2e- = Hg2+2 + 4H2O	42.987	43.185				
Hg_2OH^{3+}	2 Hg(OH)2 + 3 H+ = Hg2OH+3 H2O			9.031			
$Hg_3(OH)_3^{3+}$	3 Hg(OH)2 + 3 H+ = Hg3(OH)3+3 + 3 H2O			12.101			
$HgBr^+$	Br- + 2H+ + Hg(OH)2 = HgBr+ + 2H2O	15.8347	15.803	15.77			
$HgBr_2$	2Br- + 2H+ + Hg(OH)2 = HgBr2 + 2H2O	23.6065	24.2725	24.29			
$HgBr_2I_2^{2-}$	2Br- + 2H+ + Hg(OH)2 + 2I- = HgBr2I2-2 + 2H2O	32.3994	32.3994	32.3994			
$HgBr_3^-$	3Br- + 2H+ + Hg(OH)2 = HgBr3- + 2H2O	25.7857	26.7025	26.67			
$HgBr_3I^{2-}$	3Br- + 2H+ + Hg(OH)2 + I- = HgBr3I-2 + 2H2O	30.1528	30.1528	30.1528			
$HgBr_4^{2-}$	4Br- + 2H+ + Hg(OH)2 = HgBr4-2 + 2H2O	27.0633	27.933	27.9			
HgBrCl	Br- + Cl- + 2H+ + Hg(OH)2 = HgBrCl + 2H2O	22.0145	22.1811	22.1811			
HgBrI	Br- + 2H+ + Hg(OH)2 + I- = HgBrI + 2H2O	27.1212	27.3133	27.3133			
$HgBrI_3^{2-}$	Br- + 2H+ + Hg(OH)2 + 3I- = HgBrI3-2 + 2H2O	34.2135	34.2135	34.2135			
HgBrOH	Br- + H+ + Hg(OH)2 = HgBrOH + H2O	11.598	12.433	12.4			
$HgCl^+$	Cl- + 2H+ + Hg(OH)2 = HgCl+ + 2H2O	12.85	13.494	13.49			
$HgCl^+$	Hg2+ Cl- = HgCl+					7.21	

Continued on next page

Table S2. Used equilibrium constants (log K values) of aqueous Hg species and complexes - Continued.

AQUEOUS COMPLEXES		EQUILIBRIUM CONSTANTS					
Name	Reaction	PHREEQC minteq.dat	PHREEQC minteq.v4.dat	Visual Minteq thermo.vdb and shmgeneric 14.vdb		WHAM default.db7	
		log K	log K	log K	ΔLK_2	log K	ΔLK_2
$HgCl_2$	2Cl- + 2H+ + Hg(OH)2 = HgCl2 + 2H2O	19.2203	20.194	20.19			
$HgCl_2$	Hg2+ 2Cl- = HgCl2					13.98	
$HgCl_3^-$	3Cl- + 2H+ + Hg(OH)2 = HgCl3- + 2H2O	20.1226	21.194	21.19			
$HgCl_3^-$	Hg2+ 3Cl- = HgCl3-					15.06	
$HgCl_4^{2-}$	Hg2+ 4Cl- = HgCl4-2					15.42	
$HgCl_4^{2-}$	4Cl- + 2H+ + Hg(OH)2 = HgCl4-2 + 2H2O	20.5338	21.794	21.79			
HgClI	Cl- + 2H+ + Hg(OH)2 + I- = HgClI + 2H2O	25.3532	25.532	25.532			
HgClOH	Cl- + H+ + Hg(OH)2 = HgClOH + H2O	9.317	10.444	10.444			
$HgCyanide^+$	Cyanide- + 2H+ + Hg(OH)2 = HgCyanide+ + 2H2O	24.1738	23.194	23.16			
$HgCO_3$	Hg(OH)2 + 2H+ + CO3-2 = HgCO3 + 2H2O		18.272	18.29			
HgF^+	F- + 2H+ + Hg(OH)2 = HgF+ + 2H2O	8.0848	7.763	7.76			
$HgHCO_3^+$	Hg(OH)2 + 3H+ + CO3-2 = HgHCO3+ + 2H2O		22.542				
$HgHS_2^-$	Hg(OH)2 + H+ + 2HS- = HgHS2- + 2H2O		38.122 / *38.642**	38.09 / *38.642**			
HgI^+	2H+ + Hg(OH)2 + I- = HgI+ + 2H2O	18.8949	19.603	19.57			
HgI_2	2H+ + Hg(OH)2 + 2I- = HgI2 + 2H2O	30.1081	30.8225	30.79			
HgI_3^-	2H+ + Hg(OH)2 + 3I- = HgI3- + 2H2O	33.7935	34.6025	34.57			
HgI_4^{2-}	2H+ + Hg(OH)2 + 4I- = HgI4-2 + 2H2O	35.7858	36.533	36.5			
$HgR^+{\sim}_{\text{fulvic acid}}$	Hg2+ + R~ = HgR+~					(3.51)	5.1

Continued on next page

Table S2. Used equilibrium constants (log K values) of aqueous Hg species and complexes - Continued.

AQUEOUS COMPLEXES		EQUILIBRIUM CONSTANTS					
Name	**Reaction**	**PHREEQC minteq.dat**	**PHREEQC minteq.v4.dat**	**Visual Minteq thermo.vdb and shmgeneric 14.vdb**		**WHAM default.db7**	
		log K	**log K**	**log K**	**ΔLK_2**	**log K**	**ΔLK_2**
HgOHR~ fulvic acid	HgOH+ + R~ = HgR+~					(3.51)	5.1
HgR^+~ humic acid	Hg2+ + R~ = HgR+~					(3.51)	5.1
HgOHR~ humic acid	HgOH+ + R~ = HgR+~					(3.51)	5.1
$HgNH_3^{2+}$	H+ + Hg(OH)2 + NH4+ = HgNH3+2 + 2H2O	5.6139	5.75				
HgN_3^+	2H+ + Hg(OH)2 + N3- = HgN3+ + 2H2O			13.96			
$HgNO_2^+$	2H+ + Hg(OH)2 + NO2- = HgNO2+ + 2H2O			12.1			
$HgNO_3^+$	2H+ + Hg(OH)2 + NO3- = HgNO3+ + 2H2O	6.4503	5.7613	5.7613			
$HgOH^+$	H+ + Hg(OH)2 = HgOH+ + H2O	2.6974	2.797	2.767			
$HgOH^+$	Hg2+ + OH- = HgOH+					10.6	
$HgOH_2$	Hg2+ +2 OH- = HgOH2					21.83	
$HgOH_3^-$	Hg2+ +3 OH- = HgOH3-					20.9	
$HgOHCO_3^-$	Hg(OH)2 + CO3-2 + H+ = HgOHCO3- + H2O			11.36			
HgOHI	1H+ + Hg(OH)2 + I- = HgOHI + H2O			9.41			
HgOHgSH	Hg(OH)2 + HS- + H+ = HOHgSH + H2O		*22.447* [#]				
HgOHSCN	Hg(OH)2 + SCN-1 + H+ = HgOHSCN + H2O			12.61			
$HgSR^+$	RS- + Hg(OH)2 + 2H+ = HgSR+ + 2H2O		*26.145°*				

Continued on next page

Table S2. Used equilibrium constants (log K values) of aqueous Hg species and complexes - Continued.

AQUEOUS COMPLEXES		EQUILIBRIUM CONSTANTS					
Name	Reaction	PHREEQC minteq.dat	PHREEQC minteq.v4.dat	Visual Minteq thermo.vdb and shmgeneric 14.vdb		WHAM default.db7	
		log K	log K	log K	ΔLK_2	log K	ΔLK_2
$HgSR^+$	Hg2+ + RS- = HgSR+					*20°*	
HgS_2^{2-}	2HS- + Hg(OH)2 = HgS2-2 + 2H2O	31.2398	29.414 / *29.342**	29.38			
$HgSCN^+$	Hg(OH)2 + SCN-1 + 2 H+ = HgSCN+ + 2 H2O			15.8			
$HgSO_4$	2H+ + Hg(OH)2 + SO4-2 = HgSO4 + 2H2O	7.4911	8.612	8.63			
$HgSO_4$	Hg2+ +SO4-2- = HgSO4					2	
RSH	RS- + H+		*-10°*	*-10°*		*-10°*	

values in itialics were updated in the database in scenario 5 to 8

values in brackets are intrinsic constants for Hg binding in the Stockholm Humic Model (Visual MINTEQ) or the Humic Ion Binding Model VII (WHAM), respectively.

* log K from Drott et al. 2013

log K from Dyrssen & Wedborg (1991) as published in Skyllberg (2008). The lower of the two published constants was chosen according to Drott et al. (2013)

° log K from Skyllberg (2008)

All log K conversions necessary to fit formats of respective databases were performed using thermodynamic data from Wagman et al. (1982).

Table S3. Applied modeling scenarios.

	Scenario	Name	DOM composition	database	applied codes
no DOM	1	"no DOM"	no implementation of DOM	unchanged	PHREEQC, Visual MINTEQ
DOM as FA+HA	2	"100% FA"	100% fulvic acid	unchanged	Visual MINTEQ, WHAM
	3	"default DOM"	100% fulvic acid, 82.5% active	unchanged	Visual MINTEQ
	4	"Malcolm"	13% fulvic acid, 1.5% humic acid*	unchanged	Visual MINTEQ, WHAM
DOM as thiols	5	"0.15% thiols"	0.15wt.% of DOC thiol groups†	thiol groups added, Hg-sulfides updated	PHREEQC, Visual MINTEQ, WHAM
	6	"optimized thiols"	0.04375wt.% of DOC thiol groups	thiol groups added, Hg-sulfides updated	PHREEQC, Visual MINTEQ, WHAM
DOM as thiols and FA+HA	7	"Malcolm + optimized thiols"	13% fulvic acid, 1.5% humic acid*, 0.04375wt.% of DOC thiol groups	thiol groups added, Hg-sulfides updated, intrinsic Hg constants in SHM and Model VII lowered to 0.1 and 1.125, respectively.	Visual MINTEQ, WHAM
	8	"best fit"	13% fulvic acid, 1.5% humic acid*, 0.03wt.% of DOC "reactive" thiol groups#	thiol groups added, Hg-sulfides updated, intrinsic Hg constants in Model VII set to 3.1 and 3.3 for FA and HA, respectively. ΔLK_2 set to 1.7	WHAM

*Malcolm, R. L. Factors to be considered in the isolation and characterization of aquatic humic substances. In *Humic substances in the aquatic and terrestrial environment*; Springer, 1991; pp 7–36.

† Skyllberg, U. Competition among thiols and inorganic sulfides and polysulfides for Hg and MeHg in wetland soils and sediments under suboxic conditions: Illumination of controversies and implications for MeHg net production. J. Geophys. Res. 2008, 113.

#Haitzer, M.; Aiken, G. R.; Ryan, J. N. Binding of Mercury(II) to Dissolved Organic Matter: The Role of the Mercury-to-DOM Concentration Ratio. Environ. Sci. Technol. 2002, 36 (16), 3564–3570.

Table S4. Hydrochemical composition of groundwater samples from Site A.

Parameter	Sample	1	2	3	4	5	6	7	8	9
pH		7.66	6.60	8.76	11.48	6.42	8.14	8.05	7.12	7.46
pe		7.48	8.66	6.52	5.45	4.91	6.63	5.81	6.31	6.48
Eh	mV	431	495	373	308	289	381	335	364	372
Temp	°C	17.0	14.5	15.1	12.2	23.8	16.1	17.0	18.0	16.1
EC	$\mu S \cdot cm^{-1}$	3770	2570	3490	6050	2670	3560	7260	17980	7040
O2	$mg \cdot L^{-1}$	2.2	4.7	7.6	6.3	5.9	4.3	1.3	1.8	1.5
DOC	$\mu mol \cdot L^{-1}$	73.1	75.1	197	121	123	114	151	94.4	104
Alkalinity	$meq \cdot L^{-1}$	3.91	2.81	5.11	6.26	*n.d.*	*n.d.*	*n.d.*	3.49	3.81
Br	$\mu mol \cdot L^{-1}$	122	162	92	159	260	206	46	520	298
Ca	$mmol \cdot L^{-1}$	1.43	5.58	2.36	0.17	3.71	0.93	1.05	5.02	1.35
Cl	$mmol \cdot L^{-1}$	29	17	20	51	13	25	72	155	66
F	$\mu mol \cdot L^{-1}$	9.9	0.0	12.9	33.3	14.3	9.8	48.4	26.1	21.6
K	$\mu mol \cdot L^{-1}$	48	57	209	36	33	43	71	163	71
Mg	$\mu mol \cdot L^{-1}$	242	447	812	29	793	194	124	511	203
Mn	$\mu mol \cdot L^{-1}$	0.2	0.1	1.0	0.0	36.4	0.0	0.1	53.2	0.7
NO_3^-	$\mu mol \cdot L^{-1}$	59	37	196	89	85	76	11	55	43
Na	$mmol \cdot L^{-1}$	31.8	12.8	28.0	54.8	17.9	30.5	68.1	173	64.2
SO_4^{2-}	$mmol \cdot L^{-1}$	5.44	6.12	7.80	5.63	7.54	5.77	5.72	7.16	6.07
Si	$\mu mol \cdot L^{-1}$	128	143	1019	1167	1081	156	113	105	101
Zn	$\mu mol \cdot L^{-1}$	0.00	0.47	0.17	0.00	0.43	0.00	0.00	0.37	0.16
Hg	$nmol \cdot L^{-1}$	118	39	60	245	84	60	22	109	43

n.d.: not determined

Table S5. Hydrochemical composition of groundwater samples from Site B.

Parameter	Sample	1	2	3	4	5	6
pH		6.62	6.63	6.63	6.58	6.58	6.59
pe		8.47	8.36	*n.d.*	7.71	7.16	7.72
Eh	mV	480	474	*n.d.*	438	407	438
Temp	°C	12.4	12.6	12.6	13.2	13.2	12.9
EC	$\mu S \cdot cm^{-1}$	373	397	401	405	421	413
O2	$mg \cdot L^{-1}$	6.9	5.5	6.8	5.8	6.2	5.5
DOC	$\mu mol \cdot L^{-1}$	64.4	56.3	58.7	76.2	46.1	47.7
Alkalinity	$meq \cdot L^{-1}$	2.60	2.99	2.85	2.85	3.06	2.90
Br	$\mu mol \cdot L^{-1}$	0.33	0.26	0.30	0.36	0.33	0.38
Ca	$mmol \cdot L^{-1}$	1.42	1.52	1.54	1.57	1.62	1.59
Cl	$\mu mol \cdot L^{-1}$	504	558	586	544	564	568
F	$\mu mol \cdot L^{-1}$	13.9	13.0	13.2	12.1	11.4	11.5
K	$\mu mol \cdot L^{-1}$	27.1	29.1	29.5	29.5	30.9	30.4
Mg	$\mu mol \cdot L^{-1}$	348	371	375	380	397	391
NO_3^-	$\mu mol \cdot L^{-1}$	268	271	257	275	280	280
Na	$\mu mol \cdot L^{-1}$	407	460	461	470	515	515
SO_4^{2-}	$\mu mol \cdot L^{-1}$	189	208	199	221	222	212
Si	$\mu mol \cdot L^{-1}$	209	212	208	212	225	231
Sr	$\mu mol \cdot L^{-1}$	1.8	1.9	2.0	1.9	2.1	2.0
Hg	$nmol \cdot L^{-1}$	287	930	1325	138	58	171

n.d.: not determined

Table S6. Hydrochemical composition of groundwater samples from Site C.

Parameter	Sample	1	2	3	4	5	6	7	8	9
pH		6.34	6.40	6.11	6.22	6.69	6.77	7.37	6.45	6.22
pe		*n.d.*	7.01	*n.d.*	*n.d.*	*n.d.*	*n.d.*	*n.d.*	9.15	*n.d.*
Eh	mV	*n.d.*	393	*n.d.*	*n.d.*	*n.d.*	*n.d.*	*n.d.*	524	*n.d.*
Temp	°C	11.9	9.7	12.2	12.0	13.0	15.2	12.3	15.2	11.8
EC	$\mu S \cdot cm^{-1}$	520	319	417	331	659	760	414	490	347
O2	$mg \cdot L^{-1}$	4.1	0.9	3.6	1.9	5.5	3.6	5.5	3.6	4.2
DOC	$\mu mol \cdot L^{-1}$	102	383	89.6	87.4	439	439	282	282	64.4
Alkalinity	$meq \cdot L^{-1}$	0.76	1.89	0.81	1.17	5.89	7.09	2.92	3.98	1.43
Ca	$mmol \cdot L^{-1}$	0.84	0.69	0.84	0.86	2.15	2.19	1.38	1.39	0.77
Cl	$mmol \cdot L^{-1}$	3.29	1.37	2.48	1.43	1.12	0.62	0.90	0.85	1.77
F	$\mu mol \cdot L^{-1}$	6.0	9.5	4.9	4.9	267	397	117	149	4.8
K	$\mu mol \cdot L^{-1}$	129	88	59	41	944	1143	304	359	51
Mg	$\mu mol \cdot L^{-1}$	360.2	212.7	400.5	344.9	439.4	451.1	247.7	266.0	367.2
Mn	$\mu mol \cdot L^{-1}$	5.0	42.6	2.2	0.1	0.6	0.8	0.9	1.0	0.4
NO_3^-	$\mu mol \cdot L^{-1}$	112.4	13.8	82.7	70.9	53.6	20.5	74.9	109.1	74.7
Na	$mmol \cdot L^{-1}$	0.4	0.9	0.5	0.3	1.2	1.3	0.9	1.0	1.1
SO_4^{2-}	$\mu mol \cdot L^{-1}$	132.4	27.6	124.9	161.9	167.2	193.0	153.9	194.7	124.4
Si	$\mu mol \cdot L^{-1}$	180.0	148.8	132.1	132.1	128.8	151.5	104.6	132.1	228.1
Hg	$nmol \cdot L^{-1}$	3899	289	2617	244	57	68	125	154	1758

n.d.: not determined

Table S7. Linear correlation analysis between measured and modeled total inorganic Hg concentrations (log(M)).

	Scenario	Name	Intercept	Slope	R^2	adj. R^2	p-value
DOM as FA+HA	2	V-MINTEQ SHM "100% FA"	10.83	2.86	0.72	0.70	1.92E-07
		V-MINTEQ ND "100% FA"	21.20	4.75	0.76	0.74	2.54E-06
		WHAM "100% FA"	10.88	2.87	0.69	0.68	5.12E-07
	3	V-MINTEQ SHM "default DOM"	9.47	2.62	0.72	0.70	1.86E-07
		V-MINTEQ ND "default DOM"	20.59	4.62	0.75	0.73	3.57E-06
	4	V-MINTEQ SHM "Malcolm"	0.56	1.10	0.89	0.89	3.31E-12
		V-MINTEQ ND "Malcolm"	10.03	2.75	0.56	0.50	1.97E-02
		WHAM "Malcolm"	1.15	1.19	0.76	0.75	2.35E-08
DOM as thiols	5	PHREEQC mit Hg0 "0.15% thiols" (minteq.v4.dat)	19.50	4.08	0.41	0.38	8.22E-04
		V-MINTEQ "0.15% thiols"	20.62	4.22	0.32	0.28	4.28E-03
		WHAM "0.15% thiols"	20.29	4.20	0.39	0.36	1.14E-03
	6	PHREEQC (minteq.v4.dat) "optimized thiols"	-0.04	0.99	0.95	0.95	3.33E-16
		V-MINTEQ "optimized thiols"	-0.04	0.99	0.95	0.95	3.33E-16
		WHAM "optimized thiols"	-0.04	0.99	0.95	0.95	3.33E-16
DOM as thiols and HA+FA	7	WHAM "Malcolm + optimized thiols"	0.07	1.01	0.96	0.96	1.11E-16
		V-Minteq SHM "Malcolm + optimized thiols"	-0.01	0.99	0.95	0.95	5.55E-16
	8	WHAM "best fit"	-0.12	0.98	0.97	0.96	1.00E-17

Table S8. Linear correlation analysis between measured and modeled DOM bound Hg concentrations (log(M)).

	Scenario	Name	Intercept	Slope	R^2	adj. R^2	p-value
DOM as FA+HA	2	V-MINTEQ SHM "100% FA"	-7.04	-0.01	0.00	-0.05	9.28E-01
		V-MINTEQ ND "100% FA"	-6.15	0.08	0.02	-0.05	6.14E-01
		WHAM "100% FA"	-6.04	0.11	0.05	0.01	2.89E-01
	3	V-MINTEQ SHM "default DOM"	-6.97	0.00	0.00	-0.05	9.78E-01
		V-MINTEQ ND "default DOM"	-6.16	0.08	0.02	-0.04	5.95E-01
	4	V-MINTEQ SHM "Malcolm"	-7.09	0.06	0.02	-0.03	5.68E-01
		V-MINTEQ ND "Malcolm"	-9.49	-0.26	0.26	0.16	1.59E-01
		WHAM "Malcolm"	-5.96	0.19	0.21	0.17	2.51E-02
DOM as thiols	5	PHREEQC mit Hg0 "0.15% thiols" (minteq.v4.dat)	-5.95	0.20	0.33	0.30	3.05E-03
		V-MINTEQ "0.15% thiols"	-6.02	0.19	0.33	0.30	3.58E-03
		WHAM "0.15% thiols"	-5.95	0.20	0.33	0.30	3.05E-03
	6	PHREEQC (minteq.v4.dat) "optimized thiols"	-6.27	0.22	0.31	0.28	4.76E-03
		V-MINTEQ "optimized thiols"	-6.27	0.22	0.31	0.28	4.76E-03
		WHAM "optimized thiols"	-6.27	0.22	0.31	0.28	4.76E-03
DOM as thiols and HA+FA	7	WHAM "Malcolm + optimized thiols"	-6.40	0.20	0.27	0.24	8.73E-03
		V-Minteq SHM "Malcolm + optimized thiols"	-6.20	0.22	0.31	0.28	4.36E-03
	8	WHAM "best fit"	-5.83	0.27	0.45	0.42	3.37E-04

References

Aiken, G.R., 1985. Humic Substances in Soil, Sediment, and Water: Geochemistry, Isolation, and Characterization. John Wiley and Sons.

Allison, J.D., Brown, D.S., Novo-Gradac, K.J., 1991. MINTEQA2/PRODEFA2, A Geochemical Assessment Model for Environmental Systems: Version 3.0 User's Manual (No. EPA/600/3-91/021).

Amirbahman, A., Kent, D.B., Curtis, G.P., Marvin-DiPasquale, M.C., 2013. Kinetics of Homogeneous and Surface-Catalyzed Mercury(II) Reduction by Iron(II). Environ. Sci. Technol. 47, 7204–7213. doi:10.1021/es401459p

Artinger, R., Buckau, G., Geyer, S., Fritz, P., Wolf, M., Kim, J.I., 2000. Characterization of groundwater humic substances: influence of sedimentary organic carbon. Appl. Geochem. 15, 97–116. doi:10.1016/S0883-2927(99)00021-9

Barkay, T., Miller, S.M., Summers, A.O., 2003. Bacterial mercury resistance from atoms to ecosystems. FEMS Microbiol. Rev. 27, 355–384. doi:10.1016/S0168-6445(03)00046-9

Barringer, J.L., Riskin, M.L., Szabo, Z., Reilly, P.A., Rosman, R., Bonin, J.L., Fischer, J.M., Heckathorn, H.A., 2010. Mercury and Methylmercury Dynamics in a Coastal Plain Watershed, New Jersey, USA. Water. Air. Soil Pollut. 212, 251–273. doi:10.1007/s11270-010-0340-1

Bearup, L.A., Navarre-Sitchler, A.K., Maxwell, R.M., McCray, J.E., 2012. Kinetic Metal Release from Competing Processes in Aquifers. Environ. Sci. Technol. 46, 6539–6547. doi:10.1021/es203586y

Bessinger, B.A., Vlassopoulos, D., Serrano, S., O'Day, P.A., 2012. Reactive Transport Modeling of Subaqueous Sediment Caps and Implications for the Long-Term Fate of Arsenic, Mercury, and Methylmercury. Aquat. Geochem. 18, 297–326. doi:10.1007/s10498-012-9165-4

Bollen, A., Wenke, A., Biester, H., 2008. Mercury speciation analyses in HgCl2-contaminated soils and groundwater—Implications for risk assessment and remediation strategies. Water Res. 42, 91–100. doi:10.1016/j.watres.2007.07.011

Brosset, C., 1987. The behavior of mercury in the physical environment. Water. Air. Soil Pollut. 34, 145–166. doi:10.1007/BF00184757

Carling, G.T., Diaz, X., Ponce, M., Perez, L., Nasimba, L., Pazmino, E., Rudd, A., Merugu, S., Fernandez, D.P., Gale, B.K., Johnson, W.P., 2013. Particulate and Dissolved Trace Element Concentrations in Three Southern Ecuador Rivers Impacted by Artisanal Gold Mining. Water. Air. Soil Pollut. 224, 1–16. doi:10.1007/s11270-012-1415-y

Chiasson-Gould, S.A., Blais, J.M., Poulain, A.J., 2014. Dissolved Organic Matter Kinetically Controls Mercury Bioavailability to Bacteria. Environ. Sci. Technol. 48, 3153–3161. doi:10.1021/es4038484

Christensen, J.B., Botma, J.J., Christensen, T.H., 1999. Complexation of Cu and Pb by DOC in polluted groundwater: a comparison of experimental data and predictions by computer speciation models (WHAM and MINTEQA2). Water Res. 33, 3231–3238. doi:10.1016/S0043-1354(99)00020-2

Christensen, J.B., Christensen, T.H., 1999. Complexation of Cd, Ni, and Zn by DOC in Polluted Groundwater: A Comparison of Approaches Using

Resin Exchange, Aquifer Material Sorption, and Computer Speciation Models (WHAM and MINTEQA2). Environ. Sci. Technol. 33, 3857–3863. doi:10.1021/es981105t

DIN Deutsches Institut für Normung e. V., DIN German Institute for Standardization, 2008. DIN 32645 (2008-11-00) Chemical analysis - Decision limit, detection limit and determination limit under repeatability conditions - Terms, methods, evaluation (Nachweis-, Erfassungs- und Bestimmungsgrenze unter Wiederholbedingungen - Begriffe, Verfahren, Auswertung).

Drott, A., Björn, E., Bouchet, S., Skyllberg, U., 2013. Refining Thermodynamic Constants for Mercury(II)-Sulfides in Equilibrium with Metacinnabar at Sub-Micromolar Aqueous Sulfide Concentrations. Environ. Sci. Technol. 47, 4197–4203. doi:10.1021/es304824n

Dyrssen, D., Wedborg, M., 1991. The sulphur-mercury(II) system in natural waters. Water. Air. Soil Pollut. 56, 507–519. doi:10.1007/BF00342295

EN, European Committee for Standardization, 2007. Method 1483, Water quality- Determination of mercury- Method using atomic absorption spectrometry; German version.

EN, European Committee for Standardization, 2007. Method 1483, Water quality- Determination of mercury- Method using atomic absorption spectrometry; German version.

Feyte, S., Tessier, A., Gobeil, C., Cossa, D., 2010. In situ adsorption of mercury, methylmercury and other elements by iron oxyhydroxides and organic matter in lake sediments. Appl. Geochem. 25, 984–995. doi:10.1016/j.apgeochem.2010.04.005

Gemici, Ü., Tarcan, G., Melis Somay, A., Akar, T., 2009. Factors controlling the element distribution in farming soils and water around the abandoned Halıköy mercury mine (Beydağ, Turkey). Appl. Geochem. 24, 1908–1917. doi:10.1016/j.apgeochem.2009.07.004

Grassi, S., Netti, R., 2000. Sea water intrusion and mercury pollution of some coastal aquifers in the province of Grosseto (Southern Tuscany — Italy). J. Hydrol. 237, 198–211. doi:10.1016/S0022-1694(00)00307-3

Gu, B., Bian, Y., Miller, C.L., Dong, W., Jiang, X., Liang, L., 2011. Mercury reduction and complexation by natural organic matter in anoxic environments. Proc. Natl. Acad. Sci. 108, 1479–1483. doi:10.1073/pnas.1008747108

Gustafsson, J.P., 2013. Tutorial to Visual MINTEQ version 3.0.

Gustafsson, J.P., 2001. Modeling the Acid–Base Properties and Metal Complexation of Humic Substances with the Stockholm Humic Model. J. Colloid Interface Sci. 244, 102–112. doi:10.1006/jcis.2001.7871

Haitzer, M., Aiken, G.R., Ryan, J.N., 2002. Binding of Mercury(II) to Dissolved Organic Matter: The Role of the Mercury-to-DOM Concentration Ratio. Environ. Sci. Technol. 36, 3564–3570. doi:10.1021/es025699i

ISO, International Organization for Standardization, 1996. Method 9963-1, Water quality- Determination of alkalinity -Part 1: Determination of total and composite alkalinity, German version.

Johannesson, K.H., Neumann, K., 2013. Geochemical cycling of mercury in a deep, confined aquifer: Insights from biogeochemical reactive transport modeling. Geochim. Cosmochim. Acta 106, 25–43. doi:10.1016/j.gca.2012.12.010

Khwaja, A.R., Bloom, P.R., Brezonik, P.L., 2006. Binding Constants of Divalent Mercury (Hg2+) in Soil Humic Acids and Soil Organic Matter. Environ. Sci. Technol. 40, 844–849. doi:10.1021/es051085c

Kinniburgh, D.G., van Riemsdijk, W.H., Koopal, L.K., Borkovec, M., Benedetti, M.F., Avena, M.J., 1999. Ion binding to natural organic matter: competition, heterogeneity, stoichiometry and thermodynamic consistency. Colloids Surf. Physicochem. Eng. Asp. 151, 147–166. doi:10.1016/S0927-7757(98)00637-2

Leopold, K., Foulkes, M., Worsfold, P., 2010. Methods for the determination and speciation of mercury in natural waters—A review. Anal. Chim. Acta 663, 127–138. doi:10.1016/j.aca.2010.01.048

Linberg, R.D., Runnels, D., 1984. Ground water redox reactions: an analysis of equilibrium state applied to Eh measurements and geochemical modeling. Science 225, 925–927.

Lövgren, L., Sjöberg, S., 1989. Equilibrium approaches to natural water systems—7. Complexation reactions of copper(II), cadmium(II) and mercury(II) with dissolved organic matter in a concentrated bog-water. Water Res. 23, 327–332. doi:10.1016/0043-1354(89)90098-5

LUBW, 2014. Hydrogeological Map of Baden Württemberg [WWW Document]. URL http://udo.lubw.baden-wuerttemberg.de/public/pages/map/default/index.xhtml (accessed 9.24.14).

Malcolm, R.L., 1991. Factors to be considered in the isolation and characterization of aquatic humic substances, in: Humic Substances in the Aquatic and Terrestrial Environment. Springer, pp. 7–36.

Maprani, A.C., Al, T.A., MacQuarrie, K.T., Dalziel, J.A., Shaw, S.A., Yeats, P.A., 2005. Determination of Mercury Evasion in a Contaminated Headwater Stream. Environ. Sci. Technol. 39, 1679–1687. doi:10.1021/es048962j

Maurice, P.A., Leff, L.G., 2002. Hydrogeochemical controls on the organic matter and bacterial ecology of a small freshwater wetland in the New Jersey Pine Barrens. Water Res. 36, 2561–2570. doi:10.1016/S0043-1354(01)00465-1

Meili, M., Iverfeldt, A., Håkanson, L., 1991. Mercury in the surface water of Swedish forest lakes —concentrations, speciation and controlling factors. Water. Air. Soil Pollut. 56, 439–453. doi:10.1007/BF00342290

Merck, 2014. Safety Data Sheet Mercury:

Merck, 2010. Safety Data Sheet: Mercury(II)Chloride (HgCl2):

Merian, E., Anke, M., Ihnat, M., Stoeppler, M. (Eds.), 2004. Elements and their compounds in the environment: occurence, analysis and biological relevance, 2nd completely rev. and enl. ed. ed. Wiley-VCH, Weinheim.

Miller, C.L., Liang, L., Gu, B., 2012. Competitive ligand exchange reveals time dependant changes in the reactivity of Hg?dissolved organic matter complexes. Environ. Chem. 9, 495. doi:10.1071/EN12096

Milne, C.J., Kinniburgh, D.G., Tipping, E., 2001. Generic NICA-Donnan model parameters for proton binding by humic substances. Environ. Sci. Technol. 35, 2049–2059. doi:10.1021/es000123j

Milne, C.J., Kinniburgh, D.G., Van Riemsdijk, W.H., Tipping, E., 2003. Generic NICA - Donnan model parameters for metal-ion binding by humic substances. Environ. Sci. Technol. 37, 958–971. doi:10.1021/es0258879

Muresan, B., Pernet-Coudrier, B., Cossa, D., Varrault, G., 2011. Measurement and modeling of mercury complexation by dissolved organic matter isolates from freshwater and effluents of a major wastewater treatment plant. Appl. Geochem. 26, 2057–2063. doi:10.1016/j.apgeochem.2011.07.003

Nagy, K.L., Manceau, A., Gasper, J.D., Ryan, J.N., Aiken, G.R., 2011. Metallothionein-Like Multinuclear Clusters of Mercury(II) and Sulfur in Peat. Environ. Sci. Technol. 45, 7298–7306. doi:10.1021/es201025v

Neitzel, V., 2002. Calibration of Analytical Methods (part 2) non linear calibration functions (Die Kalibration von Analysenverfahren (Teil 2) Nicht lineare Kalibrationsfunktionen). Chem. Labor Biotech. 53.

Ndungu, K., 2012. Model Predictions of Copper Speciation in Coastal Water Compared to Measurements by Analytical Voltammetry. Environ. Sci. Technol. 46, 7644–7652. doi:10.1021/es301017x

Parkhurst, D.L., Apello, C.A.J., 2013. Description of Input and Examples for PHREEQC Version 3—A Computer Program for Speciation, Batch-Reaction, One-Dimensional Transport, and Inverse Geochemical Calculations (No. book 6, chap. A43), U.S. Geological Survey Techniques and Methods.

Perry, D.L., 2011. Handbook of Inorganic Compounds, Second Edition. CRC Press.

Qian, J., Skyllberg, U., Frech, W., Bleam, W.F., Bloom, P.R., Petit, P.E., 2002. Bonding of methyl mercury to reduced sulfur groups in soil and stream organic matter as determined by x-ray absorption spectroscopy and binding affinity studies. Geochim. Cosmochim. Acta 66, 3873–3885. doi:10.1016/S0016-7037(02)00974-2

Richard, J.-H., Bischoff, C., Ahrens, C.G.M., Biester, H., 2016. Mercury (II) reduction and co-precipitation of metallic mercury on hydrous ferric oxide in contaminated groundwater. Sci. Total Environ. 539, 36–44. doi:10.1016/j.scitotenv.2015.08.116

Ryaboshapko, A., Ilyin, I., Bullock, R., Ebinghaus, R., 2001. INTERCOMPARISON STUDY OF NUMERICAL MODELS FOR LONG-RANGE ATMOSPHERIC TRANSPORT OF MERCURY: Stage I. Comparison of chemical modules for mercury transformations in a cloud/fog environment, MSC-E Technical Report 2/2001. METEOROLOGICAL SYNTHESIZING CENTRE - EAST, Moscow, Russia.

Sander, R., 1999. Compilation of Henry's law constants for inorganic and organic species of potential importance in environmental chemistry. Max-Planck Institute of Chemistry, Air Chemistry Department.

Schöndorf, T., Egli, M., Biester, H., Mailahn, W., Rotard, W., 1999. Distribution, Bioavailability and Speciation of Mercury in Contaminated Soil and Groundwater of a Former Wood Impregnation Plant, in: Ebinghaus, D.R., Turner, D.R.R., Lacerda, P.D.L.D. de, Vasiliev, P.D.O., Salomons, P.D.W. (Eds.), Mercury Contaminated Sites, Environmental Science. Springer Berlin Heidelberg, pp. 181–206.

Sjöstedt, C.S., Gustafsson, J.P., Köhler, S.J., 2010. Chemical equilibrium modeling of organic acids, pH, aluminum, and iron in Swedish surface waters. Environ. Sci. Technol. 44, 8587–8593.

Skyllberg, U., 2011. Chemical Speciation of Mercury in Soil and Sediment, in: Liu, G., Cai, Y., O'Driscoll, N. (Eds.), Environmental Chemistry and Toxicology of Mercury. John Wiley & Sons, Inc., pp. 219–258.

Skyllberg, U., 2010. Mercury biogeochemistry in soils and sediments, in: Synchrotron-Based Techniques in Soils and Sediments, Developments in Soil Science. pp. 379–410.

Skyllberg, U., 2008. Competition among thiols and inorganic sulfides and polysulfides for Hg and MeHg in wetland soils and sediments under suboxic conditions: Illumination of controversies and implications for MeHg net production. J. Geophys. Res. 113. doi:10.1029/2008JG000745

Skyllberg, U., Qian, J., Frech, W., Xia, K., Bleam, W.F., 2003. Distribution of mercury, methyl mercury and organic sulphur species in soil, soil solution and stream of a boreal forest catchment. Biogeochemistry 64, 53–76. doi:10.1023/A:1024904502633

Skyllberg, U., Xia, K., Bloom, P.R., Nater, E.A., Bleam, W.F., 2000. Binding of mercury(II) to reduced sulfur in soil organic matter along upland-peat soil transects. J. Environ. Qual. 29, 855–865.

Stockdale, A., Tipping, E., Lofts, S., 2015. Dissolved trace metal speciation in estuarine and coastal waters: Comparison of WHAM/Model VII predictions with analytical results: Trace metal speciation in estuarine and coastal waters. Environ. Toxicol. Chem. 34, 53–63. doi:10.1002/etc.2789

Swift, R.S., 1999. Macromolecular properties of soil humic substances: Fact, fiction, and opinion. Soil Sci. 164, 790–802.

Thurman, E.M., Malcolm, R.L., 1981. Preparative isolation of aquatic humic substances. Environ. Sci. Technol. 15, 463–466.

Tipping, E., 2007. Modelling the interactions of Hg(II) and methylmercury with humic substances using WHAM/Model VI. Appl. Geochem., Metal interactions with natural organic matter and Watershed-scale geochemistry 15th Annual V.M. Goldschmidt Conference Selected papers of the 15th Annual V.M. Goldschmidt Conference held in Moscow, Idaho (USA), in May 2005. 22, 1624–1635. doi:10.1016/j.apgeochem.2007.03.021

Tipping, E., 1998. Humic ion-binding model VI: an improved description of the interactions of protons and metal ions with humic substances. Aquat. Geochem. 4, 3–47.

Tipping, E., 1994. WHAMC—A chemical equilibrium model and computer code for waters, sediments, and soils incorporating a discrete site/electrostatic model of ion-binding by humic substances. Comput. Geosci. 20, 973–1023. doi:10.1016/0098-3004(94)90038-8

Tipping, E., Lofts, S., Sonke, J.E., 2011. Humic Ion-Binding Model VII: a revised parameterisation of cation-binding by humic substances. Environ. Chem. 8, 225. doi:10.1071/EN11016

UNEP, 2013. Global Mercury Assessment 2013: Sources, Emissions, Releases and Environmental Transport. UNEP Chemicals Branch, Geneva, Switzerland.

UNEP, 2002. Global Mercury Assessment 2002. UNEP Chemicals Branch, Geneva, Switzerland.

Unsworth, E.R., Warnken, K.W., Zhang, H., Davison, W., Black, F., Buffle, J., Cao, J., Cleven, R., Galceran, J., Gunkel, P., Kalis, E., Kistler, D., van

Leeuwen, H.P., Martin, M., Noël, S., Nur, Y., Odzak, N., Puy, J., van Riemsdijk, W., Sigg, L., Temminghoff, E., Tercier-Waeber, M.-L., Toepperwien, S., Town, R.M., Weng, L., Xue, H., 2006. Model Predictions of Metal Speciation in Freshwaters Compared to Measurements by In Situ Techniques. Environ. Sci. Technol. 40, 1942–1949. doi:10.1021/es051246c

USEPA, 2002. Method 1631, Revision E: Mercury in Water by Oxidation, Purge and Trap, and Cold Vapor Atomic Fluorescence Spectrometry.

Wagman, D.D., Evans, W.H., Parker, V.B., Schumm, R.H., Halow, I., 1982. The NBS Tables of Chemical Thermodynamic Properties. Selected Values for Inorganic and C1 and C2 Organic Substances in SI Units.

Wiatrowski, H.A., Ward, P.M., Barkay, T., 2006. Novel Reduction of Mercury(II) by Mercury-Sensitive Dissimilatory Metal Reducing Bacteria. Environ. Sci. Technol. 40, 6690–6696. doi:10.1021/es061046g

Wollenberg, J.L., Peters, S.C., 2009. Mercury emission from a temperate lake during autumn turnover. Sci. Total Environ. 407, 2909–2918. doi:10.1016/j.scitotenv.2008.12.017

Wong, J.C.Y., Williams, D.D., 2009. Sources and seasonal patterns of dissolved organic matter (DOM) in the hyporheic zone. Hydrobiologia 647, 99–111. doi:10.1007/s10750-009-9950-2

Xia, K., Skyllberg, U.L., Bleam, W.F., Bloom, P.R., Nater, E.A., Helmke, P.A., 1999. X-ray Absorption Spectroscopic Evidence for the Complexation of Hg(II) by Reduced Sulfur in Soil Humic Substances. Environ. Sci. Technol. 33, 257–261. doi:10.1021/es980433q

Chapter 4: Performance and limitations of reactive mercury removal from contaminated groundwater through amalgamation using brass shavings[1]

Abstract

Brass shavings have been proposed as a cost-effective filter material to remove Hg from contaminated groundwater. The method, which is based on reduction of reactive Hg(II) and subsequent formation of amalgams has been shown to be fast and effective on the short term. However, the effectiveness of brass filters and their stability on the long term, especially if used in passive filter systems such as permeable reactive barriers (PRB) at high flow conditions, is yet unknown. To evaluate performance and limitations of brass shavings for Hg removal from contaminated groundwater, we performed long-term pilot scale filtration tests (6 and 28 months) at two former wood impregnation sites with severe groundwater contamination (up to 870 µg L^{-1} Hg). Results showed that even at high flow conditions (>60 m d^{-1}) 60 to 80% of Hg were removed in the first 8 millimeters of the brass shavings filter bed. Kinetics of filtration, Hg total removal performance (>99.95%), and loading capacity (164 g L^{-1}) were found to surpass those of a Hg specific synthetic resin (LEWATIT®MonoPlus TP-214) . However, at natural pH conditions (pH 6.4 and 6.7) Zn was leached from the brass and exceeded the threshold value (0.5 mg L^{-1}) in the filter outflow up to a factor of 40. Rising of pH (>8.5) diminished Zn concentrations (<0.05 mg L^{-1})

[1] this chapter has been published in revised form in Water Research DOI: 10.1016/j.watres.2016.05.007

but affected Hg removal due to formation of Zn-hydroxide/carbonate coatings on the brass. Thus, the use of brass shavings as exclusive filter material in PRBs would be restricted to aquifers with high pH. However, brass is ideal as low-cost thin-bed prefilter to remove the main Hg load from groundwater when Zn release is managed.

1 Introduction

Mercury (Hg) is known to be one of the most toxic trace metals. It has been released to the environment by numerous industrial processes and is still emitted to the atmosphere in large quantities due to the burning of fossil fuels (UNEP, 2013). The annual global Hg emissions from contaminated sites like precious metal processing and polluted industrial/urban sites are estimated to be 198 (137-260) Mg yr^{-1} (Kocman et al., 2013). Roughly 60% of these emissions (116 ± 69 Mg yr^{-1}) are estimated to be hydrologically controlled. Inorganic Hg(II) species (e.g. $HgCl_2$) are distinctly more soluble than elemental Hg(0) and are found at many Hg contaminated sites, such as chlor-alkali plants (Biester et al., 2002) or former wood treatment facilities (Bollen et al., 2008; Richard et al., 2016). When groundwater is affected, reactive Hg(II) species tend to adsorb on Mn/Fe-oxidydroxides or organic matter (Barringer et al., 2013). Hg adsorption to soil or aquifer material and related long term release of Hg into groundwater often requests long and cost-intensive remediation. At such sites in situ treatment with permeable reactive barriers (PRBs) could be an appropriate remediation strategy as extensive energy costs for long-term pumping in onsite treatment could be avoided (Obiri-Nyarko et al., 2014). A number of different filter materials exists to remove Hg from contaminated water. Sulfurized activated carbons (ACs) (Asasian and Kaghazchi, 2015), Hg specific resins, binding Hg on thiol or thiourea functional groups (Monier et al., 2015), zero valent iron (ZVI) (Vernon and Bonzongo, 2014), and mineral adsorbers such as zeolites (Azizi et al., 2013) are among the most frequently used Hg adsorbents. However, for the use in PRBs on highly Hg contaminated sites all conventional filter materials show serious drawbacks like low sorption capacity (ACs, ZVI, zeolites), biofouling (ACs, organic resins), or filter clogging (ZVIs), especially under high flow conditions. Hg amalgamation with metals such as tin (Sn) (Biester et al., 2000) or copper (Cu) (Huttenloch et al., 2003)

has been proposed as a cost effective alternative. Here, Hg(II) is reduced to elemental Hg(0) by less “noble” metals and forms insoluble amalgams (solid solution) with most metals. This method offers fast kinetics and high Hg loading capacities but also shows disadvantages such as filter instability (Sn) or elevated Cu release at the filter’s outflow. The latest approach in this field to overcome those drawbacks was the testing of brass shavings as a Hg filter material (Wenke et al., 2015). Here, Hg(II) was reduced by metallic Zn to Hg(0) and subsequently formed a Cu-Zn-amalgam, according to equation 1.

$$Hg^{2+} + Zn^0/Cu^0\ (\text{brass}) \longrightarrow Zn^{2+} + Hg^0/Zn^0/Cu^0\ (\text{amalgam}) \quad (1)$$

Based on the results of successful lab experiments (Wenke et al. 2015), we conducted long-term tests with brass shavings filters at two mercuric chloride ($HgCl_2$) contaminated sites under high flow conditions. On the first site appropriate brass type and minimum filter bed length were identified to perform further experiments at a pilot plant on the second site, where the installation of a PRB is under discussion.

2 Materials and methods

2.1 Field tests: Site description and experimental setup.

2.1.1 Pre-tests on site A

On site A, two types of brass shavings were tested with three different filter bed lengths under field conditions to determine the appropriate brass material for more detailed investigations on site B. The site is a former wood treatment facility in the Black Forrest (Southern Germany) where $HgCl_2$ was applied as a protective agent, resulting in severe contamination of soils and groundwater. A detailed site description can be found in Richard et al. (2016). Nine polymethyl methacrylate (PMMA, acrylic glass) filter columns (10 cm diameter, EMC GmbH, Germany), filled with two different types of brass shavings in three different filter bed thicknesses (2, 7, and 15 cm) were run in bypass to an existing groundwater remediation plant (see also Figure S1 in Supporting Material). The brass shavings were installed between layers of quartz sand and gravel to ensure homogeneous water distribution and steady flow. While packing the columns, the material being filled in was always kept covered with

water to avoid formation of air pockets inside the filter. To simulate conditions in a permeable reactive barrier (PRB), flow was set to 2 L h^{-1}, corresponding to an effective groundwater velocity of 21 m d^{-1}. Flow velocities were regulated with EPDM (ethylene propylene diene monomer) diaphragm valves (617, GEMÜ GmbH & Co. KG, Germany) and measured with polypropylene (PP) rotameters (871, GEMÜ GmbH & Co. KG, Germany). Duration of the experiment was 192 days.

2.1.2 Pilot plant on site B

On site B the installation of a PRB is under consideration. Therefore a pilot plant was installed to perform detailed tests on filtration performance and physico-chemical behavior of brass shavings under realistic conditions, compared to other filter materials. Total operation time of the pilot plant was 28 months. The site is located south-west of Freiburg im Breisgau (Southwestern Germany). Hg contamination of groundwater was also caused by $HgCl_2$ solution which had been used for wood conservation on the site, similar to site A. For more information see Bollen et al. (2008). The pilot plant was located in the center of the contaminant plume (see Figure S2) and contained eight polyethylene (PE) columns (150 x 31.5cm, SKZ Peine, Germany). Groundwater was pumped with a stainless steel groundwater pump (SP 2A-6, Grundfos GmbH, Germany) into a 1.5 m³ PP buffer tank inside the pilot plant. Water level of the buffer tank was kept at a constant level (192.5 ± 2.5cm). Water was transported to the test columns through polyvinylchloride (PVC) tubing following the hydraulic gradient. Each of the test columns was applied with 19 PP sampling probes for high resolution sampling inside the filter beds. On site B, only one type of brass shavings was applied (type 1). Test columns were filled with pure brass shavings (columns B7 and B8) and mixtures of brass with gravels in different ratios (brass/gravel ratios: 1 to 2 (column B2), 1 to 5 (columns B3 and B4), 1 to 10 (columns B5 and B6), and 1 to 20 (column B1)). Filter bed thicknesses of pure brass filters and of brass-gravel mixtures were 29 cm and 72 cm, respectively. All filter materials were installed between layers of borosilicate granules to ensure homogeneous water distribution and steady flow (for detailed construction schemes see Figure S3). When columns were packed, the material being installed was always kept under water to avoid air inclusions.

Water flow was from bottom to top. Flow velocity was set to 53 L h^{-1} for the first 100 m³ and was then changed to 36 L h^{-1}, corresponding to the effective groundwater velocities in a hypothetic PRB of 58 and 39 m d^{-1}, respectively. Flow velocities were regulated by means of stainless steel needle valves and measured with low-flow turbine flow meters (FCH-midi-POM, B.I.O-TECH e.K., Germany). Monitoring and recording of flow data was performed by an electronic control unit (unitronics V350, Unitronics Inc., Israel). Hydraulic conductivities of the tested filter materials were monitored by measuring permeability (*K*) according to European technical specification 17892-11 chapter 4.1.7 (CEN ISO, 2004). After filtration of roughly 100 m³ of contaminated water, columns B3 and B4 were emptied and filled with pure brass shavings filters (39 cm), B6, was packed with a Hg specific adsorber resin (28 cm filter bed length), and a mineral adsorber was installed in column B7 (72 cm bed length). To reduce Zn outflow concentrations of the brass shaving filters, pH adjustment was started. First, the buffer tank was filled with limestone chippings (grainsize 2-3cm, HeidelbergCement AG, Germany) for 99 days. As a second step, a sodium hydroxide (NaOH) solution dosing system (EH Wassertechnik GmbH, Germany) was installed at the inflow of the pilot plant for ~200 days after the limestone chippings were removed. A third approach to raise the pH was pre-filtration of raw water through filter beds of half-burnt dolomite (EN, 2014), so called Magno-Dol ($CaCO_3 \cdot MgO$). For this, columns B1, B5, and B7 were emptied and filled with three different types of Magno-Dol (Akdolit® CM G grain size 3 and Akdolit® MAGNO-DOL CM grain size 1 and 2, Lhoist, Belgium). Brass shavings filled columns B3, B4, and B8 were coupled to the Magno-Dol columns.

2.2 Lab tests: Synthetic groundwater test rig.

To study the influence of pH on Zn solubility and pretesting different pH raising approaches before installation in the pilot plant on site B, a synthetic groundwater test rig was installed at the laboratory (Figure S4). Tap water was deionized in an ion exchange unit and stored in a 220 L polyethylene (PE) reservoir tank. The process water was adjusted to groundwater condition at site B by bubbling with CO_2 and addition of precalculated amounts of Ca, Mg, K, and Na salts ($CaCO_3$, NaCl, $Ca(NO_3)_2 \cdot 4H_2O$, $MgSO_4 \cdot 7H_2O$, $MgCl_2 \cdot 6H_2O$,

$Mg(NO_3)_2 \cdot 6H_2O$, and $KHCO_3$, all p.a., Carl Roth GmbH, Germany). The process water was then pumped through PVC tubing to an overhead tank with constant water table to keep a steady pressure level. From the overhead tank, water was then transported to the four test columns (PMMA, 10 cm diameter, EMC GmbH, Germany) filled with brass shavings, following the hydraulic gradient. Water flow was regulated with PP needle valves to 5.3 L h^{-1} (≙ 58 m d^{-1}) and measured with PP rotameters (871, GEMÜ GmbH & Co. KG, Germany). To predict Zn concentrations in outflow of the filters on site B at different pH values, pH of process water in the lab test rig was set to values between 6 and 12 and continuously adjusted to the target value by bubbling with compressed air or CO_2. To achieve pH values above 8.5, NaOH solution (p.a., Carl Roth GmbH, Germany) was added. Water at the outflow of the test columns was sampled and Zn concentrations were measured.

2.3 Tested filter materials.

Two different types of brass shavings were used on site A to identify the appropriate brass type to be used in the pilot plant on site B and in the lab experiments. Both brass types were high purity copper and zinc (Zn) alloys with low lead (Pb) contents (detailed elemental composition is shown in Table S2 and Figure S5). Brass type 1 was a commercially available process media used for removal of chlorine and heavy metals from drinking water (KDF 55®, KDF Fluid treatment, Inc, USA). Brass type 2 was a recycled material made from cable scrap (M2000® Cablo GmbH, Germany). This brass type contained a black, fine, hydrophobic powder (ash particles, most likely residuals of cable sheaths) that had to be removed before use by rinsing with tap water. On site B, brass shavings type 1 were also mixed with gravels (GGK 2/8 mm RK, Knobel Bau GmbH, Germany (for grain size distribution of both materials see Figure S6). Additionally, two commercial mercury filtering materials were tested: One Hg specific adsorber resin based on sulfur-ligands (LEWATIT® MonoPlus TP 214, Lanxess AG, Germany) and one mineral adsorber (absorption agent 3, sulfurized, Dr.Ecker GmbH, Germany).

2.4 Sampling and sample treatment.

2.4.1 Water samples.

Sampling of water from the small test filters at site A and in the laboratory was performed at constant flow at the filter's in- and outlet only. On site B filters were sampled at constant flow also but water at different levels inside the filter beds was sampled as well. Stagnant water in sampling probes was removed before sampling. Outflow at the sampling probes was kept as low as possible to avoid sampling artifacts by water back-flow or hydraulic short circuits. Columns were sampled from above to below and samples were taken in 50 mL PP or 500 mL fluorinated polyethylene (FLPE) containers, when Hg speciation was determined.

Unfiltered samples for total trace element (Cu, Zn,…) and total mercury analyses were preserved with 1% (v/v) double distilled nitric acid (HNO_3). For total Hg determination, 1% (v/v) 1/60 M $K_2Cr_2O_7$ solution and 0.5% (v/v) BrCl solution were added in the field and in the lab, respectively (EN and European Committee for Standardization, 2007; USEPA, 2002). Samples for determination of "dissolved" (<0.45 µm) concentrations of major cations and anions were filtered in the field using polyamide (PA) syringe filters and PP syringes. Samples for determination of Hg species were taken according to the sampling protocol given in Richard et al. (2016) based on the methods from Brosset (1987) and Meili et al. (1991). Field parameters (pH, Eh, electric conductivity, temperature, O_2 content) were determined by conducting an air-free flow chamber to the sampling probes to avoid contact of the sampled water with the atmosphere.

2.4.2 Solid samples.

After decommissioning of a filter, the filter material was extracted in layers from above. Each layer was homogenized and sampled. Specimens of the brass shavings samples were digested in *aqua regia*, according to ISO standard method 11466 (ISO, 1996). To determine Hg concentrations of brass mixed with gravels, brass shavings were extracted from the mixtures by wet sieving with Milli-Q water (18.2 MΩ cm), using a polyamide (PA) sieve (2 mm) . Retained brass shavings were acid digested as described above.

2.5 Chemical analyses.

Total Hg concentrations and Hg speciation were determined using a cold vapor atomic absorption spectrometer (CV-AAS, mercury analyzer Hg-254 NE, Seefelder Messtechnik GmbH, Germany). Concentrations of major elements, Zn, and Cu in water and digests were performed using an inductively coupled plasma optical emission spectrometer (ICP-OES, Varian 715 ES, Agilent Technologies Inc., USA). Field parameter were determined using a SenTix® 21 pH electrode and a SenTix® ORP Eh electrode, both connected to a ProfiLine pH 3110 hand unit, a CellOx® galvanic oxygen probe connected to an Oximeter 325 hand unit, and a TetraCon® electric conductivity probe connected to a ProfiLine Cond 3110 hand unit (all WTW GmbH, Germany). Oxygen and pH probes were calibrated on a daily basis. For total cation-anion balances used in geochemical modeling and as a basis for calculating necessary amounts of metal salts in the synthetic groundwater lab experiments, alkalinity and major anions were also determined. Alkalinity was titrated in the field according to ISO standard method 9963-1 (ISO, 1996). For analyses of anions, an ion exchange chromatograph (761 Compact IC, Metrohm AG, Switzerland) was applied. Scanning electron microscope (SEM) pictures of brass shavings were taken with a JSM-6480 (Jeol Ltd., Japan) at 20 kV acceleration voltage. Energy dispersive X-Ray (EDX) spectra of the SEM specimens were obtained with an eumeX updated Kevex EDX system (eumeX Instrumentebau GmbH, Germany) coupled to the SEM.

2.6 Analytical quality assurance.

To assure quality of digests and analyses, the following standard reference materials (SRMs) were analyzed “Trace Metals” RTC 1-WP for Hg analyses in water and digests, "River Water" NRC CNRC SLRS-5 water analyses in water. For analytical limits and recovery of SRMs see Table S1 (Supporting Material).

2.7 Geochemical modeling.

For prediction of Zn solubility and precipitate composition during pH raising experiments, geochemical modeling was conducted on the basis of cation-anion-balances from site B, including field parameters (temperature, pH, dissolved O_2, alkalinity, and Eh). PhreePlot version 1 (x64) (Kinniburgh and

Cooper, 2014) was applied to calculate pH sweeps by repetitive execution of embedded PHREEQC (Parkhurst and Apello, 2013) code, using the minteq.v4.dat database as supplied with the program and an initial Zn concentration of 100 mg L^{-1}.

3 Results and discussion

3.1 Hg filtration performance.

3.1.1 Results of pre-tests at site A.

During the Hg filtration pre-test at site A, Hg concentrations ranged between 35 and 390 µg L^{-1} (average: 212 ± 118 µg L^{-1}). Average pH was 6.38 ± 0.06 and electrical conductance ranged between 560 and 630 µS cm^{-1}. The two different types of brass shavings were tested at three different filter bed thicknesses. Results are shown in Figure 1. Test columns with 2 cm filter layers were found to have lowest Hg removal rates for both brass types (average: 94.3 ± 0.05% and 92.6 ± 0.04% for brass type 1 and 2, respectively). Consistently, 7 cm filter layers were more effective (brass type 1: 99.1 ± 0.01%, brass type 2: 96.4 ± 0.04%), and maximum removal rates were achieved by 15 cm filter layers (brass type 1: 99.1 ± 0.01%, brass type 2: 99.1 ± 0.02%), with Hg outflow concentrations complying in most cases with the threshold value (1µg L^{-1}, BBodSchV, 1999). However, differences in removal rates were significant for the 2 cm layer and the other two layer thicknesses for brass type 1 (p-values: 0.010 and 0.011 for 2 cm vs. 7 cm and 1cm vs. 15 cm, respectively) and for the 2 cm and 15 cm layer columns for brass type 2 (p-value: 0.0003). After roughly 200 days (9.2 m^3), filters with both brass types still did not show decreasing filtration efficiency and no significant difference between the two brass types could be found for none of the used filter bed thicknesses. Hence, both brass types were equal in terms of Hg filtration effectiveness. Brass type 1 was chosen for the field tests on site B because it could be used without any pretreatment, in contrast to brass type 2 (see chapter 2.3). To assure compliance with the Hg threshold value of 1 µg L^{-1} a bed length of approx. 30 cm was chosen for the experiments on site B, in accordance with calculations of minimum filter bed length for the site published in Wenke et al. (2015).

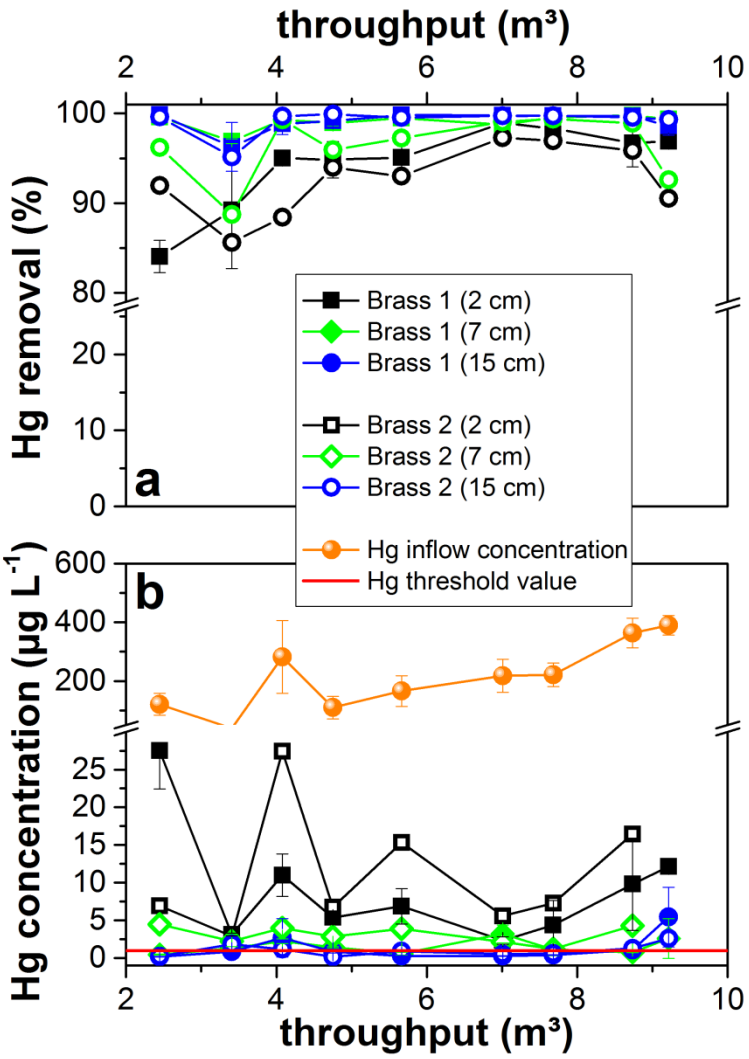

Figure 1. Mercury removal (a) and measured total Hg in- and outflow concentrations (b) of the installed brass filters on site A. Results of brass type 1 and brass type 2 are shown as squares and open circles, respectively. Different filter strengths are depicted in different colors. Values of brass type 1 are averaged results from two identical columns for each filter strength, respectively, that were run in parallel. Error bars represent twofold standard deviations of averaged data.

3.1.2 Hg removal of filters at site B.

Average inflow Hg concentrations of the pilot plant during time of operation was 203 ± 45 µg L^{-1}. Electric conductivity ranged between 430 and 508 µS cm^{-1} (459 ± 31 µS cm^{-1}) and the average pH was 6.74 ± 0.06. Hg removal results during filtration of the first 100m³ of groundwater are shown in Figure 2. Column B1, filled with a brass-gravel mixture at a ratio of 1 to 20 showed lowest removal rates (85 ± 5% Figure 2a) and highest Hg outflow concentrations (27 ± 8 µg L^{-1}). With ascending brass content Hg removal rates increased. 1 to 10 brass-gravel

mixtures (columns B3 and B4) removed 91 ± 5% of Hg (outflow concentration: 17 ± 9 µg L^{-1}), 1 to 5 mixtures (B5 and B6) retained 95 ± 3% of inflow Hg (Hg in outflow: 9 ± 6 µg L^{-1}), and the 1 to 2 mix in column B2 reached 98.5 ± 1.1% removal efficiency, equal to 2.7 ± 1.8 µg L^{-1} Hg behind the filter. Hence, none of the mixtures complied with the Hg threshold value (1 µg L^{-1}). Therefore mixtures of brass and gravel are not further discussed in this paper.

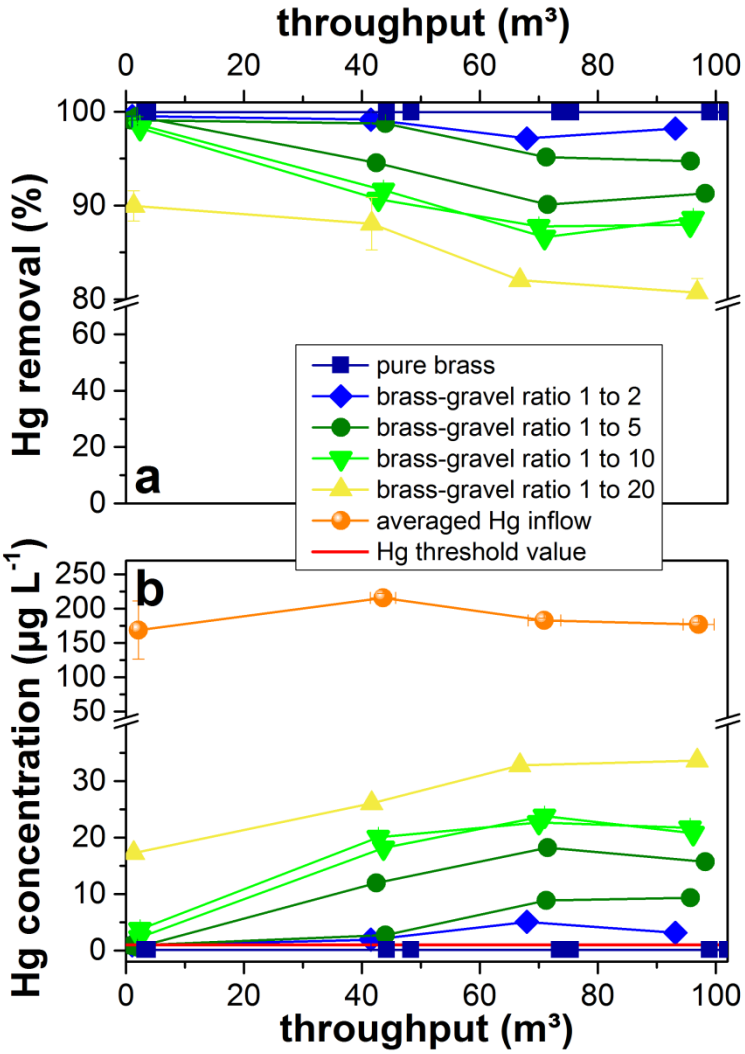

Figure 2. Mercury removal (a) and measured total Hg in- and outflow concentrations (b) of the installed filters on site B during treatment of the first 100m³ of groundwater. Shown Hg inflow concentrations are averaged inflow values from all columns.

However, filtration efficiency of the pure brass shavings in columns B7 and B8 was found to be more than 99.95 ± 0.01% and did not decrease after filtration of approx. 100 m³ of contaminated groundwater (effective velocity: 61 ± 5 m d^{-1}). Hg outflow concentrations were found to be always below limit of detection

(0.03 µg L^{-1}). Constant Hg removal of more than 80% at sampling probe 2 (8 mm filter bed length) was also remarkable (Figure 3a, bottom and Figure S7), especially when compared to the results obtained by Lewatit (Figure 3b, bottom). Lewatit showed usually less than 50% Hg removal at sampling probe 2, even though effective velocity was one third lower here (41 ± 10 m d^{-1}) indicating reaction kinetics of Hg(II) reduction and subsequent amalgamation by brass being faster than Hg complexation by sulfur functional groups of the adsorption resin. This is in particular advantageous for usage in PRBs. Hg removal performance of Lewatit (98.9 ± 1.3%) was also found to be lower than that of pure brass shavings with average Hg outflow concentrations (2.2 ± 2.7 µg L^{-1}) above the Hg threshold value (1 µg L^{-1}). However, Hg retention of the adsorber resin did not decrease during the testing period and Hg outflow concentrations even declined below threshold towards the end of the experiment. Furthermore, brass shavings and the resin filter had the same filter bed volume (22.6 L) but bulk densities of the two materials are distinctly different (3.3 and 0.68 g L^{-1}, respectively, Wenke et al., 2015 and Lanxess AG, 2011). Therefore, if compared on a filtration-per-mass basis, performance of the resin would improve significantly. The second commercial Hg filter material tested, a sulfurized mineral adsorber, never complied with the Hg threshold value. Average Hg outflow concentrations were 18.7 ± 16.6 µg L^{-1} at effective filter velocity of 38 ± 19 m d^{-1}) even though the filter bed size was more than twice the volume (56 L) of those of brass shavings and Lewatit (see Figure S3). The average Hg removal rate was 93 ± 6% and after 94 days of operation the filter was clogged and removed.

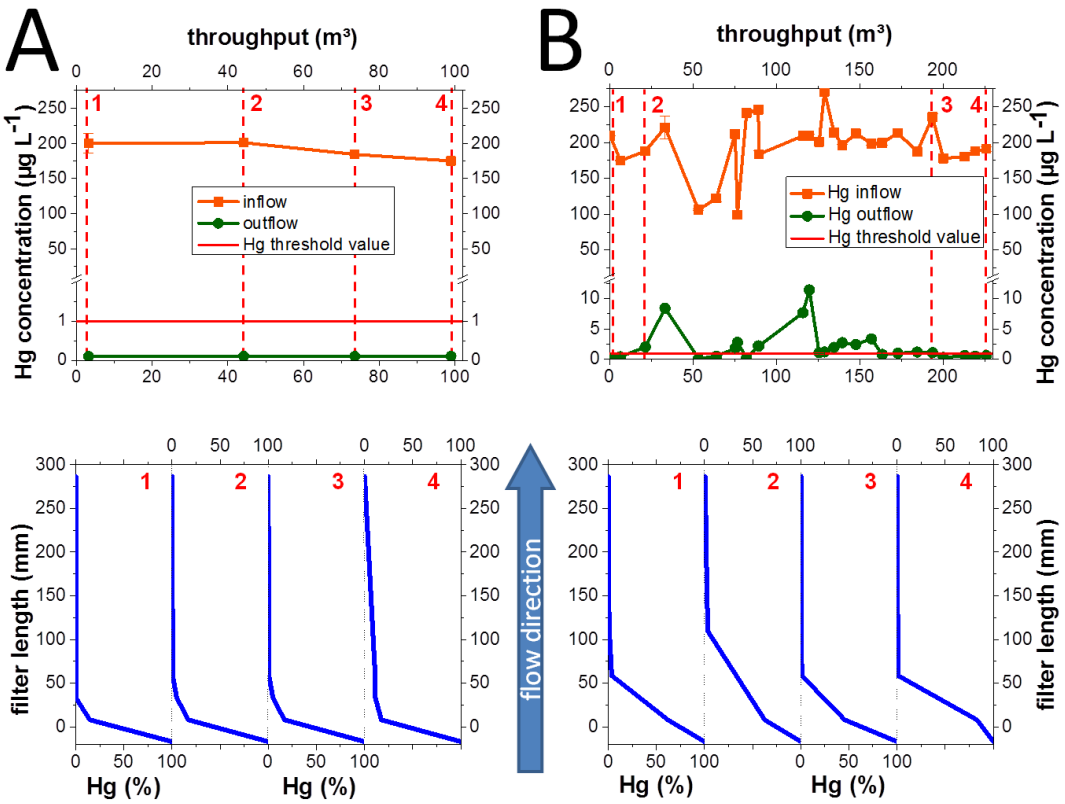

Figure 3. Total mercury concentrations at in- and outflow of two test columns (B7 and B6) on site B (top), filled with brass shavings (A) and Hg specific resin LEWATIT® MonoPlus TP 214 (B). Corresponding (normalized) Hg concentration profiles inside the filter beds (bottom). Sampling events are marked with red dashed lines in top graphs. Flow direction from bottom to top. Effective flow velocities for brass shavings and adsorption resin were 61 ± 5 and 41 ± 10 m d-1, respectively. Error bars are twofold standard deviations of duplicate measurements.

3.2 Changes of water chemistry during filtration.

Results of Hg speciation, Hg, Zn, Cu, pH, Eh, and O_2 measurements in filtered water within a brass filter from site B (column B4) are shown in Figure 4. Total Hg concentrations decreased rapidly from approximately 200 µg L^{-1} to below detection limit (0.08 µg L^{-1}) at the outlet of the filter. Lower Hg retention than usually found at the first sampling probe inside the filter bed (35 vs. 60-80%) is most likely a sampling artifact (hydraulic short circuit) due to a larger volume of water needed for multi parameter analyses. However, speciation measurements show that inorganic Hg(II) was quantitatively reduced to Hg(0) when the water-front had reached sampling probe 4 at 59 mm, and got subsequently removed from solution by amalgamation. Relative proportions of inorganic Hg(II) decreased rapidly from 90 to less than 5%, while Hg(0) proportions increased

from 4.7% to a maximum of 45% of total Hg. Particle- and DOM (dissolved organic matter) bound Hg(II) were more resistant to reduction and showed therefore relative enrichment during the filtration process, changing from <1% and 5 to maximum proportions of 28 and 40%, respectively. Nevertheless, Hg concentrations were below detection limit behind the filters, proofing that DOM bound Hg was retained by the filters either by Hg reduction or by adsorption to the filter material or precipitated Zn hydroxides or carbonates.

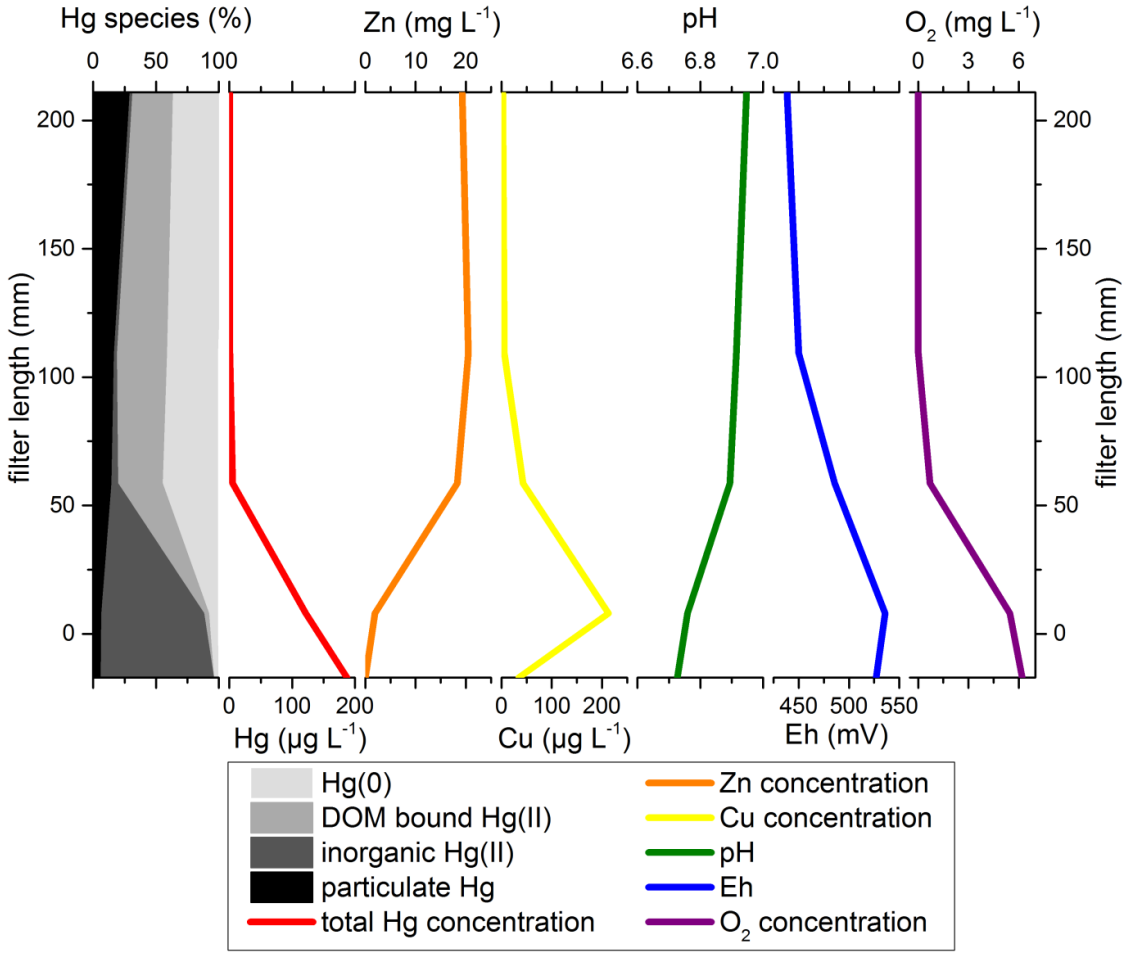

Figure 4. Changes of Hg species, total Hg, Zn, Cu, O_2 concentrations, pH, and Eh of a contaminated groundwater with natural pH (6.7) during passage of a brass shavings filter. Flow direction from bottom to top.

Zn concentration was found to exceed stoichiometry of reaction with Hg (equation 1, theoretical concentration: ~66 µg L^{-1}) and reached a plateau of roughly 20 mg L^{-1} at approximately 110 mm filter bed length (sampling probe 6). Here dissolution of metallic Zn(0) and precipitation of Zn hydroxides and

carbonates seemed to have reached equilibrium. Protons and oxygen were drawn from solution by Zn oxidation, leading to a rise of pH, oxygen depletion, and the decrease of redox potential (Eh). Copper concentrations increased to a maximum of approximately 200 µg L^{-1} in the first millimeters of the filter but decreased again rapidly to below detection limit (7 µg L^{-1}) at the outflow. The decline of Cu concentrations in the upper part of the filter can most likely be attributed to re-reduction of Cu(II) with subsequent precipitation of Cu(0) and the effective protection against further Cu(0) oxidation and dissolution, both evoked by metallic Zn(0). Zinc is more electronegative than Cu and served here as a sacrificial anode, donating electrons to Cu while itself got oxidized.

3.3 Changes of brass composition.

Oxidation and release of Zn lead to changes in the chemical composition of the filter material. Pristine brass shavings consisted of 50.5 ± 1.8% Zn and 50.1 ± 0.9% Cu on a mass basis and only trace amounts of other elements (see Figure S5 and Table S2). The composition of brass shavings after filtration of 360 m³ of Hg contaminated groundwater is shown in Figure 5 (column B8). Zn was depleted in the entire filter to a minimum concentration of 24.9 ± 0.1 wt.% at the inlet of the filter and increasing proportions in the upper parts of the filter (maximum: 48.0 ± 0.1 wt.%). Copper was also abated in the inlet region but showed a subsequent zone of enrichment between 23 and 48 mm filter length with a maximum concentration of 53.3 ± 0.1 wt.%. In this range, decreasing aqueous Cu concentrations were observed inside a brass filter (chapter 3.2.) indicating Cu(0) precipitation. Hence, true not only relative enrichment of Cu took place. Concentrations of other elements were limited to a maximum total content of 0.81 ± 0.02 wt.% with Hg being the dominant element (maximum Hg content: 0.76 ± 0.02 wt.%, (Figure 5). Highest Hg content was found in the first centimeter of the filter and concentrations decreased rapidly to a minimum of 52.9 ± 0.7 mg·kg^{-1} in accordance with the aqueous Hg concentration profile

shown in Figure 4.

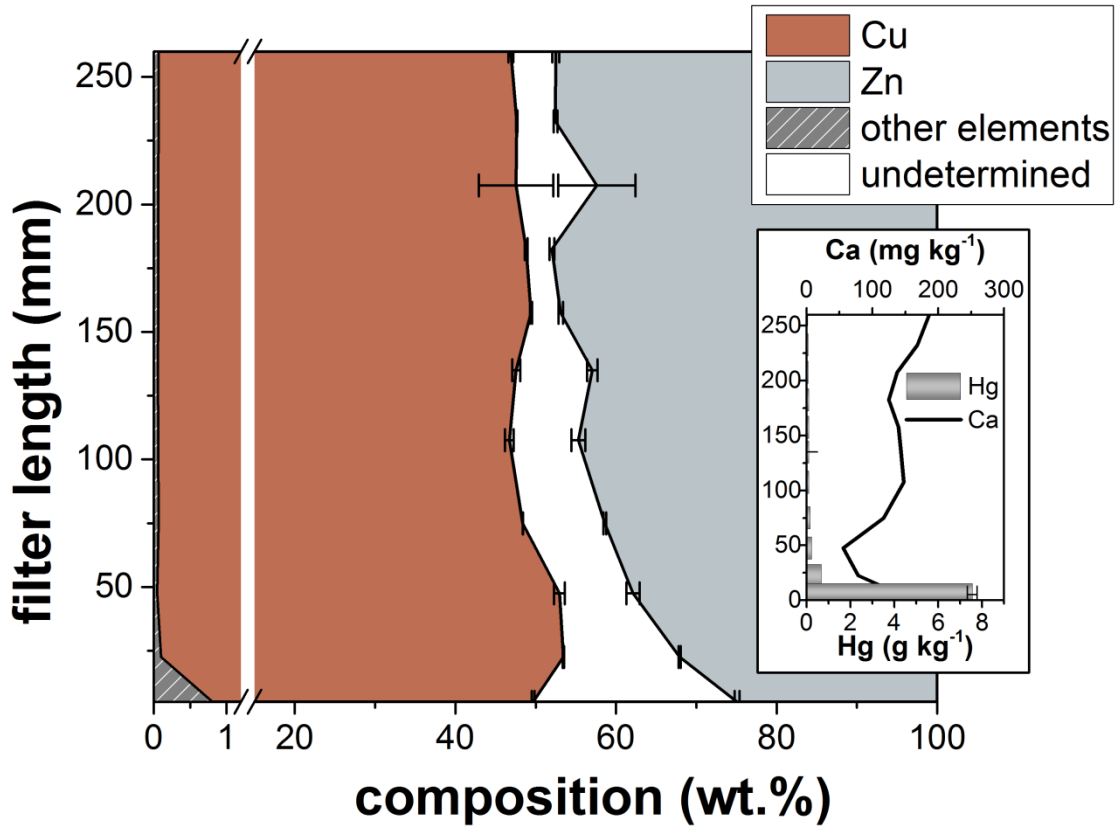

Figure 5. Composition of brass shavings from site B (filter B8) after filtration of 360 m³ Hg contaminated groundwater. “Other elements” are: Hg, Al, Ca, Cr, Mg, Pb, and Si.

However, in the 1:20 brass-gravel mix filter (column 1) maximum Hg concentrations of up to 4.98 ± 0.1 wt.% were found on the brass material (Figure S8). At a measured bulk density of 3.30 ± 0.02 g cm^{-3} (see Wenke et al., 2015) this value results in a minimal loading capacity of 164 ± 4 g L^{-1}, surpassing the one of Hg specific cation exchange resins like AMBERSEP™ GT74 (130.4 g L^{-1}; Rohm & Haas Company, 2006) and LEWATIT® MonoPlus TP 214 (100.3 g L^{-1}; Lanxess AG, 2011). Expressed on a mass basis, however, loading capacities of the resins are about three times higher (166 and 148 g kg^{-1}, for Ambersep and Lewatit, respectively) than the maximum loading found on the brass shavings, due to the low density of the resins (0.79 and 0.68 g cm^{-3} for Ambersep and Lewatit, respectively).

In contrast to the analyses of pristine brass where measured elemental concentrations summed up to a total of 100.7 ± 2.7 wt.% (Figure S5 and Table S2), a mass gap of up to 25.4 ± 0.3 wt.% to 100 was encountered (denoted as

"undetermined" in Figure 5) when summing up measured elemental content of the brass shavings that had been used as a filter material. Geochemical modeling (PHREEQC, minteq.v4.dat) indicated that the missing mass fraction was mainly comprised of oxygen, hydrogen, and carbon, since Cu and Zn oxides, hydroxides, and carbonates were predicted to form under the given conditions. Scanning electron microscope (SEM) images of brass shavings that had been exposed to groundwater from site B for eight months showed surface alteration and crystal growth. Energy dispersive X-ray (EDX) spectra revealed carbon and oxygen enrichment (Figure S9) in accordance to the modeling results. The observed mineral formation/precipitation caused a decrease in hydraulic conductivity *K* (Figure S10) when pH was raised (chapter 3.4.) but minimal permeability remained in the range of well sorted sand (Bear, 1972) with a minimum *K* value of $9.7 \cdot 10^{-4}$ m s^{-1}. Nevertheless, gradual blocking of brass filters by build-up of meringue like corrosion products as described by Sarver (2010) should be expected during long-term use under high pH conditions. In contrast filter blocking should not be a problem in low pH waters, but filter dissolution slowly is expected to take place due to Zn leaching. Cu concentrations in outflow water are also likely to increase after Zn has been lost, as Cu is not corrosion-protected any more. Therefore, the lifetime of brass shaving filters is limited at any pH and filters should be changed at times or K values, Zn and Cu concentrations should be monitored during operation to assess conditions of the filter.

3.4 Influence of pH on Zn concentrations.

As shown in chapter 3.2. aqueous Zn concentrations on site B exceeded the German threshold value for groundwater (0.5 mg L^{-1}, BBodSchV, 1999) by approximately 40 times and did not decrease significantly during filtration of the first 100m³ of contaminated water (see Figure S11). Zn leaching was likely caused by dezincification, a type of corrosion that can occur when high-zinc brass alloys are in contact with water (Zhang and Edwards, 2011). Probability of dezincification was estimated prior to conducting the experiments on site B by plotting chloride (Cl^-) concentration of groundwater from the site against alkalinity in a so called "Turner`s diagram" (Turner, 1961, taken from Sarver, 2010; see Figure S12). According to this, no dezincification should have

occurred on the site. Apparently, this prognosis method, originally developed for predicting corrosion of brass fittings in water installation, was not suitable for brass shavings. However, when Zn leaching was encountered, geochemical modeling was performed, using PhreePlot. The model predicted a decreasing Zn solubility with increasing pH (Figure 6) due to enhanced formation of Zn hydroxides and carbonates. To test this prediction lab experiments with synthetic groundwater and brass shavings in filter columns were conducted at different pH (see chapter 2.2) and measured Zn concentrations agreed well with modeling results (Figure 6).

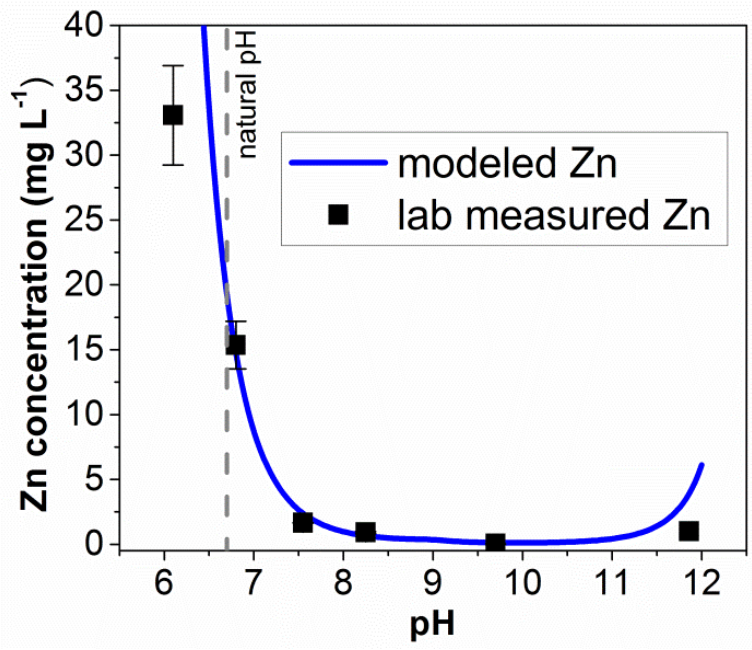

Figure 6. Dependency of Zn solubility on pH. Results from geochemical modeling (PhreePlot, minteq.v4.dat) and laboratory experiments using synthetic groundwater of site B composition.

Therefore, pH adjustment was started in the pilot plant (Figure 7a). In a first step the pumped groundwater in the pilot plant on site B was pretreated by passing through a filter bed of limestone chippings, yielding in an average pH of 7.2 ± 0.2. Resulting decrease of Zn concentrations in the outflow of the test columns was approximately 50% (10 ± 4 mg L^{-1} in the column shown in Figure 7. A further rise of pH to 7.8 ± 0.1 by using an automatic dosing system for addition of sodium hydroxide (NaOH) solution to the raw water lowered the Zn concentrations to 2.2 ± 0.3 mg L^{-1}. In a short-term test (24 h) at pH 8.49 Zn outflow concentration was reduced to 0.65 mg L^{-1}. However, the use of NaOH

to increase pH lead to precipitation of $CaCO_3$ in the tubing and to blocking of the flowmeters. Therefore, the calculated minimum pH of 8.5 necessary to comply with the threshold value could not be maintained in the long run by NaOH dosing.

A different option to rise the pH is to pretreat raw water by filtration through a filter bed of half-burnt dolomite (EN, 2014), referred to as Magno-Dol ($CaCO_3 \cdot MgO$). Hereby, MgO is transformed into Mg hydroxides and carbonates and protons and carbonic acid are bound. The so treated water had an average pH of 8.5 ± 1.2 (maximum: 10.1). Initially, Zn concentrations in the outflow of the brass shavings filters complied with the threshold value and dropped to minimum values below 0.05 mg L^{-1} (Figure 7a). However, reactivity of Magno-Dol decreased rapidly and pH could not be kept constant which resulted in fluctuating Zn concentrations in the outflow.

3.5 Influence of pH on Hg filtration.

Besides controlling Zn solubility, pH was also found to affect Hg removal efficiency. Hg concentrations were below limit of quantification (LOQ) as long as the natural pH of the groundwater was maintained (Figure 7b). When pH adjustment was started, Hg outflow concentrations slowly increased. Whereas Hg removal rates at natural pH conditions were always above 99.95%, they started to decline when water pretreatment by filtration through limestone chippings was started and reached a minimum of 98.0 ± 0.2% in Filter B8 (Figure S7) (maximum Hg outflow concentration: 5.4 ± 0.3 µg L^{-1}). Further pH increase by NaOH dosing or Magno-Dol filtration resulted in a further decline of Hg removal rates (minimum: 84.7 ± 1.7%; max. Hg outflow concentration: 28.6 ± 0.1 µg L^{-1}).

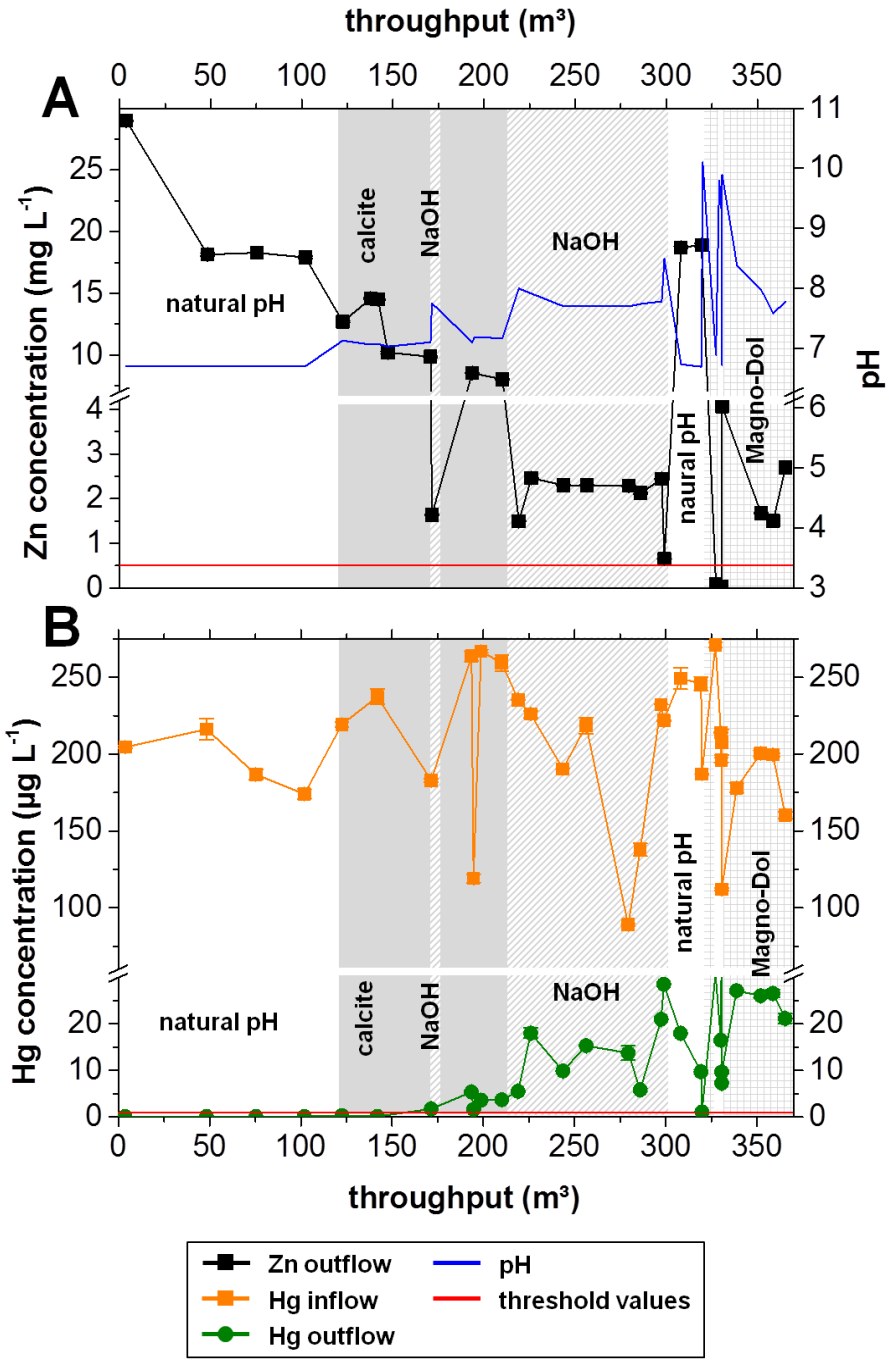

Figure 7. Water chemistry of in- and outflow water from brass shavings test column B8at site B. (A) Inflow pH and total Zn concentrations in outflow water. (B) Total Hg in- and outflow concentrations. Threshold values (BBodSchV, 1999) for Hg and Zn (1 µg·L^{-1} and 0.5 mg·L^{-1}, respectively) are drawn as red lines.

However, most interestingly Hg removal inside the filter bed was found to occur predominantly in the first section of the filter, regardless at which pH at the inflow (Figure S7). Even when the overall Hg removal rate was only 86.7% more than 60% of Hg was still removed in the first 8 millimeters. Hence,

differences in overall Hg removal rates between different inflow pH seemed to develop mainly in the upper filter bed. This could be due to enhanced precipitation of $CaCO_3$ in the upper part of the filters evoked by an increase of pH during filtration (Figure 4). This assumption is supported by increasing Ca concentrations with increasing filter-bed length (Figure 5). At inflow pH of ~7.2, Hg speciation measurements during filtration also showed impaired reduction of inorganic Hg(II) to Hg(0) (Figure S13) most likely due to carbonate/hydroxide coated brass surfaces as shown in SEM pictures (Figure S9). When pH adjustment was stopped Hg outflow concentrations started to decrease again until complying with the threshold (1µg L^{-1}) (Figure 7b). Hg removal rates also recovered and raised again to a maximum of 99.4% (Figure S7). However, Zn leaching was also reversible and responded even faster on the pH reduction, immediately reaching a similar concentration level as prior to pH adjustment, likely due to dissolution of Zn-carbonates and -hydroxides.

4 Conclusions

In summary, pure brass shavings showed excellent removal capacity and reaction kinetics at pH conditions between 6.3 and 6.7. Removal rates, reaction kinetics, and loading capacities (Hg loading per volume) exceeded the ones of tested conventional filter materials (Hg specific organic resin and sulfurized mineral adsorber). However, Zn concentrations in outflow water exceeded legal limits (0.5 mg L^{-1}) and Zn leaching can lead to filter dissolution during long-term operation. Rising pH to 8.5 could lower Zn discharge to concentrations below the threshold limit, but Hg removal was attenuated due to precipitation of Zn hydroxides and carbonates. Therefore, usage of brass shavings in a permeable reactive barrier would be limited to groundwater with naturally high pH (> 8). Moreover, hydraulic conductivity (*K*) should be monitored, as Zn hydroxides and carbonate formation can lead to decreasing *K* values. Regardless of pH, 60 to 80% of Hg removal was found to occur in the first few millimeters of the filter bed while Zn concentrations started to increase further up the filter. Therefore, usage of brass shavings in combination with other Hg filter materials like Hg specific resins is most promising. When installed as a thin layer in front of conventional filters, brass shavings could reduce Hg inflow concentrations at

the main filter by more than half and filter dimensions could be diminished significantly to save costs.

Acknowledgements

This study was financed by the regional council of Freiburg i. Brsg. (Germany). We thank the Harres Pickel Consulting Group (HPC AG, Germany) for the excellent cooperation.

Supporting information

Table S1. Analytical limits (DIN, 2008) and recovery of measured standard reference materials for most important analytes.

Analyte	Unit	Analytical Instrument	Limit of Detection (LOD)	Limit of Quantification (LOQ)	Standard Reference Material (SRM)	Certified Concentration	Measured Concentration	Recovery
Cu	$\mu g\ L^{-1}$	ICP-OES	7.0	23.0	"River Water" NRC CNRC SLRS-5	17.4 ± 1.3	17.4 ± 0.9	100.2%
Zn	$mg\ L^{-1}$	ICP-OES	0.03	0.09	"Trace Metals" RTC 1-WP*	3.1 ± 0.1	3.4 ± 0.0	108.0%
Hg	$\mu g\ L^{-1}$	CV-AAS	0.03	0.08	"Trace Metals" RTC 1-WP*	70.8 ± 3.2	69.0 ± 2.2	97.4%
Hg (in digest)	$mg\ kg^{-1}$	CV-AAS	0.06‡	0.17‡	pristine brass, fortified with Hg standard solution#	100	102.1 ± 3.6	102.1%

* Lot 018789, diluted four times less than specified in certificate.
# in lack of a suitable CRM, an inhouse reference was prepared by adding diluted Hg standard solution to pristine brass shavings before digestion
‡ converted from mass per volume to mass concentration using weight-in mass of sample

Table S2. Composition of pristine brass shavings.

	brass type 1 (wt %)			brass type 2*
Zn	50.5	±	1.8	35.1
Cu	50.1	±	0.9	61.4
Fe	0.006	±	0.001	0.3
Ni	0.0028	±	0.0001	
Pb	0.0021	±	0.0001	0.02
Sn	0.0004	±	0.0001	
As	0.0004	±	0.0001	
Ca	0.00030	±	0.00002	
V	0.000041	±	0.000003	
Cr	0.000017	±	0.000004	
Si				1.9
total	100.7	±	2.7	98.72

* data from manufacturer

Figure S1. Test column setup on site A. Columns are filled with 2 (front row), 7 (middle row), and 15 cm (back row) brass shavings layers. Brass type 1 is installed in the six columns in the middle and brass type 2 is used in the three columns on the left. The 3 columns on the right are “blank” columns.

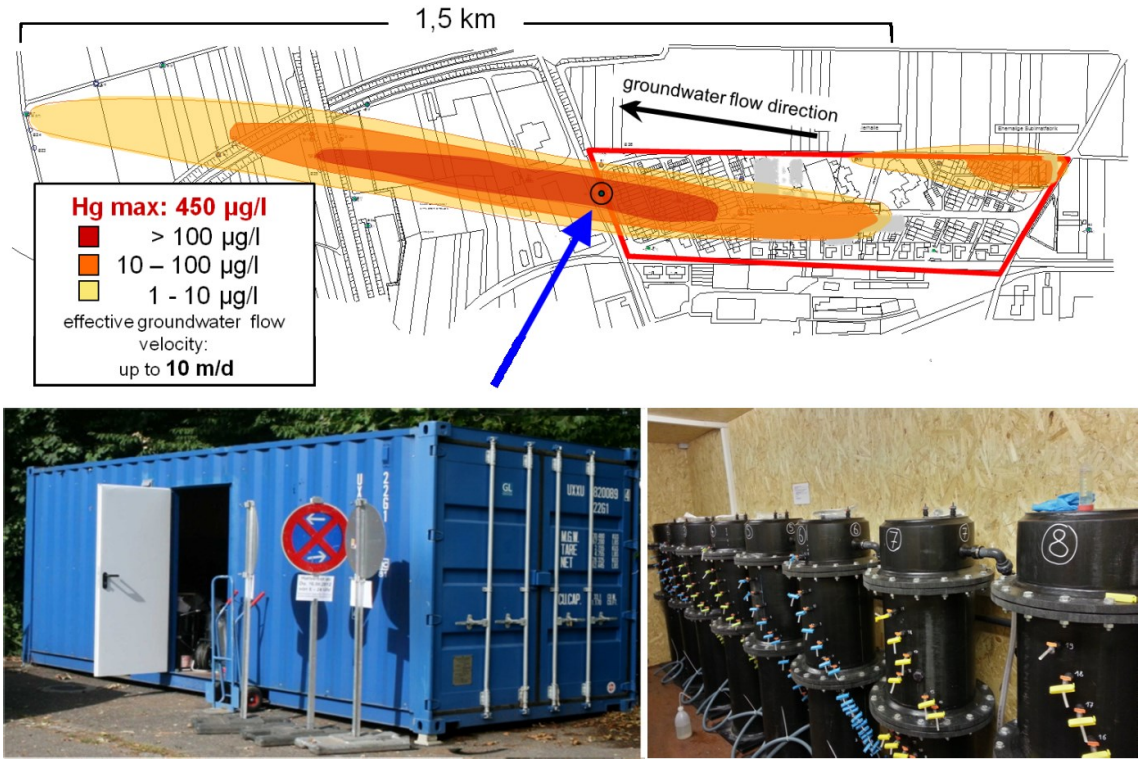

Figure S2. Site map with Hg groundwater plume and position of the pilot plant (above, basemap: HPC AG). Pilot plant and test columns (below).

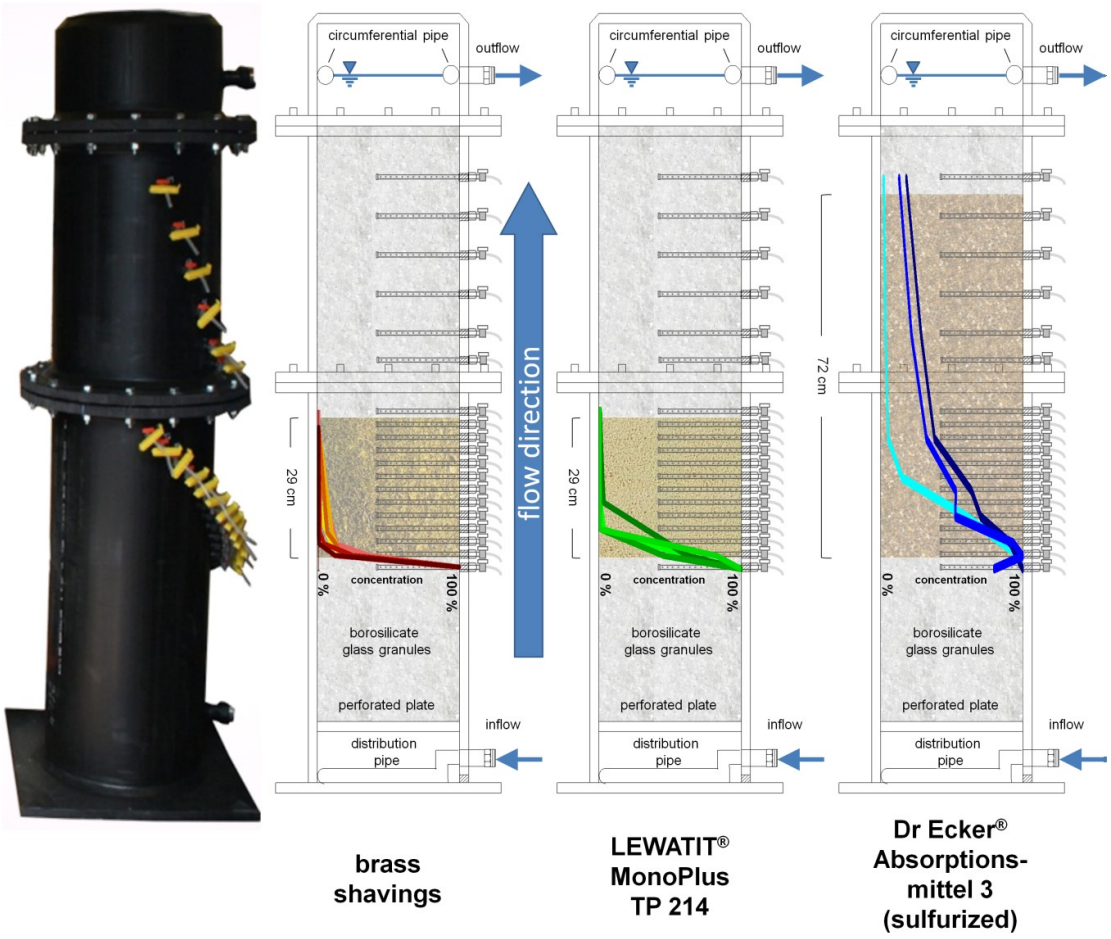

Figure S3. Filter column type applied in the pilot plant on site B. Construction schemes with filter layer thicknesses and normalized mercury concentration profiles of the tested filter materials are drawn on the right.

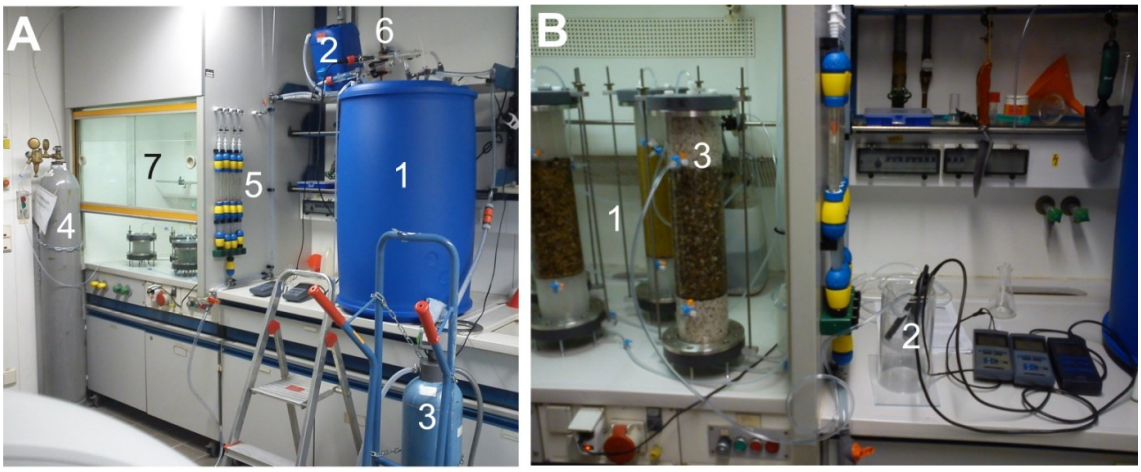

Figure S4. Synthetic groundwater lab test rig. (A) Overview with main reservoir (1), overhead tank (2) ion exchange unit (3), CO_2 gas tank (4), flow meters (5), pH/electric conductivity probes (6), and fume hood with test columns (7). (B) Detailed view of test columns (1) with pH, O_2, and Eh probes in a flow cell (2) connected to a sampling probe (3) inside a test column.

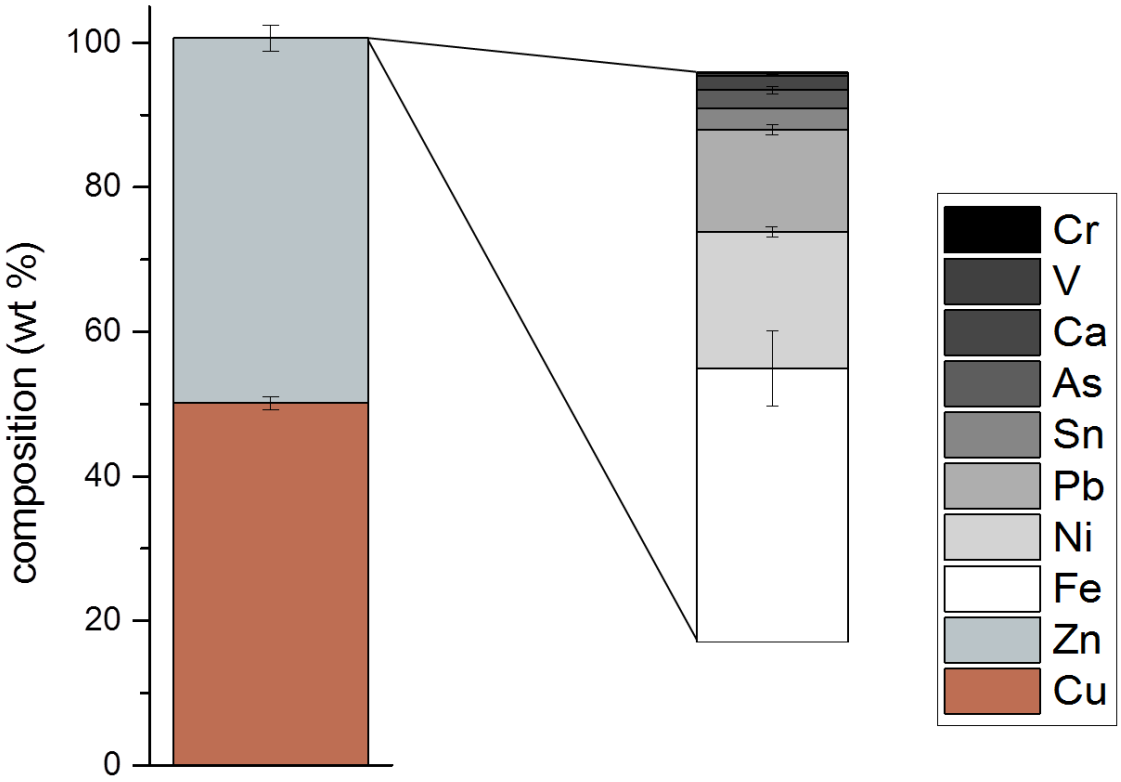

Figure S5. Composition of pristine brass shavings (type 1). The enlarged part of the bar graph represents a total proportion of 0.012 ± 0.001 wt %.

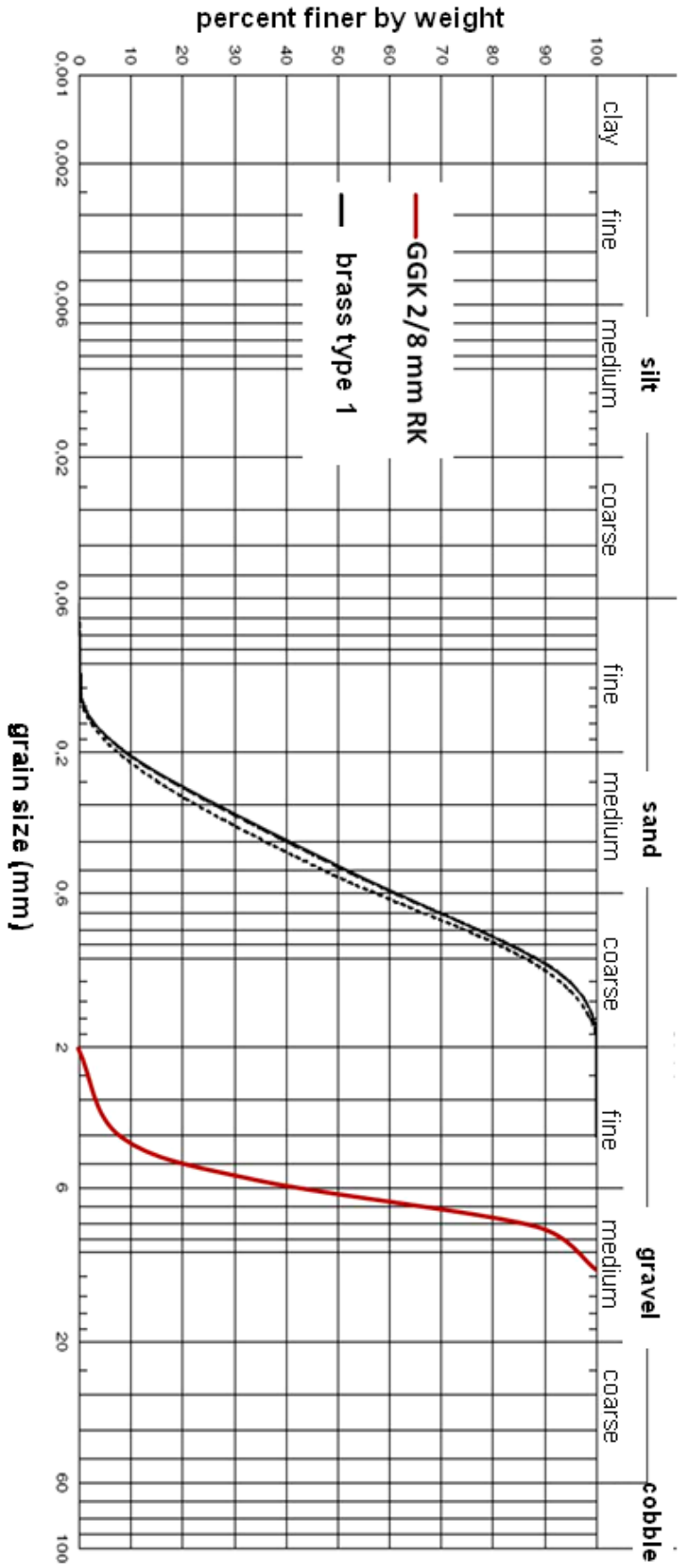

Figure S6. Grain size distribution of brass type 1 and gravel used for mixing with brass shavings.

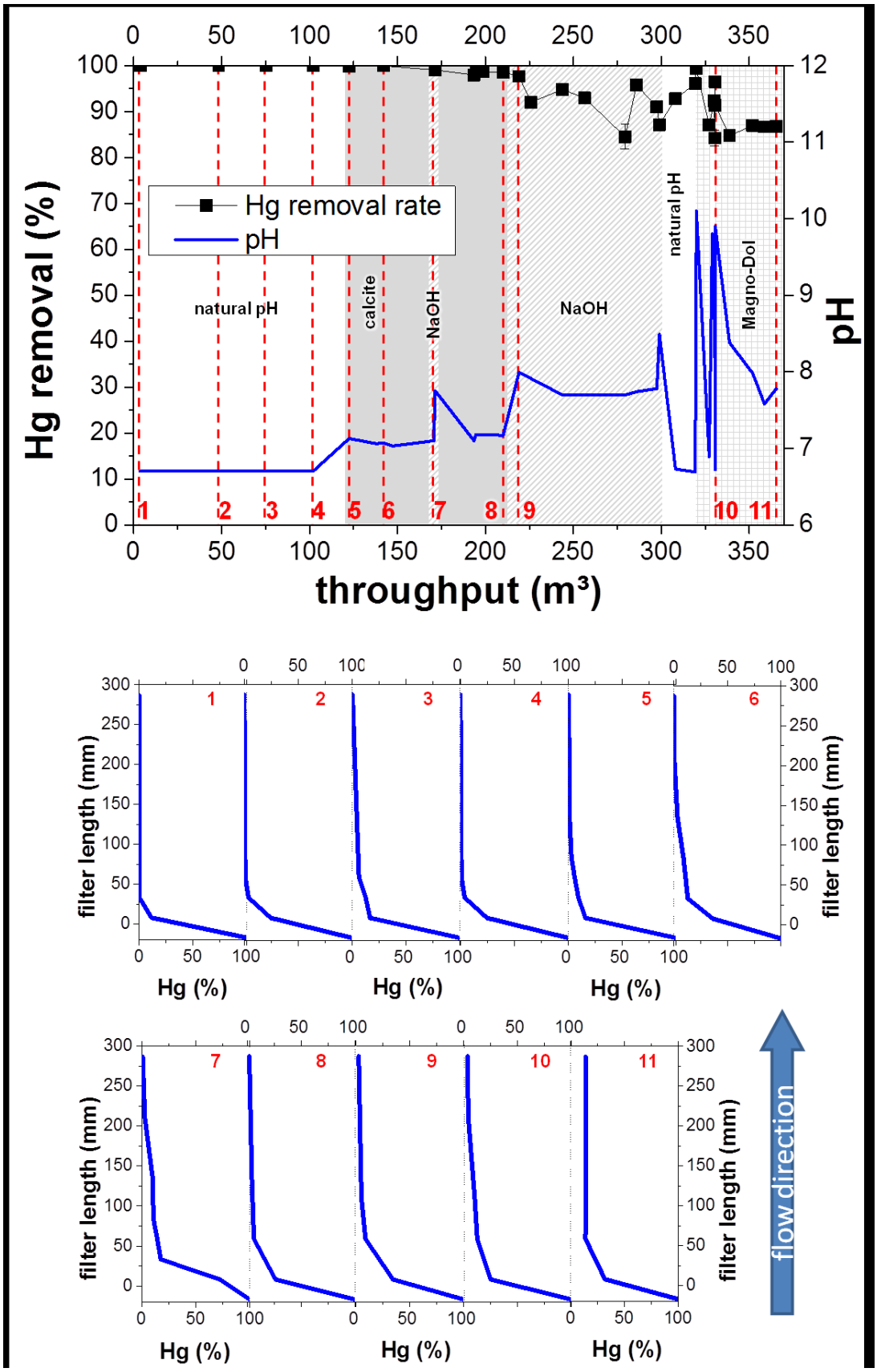

Figure S7. Hg removal rates of a brass shavings test column (B8) in the pilot plant on site B. Top: Overall Hg removal rates of the filter column, calculated from inflow and outflow concentrations. Bottom: Hg removal rates inside the filter bed, with sampling events marked with red dashed lines in top figure.

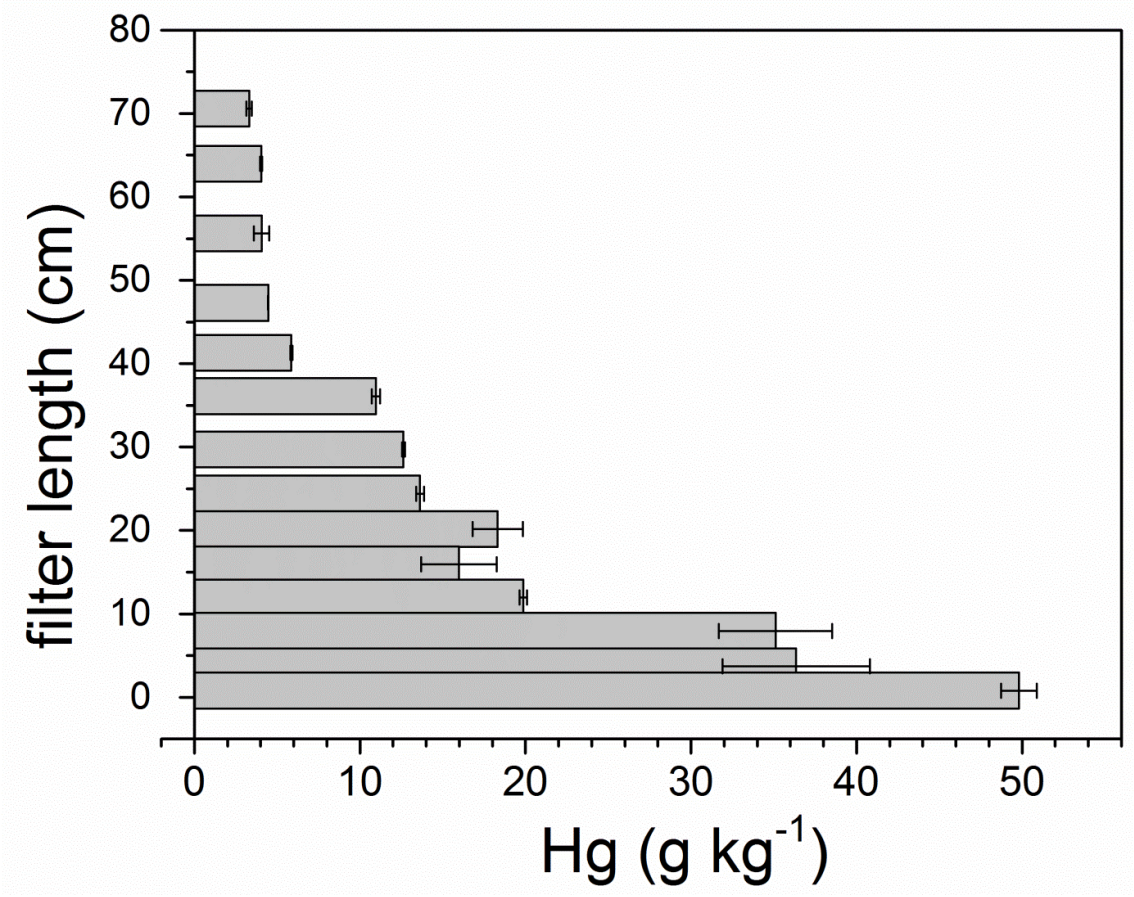

Figure S8. Hg concentration profile of brass shavings, extracted from column B1 (brass-gravel mix, ratio 1 to 20) on site B after filtration of 97 m³ of groundwater.

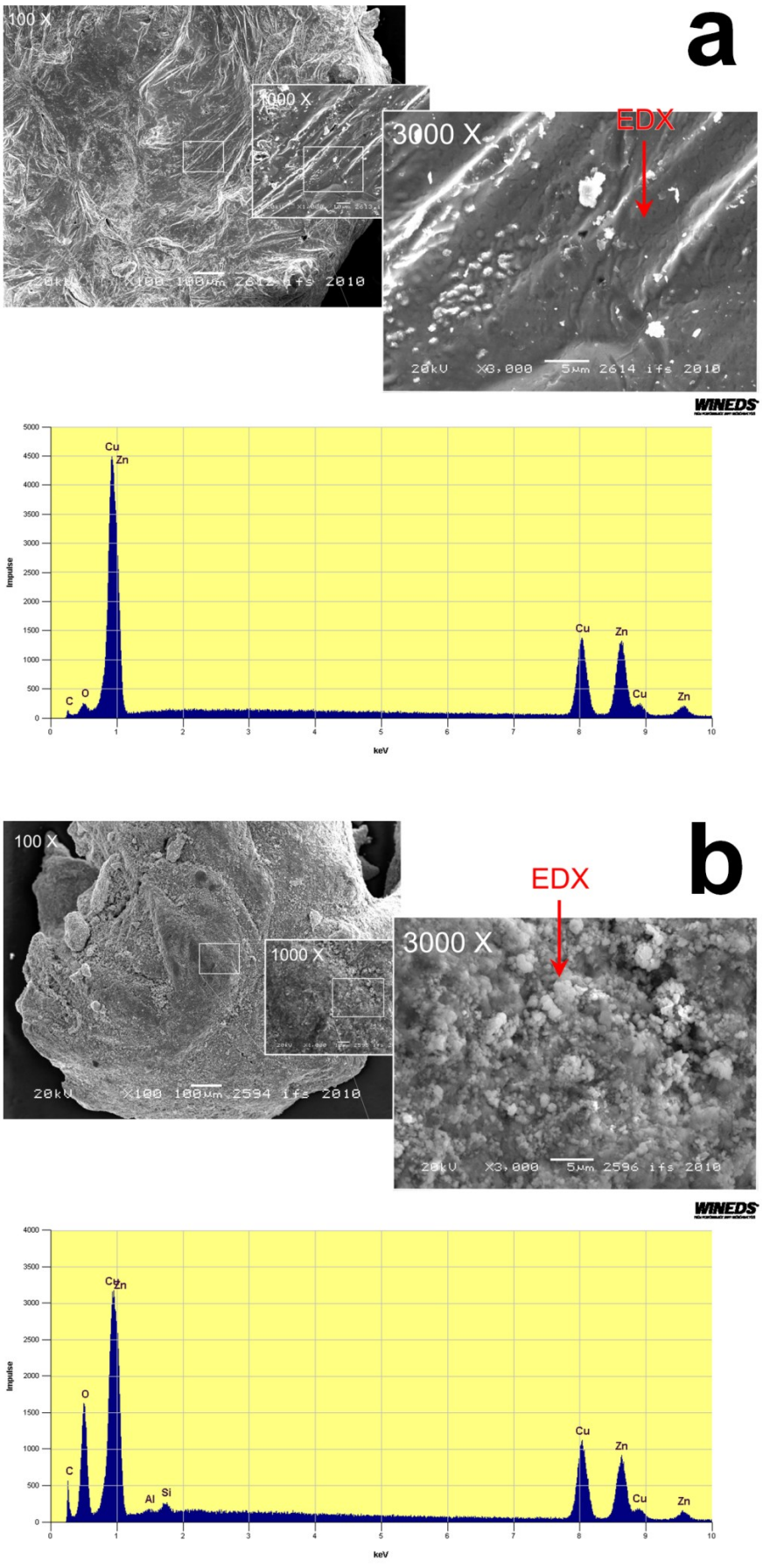

Figure S9. SEM pictures and EDX spectra of pristine (a) and altered brass shavings after eight months of exposure to groundwater from site B (b).

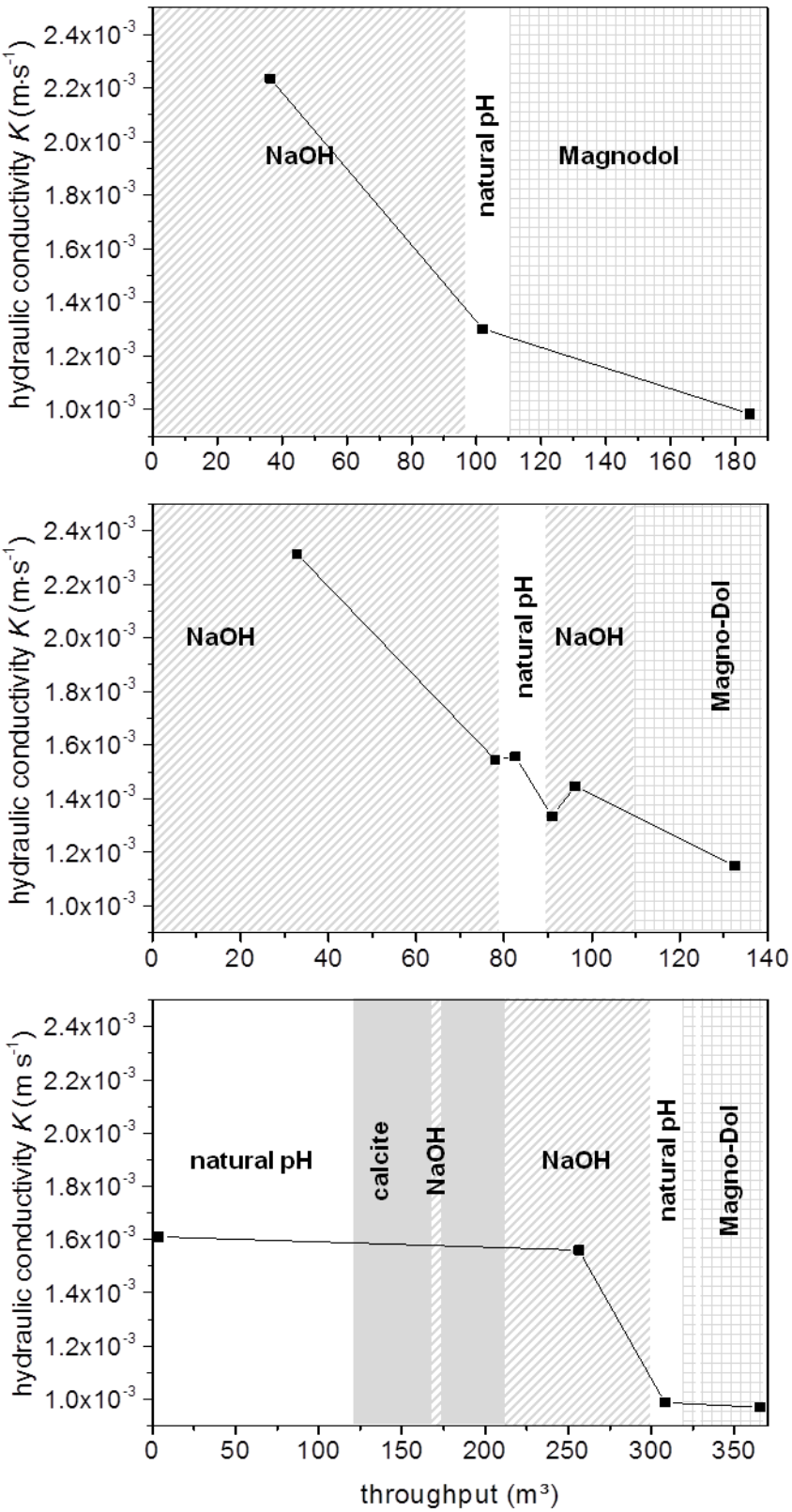

Figure S10. Hydraulic conductivity (*K*) change of three brass shavings filters from site B. Upper two graphs show less densely packed brass shavings in columns B3 and B4, lowest graph shows *K* values of filter bed in B8.

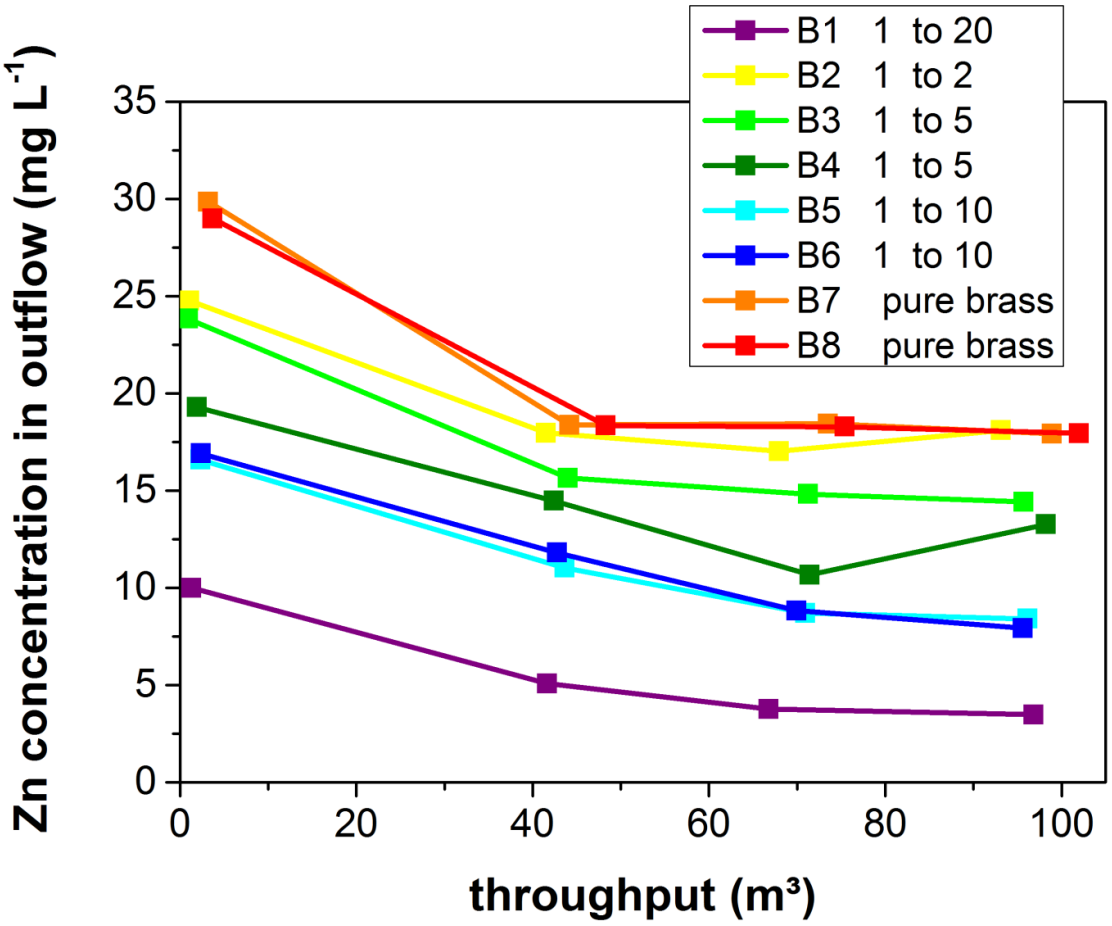

Figure S11. Zn concentrations in outflow water of filters at site B. Columns B1 to B6 contained mixtures of brass shavings and gravel at ratios shown in the legend.

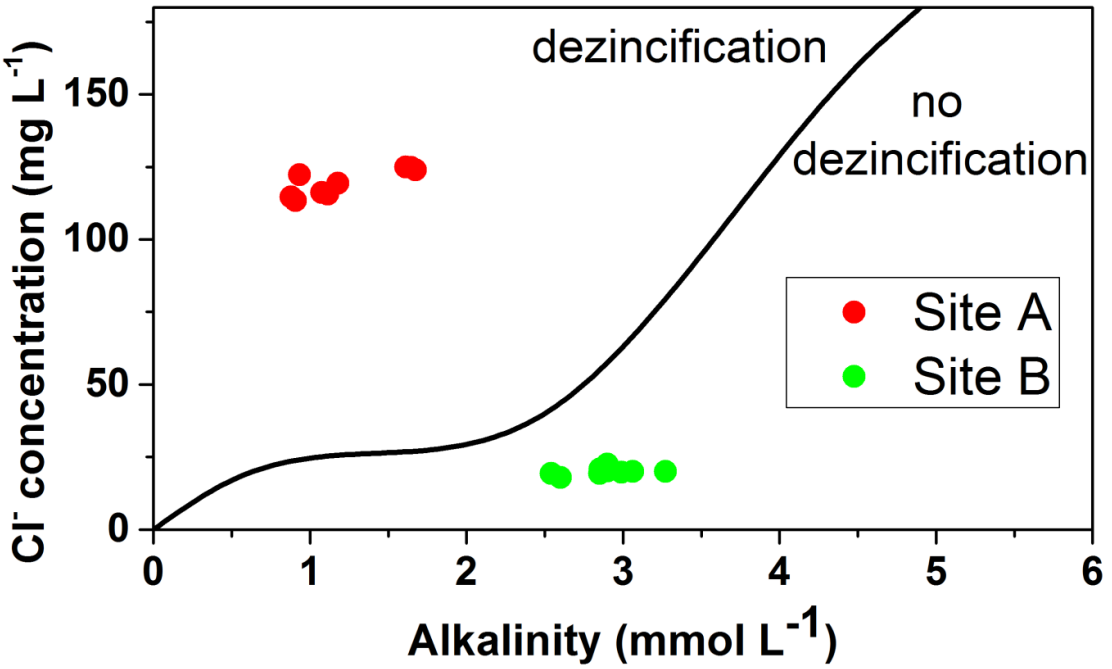

Figure S12. Turner`s diagram to predict probability of brass dezincification.

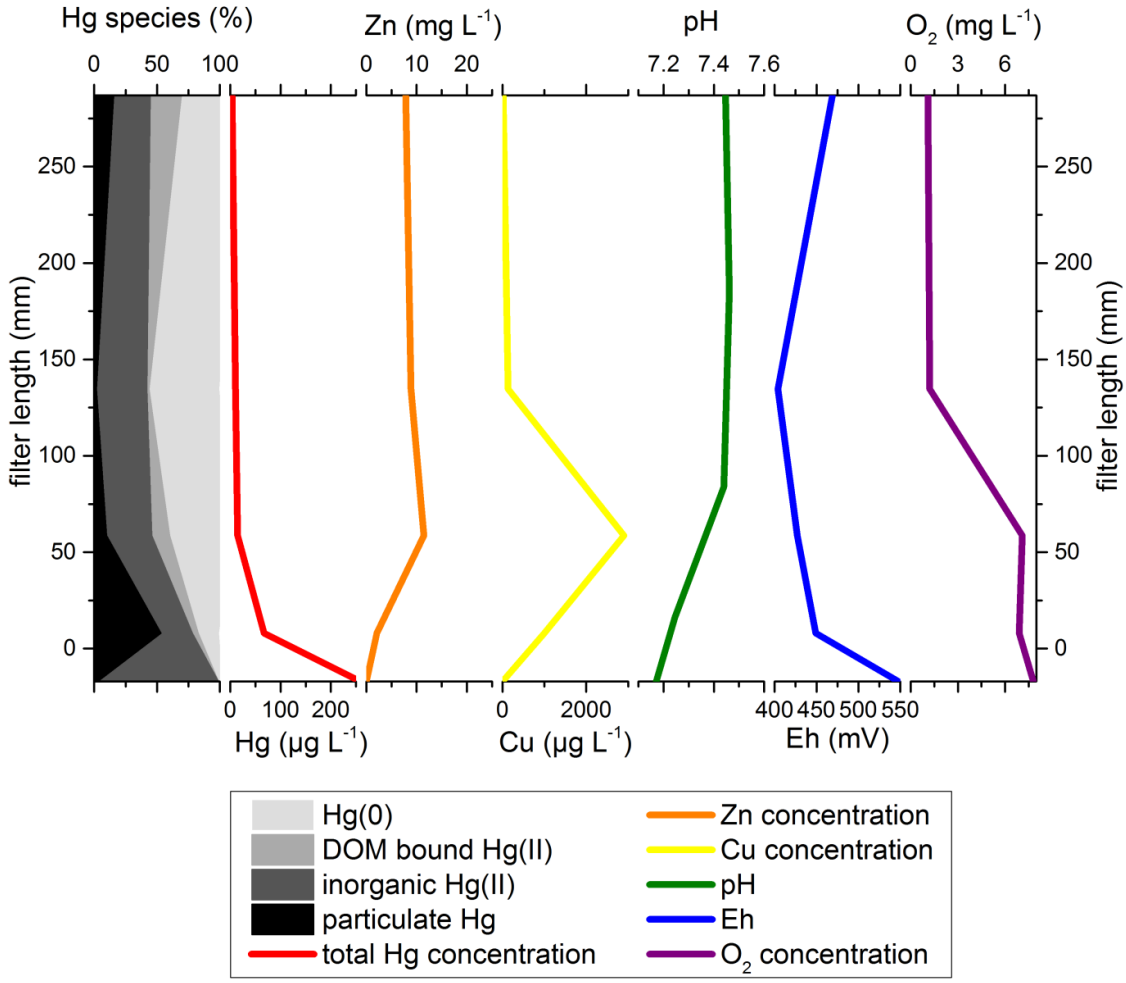

Figure S13. Changes of Hg species, Hg, Zn, Cu, O_2 concentration, pH, and Eh of a contaminated groundwater pretreated with $CaCO_3$ during passage through a brass shavings filter. Flow direction was from bottom to top.

References

Asasian, N., Kaghazchi, T., 2015. Sulfurized activated carbons and their mercury adsorption/desorption behavior in aqueous phase. Int. J. Environ. Sci. Technol. 12, 2511–2522. doi:10.1007/s13762-015-0818-x

Azizi, S.N., Dehnavi, A.R., Joorabdoozha, A., 2013. Synthesis and characterization of LTA nanozeolite using barley husk silica: Mercury removal from standard and real solutions. Mater. Res. Bull. 48, 1753–1759. doi:10.1016/j.materresbull.2012.12.068

Barringer, J.L., Szabo, Z., Reilly, P.A., 2013. Occurrence and Mobility of Mercury in Groundwater, in: Bradley, P. (Ed.), Current Perspectives in Contaminant Hydrology and Water Resources Sustainability. InTech.

BBodSchV, 1999. German Federal Soil and Legacy Regulation (Bundes-Bodenschutz- und Altlastenverordnung (BBodSchV- BGBl. I S. 1554)).

Bear, J., 1972. Dynamics of Fluids in Porous Media. Courier Corporation.

Biester, H., Müller, G., Schöler, H.., 2002. Binding and mobility of mercury in soils contaminated by emissions from chlor-alkali plants. Sci. Total Environ. 284, 191–203. doi:10.1016/S0048-9697(01)00885-3

Biester, H., Schuhmacher, P., Müller, G., 2000. Effectiveness of mossy tin filters to remove mercury from aqueous solution by Hg(II) reduction and Hg(0) amalgamation. Water Res. 34, 2031–2036. doi:10.1016/S0043-1354(99)00379-6

Bollen, A., Wenke, A., Biester, H., 2008. Mercury speciation analyses in HgCl2-contaminated soils and groundwater—Implications for risk assessment and remediation strategies. Water Res. 42, 91–100. doi:10.1016/j.watres.2007.07.011

Brosset, C., 1987. The behavior of mercury in the physical environment. Water. Air. Soil Pollut. 34, 145–166. doi:10.1007/BF00184757

CEN ISO, 2004. Geotechnical investigation and testing - Laboratory testing of soil - Part 11: Determination of permeability by constant and falling head.

DIN Deutsches Institut für Normung e. V., DIN German Institute for Standardization, 2008. DIN 32645 (2008-11-00) Chemical analysis - Decision limit, detection limit and determination limit under repeatability conditions - Terms, methods, evaluation (Nachweis-, Erfassungs- und Bestimmungsgrenze unter Wiederholbedingungen - Begriffe, Verfahren, Auswertung).

EN, European Committee for Standardization, 2014. DIN EN 1017: Chemicals used for treatment of water intended for human consumption – Half-burnt dolomite (German version).

EN, European Committee for Standardization, 2007. Method 1483, Water quality- Determination of mercury- Method using atomic absorption spectrometry; German version.

Huttenloch, P., Roehl, K.E., Czurda, K., 2003. Use of Copper Shavings To Remove Mercury from Contaminated Groundwater or Wastewater by Amalgamation. Environ. Sci. Technol. 37, 4269–4273. doi:10.1021/es020237q

ISO, International Organization for Standardization, 1996. Method 9963-1, Water quality- Determination of alkalinity -Part 1: Determination of total and composite alkalinity, German version.

Kinniburgh, D.G., Cooper, D., 2014. PhreePlot: Creating graphical output with PHREEQC.

Kocman, D., Horvat, M., Pirrone, N., Cinnirella, S., 2013. Contribution of contaminated sites to the global mercury budget. Environ. Res., Mercury in contaminated sites: identification, characterization, remediation, impact 125, 160–170. doi:10.1016/j.envres.2012.12.011

Lanxess AG, 2011. Product Information: LEWATIT-MonoPlus TP 214.

Meili, M., Iverfeldt, A., Håkanson, L., 1991. Mercury in the surface water of Swedish forest lakes —concentrations, speciation and controlling factors. Water. Air. Soil Pollut. 56, 439–453. doi:10.1007/BF00342290

Monier, M., Elsayed, N.H., Abdel-Latif, D., 2015. Synthesis and application of ion-imprinted resin based on modified melamine–thiourea for selective removal of Hg(II). Polym. Int. 64, 1465–1474. doi:10.1002/pi.4942

Obiri-Nyarko, F., Grajales-Mesa, S.J., Malina, G., 2014. An overview of permeable reactive barriers for in situ sustainable groundwater remediation. Chemosphere 111, 243–259. doi:10.1016/j.chemosphere.2014.03.112

Parkhurst, D.L., Apello, C.A.J., 2013. Description of Input and Examples for PHREEQC Version 3—A Computer Program for Speciation, Batch-Reaction, One-Dimensional Transport, and Inverse Geochemical Calculations (No. book 6, chap. A43), U.S. Geological Survey Techniques and Methods.

Richard, J.-H., Bischoff, C., Ahrens, C.G.M., Biester, H., 2016. Mercury (II) reduction and co-precipitation of metallic mercury on hydrous ferric oxide in contaminated groundwater. Sci. Total Environ. 539, 36–44. doi:10.1016/j.scitotenv.2015.08.116

Rohm & Haas Company, 2006. Ambersep-GT74: product data sheet.

Sarver, E.A., 2010. Insights into non-uniform copper and brass corrosion in potable water systems.

Turner, M.E., 1961. influence of water composition on the dezincification of duplex brass fittings. Proc Soc Water Treat. Exam. 162–174.

UNEP, 2013. Global Mercury Assessment 2013: Sources, Emissions, Releases and Environmental Transport. UNEP Chemicals Branch, Geneva, Switzerland.

USEPA, Office of Science and Technology, 2002. Method 1631, Revision E: Mercury in Water by Oxidation, Purge and Trap, and Cold Vapor Atomic Fluorescence Spectrometry.

Vernon, J.D., Bonzongo, J.-C.J., 2014. Volatilization and sorption of dissolved mercury by metallic iron of different particle sizes: Implications for treatment of mercury contaminated water effluents. J. Hazard. Mater. 276, 408–414. doi:10.1016/j.jhazmat.2014.05.054

Wenke, A., Bollen, A., Richard, J.-H., Biester, H., 2015. Potential of Brass to Remove Inorganic Hg(II) from Aqueous Solution through Amalgamation (in press). Water Environment Research.

Zhang, Y., Edwards, M., 2011. Effects of pH, chloride, bicarbonate, and phosphate on brass dezincification. J. - Am. Water Works Assoc. 103, 90–102.

Chapter 5: Synthesis and outlook

1 Synthesis

In the course of this thesis, the role of Fe-hydroxides (HFOs) for Hg species transformation was characterized, Hg speciation models were evaluated, and the long-term performance of brass shavings as Hg filter material was examined.

While the general importance of Fe mineral phases for Hg sorption, transport, and retardation has already been known, it could be shown here for the first time that precipitation of HFOs plays an important role for the formation and accumulation of Hg^0. Through Hg^{2+} reduction Hg mobility changes dramatically because i) dissolved Hg^0 sorbs less strongly to the aquifer material, and may be transported further ii) Hg^0 is volatile and can therefore become a subject of long range transport iii) Hg^0 is less soluble than Hg^{2+} and can precipitate, as demonstrated in this study by observed Hg^0 concentrations of up to 4% in HFO. Moreover, it could be shown in this thesis that geochemical models are not able to predict Hg^{2+} reduction during HFO formation, resulting in large underestimations of Hg concentrations when coprecipitation of Hg with HFOs is modeled.

This lack of agreement between Hg hydrogeochemical modeling and measured field data demonstrated the need for a systematic check of Hg speciation codes. Hence, measured and predicted Hg species in groundwater of three contaminated sites was compared. It could be shown that Hg^0 was underestimated by the applied models in most samples. This was assigned to the non-implementation of important processes for Hg^0 formation (reduction by reduced organic matter, Fe^{2+}, and microorganisms) in the models. Furthermore it could be shown in this thesis that the application of commonly used DOM parameters resulted in poor prediction accuracy for DOM bound and inorganic Hg in groundwater. Hg-DOM complexes were over- and inorganic Hg underestimated. It was demonstrated that prediction accuracy can be improved significantly by lowering the assumed proportion of strongly Hg binding thiol sites on DOM. This indicates general differences between ground and surface

water DOM and proofs that DOM parameters determined from surface water, unlike usual practice, must not be used to model Hg and trace elements in subsurface environments without prior verification.

To remediate fast flowing groundwater with high Hg concentrations through permeable reactive barriers (PRB) brass shavings were proposed as an appropriate filter material. In the present thesis their performance was assessed for the first time with real groundwater in long-term use and at a pilot scale. It could be shown that reaction kinetics of Hg filtration by brass shavings is extraordinary high even on the long run, exceeding that of all other tested filter materials (mineral adsorbers, Hg specific resins). Observed maximum Hg loading (164 g L^{-1}) was also shown to surpass that of conventional materials. However, at natural pH (6.6) Zn concentrations in the outflow exceeded the legal limits and threshold compliance was only reached above pH 8.5. Hence, brass shavings were shown to be appropriate as PRB filter material only in alkaline groundwater.

2 Outlook

The studies conducted in this thesis clearly represent a contribution to knowledge about the behavior of Hg in groundwater, our abilities to model its speciation, and the possible options to remediate Hg contaminations. Nevertheless, there is still need for further research.

While the importance of HFO precipitation for Hg^0 formation and enrichment could be demonstrated for a highly contaminated groundwater system, the significance of this process for Hg mobility still has to be investigated in aquifers with lower Hg loads. Furthermore, the main reaction mechanism behind Hg^0 formation in groundwater could not be determined. Is Hg reduction mainly triggered by oxidation of Fe^{2+} during HFO formation, or is reduction by reduced organic matter and/or microbes also major reaction pathways? We still cannot answer this question yet so further research has to untangle this. The application of Hg isotope analysis is promising here since the three mentioned processes are likely to produce different isotope fractionation signals. A follow-up project in which Hg speciation and isotope measurements will be combined is under preparation.

It was shown in this thesis that prediction accuracy of geochemical models for DOM bound and inorganic Hg could be improved significantly by lowering the assumed proportion of strongly Hg binding thiol sites on DOM. The hypothesis behind, viz. that differences between surface and groundwater DOM are responsible for the encountered lack of agreement between modeled and measured Hg speciation, is coherent but measurements still have to proof it. Hence, thiol determination in groundwater DOM should be the next step in order to resolve this issue.

The outstanding reaction kinetics and Hg loading capacity of brass shavings as Hg filter material could be demonstrated in this thesis. Nevertheless, because of Zn leaching brass shavings have turned out to be not appropriate as filter material for PRBs at sites with groundwater pH below 8.5. However, at many chlor alkali plants pH in groundwater is reported to be even higher than 8.5 due to spillage of Hg containing brines. So brass might still be used in PRBs at such sites but further research has to investigate this. Hg in flue gas of coal combustion and waste incineration units is one of the largest anthropogenic Hg sources because currently used filtration techniques have difficulties to retain Hg^0. Here, amalgamating materials could bring a clear progress and a research project is under preparation.

Acknowledgements

I would like to thank all friends and colleagues for the support of my work during the last years:

Special thanks go to my doctoral supervisor Prof. Dr. Harald Biester for giving me the necessary space and the encouragement to develop my own solutions, but still giving me all possible support and assistance whenever this was needed. Thank you very much as well for the opportunity to travel more than 100,000 km (2.6 times around the globe!) during this PhD.

I would also like to express my gratitude to the regional council and the district office of Freiburg i. Brsg. for financing a large part of my work. Thanks go out to Thomas Schöndorf from HPC AG for the excellent cooperation and to the staff of BRGM (France), namely Daniel Hube, Dr. Jennifer Harris-Hellal, Dr. Valérie Guerin, and Dr. Valérie Laperche for giving us the opportunity to work on such an extraordinary site and for the support during our field trips.

Many thanks go to the current and former members of my research group, Ayokunle Akindutire, Dr. Benjamin Gilfedder, Carluvy Baptista-Salazar, Ina Reisen, Dr. Johan Rydberg, Monica Moreno, Sara Zaferani, Tanja Broder, Dr. Thomas Riedel, and Dr. Yvonne Hermanns for the pleasant working atmosphere and the good times in the lab and in the office.

I would also like to thank Christa Wörndel for always finding an alternative solution of my problems. Special thanks go to Adelina Calean and Petra Schmidt, not only for their willing help in lab analyses but also for their reliable and manifold support throughout the years.

Moreover, thanks go to Christian Ahrens, Christina Wilms, Cornelia Bischoff, and Jacqueline Haller-Jans for helping me in the field and in the lab and for the nice discussions during long motorway journeys.

Johan und Hanna, ich danke euch für die Geduld und Ausdauer mit der ihr auf mich gewartet habt, wenn ich mal wieder viel zu spät nach Hause kam.

Fê, meu amor, eu não sei onde eu estaria hoje sem você. Este doutorado é mais ainda seu mérito como meu. Com seu amor, sua devoção e sua fé, você me deu uma nova vida que me permitiu este sucesso. Eu me alegro com o que ainda viveremos juntos. Eu te amo.

S.D.G.

Appendix

Because of the large quantity of data that has been generated during the studies for this thesis, the analytical data that has not been presented in the main sections or supporting information of chapter 2-4 can be found on an electronic storage medium that was submitted together with this thesis.